



PHD

Novel antifouling and chemically resistant membranes for water and wastewater treatment applications: Exploiting membrane preparation protocols for performance enhancement.

(Alternative Format Thesis)

Alali Alhweij, Hassan

Award date:
2022

Awarding institution:
University of Bath

[Link to publication](#)

Alternative formats

If you require this document in an alternative format, please contact:
openaccess@bath.ac.uk

Copyright of this thesis rests with the author. Access is subject to the above licence, if given. If no licence is specified above, original content in this thesis is licensed under the terms of the Creative Commons Attribution-NonCommercial 4.0 International (CC BY-NC-ND 4.0) Licence (<https://creativecommons.org/licenses/by-nc-nd/4.0/>). Any third-party copyright material present remains the property of its respective owner(s) and is licensed under its existing terms.

Take down policy

If you consider content within Bath's Research Portal to be in breach of UK law, please contact: openaccess@bath.ac.uk with the details. Your claim will be investigated and, where appropriate, the item will be removed from public view as soon as possible.



PHD

Novel antifouling and chemically resistant membranes for water and wastewater treatment applications: Exploiting membrane preparation protocols for performance enhancement.

(Alternative Format Thesis)

Alali Alhweij, Hassan

Award date:
2022

Awarding institution:
University of Bath

[Link to publication](#)

Alternative formats

If you require this document in an alternative format, please contact:
openaccess@bath.ac.uk

Copyright of this thesis rests with the author. Access is subject to the above licence, if given. If no licence is specified above, original content in this thesis is licensed under the terms of the Creative Commons Attribution-NonCommercial 4.0 International (CC BY-NC-ND 4.0) Licence (<https://creativecommons.org/licenses/by-nc-nd/4.0/>). Any third-party copyright material present remains the property of its respective owner(s) and is licensed under its existing terms.

Take down policy

If you consider content within Bath's Research Portal to be in breach of UK law, please contact: openaccess@bath.ac.uk with the details. Your claim will be investigated and, where appropriate, the item will be removed from public view as soon as possible.



Citation for published version:

Alhweij H, 2022, Novel antifouling and chemically resistant membranes for water and wastewater treatment applications: Exploiting membrane preparation protocols for performance enhancement', Ph.D., University of Bath.

Publication date:

March 2022

Document Version

Publisher's PDF, also known as Version of record

[Link to publication](#)

University of Bath

Alternative formats

If you require this document in an alternative format, please contact:
openaccess@bath.ac.uk

General rights

Copyright and moral rights for the publications made accessible in the public portal are retained by the authors and/or other copyright owners

and it is a condition of accessing publications that users recognise and abide by the legal requirements associated with these rights.

Take down policy

If you believe that this document breaches copyright, please contact us providing details, and we will remove access to the work immediately and investigate your claim.

Novel antifouling and chemically resistant
membranes for water and wastewater treatment
applications
Exploiting membrane preparation protocols for
performance enhancement

Hassan Alali Alhweij

A thesis submitted for the degree of Doctor of Philosophy

University of Bath
Department of Chemical Engineering
March 2022

Lead Supervisor: Dr Jannis Wenk

Second Supervisor: Dr Salman Shahid

Third Supervisor: Dr Emma Anna Carolina Emanuelsson

COPYRIGHT

Attention is drawn to the fact that copyright of this thesis rests with its author. A copy of this thesis has been supplied on the condition that anyone who consults it is understood to recognise that its copyright rests with its author and that they must not copy it or use material from it except as permitted by law or with the consent of the author.

This thesis may be made available for consultation within the University Library and may be photocopied or lent to other libraries for the purposes of consultation.

Signature of Author *Hassan Alhweij*

Declaration of authorship

I am the author of this thesis, and the work described therein was carried out by myself personally, with any collaborative work stated and acknowledged within the corresponding text. I also declare that I have no known competing financial interests or personal relationships that could have appeared to influence the work reported in this thesis.

Candidate's signature

A solid black rectangular box redacting the candidate's signature.

Acknowledgments

A special gratitude to my lead supervisor Dr. Jannis Wenk for his priceless help and guidance which played a vital role throughout my PhD to think, plan, and write like an academic, this study could not have been successfully conducted without. Thanks to my co-supervisors, Dr. Emma Emanuelsson and Dr. Salman Shahid for their advice and recommendations. A huge recognition to the University of Bath for research scholarship (URSA). I also appreciate the assistance provided by the Department of Chemical Engineering, and technical support provided by the legend Dr Philip Fletcher and the team in the Material and Chemical Characterisation Facility (MC²). I am also very indebted to Stantec colleagues Richard Margrett, Julie Jeavons, Lisa Barrott, Huw Jones, Tony Amato and Narinder Sunner for their kind treatment and support. A distinct appreciation to Wessex Water and Severn Trent fantastic and knowledgeable team members Will Wormald, Andrew Gulliford, Jill Smith, Nick Lowe, Stuart Lewis, Sophie Ward, Anna Nel and Sam Codd. Indeed, you have been so creative, and I have learned from you so much. All, you have been such an inspiring, kind, and unforgotten individuals who beyond shadow of a doubt had shined making the UK not only one of the best places to work, but also to learn, integrate and enjoy, what an incredible work environment! I have a great gratitude to Dr Adam Sarihan for the generous share of his lab knowledge and expertise. Also, special thanks to the lab colleagues Ida Amura, Triantafyllos Manios and Sharifah Alkandari for creating an inspiring work environment. I would like to thank my family who were forcibly displaced from Syria and dispersed all over the globe, without their encouragement and inspirations nothing of this could ever be possible. The thesis is dedicated to my father "Adnan" who passed away in Turkey while I was abroad. He guided me to where I am today and supported me with endless care, affection, encouragement, and love. To all family members, tutors and friends who were displaced and departed this life abroad, rest in peace (RIP). You are all loved and remembered.

Abstract

Development for next generation of polymeric membranes by using new classes of materials with novel preparation protocols is crucial to address the shortcomings of the existing commercial membranes such as antifouling resistance, chlorine intolerance and solvent stability. Polyaniline (PANI) membranes were foreseen a promising alternative material to existing membrane polymers, mainly due to their affordability and intrinsic antifouling behaviour, but more widespread applications were constrained by chlorine intolerance, and the need for prolonged post-treatment crosslinking to improve solute retention and solvent stability. This study presents a simplified technique to overcome these limitations by modifying PANI synthesis and tailoring the membrane preparation protocols using non-solvent induced phase separation (NIPS) technique. PANI was modified by introducing sulfonic acid groups ($-\text{SO}_3\text{H}$) resulting in sulfonated polyaniline (S-PANI) that was used for the fabrication of S-PANI membranes at the ultrafiltration (UF) separation range (molecular weight cut off (MWCO) ≈ 25 kDa and pure water permeance $69.7 \text{ L m}^{-2} \text{ h}^{-1} \text{ bar}^{-1}$). The prepared S-PANI membranes exhibited physical and chemical stability after soaking in 250 ppm sodium hypochlorite aqueous solution for 3 consecutive days whereas PANI membranes suffered from chemical degradation and complete structural damage as confirmed by visual observation, dynamic filtration tests (permeance and rejection), Fourier transform infra-red (FT-IR) spectra, scanning electron microscopy (SEM) imaging and atomic force microscopy (AFM) analysis. The dynamic filtration test using three model foulants showed enhanced antifouling behaviour of S-PANI membranes with flux recovery rate (Fr) 84%, 89% and 92% compared to 65%, 68%, 77% for the PANI membrane with *alginate acid*, *humic acid* and *bovine serum albumin*, respectively. However, the developed UF membranes would have limited application unless otherwise the solute retention is narrowed to the nanofiltration (NF) range and beyond. As such, a novel facile preparation technique was adopted to produce S-PANI NF membranes (MWCO ≈ 680 Da and pure water permeance $\approx 5 \text{ L}$

$\text{m}^{-2} \text{h}^{-1} \text{bar}^{-1}$). The presence of crosslinking sites (sulfonic and amide groups) at the polymer chains and the changes in the chemistry of the coagulation bath (1-3 M HCl) facilitated simultaneous coagulation and crosslinking. The instant stabilisation of the selective layer for the crosslinked S-PANI hindered the solvent/non-solvent exchange rate (from 2 h to ca. 24 h), enabled the production of a tailored membrane morphology with a dense skin layer (1.1-2.3 times), suppressed macro-voids (50-70%), reduced porosity (26-37%), enhanced tensile strength (2.3 times), increased hydrophilicity (21% drop in contact angle), and improved solvent stability (mass swelling degree and gel content in *tetrahydrofuran* was 88% and 90% (pristine S-PANI) compared to 3% and 100% (crosslinked S-PANI), respectively). In a water treatment scenario, the newly developed S-PANI NF membranes were compared with a commercial membrane and conventional adsorption-coagulation-flocculation, optimised for natural organic matter (NOM) removal. Artificially prepared surface water and seawater and a stabilised landfill leachate served as test solutions. S-PANI NF membranes showed best NOM separation performance for both surface water and seawater (higher by ~5-8% and ~24-41% for commercial membrane and conventional treatment, respectively). In contrast, the conventional treatment achieved higher leachate NOM removal by ~7% (S-PANI) and ~17% (commercial membrane). The S-PANI performed slightly better (~6%) in removal of chemical oxygen demand (COD) compared to the commercial membrane and conventional treatment. During long-term fouling S-PANI exhibited slower growth in transmembrane pressure (TMP) by ~52-52%, less affinity towards organic matter (~26-43% surface water, ~35-42% seawater and ~48-55% leachate) and higher flux recovery (~4-10% artificial surface and seawaters and ~12% in leachate) compared to the commercial membrane, particularly at high NOM concentration. The facile crosslinking technique was adopted for the preparation of in-situ tuneable high performance organic solvent NF S-PANI membranes (*Tetrahydrofuran* (THF) permeance was 2.1 to 16.4 $\text{L m}^{-2} \text{h}^{-1} \text{bar}^{-1}$ with apparent MWCO between 250 to 1000 g mol^{-1}). Different molecular weight organic acids (173 g mol^{-1} metanilic acid versus 800,000 g mol^{-1} poly(2-acrylamido-2-methyl-1-propanesulfonic

acid)) were incorporated and self-doped PANI membranes were fabricated at different aqueous coagulation bath acidic strength (0.1-3 M HCl). The transport properties of the OSN membranes were stable in dynamic ageing filtration test with sequential feed of dye solutions (MW range from 327 to 1470 g mol⁻¹) in *Methanol*, *acetonitrile*, and *tetrahydrofuran* over 250 h. The cast membranes in higher coagulation bath acidic strength showed increased crosslinking degree as confirmed by the mass swelling degree and gel content measurements. The higher crosslinking degree was associated with an order decline in permeance (52-92%) and an increase in solute rejection due to the contractions in the polymer intersegmental spaces. PAMPSA doped membranes were only in the tight UF separation range (MWCO \approx 1.5 kDa) due to the dopant high MW and membrane post-treatment by wet annealing was required to narrow the membrane's solute rejection to NF range without substantial compromise to the membrane permeance. The OSN filtration results were reproducible without any irreversible structural ageing. The characterisation results (SEM, AFM, mechanical properties, and hydrophilicity) indicated that no membrane ageing occurred over the static test period of 30 days with *THF*. These results indicate that the membranes exhibit good stability over a long-term period whilst still maintaining the excellent separation performances. This work has significant novelty and believed to attract research communities and engineers as it is the first study to exploit the PANI polymer synthesis and membrane preparation protocols using simplified approach to produce S-PANI membranes with noticeable improvement in antifouling behaviour, chlorine intolerance, and substantial improvement in permselective properties and solvent stability. The developed membranes have a scalability potential to suit numerous applications in water and wastewater treatment, organic solvent nanofiltration (OSN) related industries and potentially high fouling solutions in food processing applications.

Dissemination

Journal articles

- **H. Alhweij**, I. Amura, J. Wenk, E.A.C. Emanuelsson, S. Shahid, Self-doped sulfonated polyaniline ultrafiltration membranes with enhanced chlorine resistance and antifouling properties, *J. Appl. Polym. Sci.* (2021) 50756. <https://doi.org/10.1002/app.50756>.
- **H. Alhweij**, E.A. Carolina Emanuelsson, S. Shahid, J. Wenk, Simplified in-situ tailoring of cross-linked self-doped sulfonated polyaniline (S-PANI) membranes for nanofiltration applications, *J. Memb. Sci.* (2021) 119654. <https://doi.org/10.1016/j.memsci.2021.119654>.
- **H. Alhweij**, E.A. Carolina Emanuelsson, S. Shahid, J. Wenk, Organic matter removal and antifouling performance of sulfonated polyaniline nanofiltration (S-PANI NF) membranes, *Journal of Environmental Chemical Engineering*, Volume 10, Issue 3, 2022, 107906, ISSN 2213-3437, <https://doi.org/10.1016/j.jece.2022.107906>.
- **H. Alhweij**, E.A. Carolina Emanuelsson, S. Shahid, J. Wenk High performance in-situ tuned self-doped polyaniline (PANI) membranes for organic solvent (nano)filtration, *Polymer*. 245 (2022) 124682. <https://doi.org/10.1016/j.polymer.2022.124682>.

Conference presentations

- Dec 2020** **H. Alhweij**, E.A. Carolina Emanuelsson, S. Shahid, J. Wenk, Comparative study of novel antifouling sulfonated polyaniline nanofiltration membranes and conventional treatment for water and seawater (pre)treatment, 17th Network Young Membrains Meeting (NYM 2020).
- Dec 2020** **H. Alhweij**, I. Amura, J. Wenk, E.A.C. Emanuelsson, S. Shahid, Self-doped sulfonated polyaniline ultrafiltration membranes with enhanced chlorine resistance and antifouling properties, International Congress on Membranes & Membrane Processes (ICOM 2020).
- Dec 2020** **H. Alhweij**, E.A. Carolina Emanuelsson, S. Shahid, J. Wenk, Self-doped sulfonated polyaniline nanofiltration membranes, International Congress on Membranes & Membrane Processes (ICOM 2020).

Table of Contents

Declaration of authorship	i
Acknowledgments	ii
Abstract	iii
Dissemination	vi
Journal articles	vi
Conference presentations	vi
Table of Contents	vii
List of Figures	xi
List of Tables	xxiii
List of Abbreviations	xxv
Thesis Outline	xxviii
Chapter 1 Introduction and general literature review	1
1.1 Overview.....	2
1.2 Membrane treatment	3
1.3 Membrane transport theory	5
1.4 Membrane material and preparation	6
1.5 Membrane cross-linking and solvent stability applications	9
1.6 Membrane fouling.....	12
1.7 Antifouling techniques.....	13
1.7.1 Feed water pre-treatment	13
1.7.2 Chlorination.....	14
1.7.3 Surface modification	16
1.7.4 Material blending.....	18
1.7.5 Antifouling and chlorine resistant material	18

1.8 Aims and objectives	21
1.9 References	22
Chapter 2 Self-doped sulfonated polyaniline ultrafiltration membranes with enhanced chlorine resistance and antifouling properties	45
Abstract	49
2.1 Introduction	50
2.2 Experiment	53
2.2.1 Materials	53
2.2.2 Synthesis of PANI and S-PANI polymers	53
2.2.3 Membrane fabrication	54
2.2.4. Membrane characterization	55
2.3 Results and Discussion	58
2.3.1 FT-IR spectroscopic analysis of membranes	58
2.3.2 Morphology	59
2.3.3 Surface charge	64
2.3.4 Permeance and rejection tests	65
2.3.5 Hydrophilicity and fouling behaviour	68
2.4 Conclusions	72
2.5 Acknowledgements	73
2.6 References	73
Chapter 3 Simplified in-situ tailoring of cross-linked self-doped sulfonated polyaniline (S-PANI) membranes for nanofiltration applications	84
Abstract	88
3.1 Introduction	89
3.2 Experimental	91
3.2.1 Materials	91

3.2.2 Synthesis of S-PANI polymer	91
3.2.3 Membrane fabrication	92
3.2.4 Membrane characterisation.....	93
3.3 Results and Discussion	94
3.3.1 FT-IR spectroscopy, XPS and XRD analysis.....	94
3.3.2 Ion exchange capacity and water stability	97
3.3.3 Morphology and porosity	98
3.3.4 Demixing kinetics.....	101
3.3.5 Thermal and mechanical analysis.....	102
3.3.6 Solvent stability.....	104
3.3.7 Mass swelling degree and gel content	104
3.3.8 Contact Angle.....	106
3.3.9 Membrane transport properties.....	106
3.4 Conclusions.....	113
3.5 Acknowledgements.....	113
3.6 References.....	114
Supporting Information.....	123
Materials S1	124
S-PANI synthesis S2	124
S-PANI molecular weight determination S3.....	125
Energy dispersive X-ray S4.....	125
Membrane fabrication S5	126
Membrane characterisation S6.....	127
S-PANI doping S7	138
XPS spectra S8	139
Water stability S9.....	139

Morphology S10	140
Porosity S11	140
Differential scanning calorimetry S12	142
Transport properties S13	143
References S14	145
Chapter 4 Organic matter removal and antifouling performance of sulfonated polyaniline nanofiltration (S-PANI NF) membranes	146
Abstract	151
4.1 Introduction	152
4.2 Experimental	154
4.2.1 Materials	154
4.2.2 Artificially prepared waters and leachate characterization	155
4.2.3 Conventional treatment	157
4.2.4 Membrane treatment and fouling behaviour	158
4.3 Results and Discussion	161
4.3.1 Apparent molecular weight distribution (AMWD) of artificially prepared waters and leachate	161
4.3.2 Treatment of artificially prepared water	162
4.3.3 Landfill leachate treatment	168
4.3.4 Membrane fouling behaviour	170
4.4 Conclusions	178
4.5 Acknowledgements	179
4.6 References	179
Supporting Information	195
Materials S1	196
Solute fractionation S2	196

Conventional treatment S3	197
SEM S5.....	201
References S6	201
Chapter 5 High performance in-situ tuned self-doped polyaniline (PANI) membranes for organic solvent (nano)filtration	202
Abstract.....	207
5.1 Introduction	208
5.2 Experimental	210
5.2.1 Materials.....	210
5.2.2 Polymer synthesis.....	211
5.2.3 Membrane fabrication	212
5.2.4 Membrane characterisation.....	213
5.3 Results and Discussion	214
5.3.1 FT-IR spectroscopy	214
5.3.2 Morphology	215
5.3.3 Mechanical analysis.....	221
5.3.4 Contact angle	223
5.3.5 Swelling degree and gel content.....	224
5.3.6 Membrane transport properties.....	225
5.4 Conclusions.....	233
5.5 Acknowledgements.....	234
5.6 References.....	234
Supporting Information.....	246
Materials S1	247
Polymer thermal analysis S2	247
Viscosity S3.....	248

Membrane characterisation S4	248
FT-IR spectra S5.....	253
Membrane SEM S6	254
Membrane AFM S7	256
Chapter 6 General discussions of the published work.....	263
6.1 Discussions	264
Chapter 7 General conclusions and future work	269
7.1 Conclusions.....	270
7.2 Future work and impact	274
7.2.1 Future work on the specific topics of this thesis	274
Appendix: Statement of Authorship.....	276

List of Figures

Fig. 1.1 Typical flow schematic diagram for surface water treatment plant [12].	2
Fig. 1.2 The trend of published documents per annum for membranes in a) all disciplines and b) water and wastewater related applications in Scopus website database.	3
Fig. 1.3 Membrane separation process based on pore size [26].....	4
Fig. 1.4 a) general arrangement of RO membrane module [12] and b) cross-section of spiral wound reverse osmosis membrane element [34].	4
Fig. 1.5 The trend of published documents per annum for the developments in the phase inversion technique for membranes preparation.	7
Fig. 1.6 Composition paths and cross-sectional morphology of a cast film immediately after immersion ($t < 1$ s) demonstrating (a, b) instantaneous demixing and (c, d) delayed demixing, respectively; T and B represent top and bottom of the film, respectively [44,48,52,53].	9
Fig. 1.7 Descriptive sketch of three-dimensional links after cross-linking and structural stability of organic solvent membranes [61].....	10
Fig. 1.8 Flux decline over time due to membrane fouling [86].	12
Fig. 1.9 Chemical attack of polyamide membrane selective layer by chlorine oxidant [120]. ...	15
Fig. 1.10 Methods of chemical and physical surface modification of polymer surface [155]. ...	17
Fig. 1.11 Current trends in the field of organic membrane materials to develop next-generation membrane materials [20].	19
Fig. 1.12 PANI chemical structure.....	19
Fig. 1.13 Cross-linking PANI with (a) DCX, (b) GA, and (c) thermal treatment [61,189].	20
Fig. 2.1 Polymerisation scheme for S-PANI.....	54
Fig. 2.2 Process flow diagram of the crossflow rig.....	58

Fig. 2.3 FTIR spectra for S-PANI membrane soaked in water and 250 ppm sodium hypochlorite solution, respectively, at different pH values (4.5, 7.4 and 10.5) for three consecutive days. 59

Fig. 2.4 Digital micrographs of membrane coupons (a, c) pristine control S-PANI and PANI samples before chlorination soaked in pure water at pH 7.4; (b, d) S-PANI and PANI samples after chlorination with 250 ppm sodium hypochlorite solution for three consecutive days at pH 7.4; (e, f) PANI and S-PANI samples soaked in hypochlorite solution at pH 7.4. One square box is 1cm². 61

Fig. 2.5 SEM images for S-PANI membrane surface (a) soaked in water at pH 7.4 (b, c, d) soaked in sodium hypochlorite solution at pH 4.5, 7.5 and 10.5 (e) PANI soaked in water pH 7.4 (f) PANI soaked in sodium hypochlorite solution at pH 7.4 (g) PES soaked in water at pH 7.4 (h) PES soaked in sodium hypochlorite solution at pH 7.4. 62

Fig. 2.6 SEM images for membrane cross-section (a) S-PANI soaked in water at pH 7.4, (b, c, d) S-PAN soaked in hypochlorite solution at different pH values 4.5, 7.5 and 10.5, respectively, (e) PANI soaked in water at pH 7.4 (f) PANI soaked in hypochlorite solution at pH 7.4. . 63

Fig. 2.7 AFM analysis of S-PANI membrane surface (a) soaked in water at pH 7.4 (b, c, d) soaked in hypochlorite solution at different pH values 4.5, 7.5 and 10.5, respectively. 64

Fig. 2.8 S-PANI membrane surface charge at neutral pH with a standard deviation after soaking in water and 250 ppm sodium hypochlorite solution for three days at different pH values of 4.5, 7.4 and 10.5, respectively. 65

Fig. 2.9 (a) Pure water and (b) BSA solution feed permeance of the S-PANI membranes, immersed in water and hypochlorite solution with a standard deviation at different pH values under an applied pressure of 1.0 bar at room temperature. 66

Fig. 2.10 BSA rejection of the S-PANI membranes, immersed in water and hypochlorite solution with a standard deviation at different pH values with applied pressure 1.0 bar at room temperature. 67

Fig. 2.11 The contact angle of S-PANI membranes immersed in water and hypochlorite solution at different pH values.....	69
Fig. 2.12 The change in the TMP for S-PANI and PANI membranes while being fouled with <i>humic acid</i> (a, b) <i>alginate acid</i> (c, d) and <i>BSA</i> (e, f), respectively, at different initial flux values (J_0).....	70
Fig. 2.13 The change in TMP and flux for S-PANI and PANI membranes over a prolonged period of operation using an aqueous solution with a mixture of model foulants (<i>BSA</i> , <i>humic acid</i> and <i>alginate acid</i>) at feed concentration of 100 mg/L as TOC.....	72
Fig. 3.1 FT-IR spectra of membranes produced in neutral coagulation bath (M1) and acidic coagulation bath (M2- M3).....	96
Fig. 3.2 XRD patterns of S-PANI membranes M1-M3.	97
Fig. 3.3 SEM surface and cross-sectional area images of S-PANI membranes prepared in neutral coagulation bath (M1), 1M HCl acidic coagulation bath (M2) and 3M HCl acidic coagulation bath (M3).	99
Fig. 3.4 Visual and TEM images of the S-PANI polymer solution in neutral coagulation bath (a, d), 1M coagulation bath (b, e) and 3M coagulation bath (c, f).	100
Fig. 3.5 S-PANI solvent demixing kinetics in neutral (M1) and increasingly acidic (M2, 1M HCl; M3, 3M HCl) coagulation solutions.	102
Fig. 3.6 TGA curves for pristine and cross-linked S-PANI membranes (a) weight loss (b) derivative weight loss with respect to temperature from room temperature to 600°C.....	103
Fig. 3.7 Mechanical properties of the pristine M1 and cross-linked (M2-M3) S-PANI membranes.	103
Fig. 3.8 Effect of <i>DMF</i> on membrane stability after two weeks.....	104
Fig. 3.9 Mass swelling degree and gel content of pristine and crosslinked S-PANI membranes M1-M3 in different polar protic, polar aprotic and nonpolar solvents.....	105
Fig. 3.10 The contact angle of the S-PANI membranes (M1-M3).	106

Fig. 3.11 Pure water permeance for the S-PANI membranes (M1-M5) and the commercial membrane (M8).	108
Fig. 3.12 (a) PEG permeance and (b) rejection of the S-PANI membranes (M1-M5) and the commercial membrane (M8).....	112
Fig. 3.13 (a) dye feed solution (methylene blue, indigo carmine, bromothymol blue and rose bengal) permeance and (b) rejection for of the S-PANI membranes (M1-M3) and the commercial membrane (M8).....	112
Fig. 3.14 (a) The surface charge of M1-M5 membranes and the commercial M8 membrane and (b) The zeta potential of dye feed solutions (methylene blue 10 mg L ⁻¹ , indigo carmine 10 mg L ⁻¹ , bromothymol blue 50 mg L ⁻¹ and rose bengal 10 mg L ⁻¹).....	112
Fig. S3.1 Polymerisation scheme for S-PANI.	125
Fig. S3.2 Schematic diagram of the dead-end cell filtration.....	134
Fig. S3.3 The calibration curve of methylene blue dye aqueous solution as a relation between the feed solution concentration and the UV absorbance (peak absorption at wavelength 661 nm).	134
Fig. S3.4 The calibration curve of indigo carmine dye aqueous solution as a relation between the feed solution concentration and the UV absorbance (peak absorption at wavelength 612 nm).	135
Fig. S3.5 The calibration curve of bromothymol blue dye aqueous solution as a relation between the feed solution concentration and the UV absorbance (peak absorption at wavelength 430 nm).	135
Fig. S3.6 The calibration curve of rose bengal dye aqueous solution as a relation between the feed solution concentration and the UV absorbance (peak absorption at wavelength 549 nm).	135
Fig. S3.7 The calibration curve of the PEG oligomer MW 766 g mol ⁻¹ at different concentrations.	136

Fig. S3.8 The calibration curve of the PEG oligomer MW 810 g mol ⁻¹ at different concentrations.	136
Fig. S3.9 The calibration curve of the PEG oligomer MW 854 g mol ⁻¹ at different concentrations.	136
Fig. S3.10 The calibration curve of the PEG oligomer MW 898 g mol ⁻¹ at different concentrations.	137
Fig. S3.11 The calibration curve of the PEG oligomer MW 942 g mol ⁻¹ at different concentrations.	137
Fig. S3.12 The calibration curve of the PEG oligomer MW 986 g mol ⁻¹ at different concentrations.	137
Fig. S3.13 The calibration curve of the PEG oligomer MW 1030 g mol ⁻¹ at different concentrations.	138
Fig. S3.14 The calibration curve of the PEG oligomer MW 1074 g mol ⁻¹ at different concentrations.	138
Fig. S3.15 pictorial representation of both doped/dedoped M4-M5 and M1 membranes.	138
Fig. S3.16 Core-level spectra of S-PANI membranes M1-M3 (a) C 1s (b) O 1s (c) S 2p (d) N 1s.	139
Fig. S3.17 SEM surface and cross-sectional area images of HCl doped S-PANI membranes prepared in neutral coagulation bath (M4-M5), 1M HCl acidic coagulation bath (M6) and 3M HCl acidic coagulation bath (M7).	140
Fig. S3.18 The isotherm of the S-PANI membrane produced in pure water coagulation bath (M1).	140
Fig. S3.19 The isotherm of the S-PANI membrane produced in 1M HCl(aq) coagulation bath (M2).	141
Fig. S3.20 The isotherm of the S-PANI membrane produced in 3M HCl(aq) coagulation bath (M3).	141

Fig. S3.21 The cumulative pore volume versus the pore width of the S-PANI membranes prepared in a neutral coagulation bath (M1) without a support layer.	141
Fig. S3.22 The cumulative pore volume versus the pore width of the S-PANI membranes prepared in 1M HCl acidic coagulation bath (M2) without a support layer.	142
Fig. S3.23 The cumulative pore volume versus the pore width of the S-PANI membranes prepared in 3M HCl acidic coagulation bath (M3) without a support layer.	142
Fig. S3.24 DSC thermogram register from 20 to 300°C of M1 S-PANI membrane produced in DI water coagulation bath.	142
Fig. S3.25 DSC thermogram register from 150 to 350°C of M1 S-PANI membrane produced in 1M HCl coagulation bath.	143
Fig. S3.26 DSC thermogram register from 150 to 350°C of M1 S-PANI membrane produced in 3M HCl coagulation bath.	143
Fig. S3.27 pH change of the M1-M5 membranes' permeate after preconditioning and filtration.	144
Fig. S3.28 A schematic representation of asymmetric S-PANI membrane and matrix swelling and pore contraction of the membrane after HCl(aq) acid doping.	144
Fig. 4.1 Schematic diagram for the sequence of the applied conventional treatment for artificially prepared surface water and seawater solutions.	158
Fig. 4.2 Apparent molecular weight distribution of a) NOM (measured as [DOC] of 20 mg C L ⁻¹) in feed aqueous solution for artificial surface water and seawater and b) COD and DOC in landfill leachate with error bars representing one standard deviation calculated from the results of triplicate runs at the specific experimental conditions.	162
Fig. 4.3 a) NOM (measured [DOC]) removal for artificially prepared surface water and seawater feed containing different DOC concentrations using conventional treatment with error bars representing one standard deviation calculated from the results of triplicate runs at the specific experimental conditions, b) Shift in apparent molecular weight distribution of the	

NOM for conventionally treated artificial surface water and artificial seawater at [DOC] 20 mg C L⁻¹ with error bars represent one standard deviation calculated from the results of triplicate runs at the specific experimental conditions..... 165

Fig. 4.4 Permeance and DOC rejection for artificially prepared surface water and seawater solutions containing different [DOC] using S-PANI membranes (a, b) and DuraMem®500 membranes (c, d) with error bars representing one standard deviation calculated from the results of triplicate runs at the specific experimental conditions. 168

Fig. 4.5 a) Solute removal efficiency in terms of measured DOC and COD by conventional and membrane treatment and b) Shift in apparent molecular weight distribution of the DOC and COD for conventionally treated leachate at [DOC] ≈ 370 mg C L⁻¹ with error bars representing one standard deviation calculated from the results of triplicate runs at the specific experimental conditions..... 170

Fig. 4.6 The change in the transmembrane pressure (TMP) for fouled S-PANI and DuraMem®500 membranes at different [DOC] obtained from natural source (a) artificial surface water, (b) artificial seawater, at identical initial permeance values (≈ 7.0 L m⁻² h⁻¹ bar⁻¹)..... 172

Fig. 4.7 The accumulated foulant mass per unit membrane surface area for SPANI and DuraMem®500 membranes (a) mass balance derived foulant mass and (b) chemically recovered foulant mass, with error bars represent one standard deviation calculated from the results of triple runs at the specific experimental conditions. 174

Fig. 4.8 a) Development of transmembrane pressure (TMP) for fouled membranes with landfill leachate for S-PANI and DuraMem®500 at identical initial permeance values (≈ 7.0 L m⁻² h⁻¹ bar⁻¹) and (b) Mass balance derived and chemically recovered accumulated foulant mass per unit membrane surface area for SPANI and DuraMem®500 membranes, respectively. Error bars represent one standard deviation calculated from the results of triplicate runs at the specific experimental conditions..... 175

Fig. 4.9 SEM membrane surface images fouled S-PANI and DuraMem®500 in 20 mg L ⁻¹ of artificial surface water feedstock (a, d), cleaned S-PANI and DuraMem®500 by dynamic flushing with DI water (b, e) and chemically cleaned in place (CIP) S-PANI and DuraMem®500 of (c, f), respectively.....	177
Fig. 4.10 SEM membrane surface images fouled S-PANI and DuraMem®500 in landfill leachate feedstock (a, d), cleaned S-PANI and DuraMem®500 by dynamic flushing with DI water (b, e) and chemically cleaned in place (CIP) S-PANI and DuraMem®500 of (c, f), respectively.	178
Fig. S 4.1 The calibration curve for colorimetric analysis of Fulvic 25 solution as a relation between the solution concentration (mL of fulvic 25 feedstock in L of DI water) and the UV ₂₅₄ absorbance and the dissolved organic carbon (DOC).	199
Fig. S 4.2 Apparent molecular weight distribution of the natural organic matter (measured DOC) in conventionally treated artificially prepared surface water and seawater at feed [DOC] of 20 mg C L ⁻¹ with error bars representing one standard deviation calculated from the results of triplicate runs at the specific experimental conditions.....	199
Fig. S4.3 Apparent molecular weight distribution of solute fractions of treated leachate effluent by conventional treatment with error bars representing one standard deviation calculated from the results of triplicate runs at the specific experimental conditions.....	200
Fig. S4.4 The SEM surface images of the pristine a) S-PANI membrane and b) DuraMem®500 membrane.....	201
Fig. 5.1 FT-IR spectra of the cross-linked membranes M1-M7 a) before static ageing and b) after static ageing test.....	215
Fig. 5.2 SEM cross-sectional area images of M1-M8 membranes after static ageing test in <i>THF</i> solvent for 30 days.....	217
Fig. 5.3 SEM surface images of M1-M8 membranes after static ageing test in <i>THF</i> solvent for 30 days.	218

Fig. 5.4 AFM three-dimensional images of membranes M1-M8 top surface layer after static ageing test with <i>THF</i> for 30 days.....	220
Fig. 5.5 Surface roughness before and after static ageing test with <i>THF</i> solvent for 30 days a) mean roughness, R_a , and b) root mean square roughness, R_q	221
Fig. 5.6 a) Tensile strength and b) Young's modulus of the cross-linked membranes M1-M7 before and after static ageing test with <i>THF</i> for 30 days with the error bars representing single standard deviation.....	222
Fig. 5.7 Dynamic contact angle with single standard deviation after 180 seconds of membrane-water droplet contact for the membranes M1-M8 before and after ageing with <i>THF</i> for 30 days.	224
Fig. 5.8 Mass swelling degree and gel content of the cross-linked and commercial membranes M1-M8 in different polar protic and polar aprotic solvents.....	225
Fig. 5.9 DI water and pure <i>Methanol</i> , <i>acetonitrile</i> , and <i>tetrahydrofuran</i> solvent permeance of M1-M8 membranes.....	228
Fig. 5.10 Dye solution permeance and solute rejection in (a,b) aqueous solution (c,d) <i>MeOH</i> (e,f) ACN and (g,h) <i>THF</i> solvents.	232
Fig. S5.1 TGA curves for S-PANI, PANI-PAMPSA and S-PANI PAMPSA polymers (a) weight loss (b) derivative weight loss with respect to temperature from room temperature to 600°C.	247
Fig. S5.2 The calibration curve for colorimetric analysis of methyl orange solution as a relation between the solution concentration and the UV absorbance (peak absorption at wavelength 461 nm).....	252
Fig. S5.3 The calibration curve for colorimetric analysis of acid red 1 dye solution as a relation between the solution concentration and the UV absorbance (peak absorption at wavelength 530.5 nm).....	252

Fig. S5.4 The calibration curve for colorimetric analysis of congo red dye solution as a relation between the solution concentration and the UV absorbance (peak absorption at wavelength 496.5 nm).....	252
Fig. S5.5 The calibration curve for colorimetric analysis of rose bengal dye solution as a relation between the solution concentration and the UV absorbance (peak absorption at wavelength 548 nm).....	253
Fig. S5.6 FT-IR spectra of a) pristine S-PANI, PANI-PAMPSA and S-PANI PAMPSA and b) commercial modified polyimide membrane DuraMem®500 before and after static ageing test.....	253
Fig. S5.7 SEM cross-sectional area images of M1-M8 membranes before static ageing test in <i>THF</i> solvent.....	254
Fig. S5.8 SEM surface images of M1-M8 membranes before static ageing test in <i>THF</i> solvent.	254
Fig. S5.9 SEM cross-sectional area images of M2-M7 membranes after static ageing test in <i>DMF</i> solvent for 30 days.....	255
Fig. S5.10 SEM surface images of M2-M7 membranes after static ageing test in <i>DMF</i> solvent for 30 days.	255
Fig. S5.11 AFM three dimensional images of membranes M1-M8 top surface layer before static ageing test in <i>THF</i> solvent.	256
Fig. S5.12 The percentage increase in the membranes M1-M8 top layer mean roughness, Ra and root mean square roughness, Rq roughness after static ageing test with <i>THF</i> solvent for 30 days.	257
Fig. S5.13 The stress-strain curves of the M1 membrane film before and after static ageing test with <i>THF</i> solvent for 30 days.	257
Fig. S5.14 The stress-strain curves of the M2 membrane film before and after static ageing test with <i>THF</i> solvent for 30 days.	257

Fig. S5.15 The stress-strain curves of the M3 membrane film before and after static ageing test with <i>THF</i> solvent for 30 days.	258
Fig. S5.16 The stress-strain curves of the M4 membrane film before and after static ageing test with <i>THF</i> solvent for 30 days.	258
Fig. S5.17 The stress-strain curves of the M5 membrane film before and after static ageing test with <i>THF</i> solvent for 30 days.	258
Fig. S5.18 The stress-strain curves of the M6 membrane film before and after static ageing test with <i>THF</i> solvent for 30 days.	259
Fig. S5.19 The stress-strain curves of the M7 membrane film before and after static ageing test with <i>THF</i> solvent for 30 days.	259
Fig. S5.20 Mass swelling degree and gel content of the cross-linked membranes M2-M7 in <i>DMF</i> solvent.	260
Fig. S5.21 The dye retention and apparent MWCO of the S-PANI membrane (M1) prepared in 0.1 M HCl(aq) coagulation bath.	260
Fig. S5.22 The dye retention and apparent MWCO of the S-PANI membrane (M2) prepared in 0.5 M HCl(aq) coagulation bath.	260
Fig. S5.23 The dye retention and apparent MWCO of the S-PANI membrane (M3) prepared in 1.0 M HCl(aq) coagulation bath.	261
Fig. S5.24 The dye retention and apparent MWCO of the S-PANI membrane (M4) prepared in 3.0 M HCl(aq) coagulation bath.	261
Fig. S5.25 The dye retention and apparent MWCO of PANI-PAMPSA membrane (M4) prepared in 1.0 M HCl(aq) coagulation bath.	261
Fig. S5.26 The dye retention and apparent MWCO of the S-PANI PAMPSA membrane (M6) prepared in 1.0 M HCl(aq) coagulation bath.	262
Fig. S5.27 The dye retention and apparent MWCO of the S-PANI membrane (M7) cross-linked with <i>glutaraldehyde</i>	262

Fig. S5.28 The dye retention and apparent MWCO of the commercial modified polyimide (M8).

..... 262

List of Tables

Table 2.1 The quantification of the AFM roughness data for the S-PANI membrane surface. .	64
Table 2.2 Pure water permeance and <i>BSA</i> rejection with a standard deviation of the S-PANI and commercial PES membranes, immersed in water and 250ppm sodium hypochlorite solution at pH 7.4 for three days at room temperature.....	67
Table 2.3 Fouling indicators for PANI and S-PANI membranes related to the initial cleaning-fouling cycle at equal initial flux.	71
Table 3.1 In-situ and post-treatment conditions of the tested S-PANI membranes.....	93
Table 3.2 Ion exchange capacity (IEC) and water uptake of S-PANI membranes M1-M3.	97
Table 3.3 Porosity measurements of S-PANI membranes M1-M3.	101
Table 3.4 The MWCO determination of the NF membrane (M3) using sugar solutes.	109
Table. S3.1 Element analysis (Atomic % and weight%) of S-PANI powder.....	126
Table. S3.2 Hydrolytic and alkalinity stability of S-PANI membranes M1-M3.	139
Table. S3.3 The dye removal mechanism of the S-PANI M1 membrane.	144
Table 4.1 Properties of artificially prepared surface water and seawater at different natural source [DOC].	156
Table 4.2 Characterization of a stabilized solid waste landfill leachate.	156
Table 4.3 Characterization of the S-PANI and DuraMem®500 membranes.	160
Table 4.4 Fouling indicators for S-PANI and commercial DuraMem®500 membranes related to the initial cleaning-fouling cycle at equal initial permeance.....	176
Table. S 4.1 Details of utilised membranes for solute fractionation.....	196
Table. S 4.2 The zeta potential of the treated artificial surface water, artificial seawater, and leachate by conventional and membrane processes.	200
Table. S 4.3 The DOC removal through PAC adsorption of artificially prepared surface water and seawater sample at [DOC] of 20 mg L ⁻¹	200

Table 5.1 Preparation condition and properties of the tested membrane systems.	213
Table 5.2 Dope solution composition and viscosity.	217
Table 5.3 Comparison of membrane performance with other published data using polymeric membranes with <i>THF</i> solvent.	230
Table. S5.1 Elongation at break of the M1-M7 free-standing membrane films before and after ageing with <i>THF</i> solvent for 30 days.	259

List of Abbreviations

AC	<i>Acetone</i>
ACN	<i>Acetonitrile</i>
AFM	Atomic force microscopy
AMWD	Apparent molecular weight distribution
AOC	Assimilable organic carbon
APS	Ammonium persulfate
ATR	Attenuated total reflectance
BE	Binding energy
BET	Brunauer-Emmet-Teller
BOD	Biological oxygen demand
BSA	<i>Bovine serum albumin</i>
CA	Contact angle
CIP	Chemical cleaning in place
COD	Chemical oxygen demand
DAF	Dissolved air flotation
DBPs	Disinfection by products
DI	Deionised
DMF	<i>N,N-dimethylformamide</i>
DRI	Differential refractive index
DSC	Differential scanning calorimetry
DTA	Differential thermal analysis
EDX	Energy dispersive X-ray
ELSD	Evaporative light scattering
EPS	Extracellular polymeric substances
FT-IR	Fourier-transform infrared spectroscopy
GA	<i>Glutaraldehyde</i>
GAC	Granular activated charcoal
GPC	Gel permeation chromatography
HA	<i>Humic acid</i>
HPLC	High-performance liquid chromatography
IEC	Ion exchange capacity
IPA	<i>Isopropanol</i>

ISA	Integrally skinned asymmetric
LMW	Low molecular weight
LS	Light scatters
MA	Metanilic acid
MENA	Middle East and North Africa
4MP	4-methylpiperidine
<i>MeOH</i>	<i>Methanol</i>
MF	Microfiltration
MW	Molecular weight
MWCO	molecular weight cut off
NF	Nanofiltration
NIPS	Non-solvent induced phase inversion
<i>NMP</i>	<i>N-methyl-2-pyrrolidone</i>
NOM	Natural organic matter
OSN	Organic solvent nanofiltration
PA	Polyamide
PAC	Powder activated charcoal
PAMPSA	Poly (2-acrylamido-2-methyl-1-propanesulfonic acid)
PAN	Polyacrylonitrile
PANI	Polyaniline
PDMS	Polydimethylsiloxane
PE	Polyethylene
PEG	Polyethylene glycol
PES	Polyether sulfone
PIMs	Polymers of intrinsic microporosity
PMA	Phosphomolybdic acid
PP	Polypropylene
PS	Polysulfone
PVA	Polyvinyl alcohol
PVDF	Polyvinylidene fluoride
PVP	Poly(vinyl pyrrolidone)
PWF	Pure water flux
RO	Reverse osmosis
SD	Swelling degree

SEM	Scanning electron microscopy
SI	Supporting information
S-PANI	Sulfonated polyaniline
SUVA	Specific ultraviolet absorption
SW	Spiral wound
TEM	Transmission electron microscopy
TGA	Thermogravimetric analysis
<i>THF</i>	<i>Tetrahydrofuran</i>
TMP	Transmembrane pressure
TOC	Total organic carbon
TOL	<i>Toluene</i>
UF	Ultrafiltration
UV	Ultraviolet radiation
UV-Vis	Ultraviolet-visible
VS	Viscometry
WU	Water uptake
XPS	X-ray photoelectron spectroscopy
XRD	X-ray diffractometry

Thesis Outline

This thesis was written in the alternative format.

Chapter 1 provides a general introduction on the emerge of membrane processes for water and wastewater treatment compared to the conventional treatment processes. The chapter discusses membrane materials, preparation, and cross-linking protocols as well as ongoing challenges and solution approaches such as membrane fouling and antifouling techniques. The research aims and objectives are also embedded in this chapter. Chapters 2 to 5 consist of research results, presented in paper format and either published in peer-reviewed journals (Chapters 2, 3 and 4), or submitted for peer-review (Chapter 5). Each chapter contains an introductory section reviewing relevant literature, a methods section, a results and discussion section, a conclusions section. In addition, supplementary Information (SI) sections are available for chapters 3 to 5.

Chapter 2 illustrates the preparation and characterisation of self-doped sulfonated polyaniline (S-PANI) membranes with enhanced chlorine resistance and improved antifouling properties compared to polyaniline (PANI) membranes.

Chapter 3 presents a novel and scalable approach to produce in-situ cross-linked S-PANI membranes at nanofiltration (NF) separation range via non-solvent induced phase separation (NIPS).

Chapter 4 offers inter-process comparison between a conventional treatment process and membrane processes including the developed S-PANI NF membrane across highly different water matrices that exists in drinking water, seawater desalination and landfill leachate treatment.

Chapter 5 describes a new technique to produce high performance PANI membranes with in-situ tuned transport properties to suit a broad range of organic solvent nanofiltration (OSN) applications benefitting from the newly developed cross-linking method reported in chapter 3. The membrane permselective properties were optimised via using self-dopants of different

molecular weight and altering the cross-linking degree to suit different solvents within NF filtration range.

Chapter 6 draws the discussion of the three important story lines which includes a) the application of S-PANI membranes to prevent fouling (chlorine tolerance), b) the simplified S-PANI production method developed in this work, and c) the organic solvent nanofiltration application.

Chapter 7 contains general conclusions drawn from the work presented in this thesis and recommendations for future research.

Chapter 1

Introduction and general literature review

1.1 Overview

A significant proportion of conventional separation processes is expected to be substituted by membrane process whose application has been increasing widely [1]. A conventional treatment system, in water treatment for instance, typically consists of coarse strainers, chemical conditioning (anti-scaling, acid or lime addition), coagulation, flocculation, clarification by sedimentation or dissolved air flotation (DAF), filtration and disinfection as shown in Fig. 1.1 [2–4]. However, these processes still possess few shortcomings. The performance of these processes is directly affected by the feed characteristics such as salinity, temperature, ionic strength, natural organic matter (NOM), algae, turbidity, pH, alkalinity and the type of dosed coagulant [5–9]. This requires continuous tuning and control of the chemical dose and also contributes to a surplus sludge production which implies sludge disposal management to comply with state landfill regulations [10,11]. The conventional treatment is also associated with a considerable footprint and high capital expenditure which entails 30-40% of the capital cost and 20-25% of the operating cost of the system in seawater industry, for instance [12–14]. Likewise, the successful application of membrane processes in organic solvents favoured takeover of traditional purification and separation processes (such as distillation, evaporation, adsorption, extraction, and chromatography) in wide range of industrial applications [15–18]. However, replacement for all these processes, especially in water treatment, might be quite challenging due to the heritage infrastructure in place [19].

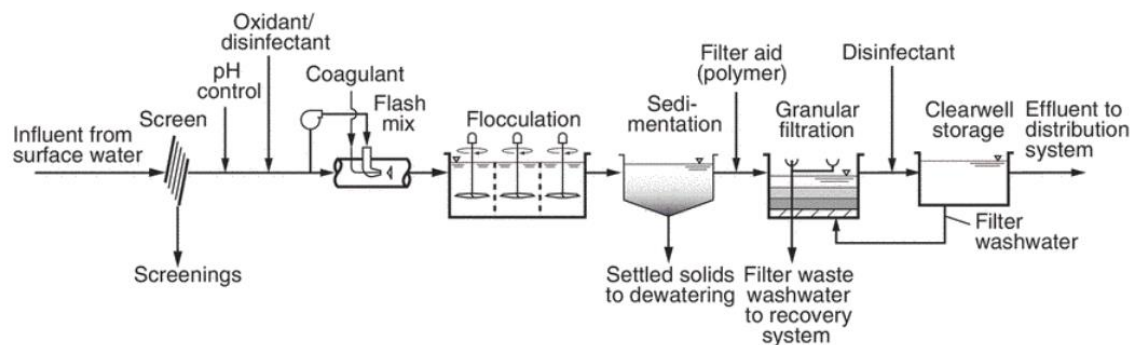


Fig. 1.1 Typical flow schematic diagram for surface water treatment plant [12].

In recent years, the application of pressure driven membranes had been widely investigated in many areas such as water purification [20] wastewater treatment [21], pharmaceutical industry [22] organic solvent nanofiltration [23] and textile effluent treatment [24]. Fig 1.2a shows the trend in published documents per annum for membranes in wide range of subject areas with particular focus in water and wastewater treatment shown in Fig 1.2b. A rapid rise in research interest in membrane development for different applications including water and wastewater treatment was observed in the 1990s which has been increasingly expanding until today echoing the importance of membrane processes.

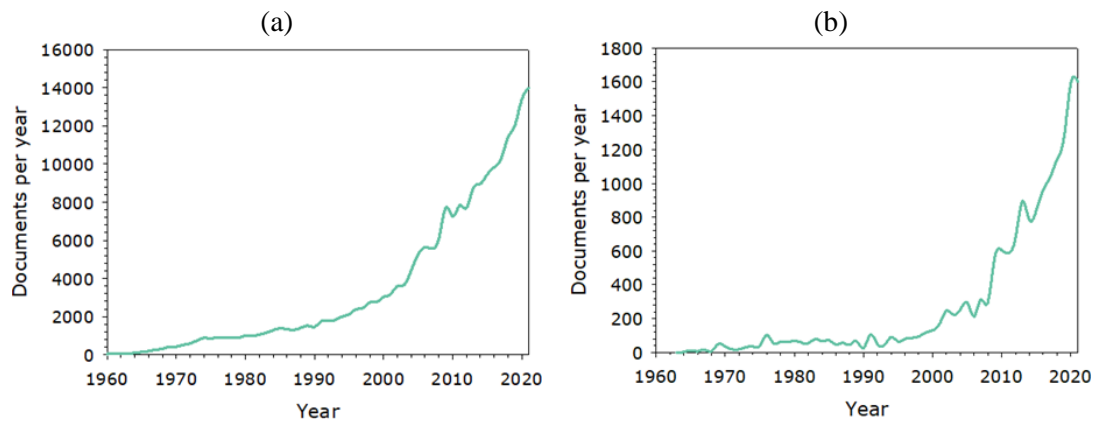


Fig. 1.2 The trend of published documents per annum for membranes in a) all disciplines and b) water and wastewater related applications in Scopus website database.

1.2 Membrane treatment

Membrane processes are a selective separation technique of mixtures and multicomponent solutions for solids, colloidal particles, macromolecules, and dissolved solutes [25]. The pressure-driven membranes processes involve the utilisation of great variety of materials and structures for restricting the passage of different components in a very specific manner at the feed [26]. The membranes benefits from numerous advantages such as a) not requiring a phase change for solute or the carrier solvent, b) exceptional combination of permselective properties, and (c) no necessity for regeneration of solid or liquid sorbents [27]. As such, membranes are widely used in many important chemical, biological, and environmental applications. Microfiltration (MF) membranes have a large pore size range 0.1-10.0 μm compared to 0.005-0.09 μm for the ultrafiltration (UF)

membranes [28] as shown in Fig 1.3. Nanofiltration (NF) membranes are closely related to RO and is sometimes called “loose RO” with pore size of 1-5 nm and a molecular weight cut-off (MWCO) 200-1000 g mol⁻¹ compared to ~0.5 nm pore size and MWCO below 200 g mol⁻¹ for the RO membranes [29,30]. The membrane processes can deliver consistent permeate quality despite fluctuations in the feed properties showing full removal of suspended solids and a substantial to full reduction in microbial species within a small footprint [31–33].

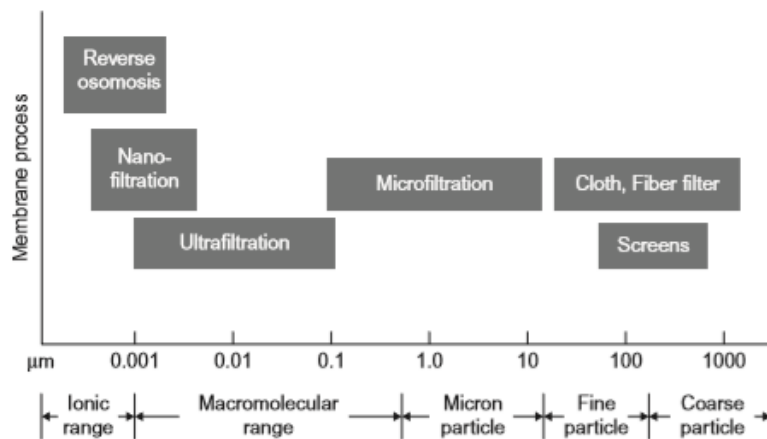


Fig. 1.3 Membrane separation process based on pore size [26].

A membrane module consists of multiple pressure vessels which are connected in parallel as shown in Fig 1.4a. Each pressure vessel accommodates few membrane elements which are mounted in series. The feedwater passes through the spacer of the spiral wound (SW) membrane element where the solvent/solute separation process occurs through the membrane active layer. The permeate is collected and carried by the permeate inner pipe as shown in Fig 1.4b.

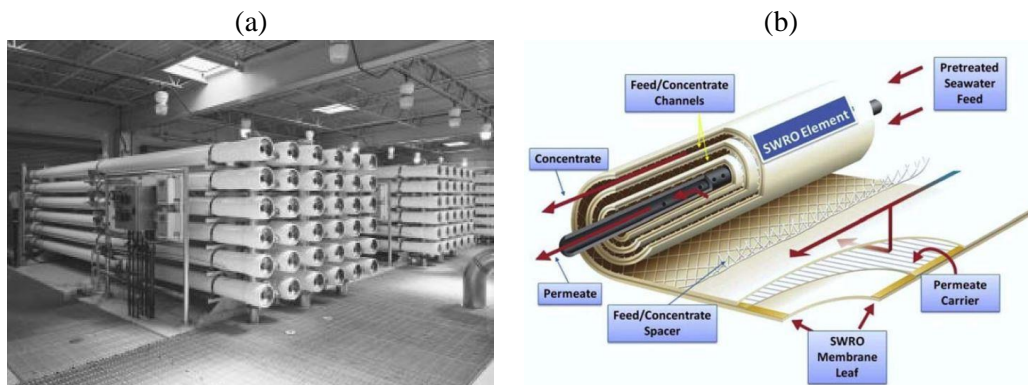


Fig. 1.4 a) general arrangement of RO membrane module [12] and b) cross-section of spiral wound reverse osmosis membrane element [34].

1.3 Membrane transport theory

The transport rate for certain components through a membrane, flux, is determined by both driving force and the permeability of the membrane which could be described by Darcy's law as shown in the following equation [35]:

$$J = -P \frac{dx}{dz} \quad \text{Equation 1.1}$$

where J , P and $\frac{dx}{dz}$ represents the flux or volumetric flow per unit membrane area, phenomenological coefficient which expresses the membrane permeability, and the driving force, respectively. The gradients in either pressure, electric potential or chemical potential establish the driving forces that could results in mass convection, ion migration and molecule diffusion, respectively [36]. The membrane processes can be classified based on the type of the driving force into dialysis (concentration driven), pervaporation (partial pressure driven), dialysis and electrolysis (electrical potential driven) and pressure driven which includes MF/UF, NF, RO and gas separation membranes [37]. The ratio of the volumetric flow rate over an active membrane filtration area at certain operating conditions defines the permeating flow rate also known as liquid permeability. This is used to describe the membrane productivity and passage of pure solvent or solution and can be expressed in volumetric ($\text{L m}^{-2} \text{h}^{-1} \text{bar}^{-1}$) or gravimetric units ($\text{kg m}^{-2} \text{h}^{-1} \text{bar}^{-1}$), respectively [38]. The liquid permeability can be dependent on the transmembrane pressure (TMP), particularly if the membrane's selective layers possess affinity to the solvent like for organic solvent nanofiltration (OSN). As such, partial and reversible decline in liquid permeability could take place due to the partial compaction of swollen polymer matrix as a result of the increase in the TMP across the membrane [23]. Filtration experiments in dead-end or cross-flow regimes are interchangeably used to determine the liquid permeability [39]. Despite no difference between the two regimes for filtration of pure solvents or dilute solutions of solutes with no specific interaction with membrane material, the filtration test in cross-flow membrane cells is preferably due to the high linear velocity (shear force) to minimize concentration

polarisation effect or membrane fouling during the filtration of real mixtures (e.g., ground or wastewater). Liquid permeability is constant for specific membranes in certain ranges of operating pressure since it is normalised by the applied TMP at constant feed composition and temperature [36]. This parameter allows to compare performance across a diverse number of membranes, tested in accordance with different filtration protocols. The liquid permeability of commercially sourced membranes is usually given by manufacturers along with values of molecular weight cut-off (MWCO). The latter is characterised the ability of the membrane to retain 90% of the solutes at certain molecular weight [40]. The critical flux concept was introduced and defined in two ways a) the flux at which the TMP starts to deviate from the pure water line or b) the first permeate flux for which irreversible fouling appears on the membrane surface [41]. Exceedance of the critical flux can accelerate membrane fouling which could lead to a combination of reversible and irreversible decline in liquid permeability [42].

1.4 Membrane material and preparation

Many types of synthetic materials are used for preparing membranes which are grouped into polymeric (organic polymers including crystalline and amorphous, glassy and rubbery) and inorganic (oxides, ceramics, metals, carbon) membranes [43]. Membrane preparation involves a number of techniques such as sintering, stretching, track-etching, template leaching, and dip-coating, to obtain a membrane structure with desired morphology tailored for a specific [44]. Phase inversion/separation techniques are among the most vital and commonly used processes for making membranes from a large variety of polymeric building blocks. Fig 1.5 illustrates an exponential trend in publications related to phase inversion more noticeably in the past three decades.

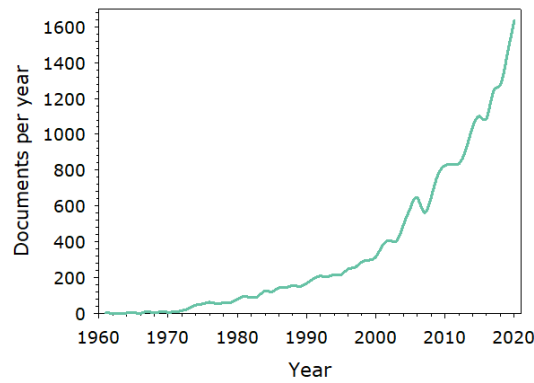


Fig. 1.5. The trend of published documents per annum for the developments in the phase inversion technique for membranes preparation.

In 1960s, a major breakthrough in the development of integrally skinned asymmetric (ISA) membranes took place by Loeb and Sourirajan [45]. The research method was utilised for a controlled transformation of polymer solution (also known as dope solution) to a solid form. Since then, a wealth of knowledge has been engendered about phase inversion membranes formed by immersion precipitation, also known as non-solvent induced phase separation (NIPS). The preparation of flat sheet membranes occurs by casting a thin film of polymer solution over a porous mechanical support layer. The applied dope solution consists of at least one polymer, at least one excellent solvent, and may contain additives. The thin film over the support layer is then immersed into a coagulation bath, which consists of a poor solvent, i.e., the nonsolvent (typically water), and may contain additives. The exchange of the solvent and nonsolvent (known as demixing) which must be miscible leads to precipitation (solidification) of polymer film [46,47]. Demands for membranes with certain physicochemical properties for different separation processes encouraged further investigation of key factors affecting the preparation process [48]. The main parameters that influence membrane formation by phase inversion include but are not limited to solvent type, polymer type and concentration, non-solvent system and composition, additives to the polymer solution, and casting conditions [49]. The thermodynamic aspects of instantaneous and delayed demixing processes which lead to different types of membrane conformations were studied using ternary phase diagram as shown in Fig 1.6a-c. The polymer, solvent and non-solvent are represented in the triangle angles, while any point within the triangle

represents a mixture of the three components. This helps to schematically define the composition path of a polymer film at a certain time of immersion in a non-solvent bath. The system consists of two regions: a one-phase region where all components are miscible and a two-phase region where the system separates into polymer-rich and polymer-poor phases. The line which connects a pair of equilibrium compositions in the phase diagram is called a tie line. The is the so-called binodal. Every composition inside the binodal curve will demixing into two liquid phases which differ in composition, but which are in thermodynamic equilibrium with each other. The cloud point is measured via rapid titration method and a turbidity measurement method in order to determine liquid-liquid phase boundary, known as binodal [50]. A two fundamentally different structures depending on the rate of polymer precipitation by NIPS [51]. Precipitation rate is measured as the time between immersing the casting solution in a precipitation bath and the time when that solution turns opaque or when the membrane separates from the glass plate. A slow precipitation rates produced membranes with “sponge-like” morphologies compared to large “finger-like” macro-voids in the substructure at fast precipitation rates as shown in Fig. 1.6b-d.

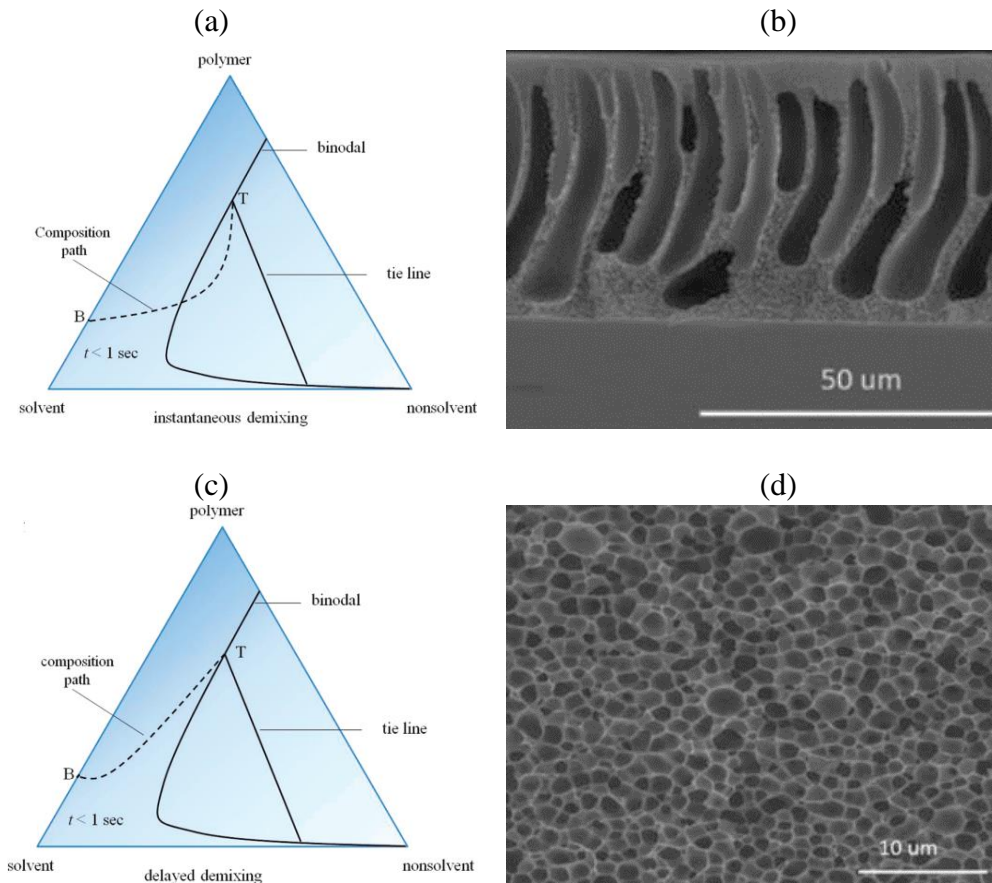


Fig. 1.6. Composition paths and cross-sectional morphology of a cast film immediately after immersion ($t < 1 \text{ s}$) demonstrating (a, b) instantaneous demixing and (c, d) delayed demixing, respectively; T and B represent top and bottom of the film, respectively [44,48,52,53].

1.5 Membrane cross-linking and solvent stability applications

The transformation process of polymer chains to an integral three-dimensional network by the interactions of linear or branched polymer chains using the chemical or physical modification is known as cross-linking [54]. The physical cross-linking takes place by heating or photo initiation and involves the development of van der Waals forces and hydrogen bond between the functional groups of the polymers and cross-linking agents and polymer chains [54,55]. The hydrogen bond of the physically cross-linked membranes is small with long bond length compared to the covalent bonds. However, the strong physical interactions of the large amount of hydrogen bonds makes them steadily exist at low pressure [56]. Chemical cross-linking occurs via polycondensation or polyaddition cross-link where a covalent bonding is formed between the functional groups of the

polymers and cross-linking agents due the interaction process of linear or branched polymer [57,58]. Small molecular compounds in the range of 200–400 g mol⁻¹, that possess two or more functional groups such as amine group are commonly used as cross-linking agents [59]. The gap spaces between the polymer chain segments become smaller after cross-linking resulting in limited vibration of the polymer chain segment as shown in Fig. 1.7 [54,60]. As such, cross-linking leads to enhanced molecular separation, chemical stability, mechanical stability, anti-swelling properties and overall capacities to undertake extreme operating conditions such as treatment of organic solvents at the expense of lower flux [61]. Separation and purification of streams containing organic solvents is challenging but inevitable in many chemical and pharmaceutical processes due to the stringent environmental legislation and the increased cost of organic solvents [15,62–64].

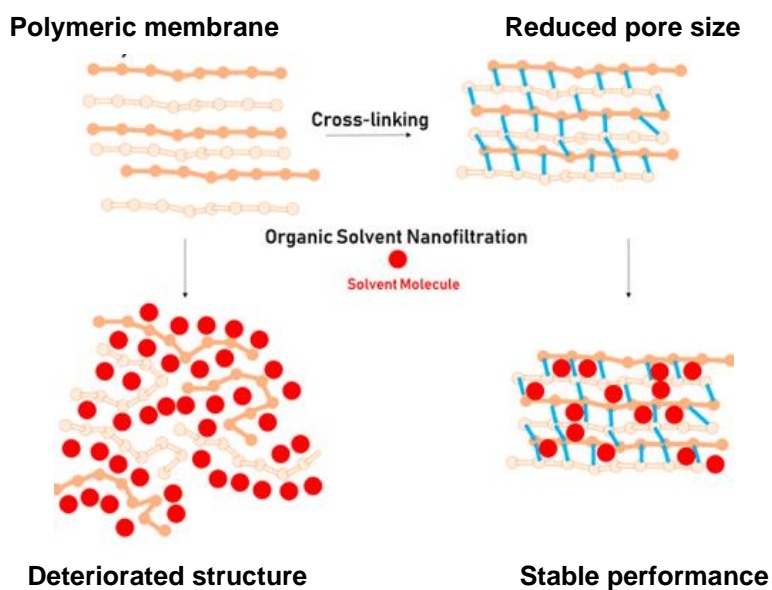


Fig. 1.7 Descriptive sketch of three-dimensional links after cross-linking and structural stability of organic solvent membranes [61].

Membrane cross-linking modifications takes place by three different methods. Post-treatment is achieved when the prepared membrane is heated to the cross-linking degree or immersed in the cross-linking solution to achieve physical or chemical cross-linking, respectively [65,66]. In contrast, simultaneous modification occurs when the cast film is immersed in a coagulation bath

containing the cross-linker [67,68]. The third type is known as pressure-assisted cross-linking where the cross-linker is forced through the bulk membrane to increase the cross-linking degree [61].

The sensitivity of most pharmaceutical products to temperature and the demand for high quality products favours the application of a membrane-based technique known as organic solvent nanofiltration (OSN) [69]. The OSN membranes are considered as a robust alternative to thermal separation processes that allows for broad market presence and core applications in the oil and petrochemical industry, food and bioproduct industry, pharmaceutical industry, bulk chemical and fine-chemical industry due process reliability, ecological and economic benefits [70–72]. OSN membranes also combine low-temperature with continuous separation of mixtures down to a molecular level without thermal energy, chemical additives or recycle streams which makes it competing with conventional separation techniques like crystallisation, chromatography, evaporation, distillation, adsorption and absorption [73]. There is a continuous demand for a wide range of different membrane materials and different MWCOs because each application has its special requirements for solute retention as well as a unique solvent system [74]. OSN applications grew early in the oil and petrochemical industry for dewaxing of lube oil followed by conditioning of liquid hydrocarbons, biodiesel production and edible oil extraction [75]. Other applications in natural oil processing involve decolourisation, deacidification and solvent recovery from the degumming extraction step [76]. These membranes are also broadly used in the food and bioproduct industry for the extraction and separation of lactoferrin (milk), lysozyme (eggs), organic acids, zeaxanthin, omega-3 fatty acids and oligosaccharides (soy) [77]. OSN membranes have also contributed to purification of organic solvent streams as well as recovery of valuable homogenous catalyst systems of different kind of chemical reactions such as palladium catalyst systems which offered cost and energy savings in bulk chemistry applications [78]. The OSN membranes is playing a key role in the synthesis, purification and concentration of active pharmaceutical ingredients (APIs) and the production of high value natural compounds

(HVNCs) including non-thermal solvent recovery and non-thermal solvent exchange processes [79–81].

1.6 Membrane fouling

Despite the widespread application of the membranes, there is still a number of technical challenges to overcome [82]. Membrane longevity decreases as a result of scaling, fouling and biofouling due to presence of particulate foulants, colloidal foulants, organic foulant and microbial foulants in the feed stream [83,84]. Foulants accumulate at the membrane outer shell and clog membrane pores leading to formation of external fouling and internal fouling, respectively. Both fouling types result in flux decline and potential increase in membrane rejection [85]. Membrane fouling exposes the plant production to crucial threat throughout the operating life due to the gradual flux decline as shown in Fig1.8.

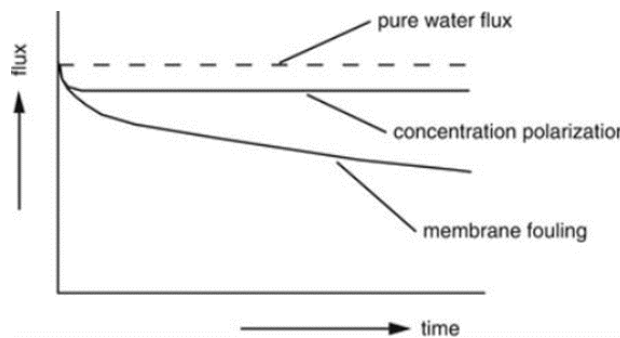


Fig. 1.8 Flux decline over time due to membrane fouling [86].

In particular, organic matter, which serves as a nutrient for microbial foulants, cause the most severe type of fouling known as biofouling [84]. During biofouling growth, the microorganisms accumulate developing extracellular polymeric substances (EPS) which can protect the biofouling bacterial species from toxins and biocides [87]. Biofouling leads to significant irreversible performance loss, decreases process reliability and increase both, operating and maintenance costs [88]. As a result, this requires membrane replacement which contributes to 14-20% of the initial membrane installation cost [14]. Biofouling forms more than 45% of membrane fouling and identified as “Achilles heel” of membrane processes [89]. To imagine the progressive

academic interest in this problematic issue, over 3000 papers were published between 1992 and 2016 and the number is expected to double by 2022 [3].

1.7 Antifouling techniques

1.7.1 Feed water pre-treatment

Several studies showed that pre-treatment of the membrane feed water could improve the overall operational performance by preventing rapid membrane fouling [90,91]. At certain times, the feed water may contain constituents such as colloidal material, suspended solids, organic compounds, and bacteria that cause irreversible fouling of downstream membrane systems [92]. Key threshold seawater quality parameters that have significant impact on the selection and configuration of the pretreatment system upstream the RO membranes were established. For instance, the TOC should be $< 2 \text{ mg L}^{-1}$, turbidity $\leq 0.1 \text{ NTU}$, silt density index (SDI) < 2 , $\text{Fe}^{+3} \leq 2 \text{ mg L}^{-1}$, $\text{Mn}^{+2} \leq 0.1 \text{ mg L}^{-1}$, silica $\leq 20 \text{ mg L}^{-1}$ and oil and grease $\leq 0.02 \text{ mg L}^{-1}$ [93]. Ideally, the role of pre-treatment processes is to minimise the scaling potential, fouling and biofouling growth at the membrane surface and maintain a consistent feed water quality to the downstream membrane processes [94,95]. These pre-treatment technologies include but are not limited to coagulation, scale inhibition, flocculation, clarification, filtration, biofiltration, disinfection and low-pressure membranes (MF/UF) ahead of the RO membranes [3,96]. Coagulation is a physio-chemical process which aims to reduce the repulsive potential of the electrical double layer of colloids using various coagulants such as ferric chloride [97]. With the addition of coagulants, colloidal microparticles start to develop and then agglomerate into larger particles called micro flocs [12]. Feed waters that are associated with harmful algae blooms or oily wastes have severe impact on the membrane processes and pre-treatment with coagulation and DAF is deemed to be vital [98]. Dual media filtration (*DMF*) preceded by coagulation was reported to decrease the fouling of downstream membrane processes and remove more than 90% of micro-algae at low power consumption $< 1.0 \text{ kWh m}^{-3}$ [99,100]. Likewise, the addition of coagulants upstream low pressure

membranes helped to reduce the TMP, minimise the extent of none back-washable fouling and decreases pore blocking due to the formation of a permeable cake/gel layer on the membrane surface [101,102]. High organic matter removal, 70% dissolved organic carbon (DOC) and 90% transparent exopolymer particles (TEP), was also achieved by using granular activated carbon (GAC) adsorbents followed by low-pressure membranes [103]. Operating the *DMF* under biological mode (biofiltration) enhanced the NOM removal [104]. However, the biofiltration with GAC media revealed higher organic matter removal rates than biologically operated *DMF* due to the availability of a large surface area of the GAC media [105,106]. The bioactivity in *DMF* improved the removal of the biologically degradable organic carbon related compounds which reduced the biofouling formation on RO membrane surfaces [107]. Disinfection by ozonation disables the bacterial activity and hinders the fouling formation in principle. However, ozonation converts most of the NOM to assimilable organic carbon (AOC) and oxidises the phosphonate based anti-scale which increase the fouling and scaling potential on RO membranes, respectively [108–110]. The pre-treatment process is crucial to deliver a consistent feed water quality to increase the downstream membrane longevity. However, in-depth understanding of the feed water quality including seasonal variations is essential for proper process selection and design. The process performance dependence on feedwater quality changes also demands for continuous control and monitoring that involves manual intervention [10–12]. Additionally, the pre-treatment process entails considerable footprint, high capital expenditure, backwash water balancing and sludge waste management [12,111].

1.7.2 Chlorination

Chlorine is the most widely used disinfectant in water and wastewater treatment [89]. The application of continuous chlorination was most often used in the 1990s where sodium hypochlorite, for instance, is used to control and suppress the growth microorganisms and algae species within the membrane treatment system [2]. Sodium hypochlorite is one of the commonly

used chemicals for particle removal from the membrane surface and the pores due to its strong oxidizing potential [112]. Intermittent chlorination (1-4 times a day) or shock chlorination (1-3 times a week) were favoured continuous chlorination due to the formation of extra-cellular polysaccharides after long-term exposure to chlorine [113]. However, biofouling cannot be simply eliminated by inactivation of the microorganisms via the disinfection. Dead biomass remain and serves as substrate for other bacteria [114]. The reaction of disinfectants such as chlorine, chlorine dioxide and ozone with *humic acid* enhance the formation of AOC and therefore increase in biodegradability of organic matter which enhance biofouling growth [104]. Also, most of the aromatic polymeric membranes suffers from performance degradation (18%) due to the high sensitivity to free chlorine [115]. Aromatic membrane chlorination takes place when the hydrogen on the polymeric ring is substituted by chloride ion followed by ring chlorination which is irreversible process as shown in Fig. 1.9 [116]. The free chlorine also attacks N-H group within the aromatic polymer structure and convert it to N-Cl group leading to increase in membrane flux, decrease in solute rejection and hence resulting in performance degradation [117]. Therefore, membrane chlorine sensitivity is still a crucial limitation for most aromatic based commercial membranes [118]. Disinfectants such as chlorine decrease the longevity of the membranes, and therefore this is not a viable solution, unless chlorine resistant membranes can be developed [119].

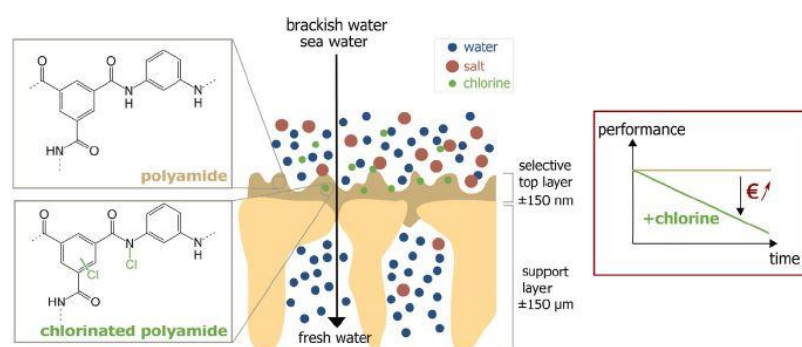


Fig. 1.9 Chemical attack of polyamide membrane selective layer by chlorine oxidant [120].

1.7.3 Surface modification

Most pressure driven commercial membranes are made of hydrophobic polymers such as PVDF (Polyvinylidene fluoride), PES (Polyether sulfone), PS (Polysulfone), PP (Polypropylene), PAN (Polyacrylonitrile), PA (Polyamide) and PE (Polyethylene) [121,122]. The attachment of the organic and bacterial species is more favourable with hydrophobic and non-polar membrane surfaces [123]. In contrast with the hydrophilic membranes, the hydrophobic membranes do not tend to form hydrogen bonding interactions between the membrane interfaces and the water. Therefore, this spontaneous process leads to an increased entropy and foulant adsorption which dominates the boundary layer [112,124,125]. As such, highly hydrophilic membrane surfaces are effective to inhibit the adsorption and deposition of pollutants leading to reduced fouling [126,127]. Therefore, massive efforts were carried out till date to develop functional materials and employ effective techniques to improve membrane hydrophilicity. Neutral or highly negative surface charge, less hydrophobic, and smooth surfaces are identified as key features of the antifouling membranes [128]. Membrane hydrophilicity plays a dominant role in membrane fouling tendency over the surface roughness which provides higher surface area for more foulants to be attached [129]. One of the most common techniques to characterize the membrane hydrophilicity/hydrophobicity is the measurement of the contact angle (CA). Purely hydrophilic membranes retain $CA=0^\circ$ compared to semi hydrophilic $0^\circ < CA < 90^\circ$ and hydrophobic $CA \geq 90^\circ$ [130].

Most recent studies concluded that the development in membrane fabrication and modification is a key solution to solve fouling challenge [3,125,131,132]. Fig. 1.10 shows a pictorial image of surface modification techniques which involves physical methods such as adsorption and coating, and chemical methods such as grafting, plasma polymerization and the addition of organic or inorganic nanoparticles (TiO_2 , silver, carbon nanotubes and graphene) to improve membrane fouling and biofouling resistance [133–138]. Surface grafting helps to amend the hydrophobic properties of the polyamide-based membrane, for instance, and deliver antifouling membrane

layer with easy cleaning properties and higher chlorine tolerance [139–141]. Plasma polymerization, UV grafting, coating or blending with hydrophilic additives are applied to produce antifouling membranes [142]. For instance, polyvinyl alcohol (PVA), graphene oxide functionalized chitosan, polydopamine, carbodiimide, polyethylene glycol (PEG) derivatives, polycations (polyethyleneimine) and chitosan were applied at laboratory scale as a coating material on PA membrane and exhibit antifouling behaviour through the improved hydrophilicity [135,143–149]. Despite these advantages, the coating layer might be sloughed off easily resulting in loss of membrane properties and flux fluctuation [150]. Likewise, the use of biocidal inorganic nanoparticles particles such as silver, copper, carbon nanotubes and graphene is still limited because these nanoparticles could either leach after long-term operation or lose their functionality over time [151]. Plasma is used to deposit the polymer onto membrane surfaces or to activate the membrane surface to generate oxide or hydroxide groups [152]. However, this process is not suitable for large-scale operation. In addition to other concerns such as high energy radiation, high power demand and the difficulty to control the reaction on the surface which might affect the original membrane characteristics [153]. The surface modification is still at an early stage and more intensive studies are needed [154]. Long-term chemical stability, partial removal of the biofouling layer, short term laboratory test and unavailability of commercial scale are ongoing hurdles towards the adoption of membrane surface modification techniques [132].

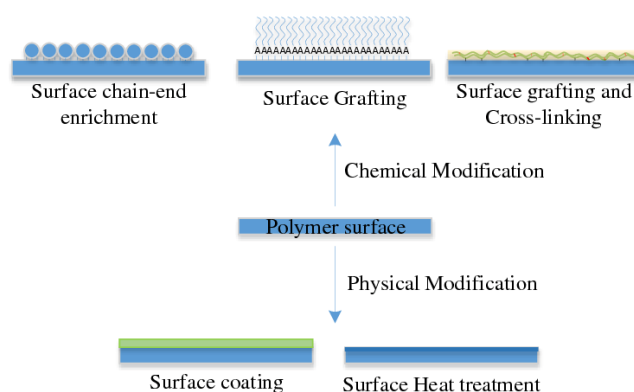


Fig. 1.10 Methods of chemical and physical surface modification of polymer surface [155].

1.7.4 Material blending

The blending of the polymers can efficiently generate new materials with synergistic advantages that cannot be obtained by the individual polymers. Polymer blending approach involves mixing several types of polymers at different loading rates which is extensively utilised in polymeric membrane preparation due to its ability and versatility to integrate desired membrane properties [156,157]. The common intention of the polymer blending is to improve the final structural morphology, wettability, permselective properties and fouling resistance [158]. Polymer blending was foreseen as one of the most straight-forward approaches to impose hydrophilic property and improve the membrane performance [142,159]. Many types of organic and inorganic materials have been used to improve the characteristics of the polymeric membranes such as polyethylene glycol (PEG) [160,161], polyvinylpyrrolidone (PVP) [162,163], cellulose acetate phthalate (CAP) [164] alcohols [165], polyaniline (PANI) [166–168], silica [169], silver [170], aluminium oxide [171] and titanium dioxide [172]. Despite the simplistic preparation protocols, there are many factors effecting the process such as additive loading rate and molecular weights, the miscibility characteristics, the compatibility properties (for inorganic materials), and the solvent type can influence the performance of these additives [172].

1.7.5 Antifouling and chlorine resistant material

A significant attention on the improvement of next generation of membrane materials for the synthesis/processing to develop novel polymeric membranes and novel functionality as shown in Fig. 1.11. Generally, there is no single commercial polymeric membrane material mentioned in the above sections that simultaneously presents antifouling resistance, antibacterial growth, chlorine intolerance, solvent stability, thermal stability, oxidation/pH resistance, and mechanical strength. As such, substantial effort has been directed toward enhancing permselective properties and membrane material longevity.

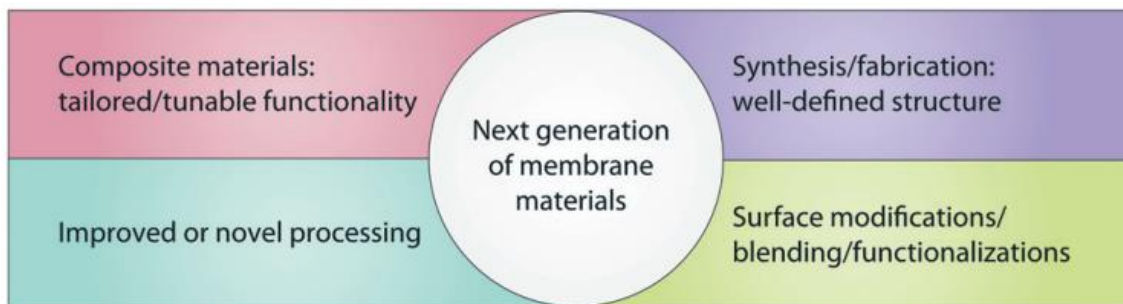


Fig. 1.11 Current trends in the field of organic membrane materials to develop next-generation membrane materials [20].

Cellulose-based membrane materials is another widely used class of organic membranes [173]. Cellulose acetate (CA) membranes were among the first polymeric membrane materials which benefits from relative low cost and hydrophilicity [174]. Due to its high hydrophilicity, CA polymer is often blended with other widely used hydrophobic polymers to produce composite membranes such as PES and PVDF [175,176]. However, CA membranes lack long-term chemical, thermal, and biological stability [177].

Recent reports addressed the utilisation of functional polymeric membranes such as polyacrylic acid (PAA) and polymethyl methacrylate (PMMA), and conductive polymers such as PANI as blending polymers to produce tuneable membranes through improving the stimuli-responsive behaviour [20,178]. PANI, a π -conjugated structure with alternating single and double bonds (Fig. 1.12) is one of the most studied polymers in the last decade due to its superior built-in antifouling properties and antibacterial behaviour [179–181].

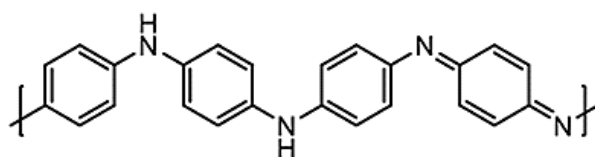


Fig. 1.12 PANI chemical structure.

PANI was used either as a membrane main building block [178] or as an additive to enhance antifouling behaviour of other commercial polymers [182–184]. Membrane conductivity, easy fabrication and abundance of PANI material raises its significance for treating feed streams enriched with organic matter [185,186]. PANI has a cross-linkable nature which could shift the

molecular separation towards NF range making it a suitable material for further OSN applications. Successfully thermal [187] and chemical [188,189] cross-linking of PANI membranes was reported in the literature (Fig. 1.13).

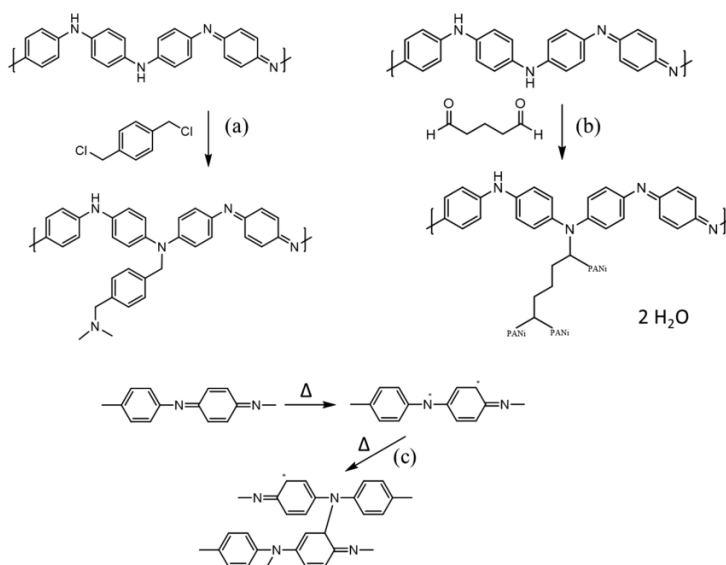


Fig. 1.13 Cross-linking PANI with (a) DCX, (b) GA, and (c) thermal treatment [61,189].

However, all the reported prepared membranes with PANI polymer blends have a MWCO in the UF separation range (above 50 kDa) which limits further applications at NF range and beyond. Additionally, PANI membranes are chlorine intolerant due to the oxidation of the aromatic structural after exposure to free chlorine [190]. The only reported chlorine resistance PANI derivative membrane is poly(*n*-2-hydroxyethyl aniline) (MF border line) which was tested at 250 ppm free chlorine for prolonged period [190]. The PANI derivative membrane benefits from the presence of the hydroxyl group which altered the hydrogen bond which makes enhanced the chlorine resistance and hydrophilicity [191]. The cross-linked PANI membrane in NF range enjoyed high stability in harsh organic solvents but suffered from considerable compromise to the membrane permeance due to the high cross-linking density. The cross-linking process lacks interest of scalability due to the use of toxic and hazardous solvents with tedious post-synthetic treatment up to 6 days [67]. Therefore, the development of chlorine tolerant and solvent stable

membranes in NF range and beyond using scalable methods is of high interest to unlock the potential of the intrinsic antifouling properties of PANI membranes.

1.8 Aims and objectives

The research was focused on addressing important research gaps in membrane synthesis processes and PANI membrane were chosen as material of interest. The aim of this PhD thesis is to a) improve the chlorine resistance and enhance the antifouling properties of PANI membranes, b) lay out the techniques for in-situ preparation of PANI membranes with the desired performance, morphology, and stability in NF separation range, c) benchmark the performance of the developed membrane with the conventional treatment processes and d) explore simplified techniques to tune the PANI membrane permselective properties with enhanced permeance for tight UF and NF applications. These aims were addressed through the following objectives:

- Introduction of electron-withdrawing sulfonic acid functional groups ($-\text{SO}_3\text{H}$) into the aromatic PANI polymer chain to a) reduce the electron density on amino groups and diminish the reactivity of polymer backbone with chemical agents such as chlorine and b) improve antifouling behaviour.
- Exploiting the presence of cross-linkable functional groups in the sulfonated polyaniline (S-PANI) polymer chain and chemical changes of the coagulation bath during the preparation of to yield cross-linked membranes in the NF range.
- Determine the suitability of S-PANI NF membranes for organic matter separation and compare with both a commercial membrane and a conventional treatment option using representative feed solutions of surface water, seawater, and leachate wastewater treatment.
- Incorporating organic acids of different molecular weight, acidity, and hydrophilicity during polymerisation in addition to the changes in the coagulation bath chemistry to in-situ tune the permselective properties of the prepared cross-linked membranes.
-

1.9 References

- [1] R.W. Baker, *Membrane Technology and Applications*, John Wiley & Sons, Ltd, Chichester, UK, 2004. <https://doi.org/10.1002/0470020393>.
- [2] S. Jamaly, N.N. Darwish, I. Ahmed, S.W. Hasan, A short review on reverse osmosis pretreatment technologies, *DES.* 354 (2014) 30–38. <https://doi.org/10.1016/j.desal.2014.09.017>.
- [3] S. Jiang, Y. Li, B.P. Ladewig, A review of reverse osmosis membrane fouling and control strategies, *Sci. Total Environ.* 595 (2017) 567–583. <https://doi.org/10.1016/j.scitotenv.2017.03.235>.
- [4] L.K. Wang, Y.-T. Hung, N.K. Shammass, eds., *Physicochemical Treatment Processes*, Humana Press, Totowa, NJ, 2005. <https://doi.org/10.1385/159259820x>.
- [5] B. Ghernaout, D. Ghernaout, A. Saiba, Algae and cyanotoxins removal by coagulation/flocculation: A review, *Desalin. Water Treat.* 20 (2010) 133–143. <https://doi.org/10.5004/dwt.2010.1202>.
- [6] F. Xiao, J.C.H. Huang, B. jie Zhang, C. wei Cui, Effects of low temperature on coagulation kinetics and floc surface morphology using alum, *Desalination.* 237 (2009) 201–213. <https://doi.org/10.1016/j.desal.2007.12.033>.
- [7] B.C. Cao, B.Y. Gao, C.H. Xu, Y. Fu, X. Liu, Effects of pH on coagulation behavior and floc properties in Yellow River water treatment using ferric based coagulants, *Chinese Sci. Bull.* 55 (2010) 1382–1387. <https://doi.org/10.1007/s11434-010-0087-5>.
- [8] M. Yan, D. Wang, J. Qu, J. Ni, C.W.K. Chow, Enhanced coagulation for high alkalinity and micro-polluted water: The third way through coagulant optimization, *Water Res.* 42 (2008) 2278–2286. <https://doi.org/10.1016/j.watres.2007.12.006>.
- [9] J.K. Edzwald, J. Haarhoff, *Seawater pretreatment for reverse osmosis: Chemistry, contaminants, and coagulation*, *Water Res.* (2011).

- <https://doi.org/10.1016/j.watres.2011.08.014>.
- [10] Y. Taniguchi, An overview of pretreatment technology for reverse osmosis desalination plants in Japan, *Desalination*. 110 (1997) 21–36.
- [11] E.L. Sharp, S.A. Parsons, B. Jefferson, Seasonal variations in natural organic matter and its impact on coagulation in water treatment, 363 (2006) 183–194. <https://doi.org/10.1016/j.scitotenv.2005.05.032>.
- [12] J.C. Crittenden, R.R. Trussell, D.W. Hand, K.J. Howe, G. Tchobanoglous, *Water Treatment principle and design*, 2012. <https://doi.org/10.1002/9781118131473.ch5>.
- [13] C.B.M. Kimber, *Basic Water Treatment*, 5th Editio, ICE Publishing, 2013. <https://app.knovel.com/hotlink/toc/id:kpBWTE0002/basic-water-treatment/basic-water-treatment>.
- [14] N. Voutchkov, *Desalination Engineering Planning and Design*, 2013. <https://doi.org/10.1017/CBO9781107415324.004>.
- [15] P. Vandezande, L.E.M. Gevers, I.F.J. Vankelecom, Solvent resistant nanofiltration: separating on a molecular level, *Chem. Soc. Rev.* 37 (2008) 365–405. <https://doi.org/10.1039/B610848M>.
- [16] J. Geens, B. De Witte, B. Van der Bruggen, Removal of API's (Active Pharmaceutical Ingredients) from Organic Solvents by Nanofiltration, *Sep. Sci. Technol.* 42 (2007) 2435–2449. <https://doi.org/10.1080/01496390701477063>.
- [17] L. Peeva, J. Arbour, A. Livingston, On the Potential of Organic Solvent Nanofiltration in Continuous Heck Coupling Reactions, *Org. Process Res. Dev.* 17 (2013) 967–975. <https://doi.org/10.1021/op400073p>.
- [18] P. Marchetti, M.F. Jimenez Solomon, G. Szekely, A.G. Livingston, Molecular Separation with Organic Solvent Nanofiltration: A Critical Review, *Chem. Rev.* 114 (2014) 10735–10806. <https://doi.org/10.1021/cr500006j>.
- [19] *Water 4.0: the past, present, and future of the world's most vital resource*, *Choice Rev.*

- Online. 52 (2014) 52-0292-52–0292. <https://doi.org/10.5860/CHOICE.52-0292>.
- [20] A. Lee, J.W. Elam, S.B. Darling, Membrane materials for water purification: design, development, and application, *Environ. Sci. Water Res. Technol.* 2 (2016) 17–42. <https://doi.org/10.1039/C5EW00159E>.
- [21] E. Obotey Ezugbe, S. Rathilal, Membrane Technologies in Wastewater Treatment: A Review, *Membranes (Basel)*. 10 (2020) 89. <https://doi.org/10.3390/membranes10050089>.
- [22] D. Dolar, K. Košutić, Removal of Pharmaceuticals by Ultrafiltration (UF), Nanofiltration (NF), and Reverse Osmosis (RO), in: 2013: pp. 319–344. <https://doi.org/10.1016/B978-0-444-62657-8.00010-0>.
- [23] A. V Volkov, G.A. Korneeva, G.F. Tereshchenko, Organic solvent nanofiltration: prospects and application, *Russ. Chem. Rev.* 77 (2008) 983–993. <https://doi.org/10.1070/RC2008v077n11ABEH003795>.
- [24] C. Fersi, L. Gzara, M. Dhahbi, Treatment of textile effluents by membrane technologies, *Desalination*. 185 (2005) 399–409. <https://doi.org/10.1016/j.desal.2005.03.087>.
- [25] M. Cheryan, *Ultrafiltration and Microfiltration Handbook*, CRC Press, 1998. <https://doi.org/10.1201/9781482278743>.
- [26] Z.F. Cui, Y. Jiang, R.W. Field, *Fundamentals of Pressure-Driven Membrane Separation Processes*, First Edit, Elsevier Ltd, 2010. <https://doi.org/10.1016/B978-1-85617-632-3.00001-X>.
- [27] G.R. Guillen, Y. Pan, M. Li, E.M.V. Hoek, Preparation and characterization of membranes formed by nonsolvent induced phase separation: A review, *Ind. Eng. Chem. Res.* 50 (2011) 3798–3817. <https://doi.org/10.1021/ie101928r>.
- [28] L.K.W. Nazih K. Shammam, *Water Engineering: Hydraulics, Distribution and Treatment*, First, WILEY, 2015.
- [29] S. Rajindar, *Membrane Technology and Engineering for Water Purification - Application, Systems Design and Operation*, (2015) 1–80. <https://doi.org/10.1007/978-1-4613-3135-3>.

- [30] R. Singh, N.P. Hankins, Introduction to Membrane Processes for Water Treatment, in: Emerg. Membr. Technol. Sustain. Water Treat., Elsevier, 2016: pp. 15–52. <https://doi.org/10.1016/B978-0-444-63312-5.00002-4>.
- [31] F. Knops, S. van Hoof, H. Futselaar, L. Broens, Economic evaluation of a new ultrafiltration membrane for pretreatment of seawater reverse osmosis, Desalination. (2007). <https://doi.org/10.1016/j.desal.2006.04.013>.
- [32] J.Z. Hamad, C. Ha, M.D. Kennedy, G.L. Amy, Application of ceramic membranes for seawater reverse osmosis (SWRO) pre-treatment, Desalin. Water Treat. 51 (2013) 4881–4891. <https://doi.org/10.1080/19443994.2013.795211>.
- [33] D.F. Halpern, J. McArdle, B. Antrim, UF pretreatment for SWRO: Pilot studies, Desalination. 182 (2005) 323–332. <https://doi.org/10.1016/j.desal.2005.02.031>.
- [34] N. Voutchkov, Pretreatment for Reverse Osmosis Desalination, Elsevier. (2017).
- [35] X. Li, J. Li, Fluxes and Driving Forces in Membrane Separation Processes, in: Encycl. Membr., Springer Berlin Heidelberg, Berlin, Heidelberg, 2015: pp. 1–3. https://doi.org/10.1007/978-3-642-40872-4_2197-1.
- [36] G.T. (Author) John C. Crittenden (Author), R. Rhodes Trussell (Author), David W. Hand (Author), Kerry J. Howe (Author), MWH's Water Treatment: Principles and Design, 2012.
- [37] H. Strathmann, Membrane separation processes: Current relevance and future opportunities, AIChE J. 47 (2001) 1077–1087. <https://doi.org/10.1002/aic.690470514>.
- [38] G. Barbieri, Permeating Flux, in: Encycl. Membr., Springer Berlin Heidelberg, Berlin, Heidelberg, 2015: pp. 1–1. https://doi.org/10.1007/978-3-642-40872-4_448-1.
- [39] H. Alhweij, E.A. Carolina Emanuelsson, S. Shahid, J. Wenk, Simplified in-situ tailoring of cross-linked self-doped sulfonated polyaniline (S-PANI) membranes for nanofiltration applications, J. Memb. Sci. (2021) 119654. <https://doi.org/10.1016/j.memsci.2021.119654>.

- [40] C.J. Davey, Z.-X. Low, R.H. Wirawan, D.A. Patterson, Molecular weight cut-off determination of organic solvent nanofiltration membranes using poly(propylene glycol), *J. Memb. Sci.* 526 (2017) 221–228. <https://doi.org/10.1016/j.memsci.2016.12.038>.
- [41] P. BACCHIN, P. AIMAR, R. FIELD, Critical and sustainable fluxes: Theory, experiments and applications, *J. Memb. Sci.* 281 (2006) 42–69. <https://doi.org/10.1016/j.memsci.2006.04.014>.
- [42] *Comprehensive Membrane Science and Engineering*, Elsevier, 2010. <https://doi.org/10.1016/C2009-1-28385-7>.
- [43] L.K. Wang, J.P. Chen, Y.-T. Hung, N.K. Shamas, eds., *Membrane and Desalination Technologies*, Humana Press, Totowa, NJ, 2011. <https://doi.org/10.1007/978-1-59745-278-6>.
- [44] M. Mulder, *Basic Principles of Membrane Technology*, Springer Netherlands, Dordrecht, 1996. <https://doi.org/10.1007/978-94-009-1766-8>.
- [45] S. LOEB, S. SOURIRAJAN, Sea Water Demineralization by Means of an Osmotic Membrane, in: 1963: pp. 117–132. <https://doi.org/10.1021/ba-1963-0038.ch009>.
- [46] M. Guillotin, C. Lemoyne, C. Noel, L. Monnerie, Physicochemical processes occurring during the formation of cellulose diacetate membranes. Research of criteria for optimizing membrane performance. IV. Cellulose diacetate-*Acetone*-organic additive casting solutions, *Desalination*. 21 (1977) 165–181. [https://doi.org/10.1016/S0011-9164\(00\)80314-8](https://doi.org/10.1016/S0011-9164(00)80314-8).
- [47] L. Broens, F.W. Altena, C.A. Smolders, D.M. Koenhen, Asymmetric membrane structures as a result of phase separation phenomena, *Desalination*. 32 (1980) 33–45. [https://doi.org/10.1016/S0011-9164\(00\)86004-X](https://doi.org/10.1016/S0011-9164(00)86004-X).
- [48] G.R. Guillen, Y. Pan, M. Li, E.M. V. Hoek, Preparation and Characterization of Membranes Formed by Nonsolvent Induced Phase Separation: A Review, *Ind. Eng. Chem. Res.* 50 (2011) 3798–3817. <https://doi.org/10.1021/ie101928r>.

- [49] A.K. Ghosh, B.-H. Jeong, X. Huang, E.M.V. Hoek, Impacts of reaction and curing conditions on polyamide composite reverse osmosis membrane properties, *J. Memb. Sci.* 311 (2008) 34–45. <https://doi.org/10.1016/j.memsci.2007.11.038>.
- [50] J.. Wijmans, J. Kant, M.H.. Mulder, C.. Smolders, Phase separation phenomena in solutions of polysulfone in mixtures of a solvent and a nonsolvent: relationship with membrane formation, *Polymer (Guildf)*. 26 (1985) 1539–1545. [https://doi.org/10.1016/0032-3861\(85\)90090-4](https://doi.org/10.1016/0032-3861(85)90090-4).
- [51] H. Strathmann, K. Kock, P. Amar, R.W. Baker, The formation mechanism of asymmetric membranes, *Desalination*. 16 (1975) 179–203. [https://doi.org/10.1016/S0011-9164\(00\)82092-5](https://doi.org/10.1016/S0011-9164(00)82092-5).
- [52] T. He, Finger-Like Structure, in: *Encycl. Membr.*, Springer Berlin Heidelberg, Berlin, Heidelberg, 2015: pp. 1–2. https://doi.org/10.1007/978-3-642-40872-4_1959-1.
- [53] T. He, Spongelike Structure, in: *Encycl. Membr.*, Springer Berlin Heidelberg, Berlin, Heidelberg, 2016: pp. 1814–1815. https://doi.org/10.1007/978-3-662-44324-8_1954.
- [54] Z. Wang, Cross-Link, in: *Encycl. Membr.*, Springer Berlin Heidelberg, Berlin, Heidelberg, 2016: pp. 479–480. https://doi.org/10.1007/978-3-662-44324-8_1809.
- [55] Y. Chujo, ed., *Conjugated Polymer Synthesis*, Wiley-VCH Verlag GmbH & Co. KGaA, Weinheim, Germany, 2010. <https://doi.org/10.1002/9783527632664>.
- [56] S. Basu, A.L. Khan, A. Cano-Odena, C. Liu, I.F.J. Vankelecom, Membrane-based technologies for biogas separations, *Chem. Soc. Rev.* 39 (2010) 750–768. <https://doi.org/10.1039/B817050A>.
- [57] T. Beryozkina, K. Boyko, N. Khanduyeva, V. Senkovskyy, M. Horecha, U. Oertel, F. Simon, M. Stamm, A. Kiriya, Grafting of Polyfluorene by Surface-Initiated Suzuki Polycondensation, *Angew. Chemie Int. Ed.* 48 (2009) 2695–2698. <https://doi.org/10.1002/anie.200806217>.
- [58] P. Luis, T. Van Gerven, B. Van der Bruggen, Recent developments in membrane-based

- technologies for CO₂ capture, *Prog. Energy Combust. Sci.* 38 (2012) 419–448.
<https://doi.org/10.1016/j.pecs.2012.01.004>.
- [59] P. Bernardo, E. Drioli, G. Golemme, Membrane Gas Separation: A Review/State of the Art, *Ind. Eng. Chem. Res.* 48 (2009) 4638–4663. <https://doi.org/10.1021/ie8019032>.
- [60] Y.L. Xue, J. Huang, C.H. Lau, B. Cao, P. Li, Tailoring the molecular structure of crosslinked polymers for pervaporation desalination, *Nat. Commun.* 11 (2020) 1461. <https://doi.org/10.1038/s41467-020-15038-w>.
- [61] A. Asadi Tashvigh, Y. Feng, M. Weber, C. Maletzko, T.-S. Chung, 110th Anniversary: Selection of Cross-Linkers and Cross-Linking Procedures for the Fabrication of Solvent-Resistant Nanofiltration Membranes: A Review, *Ind. Eng. Chem. Res.* 58 (2019) 10678–10691. <https://doi.org/10.1021/acs.iecr.9b02408>.
- [62] J. Rantanen, J. Khinast, The Future of Pharmaceutical Manufacturing Sciences, *J. Pharm. Sci.* 104 (2015) 3612–3638. <https://doi.org/10.1002/jps.24594>.
- [63] C. Gadipelly, A. Pérez-González, G.D. Yadav, I. Ortiz, R. Ibáñez, V.K. Rathod, K. V. Marathe, Pharmaceutical Industry Wastewater: Review of the Technologies for Water Treatment and Reuse, *Ind. Eng. Chem. Res.* 53 (2014) 11571–11592. <https://doi.org/10.1021/ie501210j>.
- [64] X.Q. Cheng, Y.L. Zhang, Z.X. Wang, Z.H. Guo, Y.P. Bai, L. Shao, Recent Advances in Polymeric Solvent-Resistant Nanofiltration Membranes, *Adv. Polym. Technol.* 33 (2014) n/a-n/a. <https://doi.org/10.1002/adv.21455>.
- [65] I.-C. Kim, H.-G. Yun, K.-H. Lee, Preparation of asymmetric polyacrylonitrile membrane with small pore size by phase inversion and post-treatment process, *J. Memb. Sci.* 199 (2002) 75–84. [https://doi.org/10.1016/S0376-7388\(01\)00680-9](https://doi.org/10.1016/S0376-7388(01)00680-9).
- [66] J. Shen, S. Shahid, A. Sarihan, D.A. Patterson, E.A.C. Emanuelsson, Effect of polyacid dopants on the performance of polyaniline membranes in organic solvent nanofiltration, *Sep. Purif. Technol.* 204 (2018) 336–344. <https://doi.org/10.1016/j.seppur.2018.04.034>.

- [67] K. Vanherck, A. Cano-Odena, G. Koeckelberghs, T. Dedroog, I. Vankelecom, A simplified diamine crosslinking method for PI nanofiltration membranes, *J. Memb. Sci.* 353 (2010) 135–143. <https://doi.org/10.1016/j.memsci.2010.02.046>.
- [68] A. Asadi Tashvigh, L. Luo, T.-S. Chung, M. Weber, C. Maletzko, A novel ionically cross-linked sulfonated polyphenylsulfone (sPPSU) membrane for organic solvent nanofiltration (OSN), *J. Memb. Sci.* 545 (2018) 221–228. <https://doi.org/10.1016/j.memsci.2017.09.076>.
- [69] S. Darvishmanesh, J.C. Jansen, F. Tasselli, E. Tocci, P. Luis, J. Degrève, E. Drioli, B. Van der Bruggen, Novel polyphenylsulfone membrane for potential use in solvent nanofiltration, *J. Memb. Sci.* 379 (2011) 60–68. <https://doi.org/10.1016/j.memsci.2011.05.045>.
- [70] L.G. Peeva, E. Gibbins, S.S. Luthra, L.S. White, R.P. Stateva, A.G. Livingston, Effect of concentration polarisation and osmotic pressure on flux in organic solvent nanofiltration, *J. Memb. Sci.* 236 (2004) 121–136. <https://doi.org/10.1016/j.memsci.2004.03.004>.
- [71] S.-P. Sun, T.-S. Chung, K.-J. Lu, S.-Y. Chan, Enhancement of flux and solvent stability of Matrimid® thin-film composite membranes for organic solvent nanofiltration, *AIChE J.* 60 (2014) 3623–3633. <https://doi.org/10.1002/aic.14558>.
- [72] M.F. Jimenez Solomon, Y. Bhole, A.G. Livingston, High flux membranes for organic solvent nanofiltration (OSN)—Interfacial polymerization with solvent activation, *J. Memb. Sci.* 423–424 (2012) 371–382. <https://doi.org/10.1016/j.memsci.2012.08.030>.
- [73] M.G. Buonomenna, J. Bae, Organic Solvent Nanofiltration in Pharmaceutical Industry, *Sep. Purif. Rev.* 44 (2015) 157–182. <https://doi.org/10.1080/15422119.2014.918884>.
- [74] H. Alhweij, E.A. Carolina Emanuelsson, S. Shahid, J. Wenk, High performance in-situ tuned self-doped polyaniline (PANI) membranes for organic solvent (nano)filtration, *Polymer (Guildf)*. 245 (2022) 124682. <https://doi.org/10.1016/j.polymer.2022.124682>.
- [75] S. Darvishmanesh, T. Robberecht, P. Luis, J. Degrève, B. Van der Bruggen, Performance

- of Nanofiltration Membranes for Solvent Purification in the Oil Industry, *J. Am. Oil Chem. Soc.* 88 (2011) 1255–1261. <https://doi.org/10.1007/s11746-011-1779-y>.
- [76] M. V. Tres, S. Mohr, M.L. Corazza, M. Di Luccio, J.V. Oliveira, Separation of n-butane from soybean oil mixtures using membrane processes, *J. Memb. Sci.* 333 (2009) 141–146. <https://doi.org/10.1016/j.memsci.2009.02.008>.
- [77] M. Priske, M. Lazar, C. Schnitzer, G. Baumgarten, Recent Applications of Organic Solvent Nanofiltration, *Chemie Ing. Tech.* 88 (2016) 39–49. <https://doi.org/10.1002/cite.201500084>.
- [78] J.M. Dreimann, M. Skiborowski, A. Behr, A.J. Vorholt, Recycling Homogeneous Catalysts Simply by Organic Solvent Nanofiltration: New Ways to Efficient Catalysis, *ChemCatChem*. 8 (2016) 3330–3333. <https://doi.org/10.1002/cctc.201601018>.
- [79] C. Schnitzer, D. Kruse, M. Lazar, M. Priske, A. Kobus, Die organophile Nanofiltration als neue Grundoperation der Fluidverfahrenstechnik, *Chemie Ing. Tech.* 86 (2014) 589–593. <https://doi.org/10.1002/cite.201300162>.
- [80] J.C.-T. Lin, A.G. Livingston, Nanofiltration membrane cascade for continuous solvent exchange, *Chem. Eng. Sci.* 62 (2007) 2728–2736. <https://doi.org/10.1016/j.ces.2006.08.004>.
- [81] I. Sereewatthanawut, F.W. Lim, Y.S. Bhole, D. Ormerod, A. Horvath, A.T. Boam, A.G. Livingston, Demonstration of Molecular Purification in Polar Aprotic Solvents by Organic Solvent Nanofiltration, *Org. Process Res. Dev.* 14 (2010) 600–611. <https://doi.org/10.1021/op100028p>.
- [82] H.T. El-Dessouky, H.M. Ettouney, Introduction, in: *Fundam. Salt Water Desalin.*, Elsevier, 2002: pp. 1–17. <https://doi.org/10.1016/B978-044450810-2/50003-8>.
- [83] I.G. Wenten, Khoiruddin, Reverse osmosis applications: Prospect and challenges, *Desalination*. 391 (2016) 112–125. <https://doi.org/10.1016/j.desal.2015.12.011>.
- [84] S.C. Leterme, C. Le Lan, D.A. Hemraj, A. V. Ellis, The impact of diatoms on the

- biofouling of seawater reverse osmosis membranes in a model cross-flow system, *Desalination*. 392 (2016) 8–13. <https://doi.org/10.1016/j.desal.2016.04.019>.
- [85] Q. She, R. Wang, A.G. Fane, C.Y. Tang, Membrane fouling in osmotically driven membrane processes: A review, *J. Memb. Sci.* 499 (2016) 201–233. <https://doi.org/10.1016/j.memsci.2015.10.040>.
- [86] D.N. Giorno L., *Encyclopedia of Membranes*, Springer. (2016).
- [87] R.A. Al-juboori, T. Yusaf, Biofouling in RO system: Mechanisms, monitoring and controlling, *DES*. 302 (2012) 1–23. <https://doi.org/10.1016/j.desal.2012.06.016>.
- [88] M.A. Saad, Early discovery of RO membrane fouling and real-time monitoring of plant performance for optimizing cost of water, *Desalination*. 165 (2004) 183–191. <https://doi.org/10.1016/j.desal.2004.06.021>.
- [89] T. Nguyen, F.A. Roddick, L. Fan, Biofouling of Water Treatment Membranes: A Review of the Underlying Causes, Monitoring Techniques and Control Measures, (2012) 804–840. <https://doi.org/10.3390/membranes2040804>.
- [90] I. Sutzkover-Gutman, D. Hasson, Feed water pretreatment for desalination plants, *Desalination*. 264 (2010) 289–296. <https://doi.org/10.1016/j.desal.2010.07.014>.
- [91] C. V. Vedavyasan, Pretreatment trends - an overview, *Desalination*. 203 (2007) 296–299. <https://doi.org/10.1016/j.desal.2006.04.012>.
- [92] J. Zhang, K. Northcott, M. Duke, P. Scales, S.R. Gray, Influence of pre-treatment combinations on RO membrane fouling, *Desalination*. 393 (2016) 120–126. <https://doi.org/10.1016/j.desal.2016.02.020>.
- [93] N. Voutchkov, Considerations for selection of seawater filtration pretreatment system, *Desalination*. (2010). <https://doi.org/10.1016/j.desal.2010.07.002>.
- [94] Y.M. Kim, S.J. Kim, Y.S. Kim, S. Lee, I.S. Kim, J.H. Kim, Overview of systems engineering approaches for a large-scale seawater desalination plant with a reverse osmosis network, *Desalination*. 238 (2007) 312–332. <https://doi.org/10.1016/j.desal.2007.04.012>.

- [95] J. Xu, G. Ruan, X. Gao, X. Pan, B. Su, C. Gao, Pilot study of inside-out and outside-in hollow fiber UF modules as direct pretreatment of seawater at low temperature for reverse osmosis, *Desalination*. 219 (2008) 179–189. <https://doi.org/10.1016/j.desal.2007.04.055>.
- [96] L. Henthorne, B. Boysen, State-of-the-art of reverse osmosis desalination pretreatment, *Desalination*. 356 (2015) 129–139. <https://doi.org/10.1016/j.desal.2014.10.039>.
- [97] M. Sillanpää, M.C. Ncibi, A. Matilainen, M. Vepsäläinen, Removal of natural organic matter in drinking water treatment by coagulation: A comprehensive review, *Chemosphere*. 190 (2018) 54–71. <https://doi.org/10.1016/j.chemosphere.2017.09.113>.
- [98] J. Haarhoff, J.K. Edzwald, Adapting dissolved air flotation for the clarification of seawater, *Desalination*. 311 (2013) 90–94. <https://doi.org/10.1016/j.desal.2012.10.035>.
- [99] E.M. Van Wagner, A.C. Sagle, M.M. Sharma, B.D. Freeman, Effect of crossflow testing conditions, including feed pH and continuous feed filtration, on commercial reverse osmosis membrane performance, *J. Memb. Sci.* (2009). <https://doi.org/10.1016/j.memsci.2009.08.033>.
- [100] N.E. Sabiri, J.B. Castaing, A. Massé, P. Jaouen, Environmental Technology Performance of a sand filter in removal of micro- algae from seawater in aquaculture production systems Performance of a sand filter in removal of micro-algae from seawater in aquaculture production systems, *Environ. Technol.* 33 (2012) 667–676. <https://doi.org/10.1080/09593330.2011.587027>.
- [101] S.A. Alizadeh Tabatabai, J.C. Schippers, M.D. Kennedy, Effect of coagulation on fouling potential and removal of algal organic matter in ultrafiltration pretreatment to seawater reverse osmosis, *Water Res.* (2014). <https://doi.org/10.1016/j.watres.2014.04.001>.
- [102] R. Schurer, A. Janssen, L. Villacorte, M. Kennedy, Performance of ultrafiltration and coagulation in an UF-RO seawater desalination demonstration plant, *Desalin. Water Treat.* 42 (2012) 57–64. <https://doi.org/10.1080/19443994.2012.683107>.
- [103] M. Monnot, S. Laborie, C. Cabassud, Granular activated carbon filtration plus

- ultrafiltration as a pretreatment to seawater desalination lines: Impact on water quality and UF fouling, *Desalination*. 383 (2016) 1–11. <https://doi.org/10.1016/j.desal.2015.12.010>.
- [104] S.L. Sanghyun Jeong , Robert Vollprecht, Kyungjin Cho, TorOve Leiknes, Saravanamuthu Vigneswaran , Hyokwan Bae, Advanced organic and biological analysis of dual media filtration used as a pretreatment in a full-scale seawater desalination plant, *Desalination*. 385 (2016) 83–92. <https://doi.org/10.1016/j.desal.2016.02.017>.
- [105] Y. Cohen, Biofiltration - The treatment of fluids by microorganisms immobilized into the filter bedding material: a review, *Bioresour. Technol.* 77 (2001) 257–274. [https://doi.org/10.1016/S0960-8524\(00\)00074-2](https://doi.org/10.1016/S0960-8524(00)00074-2).
- [106] R.M. Hozalski, E.J. Bouwer, Non-steady state simulation of BOM removal in drinking water biofilters: Applications and full-scale validation, *Water Res.* 35 (2001) 211–223. [https://doi.org/10.1016/S0043-1354\(00\)00226-8](https://doi.org/10.1016/S0043-1354(00)00226-8).
- [107] S. Jeong, S. Vigneswaran, Assessment of biological activity in contact flocculation filtration used as a pretreatment in seawater desalination, *Chem. Eng. J.* 228 (2013) 976–983. <https://doi.org/10.1016/j.cej.2013.05.085>.
- [108] B.S. Oh, H.Y. Jang, J. Cho, S. Lee, E. Lee, I.S. Kim, T.M. Hwang, J.W. Kang, Effect of ozone on microfiltration as a pretreatment of seawater reverse osmosis, *Desalination*. 238 (2009) 90–97. <https://doi.org/10.1016/j.desal.2008.01.039>.
- [109] M.K. Ramseier, A. Peter, J. Traber, U. Von Gunten, Formation of assimilable organic carbon during oxidation of natural waters with ozone , chlorine dioxide , chlorine , permanganate , and ferrate, *Water Res.* 45 (2010) 2002–2010. <https://doi.org/10.1016/j.watres.2010.12.002>.
- [110] L.F. Greenlee, B.D. Freeman, D.F. Lawler, Ozonation of phosphonate antiscalants used for reverse osmosis desalination: Parameter effects on the extent of oxidation, *Chem. Eng. J.* 244 (2014) 505–513. <https://doi.org/10.1016/j.cej.2014.02.002>.
- [111] M. Beery, G. Wozny, J.U. Repke, Sustainable design of different seawater reverse osmosis

- desalination pretreatment processes, *Comput. Aided Chem. Eng.* (2010).
[https://doi.org/10.1016/S1570-7946\(10\)28179-8](https://doi.org/10.1016/S1570-7946(10)28179-8).
- [112] N. Hilal, O.O. Ogunbiyi, N.J. Miles, R. Nigmatullin, N. Hilal, O.O. Ogunbiyi, N.J. Miles, R. Nigmatullin, Methods Employed for Control of Fouling in MF and UF Membranes : A Comprehensive Review, 6395 (2007). <https://doi.org/10.1081/SS-200068409>.
- [113] M. Badruzzaman, N. Voutchkov, L. Weinrich, J.G. Jacangelo, Selection of pretreatment technologies for seawater reverse osmosis plants: A review, *Desalination*. 449 (2019) 78–91. <https://doi.org/10.1016/j.desal.2018.10.006>.
- [114] J. Lee, I.S. Kim, Microbial community in seawater reverse osmosis and rapid diagnosis of membrane biofouling, *Desalination*. 273 (2011) 118–126. <https://doi.org/10.1016/j.desal.2010.12.005>.
- [115] J.M. Gohil, A.K. Suresh, Chlorine attack on reverse osmosis membranes: Mechanisms and mitigation strategies, *J. Memb. Sci.* 541 (2017) 108–126. <https://doi.org/10.1016/j.memsci.2017.06.092>.
- [116] Q. Wang, H. Zeng, Z. Wu, J. Cao, Impact of sodium hypochlorite cleaning on the surface properties and performance of PVDF membranes, *Appl. Surf. Sci.* 428 (2018) 289–295. <https://doi.org/10.1016/j.apsusc.2017.09.056>.
- [117] D.H. Shin, N. Kim, Y.T. Lee, Modification to the polyamide TFC RO membranes for improvement of chlorine-resistance, *J. Memb. Sci.* 376 (2011) 302–311. <https://doi.org/10.1016/j.memsci.2011.04.045>.
- [118] G. Kang, C. Gao, W. Chen, X. Jie, Y. Cao, Q. Yuan, Study on hypochlorite degradation of aromatic polyamide reverse osmosis membrane, 300 (2007) 165–171. <https://doi.org/10.1016/j.memsci.2007.05.025>.
- [119] V.T. Do, C.Y. Tang, M. Reinhard, J.O. Leckie, Degradation of Polyamide Nanofiltration and Reverse Osmosis Membranes by Hypochlorite, (2012). <https://doi.org/10.1021/es203090y>.

- [120] R. Verbeke, V. Gómez, I.F.J. Vankelecom, Chlorine-resistance of reverse osmosis (RO) polyamide membranes, *Prog. Polym. Sci.* 72 (2017) 1–15. <https://doi.org/10.1016/j.progpolymsci.2017.05.003>.
- [121] Nidal Hilal; Ahmad Fauzi Ismail; Chris J Wright, *Membrane Fabrication*, CRC Press, 2015. <https://doi.org/10.1201/b18149>.
- [122] S. Al Aani, C.J. Wright, N. Hilal, Investigation of UF membranes fouling and potentials as pre-treatment step in desalination and surface water applications, *Desalination*. 432 (2018) 115–127. <https://doi.org/10.1016/j.desal.2018.01.017>.
- [123] A. Matin, Z. Khan, S.M.J. Zaidi, M.C. Boyce, Biofouling in reverse osmosis membranes for seawater desalination: Phenomena and prevention, *Desalination*. 281 (2011) 1–16. <https://doi.org/10.1016/j.desal.2011.06.063>.
- [124] A.G.F. and C.J.D. FELL, A Review of Fouling and Fouling Control in Ultrafiltration, 62 (1987) 117–136.
- [125] S.F. Anis, R. Hashaikh, N. Hilal, Reverse osmosis pretreatment technologies and future trends: A comprehensive review, *Desalination*. 452 (2019) 159–195. <https://doi.org/10.1016/j.desal.2018.11.006>.
- [126] H. Qin, C. Sun, C. He, D. Wang, C. Cheng, S. Nie, S. Sun, C. Zhao, High efficient protocol for the modification of polyethersulfone membranes with anticoagulant and antifouling properties via in situ cross-linked copolymerization, *J. Memb. Sci.* 468 (2014) 172–183. <https://doi.org/10.1016/j.memsci.2014.06.006>.
- [127] G. Kang, Y. Cao, Application and modification of poly(vinylidene fluoride) (PVDF) membranes – A review, *J. Memb. Sci.* 463 (2014) 145–165. <https://doi.org/10.1016/j.memsci.2014.03.055>.
- [128] D. Norberg, S. Hong, J. Taylor, Y. Zhao, Surface characterization and performance evaluation of commercial fouling resistant low-pressure RO membranes, 202 (2007) 45–52. <https://doi.org/10.1016/j.desal.2005.12.037>.

- [129] K. Boussu, A. Belpaire, A. Volodin, C. Van Haesendonck, P. Van Der Meeren, C. Vandecasteele, B. Van Der Bruggen, Influence of membrane and colloid characteristics on fouling of nanofiltration membranes, 289 (2007) 220–230. <https://doi.org/10.1016/j.memsci.2006.12.001>.
- [130] J.A.B. Amy Childress, Characterization of the Hydrophobicity of Polymeric Reverse Osmosis and Nanofiltration Membranes : Implications to Membrane Fouling, (2000).
- [131] K.P. Lee, T.C. Arnot, D. Mattia, A review of reverse osmosis membrane materials for desalination-Development to date and future potential, J. Memb. Sci. 370 (2011) 1–22. <https://doi.org/10.1016/j.memsci.2010.12.036>.
- [132] V. Kochkodan, N. Hilal, A comprehensive review on surface modified polymer membranes for biofouling mitigation, Desalination. 356 (2015) 187–207. <https://doi.org/10.1016/j.desal.2014.09.015>.
- [133] L. Zou, I. Vidalis, D. Steele, A. Michelmore, S.P. Low, J.Q.J.C. Verberk, Surface hydrophilic modification of RO membranes by plasma polymerization for low organic fouling, J. Memb. Sci. 369 (2011) 420–428. <https://doi.org/10.1016/j.memsci.2010.12.023>.
- [134] K.Y. Jee, D.H. Shin, Y.T. Lee, Surface modification of polyamide RO membrane for improved fouling resistance, DES. 394 (2016) 131–137. <https://doi.org/10.1016/j.desal.2016.05.013>.
- [135] J. Nikkola, X. Liu, Y. Li, M. Raulio, H. Alakomi, Surface modification of thin film composite RO membrane for enhanced anti-biofouling performance, 444 (2013) 192–200. <https://doi.org/10.1016/j.memsci.2013.05.032>.
- [136] M.L. Lind, D.E. Suk, E.M. V Hoek, Tailoring the Structure of Thin Film Nanocomposite Membranes to Achieve Seawater RO Membrane Performance, 44 (2010) 8230–8235.
- [137] A. Matin, Z. Khan, S.M.J. Zaidi, M.C. Boyce, Biofouling in reverse osmosis membranes for seawater desalination: Phenomena and prevention, Desalination. 281 (2011) 1–16.

- <https://doi.org/10.1016/j.desal.2011.06.063>.
- [138] S. Munirasu, F. Banat, A.A. Durrani, M.A. Haija, Intrinsically superhydrophobic PVDF membrane by phase inversion for membrane distillation, *Desalination*. 417 (2017) 77–86. <https://doi.org/10.1016/j.desal.2017.05.019>.
- [139] J. Meng, Z. Cao, L. Ni, Y. Zhang, X. Wang, X. Zhang, E. Liu, A novel salt-responsive TFC RO membrane having superior antifouling and easy-cleaning properties, *J. Memb. Sci.* 461 (2014) 123–129. <https://doi.org/10.1016/j.memsci.2014.03.017>.
- [140] M. Liu, Q. Chen, L. Wang, S. Yu, C. Gao, Improving fouling resistance and chlorine stability of aromatic polyamide thin-film composite RO membrane by surface grafting of polyvinyl alcohol (PVA), *DES.* 367 (2015) 11–20. <https://doi.org/10.1016/j.desal.2015.03.028>.
- [141] G.R. Xu, J.N. Wang, C.J. Li, Strategies for improving the performance of the polyamide thin film composite (PA-TFC) reverse osmosis (RO) membranes: Surface modifications and nanoparticles incorporations, *Desalination*. 328 (2013) 83–100. <https://doi.org/10.1016/j.desal.2013.08.022>.
- [142] M. Asadollahi, D. Bastani, S.A. Musavi, Enhancement of surface properties and performance of reverse osmosis membranes after surface modification: A review, *Desalination*. 420 (2017) 330–383. <https://doi.org/10.1016/j.desal.2017.05.027>.
- [143] Q. Zhang, C. Zhang, J. Xu, Y. Nie, S. Li, S. Zhang, C. Peg, Effect of poly (vinyl alcohol) coating process conditions on the properties and performance of polyamide reverse osmosis membranes, *DES.* 379 (2016) 42–52. <https://doi.org/10.1016/j.desal.2015.10.012>.
- [144] L.Z. Hanaa M.Hegab, Yasodinee Wimalasiri, Milena Ginic-Markovic, Improving the fouling resistance of brackish water membranes via surface modification with graphene oxide functionalized chitosan, (2015).
- [145] A. Akbari, Z. Derikvandi, S. Majid, M. Rostami, *Journal of Industrial and Engineering*

- Chemistry Influence of chitosan coating on the separation performance , morphology and anti-fouling properties of the polyamide nanofiltration membranes, *J. Ind. Eng. Chem.* 28 (2015) 268–276. <https://doi.org/10.1016/j.jiec.2015.03.002>.
- [146] W. Falath, A. Sabir, K.I. Jacob, Novel reverse osmosis membranes composed of modified PVA / Gum Arabic conjugates : Biofouling mitigation and chlorine resistance enhancement, *Carbohydr. Polym.* 155 (2017) 28–39. <https://doi.org/10.1016/j.carbpol.2016.08.058>.
- [147] A.J. Blok, R. Chhasatia, J. Dilag, A. V Ellis, Surface initiated polydopamine grafted poly ([2- (methacryoyloxy) ethyl] trimethylammonium chloride) coatings to produce reverse osmosis desalination membranes with anti-biofouling properties, *J. Memb. Sci.* 468 (2014) 216–223. <https://doi.org/10.1016/j.memsci.2014.06.008>.
- [148] J.-S. Kang, S.C. Sung, J.J. Lee, H.-S. Kim, Application of ceramic membrane for seawater desalination pretreatment, *Desalin. Water Treat.* 3994 (2016) 1–6. <https://doi.org/10.1080/19443994.2016.1189702>.
- [149] Y. Zhou, S. Yu, C. Gao, X. Feng, Surface modification of thin film composite polyamide membranes by electrostatic self deposition of polycations for improved fouling resistance, *66* (2009) 287–294. <https://doi.org/10.1016/j.seppur.2008.12.021>.
- [150] C.J.W. Nidal Hilal, Mohamed Khayet, *Membrane Modification*, CRC Press, 2016. <https://doi.org/10.1201/b12160>.
- [151] N. Misdan, A.F. Ismail, N. Hilal, Recent advances in the development of (bio)fouling resistant thin film composite membranes for desalination, *Desalination.* 380 (2016) 105–111. <https://doi.org/10.1016/j.desal.2015.06.001>.
- [152] G. Kang, Y. Cao, Development of antifouling reverse osmosis membranes for water treatment : A review, *Water Res.* 46 (2011) 584–600. <https://doi.org/10.1016/j.watres.2011.11.041>.
- [153] W. Sun, J. Liu, H. Chu, B. Dong, Pretreatment and Membrane Hydrophilic Modification

- to Reduce Membrane Fouling, (2013) 226–241.
<https://doi.org/10.3390/membranes3030226>.
- [154] N. Misdan, W.J. Lau, A.F. Ismail, Seawater Reverse Osmosis (SWRO) desalination by thin-film composite membrane—Current development, challenges and future prospects, *Desalination*. 287 (2012) 228–237. <https://doi.org/10.1016/j.desal.2011.11.001>.
- [155] S. Yeo, S. Yong, A.W. Mohammad, Post-treatment of Polymer Membrane through Chemical and Physical Surface Modifications- A Review, *J. Appl. Sci. Agric.* 10 (2015) 104–111.
- [156] T. Rajasekhar, M. Trinadh, P. Veera Babu, A.V.S. Sainath, A.V.R. Reddy, Oil–water emulsion separation using ultrafiltration membranes based on novel blends of poly(vinylidene fluoride) and amphiphilic tri-block copolymer containing carboxylic acid functional group, *J. Memb. Sci.* 481 (2015) 82–93.
<https://doi.org/10.1016/j.memsci.2015.01.030>.
- [157] E.S. Awad, T.M. Sabirova, N.A. Tretyakova, Q.F. Alsalhy, A. Figoli, I.K. Salih, A Mini-Review of Enhancing Ultrafiltration Membranes (UF) for Wastewater Treatment: Performance and Stability, *ChemEngineering*. 5 (2021) 34.
<https://doi.org/10.3390/chemengineering5030034>.
- [158] N.H. Ismail, W.N.W. Salleh, A.F. Ismail, H. Hasbullah, N. Yusof, F. Aziz, J. Jaafar, Hydrophilic polymer-based membrane for oily wastewater treatment: A review, *Sep. Purif. Technol.* 233 (2020) 116007. <https://doi.org/10.1016/j.seppur.2019.116007>.
- [159] U. Fathanah, I. Machdar, M. Riza, N. Arahman, M. Yusuf, S. Muchtar, M.R. Bilad, N.A.H. Nordin, Enhancement of antifouling of ultrafiltration polyethersulfone membrane with hybrid mg (oh)₂/chitosan by polymer blending, *J. Membr. Sci. Res.* 6 (2020) 375–382.
<https://doi.org/10.22079/JMSR.2020.124107.1365>.
- [160] Y. Liu, G.. Koops, H. Strathmann, Characterization of morphology controlled polyethersulfone hollow fiber membranes by the addition of polyethylene glycol to the

- dope and bore liquid solution, *J. Memb. Sci.* 223 (2003) 187–199. [https://doi.org/10.1016/S0376-7388\(03\)00322-3](https://doi.org/10.1016/S0376-7388(03)00322-3).
- [161] Z.-L. Xu, F.A. Qusay, Effect of polyethylene glycol molecular weights and concentrations on polyethersulfone hollow fiber ultrafiltration membranes, *J. Appl. Polym. Sci.* 91 (2004) 3398–3407. <https://doi.org/10.1002/app.13580>.
- [162] I.M. Wienk, F.H.A. Olde Scholtenhuis, T. van den Boomgaard, C.A. Smolders, Spinning of hollow fiber ultrafiltration membranes from a polymer blend, *J. Memb. Sci.* 106 (1995) 233–243. [https://doi.org/10.1016/0376-7388\(95\)00088-T](https://doi.org/10.1016/0376-7388(95)00088-T).
- [163] B. Su, P. Fu, Q. Li, Y. Tao, Z. Li, H. Zao, C. Zhao, Evaluation of polyethersulfone highflux hemodialysis membrane in vitro and in vivo, *J. Mater. Sci. Mater. Med.* 19 (2008) 745–751. <https://doi.org/10.1007/s10856-007-3006-9>.
- [164] A. Rahimpour, S.S. Madaeni, M. Jahanshahi, Y. Mansourpanah, N. Mortazavian, Development of high performance nano-porous polyethersulfone ultrafiltration membranes with hydrophilic surface and superior antifouling properties, *Appl. Surf. Sci.* 255 (2009) 9166–9173. <https://doi.org/10.1016/j.apsusc.2009.06.123>.
- [165] Z.-L. Xu, F. Alsalhy Qusay, Polyethersulfone (PES) hollow fiber ultrafiltration membranes prepared by PES/non-solvent/*NMP* solution, *J. Memb. Sci.* 233 (2004) 101–111. <https://doi.org/10.1016/j.memsci.2004.01.005>.
- [166] D. Wandera, S.R. Wickramasinghe, S.M. Husson, Stimuli-responsive membranes, *J. Memb. Sci.* 357 (2010) 6–35. <https://doi.org/10.1016/j.memsci.2010.03.046>.
- [167] Y. Zhang, L. Zou, B.P. Ladewig, D. Mulcahy, Synthesis and characterisation of superhydrophilic conductive heterogeneous PANI / PVDF anion-exchange membranes, *DES.* 362 (2015) 59–67. <https://doi.org/10.1016/j.desal.2015.02.004>.
- [168] S.B. Teli, S. Molina, E.G. Calvo, A.E. Lozano, J. De Abajo, Preparation, characterization and antifouling property of polyethersulfone – PANI / PMA ultra filtration membranes, *DES.* 299 (2012) 113–122. <https://doi.org/10.1016/j.desal.2012.05.031>.

- [169] J. Shen, H. Ruan, L. Wu, C. Gao, Preparation and characterization of PES–SiO₂ organic–inorganic composite ultrafiltration membrane for raw water pretreatment, *Chem. Eng. J.* 168 (2011) 1272–1278. <https://doi.org/10.1016/j.cej.2011.02.039>.
- [170] H. Basri, A.F. Ismail, M. Aziz, K. Nagai, T. Matsuura, M.S. Abdullah, B.C. Ng, Silver-filled polyethersulfone membranes for antibacterial applications — Effect of PVP and TAP addition on silver dispersion, *Desalination*. 261 (2010) 264–271. <https://doi.org/10.1016/j.desal.2010.05.009>.
- [171] N. Maximous, G. Nakhla, K. Wong, W. Wan, Optimization of Al₂O₃/PES membranes for wastewater filtration, *Sep. Purif. Technol.* 73 (2010) 294–301. <https://doi.org/10.1016/j.seppur.2010.04.016>.
- [172] A.L. Ahmad, A.A. Abdulkarim, B.S. Ooi, S. Ismail, Recent development in additives modifications of polyethersulfone membrane for flux enhancement, *Chem. Eng. J.* 223 (2013) 246–267. <https://doi.org/10.1016/j.cej.2013.02.130>.
- [173] N. Gizli, M. Demircioğlu, Morphological characterization of cellulose acetate based reverse osmosis membranes by atomic force microscopy (AFM)-effect of evaporation time, *Chem. Biochem. React. Kinet. Mech.* 5 (2011) 257–267. <https://doi.org/10.23939/chcht05.03.327>.
- [174] T. Mohammadi, E. Saljoughi, Effect of production conditions on morphology and permeability of asymmetric cellulose acetate membranes, *Desalination*. 243 (2009) 1–7. <https://doi.org/10.1016/j.desal.2008.04.010>.
- [175] A. Rahimpour, S.S. Madaeni, Polyethersulfone (PES)/cellulose acetate phthalate (CAP) blend ultrafiltration membranes: Preparation, morphology, performance and antifouling properties, *J. Memb. Sci.* 305 (2007) 299–312. <https://doi.org/10.1016/j.memsci.2007.08.030>.
- [176] I. Ounifi, Y. Guesmi, C. Ursino, S. Santoro, S. Mahfoudhi, A. Figoli, E. Ferjanie, A. Hafiane, Antifouling membranes based on cellulose acetate (CA) blended with

- poly(acrylic acid) for heavy metal remediation, *Appl. Sci.* 11 (2021).
<https://doi.org/10.3390/app11104354>.
- [177] J. Puls, S.A. Wilson, D. Höltzer, Degradation of Cellulose Acetate-Based Materials: A Review, *J. Polym. Environ.* 19 (2011) 152–165. <https://doi.org/10.1007/s10924-010-0258-0>.
- [178] L. Xu, S. Shahid, A.K. Holda, E.A.C. Emanuelsson, D.A. Patterson, Stimuli responsive conductive polyaniline membrane: In-filtration electrical tuneability of flux and MWCO, *J. Memb. Sci.* 552 (2018) 153–166. <https://doi.org/10.1016/j.memsci.2018.01.070>.
- [179] F. Ahmed, B.S. Lalia, V. Kochkodan, N. Hilal, R. Hashaikeh, Electrically conductive polymeric membranes for fouling prevention and detection: A review, *Desalination*. 391 (2016) 1–15. <https://doi.org/10.1016/j.desal.2016.01.030>.
- [180] N.F. Razali, A.W. Mohammad, N. Hilal, Effects of polyaniline nanoparticles in polyethersulfone ultrafiltration membranes: Fouling behaviours by different types of foulant, *J. Ind. Eng. Chem.* 20 (2014) 3134–3140. <https://doi.org/10.1016/j.jiec.2013.11.056>.
- [181] N. Faizah, A. Wahab, N. Hilal, C. Peng, J. Alam, Optimisation of polyethersulfone / polyaniline blended membranes using response surface methodology approach, *DES*. 311 (2013) 182–191. <https://doi.org/10.1016/j.desal.2012.11.033>.
- [182] Z. Fan, Z. Wang, N. Sun, J. Wang, S. Wang, Performance improvement of polysulfone ultrafiltration membrane by blending with polyaniline nanofibers, 320 (2008) 363–371. <https://doi.org/10.1016/j.memsci.2008.04.019>.
- [183] D.A. Cerqueira, A.J.M. Valente, G.R. Filho, H.D. Burrows, Synthesis and properties of polyaniline – cellulose acetate blends : The use of sugarcane bagasse waste and the effect of the substitution degree, *Carbohydr. Polym.* 78 (2009) 402–408. <https://doi.org/10.1016/j.carbpol.2009.04.016>.
- [184] A. Al-ahmed, F. Mohammad, M.Z. Ab, Composites of polyaniline and cellulose acetate :

- preparation , characterization , thermo-oxidative degradation and stability in terms of DC electrical conductivity retention, 144 (2004) 29–49. <https://doi.org/10.1016/j.synthmet.2004.01.007>.
- [185] I. Mav, M. Žigon, A. Šebenik, Sulfonated polyaniline, *Synth. Met.* 101 (1999) 717–718. [https://doi.org/10.1016/S0379-6779\(98\)01166-7](https://doi.org/10.1016/S0379-6779(98)01166-7).
- [186] J. Pellegrino, The Use of Conducting Polymers in Membrane-Based Separations, *Ann. N. Y. Acad. Sci.* 984 (2003) 289–305. <https://doi.org/10.1111/j.1749-6632.2003.tb06007.x>.
- [187] P. Chapman, X.X. Loh, A.G. Livingston, K. Li, T.A.C. Oliveira, Polyaniline membranes for the dehydration of *tetrahydrofuran* by pervaporation, 309 (2008) 102–111. <https://doi.org/10.1016/j.memsci.2007.10.016>.
- [188] M. Sairam, X.X. Loh, Y. Bhole, I. Sereewatthanawut, K. Li, A. Bismarck, J.H.G. Steinke, A.G. Livingston, Spiral-wound polyaniline membrane modules for organic solvent nanofiltration (OSN), *J. Memb. Sci.* 349 (2010) 123–129. <https://doi.org/10.1016/j.memsci.2009.11.039>.
- [189] X.X. Loh, M. Sairam, A. Bismarck, J.H.G. Steinke, A.G. Livingston, K. Li, Crosslinked integrally skinned asymmetric polyaniline membranes for use in organic solvents, 326 (2009) 635–642. <https://doi.org/10.1016/j.memsci.2008.10.045>.
- [190] R. Huang, X., Mcverry, B., Marambio-Jones, C., Wong, M., Hoek, E., & Kaner, Novel Chlorine Resistant Low-Fouling Ultrafiltration Membrane Based on a Hydrophilic Polyaniline Derivative, *R. Soc. Chem.* (2012). <https://doi.org/10.1039/C5TA00900F>.
- [191] M. Paul, S.D. Jons, Chemistry and fabrication of polymeric nano filtration membranes: A review, *Polymer (Guildf)*. 103 (2016) 417–456. <https://doi.org/10.1016/j.polymer.2016.07.085>.
- [192] P. Marchetti, A.G. Livingston, Predictive membrane transport models for Organic Solvent Nanofiltration: How complex do we need to be?, *J. Memb. Sci.* 476 (2015) 530–553. <https://doi.org/10.1016/j.memsci.2014.10.030>.

- [193] A. Kudasheva, S. Sorribas, B. Zornoza, C. Téllez, J. Coronas, Pervaporation of water/ethanol mixtures through polyimide based mixed matrix membranes containing ZIF-8, ordered mesoporous silica and ZIF-8-silica core-shell spheres, *J. Chem. Technol. Biotechnol.* 90 (2015) 669–677. <https://doi.org/10.1002/jctb.4352>.
- [194] H. Alhweij, I. Amura, J. Wenk, E.A.C. Emanuelsson, S. Shahid, Self-doped sulfonated polyaniline ultrafiltration membranes with enhanced chlorine resistance and antifouling properties, *J. Appl. Polym. Sci.* (2021) 50756. <https://doi.org/10.1002/app.50756>.

Chapter 2

Self-doped sulfonated polyaniline ultrafiltration membranes with enhanced chlorine resistance and antifouling properties

The work presented in this chapter has been published to Journal of Applied Polymer Science March 2021. Alhweij H, Amura I, Wenk J, Emanuelsson EAC, Shahid S. Self-doped sulfonated polyaniline ultrafiltration membranes with enhanced chlorine resistance and antifouling properties. J Appl Polym Sci. 2021;138:e50756. <https://doi.org/10.1002/app.50756>.

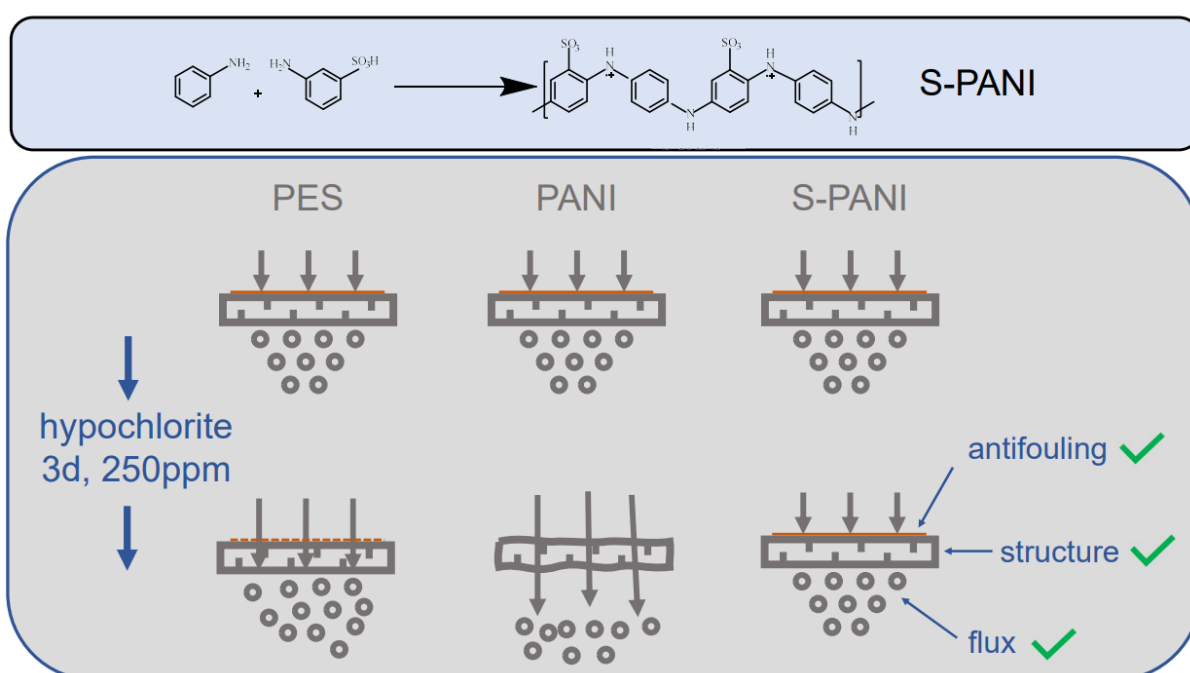
Context:

Improving chlorine stability of membranes consisting of aromatic polymers will be highly advantageous to current membrane-based separation processes which struggle with membrane longevity and unavoidable fouling issues. Membranes heavily rely on chlorination to diminish (bio)fouling growth, but chlorination can also lead to membrane degradation. The potential cost savings are associated with chlorine tolerant membranes and as such, waiving the need for existing dechlorination and re-chlorination processes applied upstream and downstream of the membranes. This work aims at developing chlorine tolerant self-doped sulfonated polyaniline (S-PANI) membranes that can overcome the current limitations of its precursor i.e., polyaniline (PANI) membranes, such as chlorine degradation and low fouling resistance. The S-PANI polymer was prepared in-situ and membranes were fabricated through Non-solvent Induced Phase Separation (NIPS) technique. The membranes' performance was evaluated under harsh chlorine conditions (250 ppm hypochlorite for three days under different conditions). The S-PANI membranes showed much higher resistance to chlorine compared to lab-fabricated PANI membranes and commercial Polyethersulfone (PES) UF membranes. The S-PANI membranes exhibited a stable pure water flux and complete rejection of *bovine serum albumin* (BSA) on chlorine exposure under different pH conditions. In comparison, on exposure to chlorine, PANI membranes suffered critical structural damage with complete leakage whilst PES membranes showed a 76% increase in pure water flux and a noticeable decrease in BSA rejection due to the poly(vinyl pyrrolidone) (PVP) addition. Additionally, the S-PANI membranes showed better antifouling properties with a high flux recovery ratio in comparison to PANI membranes using *alginate acid*, *humic acid* and BSA model foulants. Chemical cleaning by chlorine hypochlorite re-instated the transport properties to its initial condition. Overall, the high chlorine tolerance and enhanced fouling resistance make S-PANI a promising material to overcome the outstanding challenges (i.e., fouling, membrane longevity and cost) of polymeric membranes.

Contributions:

Hassan Alhweij: Conceptualization, Methodology, Validation, Formal analysis, Investigation, Writing Original Draft, Writing Review & Editing, Visualization; Ida Amura: Writing Review & Editing; Emma Anna Carolina Emanuelsson: Supervision, Funding acquisition; Salman Shahid: Conceptualization, Methodology, Supervision, Project administration, Writing Review & Editing; Jannis Wenk: Conceptualization, Writing Review & Editing, Visualization, Supervision, Project administration, Funding acquisition.

Graphical Abstract



Self-doped sulfonated polyaniline ultrafiltration membranes with enhanced chlorine resistance and antifouling properties

Hassan Alhweij^{a,c,d}, Ida Amura^{a,b}, Jannis Wenk^{a,c,*}, Emma Anna Carolina Emanuelsson^{a,b}, Salman Shahid^{a,b,c,*}

^a Department of Chemical Engineering, University of Bath, Bath BA2 7AY, United Kingdom

^b Centre for Advanced Separations Engineering, University of Bath, Bath BA2 7AY, United Kingdom

^c Water Innovation and Research Centre (WIRC@Bath), University of Bath, Bath, BA2 7AY, United Kingdom

^d Department of process engineering, Stantec UK Limited, Dominion House, Warrington, WA3 6GD, United Kingdom

* Corresponding authors

Jannis Wenk: j.h.wenk@bath.ac.uk

Salman Shahid: ss2840@bath.ac.uk

Abstract

Membranes heavily rely on chlorination to diminish (bio)fouling, but chlorination can also lead to membrane degradation. We developed sulfonated polyaniline (S-PANI) ultrafiltration (UF) membranes with improved chlorine resistance and intrinsic antifouling properties. The S-PANI membranes were synthesised through Non-solvent Induced Phase Separation (NIPS). Membrane performance was evaluated under harsh chlorine conditions (250 ppm sodium hypochlorite for 3 days under different pH conditions). The S-PANI membranes showed improved chlorine resistance including a stable performance without changes in model foulant *BSA* rejection. In contrast, PANI membranes suffered critical structural damage with complete leakage and commercial PES membranes showed a 76% increase in pure water flux and a noticeable change in *BSA* rejection. Small changes in S-PANI membrane performance could be linked to membrane structural changes with pH, as confirmed by SEM, IR spectroscopy, and contact angle measurements. Additionally, the S-PANI membranes showed better antifouling properties with a high flux recovery ratio in comparison to PANI membranes using *alginate acid*, *humic acid* and *BSA* model foulants. Chemical cleaning by sodium hypochlorite re-instated the transport properties to its initial condition. Overall, the developed S-PANI membranes have a high chlorine tolerance and enhanced antifouling properties making them promising for a range of UF membrane applications.

Keywords: Sulfonated polyaniline, chlorine resistant, antifouling, ultrafiltration, water treatment.

2.1 Introduction

Membrane technology has become integral for separation processes in the water industry including seawater desalination [1–3], municipal/industrial wastewater treatment [4,5] and other industries such as food processing [6]. The success of membranes can be attributed to their high separation performance, including consistency in permeate quality, the ease of operation and significant reductions of capital and process costs [7–10]. However, fouling, including biofouling is a critical issue for every membrane system, decreasing the membrane's lifetime and limiting more widespread application [11,12]. Membrane fouling leads to a decrease in process performance by increasing the transmembrane resistance due to blockage of membrane pores and the formation of a fouling layer [13,14]. The type of membrane material plays an important role in the build-up of the fouling layer on the membrane surface. Most commercial pressure-driven membranes are prepared from hydrophobic polymers [15,16]. While hydrophobic membranes allow for high permeance and excellent mechanical properties [17,18], their hydrophobic nature makes them more prone to fouling due to strong hydrophobic interactions between the foulants and the membrane surface [14,19,20].

To remove (bio)fouling layers and limit decreases in process performance, chlorine disinfection is the most commonly applied chemical treatment to the feed stream [21,22]. Chlorine bleach (sodium hypochlorite) is used for routine chemical cleaning tasks (1-5 ppm active chlorine) due to its low cost, its ability to inactivate microorganisms and its removal efficiency of natural organic matter deposits from membrane surfaces [23–25]. However, chlorine is a strong oxidising agent and it attacks the chemical bonds of polymeric membranes, which can lead to a decline in performance due to membrane degradation [26]. Extended exposure to chlorine has been found to impact the physical and chemical properties of membranes more severely than increases in chlorine concentrations. [27].

Upon exposure to free chlorine, amides (N-H) within membranes can be chlorinated to N-Cl which is reversible by reducing agents [28,29]. Electron rich moieties (aromatic rings) are also susceptible to direct chlorination including sequential (step) chlorination of amides followed by intermolecular

rearrangement, forming various aromatic substitution products [30,31]. These reactions are known as N-chlorination and Orton re-arrangement, respectively, and can lead to degradation of membranes by creating void space openings resulting in higher water flux and/or solute carryover into the membrane permeate [8,31].

In typical water treatment works, the feed water is chlorinated to reduce membrane biofouling and then dechlorinated before membrane passage. This protects the membranes from chlorine attack followed by rechlorination to stabilize the water in the distribution network [32]. The chlorination – dechlorination – rechlorination process increases the operational costs for water treatment [33,34]. Chlorine resistant antifouling membranes could save these costs by eliminating the need for dechlorination/rechlorination and by reducing the time and frequency of membrane cleaning cycles [26]. Several methods have been reported to enhance membrane chlorine resistance, for example, replacing amidic hydrogen on the amide linkages with other moieties, for example, methyl or phenyl for polyamide membranes; preventing Orton rearrangement by adding protective groups [30,35] and; grafting the vulnerable active membrane layer with chlorine resistant material [36–38]. However, most of these methods require complex chemistry and membrane treatments and do not enhance antifouling properties. Therefore, developing stable membranes with improved chlorine tolerance and enhanced antifouling properties by appropriate materials and simple methods is of great interest. Among polymeric membrane materials polyaniline (PANI) exhibits good separation characteristics due to the preparation simplicity, high conductivity, simple doping/dedoping chemistry, chemical durability, and relatively low cost [39,40]. PANI can be used as an additive to improve membrane hydrophilicity [41–43]. Spiral-wound PANI membrane modules showed scalability for commercial applications [43].

The introduction of sulfonic acid groups ($-\text{SO}_3\text{H}$) into the aromatic polymers shows significant improvement in chemical and physical properties [44–46]. The incorporation of $-\text{SO}_3\text{H}$ groups into the polymer chain may alter membrane properties such as ion-exchange capacity, hydrophilicity, solubility in polar solvents, and electroactivity over a broad range of pH [47]. Additionally, the internal dopant anion of the sulfonated polymers may suppress anion exchange between the polymer and electrolyte during oxidation and reduction [48]. Polymeric membranes with oxygen and sulfur functional groups

have shown increased chlorine stability [49–52]. Sulfonation of aromatic rings occurs when the sulfur atom of a sulfonating agent binds to atoms with higher electronegativity such as oxygen and acts as electrophilic centre by reacting with the delocalised π electron system of the aromatic ring [53]. The presence of various substituents on the aromatic ring can result in the insertion of the $-\text{SO}_3\text{H}$ group in preferential positions [54] and hence could prevent Orton re-arrangement in the presence of a chlorine residual. The presence of electron-withdrawing sulfonate groups can significantly reduce the electron density on amino groups and the reactivity of polymer backbone with chemical agents.

The aim of this work was to produce chlorine-resistant sulfonated polyaniline (S-PANI) membranes and test them under various fouling and chlorination conditions. S-PANI polymer powder was prepared in-situ and membrane coupons were fabricated at bench-scale through the non-solvent induced phase separation (NIPS) technique. Membrane performance was tested before and after exposure to sodium hypochlorite solution, under different pH conditions, to evaluate chlorine tolerance. The membranes were characterised by Fourier-transform infrared spectroscopy (FT-IR), scanning electron microscopy (SEM), atomic force microscopy (AFM), contact angle and membrane surface charge measurement. Fouling behaviour was determined using the three model foulants *BSA*, *alginate acid* and *humic acid* to cover a wide range of molecular sizes and different charged molecules [55,56]. S-PANI has been used for proton exchange membranes and as co-polymer additive in commercial hydrophobic polymer mixtures to enhance membrane hydrophilicity, which led to high flux recovery [57–59]. The fouling behaviour of S-PANI has been investigated with *BSA* [60]. However, to the knowledge of the authors this is the first study on developing stable S-PANI membranes with improved chlorine resistance including tests on enhanced antifouling properties using a comprehensive set of different model foulants.

2.2 Experiment

2.2.1 Materials

Aniline, ammonium persulfate (APS), hydrochloric acid (HCl), ammonium hydroxide solution, 4-methylpiperidine (4MP), *N*-methyl-2-pyrrolidone (NMP), Polyethylene glycol (PEG) 20/35 kDa, *humic acid* (HA, ~2–500 kDa) as natural organic matter (NOM), *bovine serum albumin* (BSA, ~66 kDa) as protein and *alginic acid* (~12–80 kDa) from Brown algae as polysaccharide were obtained from Sigma-Aldrich, UK. *Methanol*, 3-aminobenzene sulfonic acid (metanilic acid), sodium hypochlorite and sodium hydroxide (NaOH) were obtained from VWR, UK. PET/PBT non-woven backing layer - Novatexx 2484 (120 μ m) was supplied by Freudenberg Filter technologies (Germany). Commercial UF PES membrane (Molecular weight cut-off [MWCO] 30 kDa) was sourced by Sartorius, Germany. All materials were used as received. All solutions were prepared with deionised (DI) water.

2.2.2 Synthesis of PANI and S-PANI polymers

Sulfonation reaction of aniline monomer before polymerisation (pre-sulfonation) has been reported to form S-PANI [60,61]. In this work, S-PANI polymer synthesis was modified for better polymer processability and higher membrane performance.

S-PANI was synthesised by radical polymerisation of aniline and metanilic acid in the presence of ammonium persulfate in acidic medium. For synthesis, aniline was added to HCl aqueous solution (1.0 M). The mixture was poured into glass beaker surrounded by ice for cooling. metanilic acid was added to the aniline-hydrochloric acid mixture and stirred for 5 min using an overhead mechanical mixer fitted with a Teflon coated impeller. In a separate beaker, APS was dissolved in HCl aqueous solution (1.0 M). The APS-HCl solution was added into the aniline beaker dropwise using a peristaltic pump to allow control over the reaction temperature and formation of a reasonably long-chain polymer. The aniline, metanilic acid and APS molar ratio was 1:1. After a reaction period of 24 h, which involves APS addition and extended stirring, the solution was filtered (Whatman paper) and washed multiple times with pure water and then *Methanol* until a neutral pH of the washing solution was reached. Subsequently, the powder was placed in 200 mL of ammonium hydroxide solution (1.0 M) and left to

mix using a magnetic stirrer for 1.0 h at room temperature to deprotonate the polymer salt to its base form. The powder was washed with pure water, followed by *Methanol*/water (50%, w/v), and rinsing with pure water. The filtered polymer powder was dried under vacuum for 24 h at 60°C. The dry S-PANI powder was grounded and then passed through fine mesh screen to remove any remaining clusters leaving a fine powder with 72±1% yield based on the aniline monomer. The powder was stored in plastic vials until required. Fig. 2.1 shows the chemical structure of the formed S-PANI with sulfonate functional group binding with the aromatic benzene ring. PANI was synthesised by an established method [62].

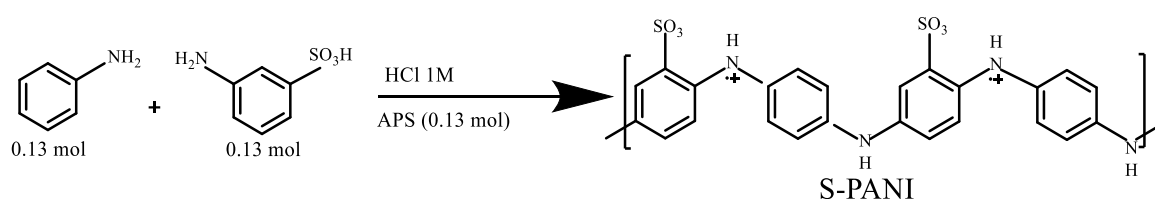


Fig. 2.1. Polymerisation scheme for S-PANI.

2.2.3 Membrane fabrication

Non-Solvent Induced Phase Separation (NIPS) was used to prepare all membranes with DI water as a coagulation bath at room temperature. To prepare the polymer solution, S-PANI (20 wt%) was added in small portions to the mixture of *NMP* (74 wt%) and anti-gelling agent 4MP (6 wt%) using a funnel (1 h). The mixture was stirred at 100 rpm for 2 h until a homogeneous solution was achieved and then left stirring at 50 rpm overnight. The polymer solution was left unstirred for 12 h for deaeration. Viscosity tests were performed using a stress-controlled rheometer (Discovery HR-3, TA Instruments, USA) equipped with a sandblasted plate-plate stainless steel geometry (40 mm) at 25°C. Approximately 1 mL of the sample was placed between the plates (with a plate-plate gap of 0.5 mm) and the flow curve was measured to study the viscosity response of the sample to shearing, with a shear rate ranging from 0.01 to 100 s⁻¹. The measured viscosity of the S-PANI polymer solution at 25°C was 14.6 Pa.s.

The support layer (Novatexx 2484) was placed on a flat glass plate before casting. Elcometer 3540 film applicator was used to cast 200 µm (clearance gap) membranes at room temperature and controlled relative humidity of ~30%. The membrane was formed after immersion precipitation in a pure water

bath at room temperature considering a consistent evaporation time of 10 s before immersing the polymer solution into the coagulation bath. All membranes were kept immersed in DI water at room temperature for at least 24 h and then rinsed with freshwater and stored in pure water until used for further characterisation. PANI membranes were prepared in the same way. Tensile strength, Young's modulus and % elongation at break of the S-PANI membranes were measured to assess the effect of the sulfonation to the membranes' mechanical properties. An Instron 3369 mechanical tester was used and the dried membrane casts without support layer were cut into rectangular strips of approximately 6×70 mm for testing. All tests were conducted with a pull speed of 2 mm min^{-1} at room temperature. Membrane thickness was measured using standard Vernier callipers.

2.2.4. Membrane characterization

Fourier-transform infrared spectroscopic analysis

The Fourier-transform infrared (FTIR) spectra of the pristine and sodium hypochlorite solution exposed membranes were obtained by using an FTIR Spectrometer (PerkinElmer, USA) fitted with an attenuated total reflectance (ATR) detector. A background scan was run prior to sample testing and spectra were recorded from 4000 to 650 cm^{-1} in transmission mode with a spectral resolution of 4 cm^{-1} and 32 scans.

Morphology

Cross-section morphologies and the surface images of the membranes were obtained using a JEOL JSM-6301F, Germany, scanning electron microscopy (SEM). The cross-sectional samples were prepared by freeze fracturing in liquid nitrogen to obtain a smooth cross-section. The samples were coated with a thin gold layer using a sputter coater (Q150T S, Quorum) to reduce electron charging. A voltage of 10 kV was used for all SEM cross section and surface images.

The topography of the membrane surface and roughness were determined by Nanoscope IIIa, Digital Instruments Atomic force microscopy (AFM). Non-contact probe (Nu Nano Ltd, UK) was used to ensure soft tapping mode in air.

Surface charge

Membrane surface charge measurement was carried out by using Zetasizer nano series model ZS, Malvern-Panalytical, UK. Zeta potential planar cell (ZEN 1020) along with tracer particles (Latex

beads, polystyrene 0.3 μm mean particle size) were used to measure the electrophoretic mobility of the particles at varying distances from the planar surface at consistent and neutral pH value.

Permeance and rejection test

Membrane permeance and rejection tests were carried out using stainless steel chemically resistant dead-end cell (Sterlitech HP4750) with an active membrane area of 14.6 cm^2 . Permeate flow rates were measured using a digital scale connected to a computer.

BSA (MW~66 kDa 6 nm in diameter [55]) solution (1 g/L) was used at neutral pH to evaluate the membrane rejection properties before and after chlorination using the dead-end cell set-up.

The *BSA* concentration in the feed and permeate samples were measured through the surrogate UV absorbance using Agilent Carry 100 UV-Vis spectroscopy.

Free chlorine concentration between 1-5 ppm is used for commercial routine cleaning. To evaluate chlorine tolerance, 250 ppm sodium hypochlorite solution was used at different pH values (4.5, 7.4 and 10.5), in agreement with literature [63–65]. Hypochlorite treatment efficacy is pH-dependent due to dissociation into hypochlorous acid (HOCl) and the less active hypochlorite (OCl^-) [66]. HOCl and OCl^- are the dominant species at pH 4.5 and pH 10.5, respectively, while at pH 7.4 both species are present [61].

Hypochlorite solution is very alkaline due to the presence of sodium hydroxide [57], therefore, the pH of the chlorinated water through sodium hypochlorite solution can increase. PANI responds to pH changes [58] including chlorine attacking the polymer more severely at lower pH. A set of membrane samples were soaked in water at different pH as controls. Chlorine stability was conducted according to literature protocols [26,67,68].

Chlorine solution was prepared by diluting sodium hypochlorite with DI water. The solution pH was adjusted by adding either hydrochloric acid or sodium hydroxide. The sodium hypochlorite solution strength was measured via HACH Pocket Colorimeter™ II chlorine test kit. The sodium hypochlorite solution strength was identical at all pH values.

A fresh membrane coupon was used for each measurement. Fresh membrane coupons were placed in sodium hypochlorite solution for 3 days, using fresh solution every 24 h, while controls were in water at different pH for 3 days. Subsequently, water flux and *BSA* rejection was measured as described above for pristine membranes.

PANI and commercial UF PES membrane coupons were soaked in sodium hypochlorite solution (250 ppm) at pH 7.4 and compared to S-PANI membranes. The MWCO of the S-PANI and the commercial PES membranes was verified by measuring PEG rejection [69].

Hydrophilicity and fouling behaviour

Dynamic droplet penetration over time was measured by using a contact angle goniometer (Contact Angle System OCA 15Pro, Dataphysics, Germany). A small droplet of water (2.0 μL) was placed onto the membrane surface at a dosing rate of 1.0 $\mu\text{L s}^{-1}$ using a Hamilton syringe. The software SCA20 was used to calculate the dynamic effective contact angle (CA) and water droplet height.

Pure water flux (PWF) and organic fouling experiments were carried out using a pilot scale crossflow rig (Fig 2.2) with an active membrane area of 14.6 cm^2 and controlled temperature of $20\pm 0.5^\circ\text{C}$. Membranes were preconditioned at 2 bar until the measured PWF stabilised. Experiments with model foulants (HA, *BSA* and NaAlg) were implemented at initial feed concentration of 100 ppm as total organic carbon (TOC) of each foulant. The fouling behaviour was also investigated over a prolonged period of 24 h by using a mixture of the model foulants with equal TOC surrogate portions to achieve total feed concentration of 100 ppm as TOC. Following that extended fouling time, the membrane flux recovery was measured after physical cleaning (30 min) with pure water and chemical cleaning with sodium hypochlorite solution (5 ppm) for 15 min at neutral pH to prevent the bias of the solution pH to the flux recovery.

Calibration curve of the feed solution TOC and the fouling test were established after passing the feed through 0.45 μm Whatman filter paper to ensure that the fouling is not biased by any particles. The pH of the feed solution was adjusted (pH 7.0) to prevent the influence on the transport properties by ionic interactions.

Fluxes of the PANI and S-PANI are slightly different [60], and thus fouling load differs. To make fouling behaviour values of the different membranes comparable a flux-step method was adopted [70,71]. The applied pressure was maintained by the dual-acting pump on the feed stream. The permeation rate was gradually increased and the pressure change was continuously monitored by precise pressure transducer (model PXM309-007-GI, OEMGA Engineering, UK) situated in the feed line, allowing accurate measurements to be recorded on a computer (Pico data logging system 1000 Series, Pico Technology, UK). Under the experimental conditions, the transmembrane pressure (TMP) assumed to vary only due to fouling.

Membrane fouling indicators were calculated following a literature method [72]. In brief, the PWF was recorded and the membranes were fouled for 1 h. Afterwards, a membrane physical cleaning cycle was initiated with pure water for 30 min and the permeance was recorded. The fouling-cleaning cycle was repeated and the permeance of the PWF after the final physical cleaning was recorded.

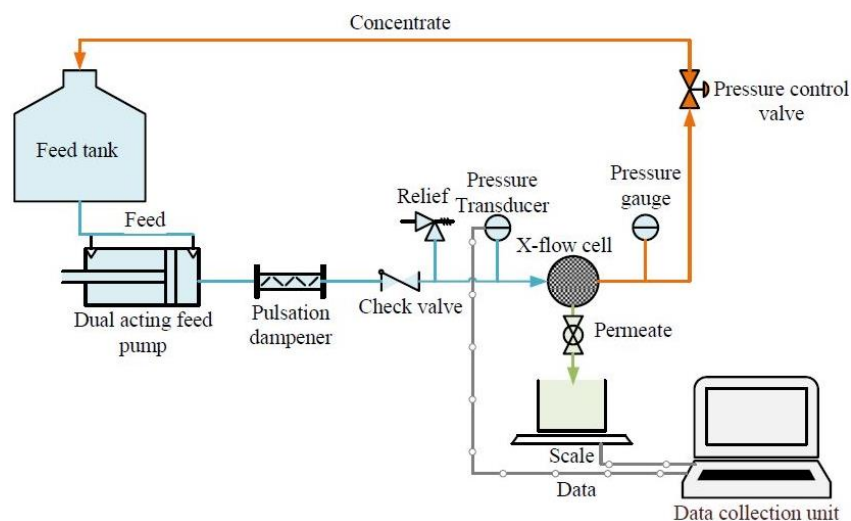


Fig. 2.2. Process flow diagram of the crossflow rig.

2.3 Results and Discussion

2.3.1 FT-IR spectroscopic analysis of membranes

Fig. 2.3 shows FTIR spectra for S-PANI membrane samples soaked in pure water and 250 ppm of sodium hypochlorite solution, respectively, for 3 days at three different pH values (4.5, 7.4 and 10.5). The pristine S-PANI membrane spectrum shows characteristic peaks at 1565, 1498 and 1296 cm^{-1} , corresponding to N = Q = N stretching of the quinoid rings, N – B – N stretching of the benzenoid

rings and C – N – C stretching of the secondary aromatic amine, respectively [73,74]. The peaks at 1169, 1034 and 722 cm^{-1} corresponded to symmetric S = O stretching [75]. The results demonstrate a successful introduction of sulfonate groups into PANI and are in agreement with the literature [57]. Soaking the membranes sample either in water or 250 ppm sodium hypochlorite solution at different pH values did not leave a residual impact on the membrane material and the membrane remains unchanged upon chlorine exposure. However, the FTIR revealed a few minor intensity shifts after being doped with hydrochloric acid at pH 4.5 in consistent with literature [76].

S-PANI membrane Young's modulus was 488 ± 15 MPa, which is almost 6 times higher than the Young's modulus of the PANI membrane reported in literature making the S-PANI membrane more brittle [77]. A high level of sulfonation can make polymeric membranes amorphous and reduce their mechanical strength [78]. The tensile strength and elongation at break of the S-PANI membrane were 3.4 ± 0.3 MPa and $5.6 \pm 1.3\%$, respectively. S-PANI membranes' tensile strength is almost 92% of the PANI counterparts reported elsewhere [62].

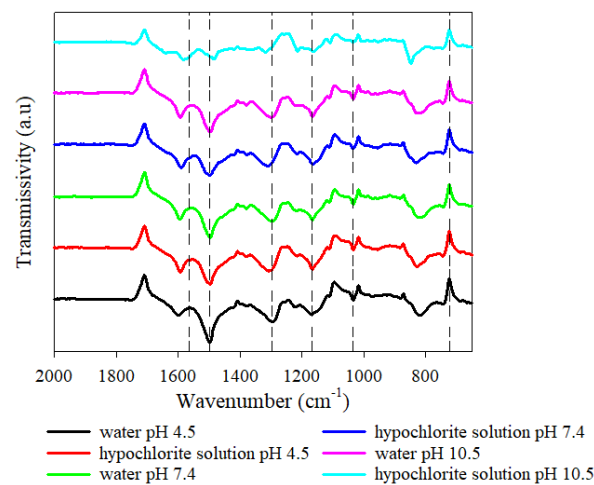


Fig. 2.3 FTIR spectra for S-PANI membrane soaked in water and 250 ppm sodium hypochlorite solution, respectively, at different pH values (4.5, 7.4 and 10.5) for three consecutive days.

2.3.2 Morphology

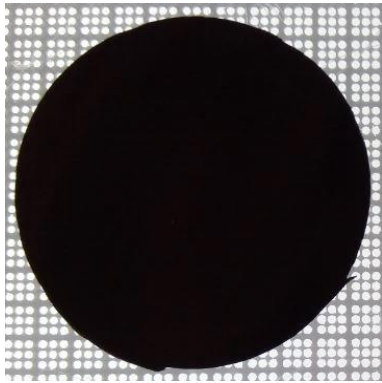
Fig. 2.4(a)-(d) shows the digital backlight photographs of S-PANI and PANI membrane coupons before and after hypochlorite treatment. Visual inspection showed no damage to the membrane surface and no bleaching (colour change) of S-PANI exposed to chlorine (Fig. 2.4(e)). In contrast for the PANI membrane, the hypochlorite solution changed colour indicating polymer degradation (Fig. 2.4(f)). After

placing the chlorinated PANI membrane in the dead-end cell a clear defect at the circumferential part of the membrane coupon developed showing compromised mechanical stability (Fig. 2.4(d)).

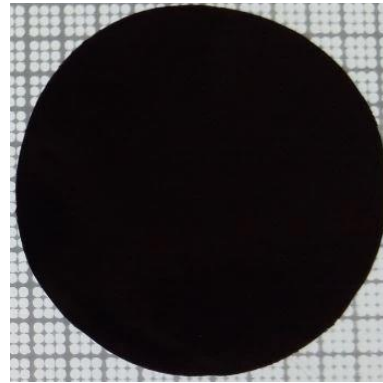
The chlorinated commercial PES membrane did not show any visual surface damage. Fig. 2.5 shows SEM images of the S-PANI membrane surface for samples soaked in water at pH 7.4 (Fig. 2.5(a)) and soaked in hypochlorite solution at different pH values (Fig. 2.5(b)-(d)). There was no indication of deterioration or imperfection on the S-PANI membrane surface after chlorine exposure within the tested pH range. Conversely, SEM images of chlorinated PANI membrane exhibit damages including surface cracks (Fig. 2.5(f)) compared to the pristine membrane (Fig. 2.5(e)). Fig. 2.6 shows SEM images for S-PANI and PANI membrane cross-sections. All membranes exhibit a morphology typical for phase inversion membranes [15,79]. From membrane cross-sectional images, the membrane skin layer appears stable without visible defects, consistent with surface SEM images. The macro-voids of the membranes soaked in water or hypochlorite solution at pH 10.5 showed a pear-like shape with a depth of *circa* 25 μm . A change in membrane macro-void depth was observed as a function of soaking solution pH. The soaked membranes at pH 7.4 and 4.5 exhibit macro-voids up to 25 μm and 14.3 μm depth, respectively. The observed morphology change in the macro-void depth could contribute to the change in membrane permeance as observed in permeation tests. The morphological change is attributed to the shrinkage or swelling of the stimuli responsive membranes when immersed in doping/dedoping solution [80]. Free volume shrinkage may take place while exposing the membrane to reducing agents, which lead to reduction or expulsion of cations. In contrast, free volume swelling occurs by the addition of cations to a fully reduced polymer [81]. This explains the tuneable properties which affect the solution transport and the slight subsequent change in membrane morphology.

Fig. 2.6(e),(f) confirm structural deterioration of PANI on exposure to chlorine as previously reported [82]. A slight change in PES surface roughness was observed after exposure to chlorine as shown in Fig. 2.5(g)-(h) whereas no changes were apparent in PES cross-sectional images. The tolerance of PES membrane can be attributed to sulfonyl groups in the polymer backbone, which is formed by the reaction between dihalo-diphenylsulfone and the salt of bisphenol compound [83].

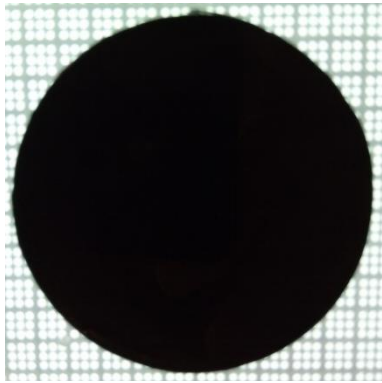
(a) S-PANI in water pH 7.4



(b) S-PANI in hypochlorite solution pH 7.4



(c) PANI in water pH 7.4



(d) PANI in hypochlorite solution pH 7.4



(e) S-PANI in hypochlorite solution pH 7.4



(f) PANI in hypochlorite solution pH 7.4



Fig. 2.4 Digital micrographs of membrane coupons (a, c) pristine control S-PANI and PANI samples before chlorination soaked in pure water at pH 7.4; (b, d) S-PANI and PANI samples after chlorination with 250 ppm sodium hypochlorite solution for three consecutive days at pH 7.4; (e, f) PANI and S-PANI samples soaked in hypochlorite solution at pH 7.4. One square box is 1cm².

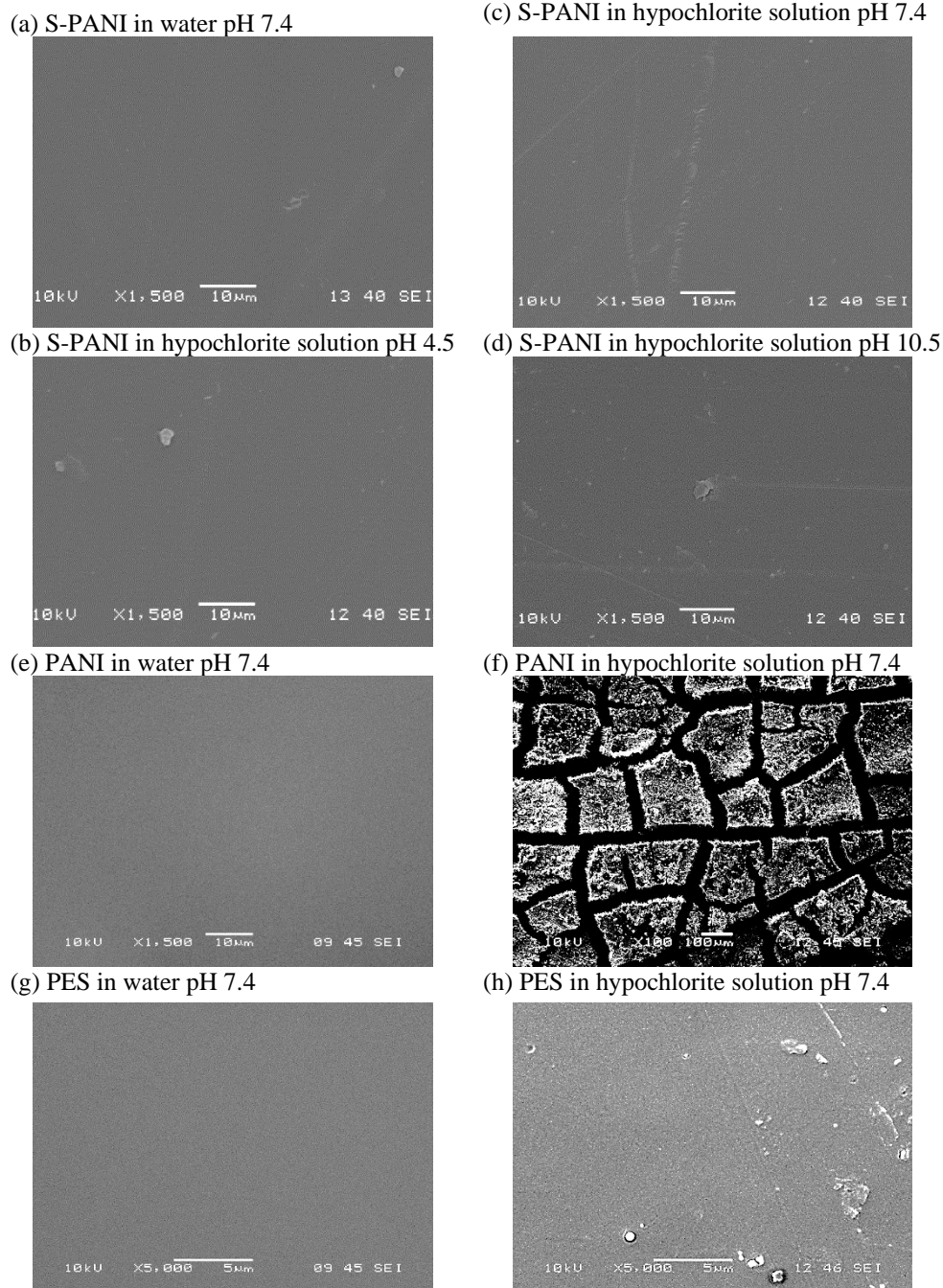


Fig. 2.5 SEM images for S-PANI membrane surface (a) soaked in water at pH 7.4 (b, c, d) soaked in sodium hypochlorite solution at pH 4.5, 7.5 and 10.5 (e) PANI soaked in water pH 7.4 (f) PANI soaked in sodium hypochlorite solution at pH 7.4 (g) PES soaked in water at pH 7.4 (h) PES soaked in sodium hypochlorite solution at pH 7.4.

Since no difference was observed in the S-PANI membrane surface by SEM images, AFM was utilised to analyse the surface topography of the chlorine exposed membranes. Surface roughness plays an important part in the fouling behaviour of membranes, for example, rougher surfaces have higher tendency to trap foulants/particles within the valleys leading to a build-up of a fouling layer [84]. Fig.

2.7 shows the change in surface roughness for S-PANI membrane samples soaked in water at pH 7.4 (Fig 2.7 (a)) and sodium hypochlorite solution at pH 4.5, 7.4 and 10.5 (Fig 2.7 (b), (d) and (c)). AFM micrographs corroborate the results of SEM on the stability of the membrane under chlorine exposure with no observed surface deterioration. SEM and AFM results are consistent with literature findings where a chlorine exposure led to an increase in surface roughness and visible surface defects for chlorine intolerant membranes whilst, no visible effects were observed for chlorine tolerant membranes [85,86].

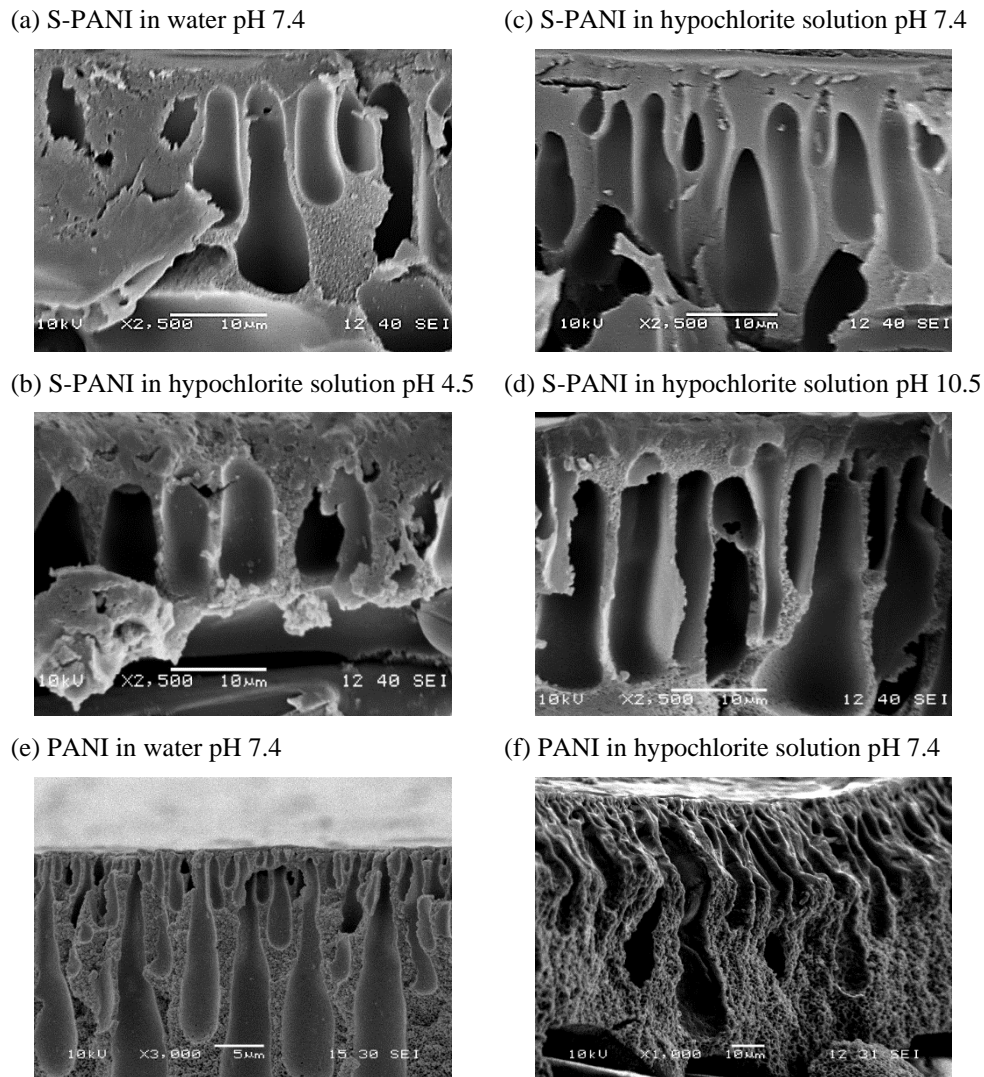
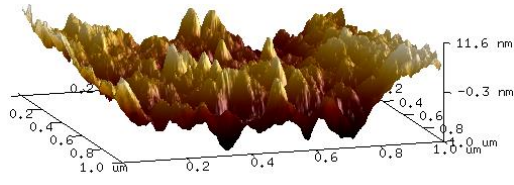
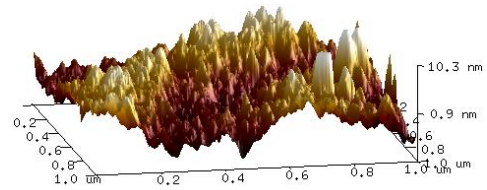


Fig. 2.6 SEM images for membrane cross-section (a) S-PANI soaked in water at pH 7.4, (b, c, d) S-PAN soaked in hypochlorite solution at different pH values 4.5, 7.5 and 10.5, respectively, (e) PANI soaked in water at pH 7.4 (f) PANI soaked in hypochlorite solution at pH 7.4.

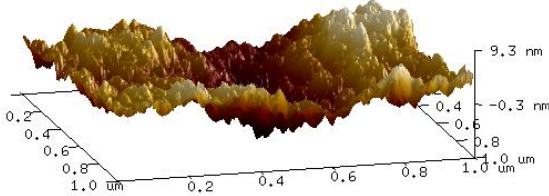
(a) water pH 7.4



(c) hypochlorite solution pH 7.4



(b) hypochlorite solution pH 4.5



(d) hypochlorite solution pH 10.5

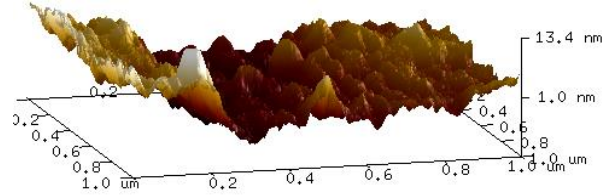


Fig. 2.7 AFM analysis of S-PANI membrane surface (a) soaked in water at pH 7.4 (b, c, d) soaked in hypochlorite solution at different pH values 4.5, 7.5 and 10.5, respectively.

Table 1 illustrates the average roughness (Ra), root mean square roughness (Rq) and the maximum roughness (Rmax) of the S-PANI membrane surface. The data suggests that there is no obvious surface deterioration after the chlorine exposure and the membrane had a smooth surface which is advantageous to prevent entrapments of foulants in the ridge and valley structure.

Table 2.1 The quantification of the AFM roughness data for the S-PANI membrane surface.

Solution	pH	Ra, nm	Rq, nm	Rmax, nm
Water	7.4	2.66	3.34	23.3
Sodium hypochlorite, 250 ppm	4.5	2.28	2.84	16.90
	7.5	2.39	2.92	21.50
	10.5	3.10	3.72	23.70

2.3.3 Surface charge

When S-PANI membranes interacted with the hypochlorite solution, the evolution of surface zeta potential with pH value became evident as shown in Fig. 2.8. For all pH values, the zeta potential of the S-PANI membrane remained positive. The zeta potential of all tested membranes decreased with increasing pH. The charge on S-PANI membranes soaked in hypochlorite solution became less positive

than that of S-PANI membranes soaked in water at neutral pH value. However, at solution pH 4.5 and pH 10.5, the zeta potential of membranes after immersion in water and hypochlorite solution is identical within error margins.

The reported surface charge of PANI emeraldine salt at pH 4.5 is around 20 mV [87] and the measured surface charge of S-PANI membrane, at similar pH, falls within the same range (Fig. 2.8). Note that at lower pH, zeta potential is higher. This can be attributed to the presence of more H^+ ions at lower pH and thus more S-PANI chains are protonated, implying an increase of positive charges on these chains. In contrast, soaking the membrane in higher pH solution enhanced the dedoping process and hence removed all residual protons leading to a decrease in surface zeta potential by 26%. The doping/dedoping process is reversible where dedoping entails the deprotonation of the original polymer without degradation of polymer backbone [88].

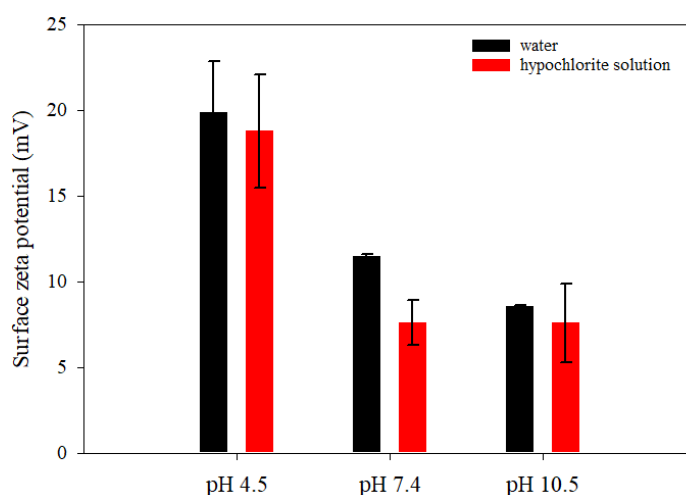


Fig. 2.8 S-PANI membrane surface charge at neutral pH with a standard deviation after soaking in water and 250 ppm sodium hypochlorite solution for three days at different pH values of 4.5, 7.4 and 10.5, respectively.

2.3.4 Permeance and rejection tests

Membrane permeance was evaluated using pure water and *BSA* feed solution. Fig. 2.9 shows S-PANI membrane permeance stability after exposure to chlorine under the different pH conditions. Fig. 2.9(a),(b) show an increase in the steady-state permeance of S-PANI membranes with an increasing pH for both water and hypochlorite solution-soaked membranes. At pH 4.5, for instance, the pure water permeance was $63.9 \text{ L m}^{-2} \text{ h}^{-1} \text{ bar}^{-1}$ compared to $72.3 \text{ L m}^{-2} \text{ h}^{-1} \text{ bar}^{-1}$ at pH 10.5 which measures a 13% increase. The relatively low permeance at pH 4.5 can be associated with doping process forcing the

membrane polymer network to reorganize in order to accommodate the proton and the counterion of the acid [66].

BSA permeance increased with increasing pH, introducing a change of 36%. The relatively low *BSA* permeance at lower pH could be explained by the repulsion between positively charged *BSA* (isoelectric point pH 5) [89] and positively charged S-PANI membrane. The *BSA* permeance of S-PANI membrane, at pH 4.5, accounts only for 39% of pure water permeance due to the accumulation of the *BSA* fouling protein on the membrane surface layer.

The pure water permeance of S-PANI membrane soaked in hypochlorite solution also showed a slight increase in value with pH (2.1% (pH 4.5) to 3.6% (pH 10.5)). Note that this negligible permeance change is not necessarily due to the chlorine oxidant attack to the polymeric structure and can be attributed to the swelling of the membrane with increasing pH [75,90].

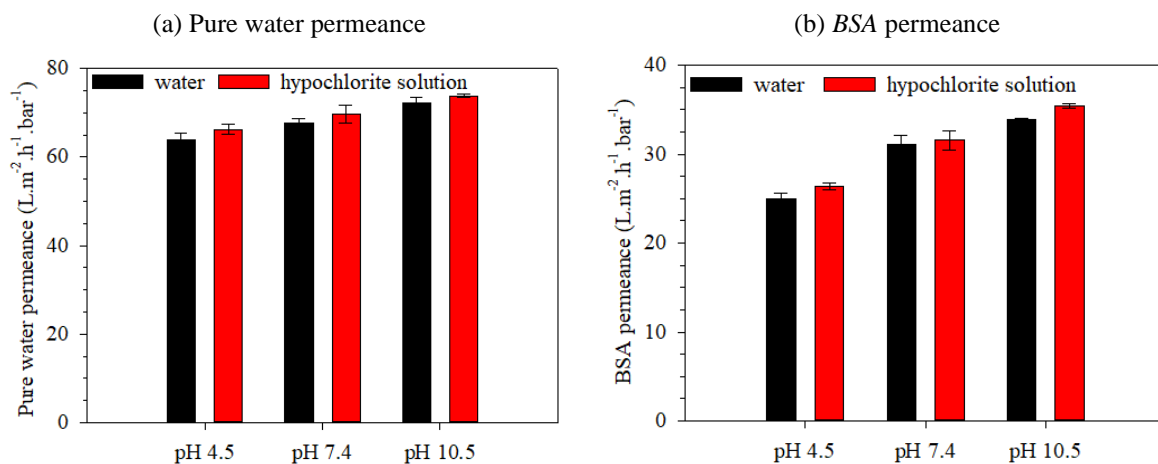


Fig. 2.9 (a) Pure water and (b) *BSA* solution feed permeance of the S-PANI membranes, immersed in water and hypochlorite solution with a standard deviation at different pH values under an applied pressure of 1.0 bar at room temperature.

Fig. 2.10 shows the *BSA* rejection of S-PANI membranes soaked in water and hypochlorite solution at different pH values. The rejection of *BSA* remained almost unchanged for all membranes, which suggests that the interior cross-section (pore size) of the membrane had not been affected by chlorine exposure. The minor difference in *BSA* rejection results was due to the use of different membrane coupons for each measurement.

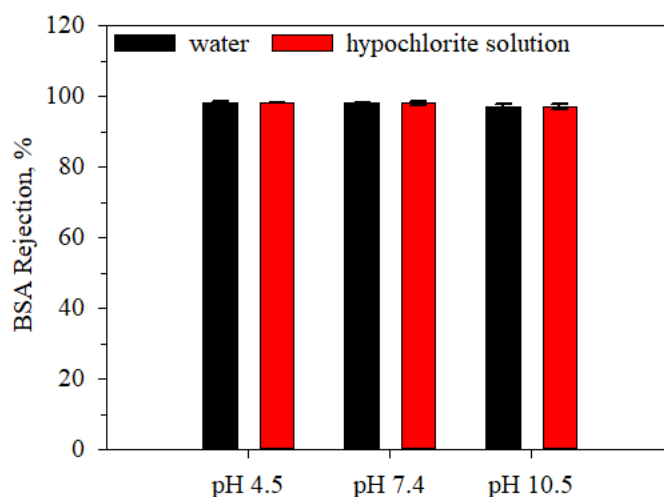


Fig. 2.10 *BSA* rejection of the S-PANI membranes, immersed in water and hypochlorite solution with a standard deviation at different pH values with applied pressure 1.0 bar at room temperature.

Table 2.2 exhibits a noticeable change of the commercial PES membrane pure water permeance and *BSA* rejection before and after exposure to hypochlorite solution at pH 7.4. The observed finding is in agreement with the reported performance of PES membranes on chlorine exposure [91]. PES membranes were selected to emphasise the role of the sulfonated backbone for membrane chlorine stability. Although PES membrane permeance increased by 74% after chlorine exposure, SEM images confirmed that there were no observed structural damages. PES membranes, including the one used, often contain poly(vinyl pyrrolidone) (PVP) as additive to improve the surface hydrophilicity and prevent macro-void formation during membrane preparation. PVP is vulnerable to chlorine attack causing PES/PVP membranes to be more permeable after chlorine treatment [92], which was observed here.

Table 2.2 Pure water permeance and *BSA* rejection with a standard deviation of the S-PANI and commercial PES membranes, immersed in water and 250ppm sodium hypochlorite solution at pH 7.4 for three days at room temperature.

Membrane type	MWCO	Pristine sample*		After sodium hypochlorite exposure (pH 7.4, 3 days at 250 ppm)	
	kDa	Pure water permeance (L m ⁻² h ⁻¹ bar ⁻¹)	<i>BSA</i> rejection (%)	Pure water permeance (L m ⁻² h ⁻¹ bar ⁻¹)	<i>BSA</i> rejection (%)
S-PANI	25±4.0	67.74±1.02	98.0±0.16	69.72±1.93	98.0±0.57
PES	34±6.0	122.0±1.0	100±0.30	215.0±10	94.0±4.3

* Controlled samples soaked in pure water at pH 7.4 before pure water filtration.

2.3.5 Hydrophilicity and fouling behaviour

Hydrophobic and non-polar membranes have a higher tendency to foul [93]. Therefore, highly charged (more hydrophilic), and smooth surface morphology are identified as key features of anti-fouling membranes [94]. Membrane hydrophilicity and the wettability of the prepared S-PANI membranes were determined by the sessile drop contact angle technique. Fig. 2.11 shows that the contact angle remained the same with no noticeable change for S-PANI membranes soaked in water under different pH values. However, the contact angle dropped by 21.5% and 22.0% after soaking the S-PANI membranes in hypochlorite solution at pH 4.5 and 7.4, respectively. Conversely, the S-PANI membrane soaked in hypochlorite solution at pH 10.5 showed a similar contact angle to the samples soaked in water at pH 10.5.

Hypochlorous acid influences the surface characteristics of S-PANI. Therefore, higher exposure levels can induce a higher concentration of ionic moiety in the conducting polymers. The decrease in the contact angles of water for doped S-PANI suggests that the wetting of the water on a doped S-PANI surface is better for low pH than for high pH-soaked S-PANI. This may be indicative of a stronger intermolecular attraction between water and doped S-PANI at lower pH values and less interaction at a higher pH value [62,95]. This also suggests that S-PANI membranes doped at lower pH could form a hydration layer at their surface, which prevents foulants from adsorbing on the surface [96].

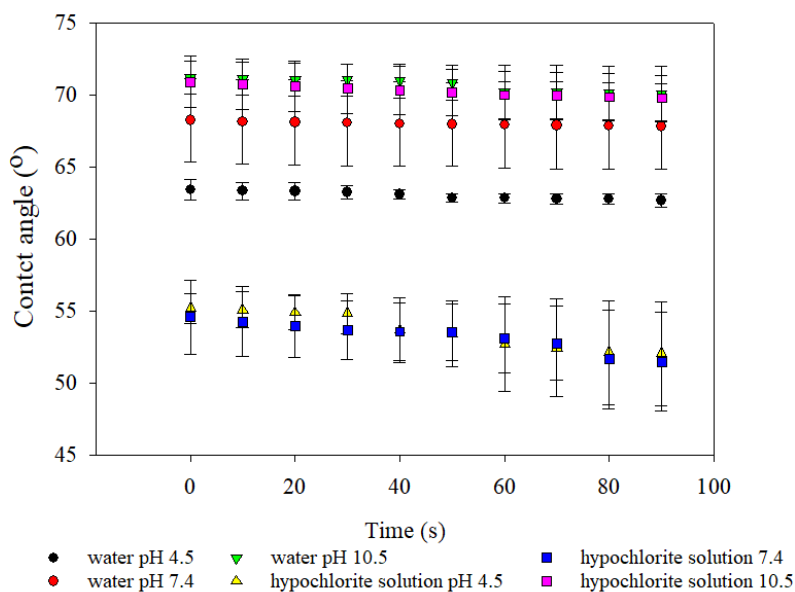


Fig. 2.11 The contact angle of S-PANI membranes immersed in water and hypochlorite solution at different pH values.

The change in the TMP was derived to depict fouling behaviour and identify the critical flux at identical feed concentration and crossflow conditions. Fig. 2.12 shows that a zero rate of TMP increase over time was not obtained, including critical flux, during the trial. However, the experiment provided useful data on comparative fouling propensity. The TMP was slightly increased and then stabilised for an arbitrary test period of 30 min at initial flux (J_0) of 60 to 100 L m⁻² h⁻¹ whereas significant TMP increase was observed at higher flux values for all model foulants. The dramatic TMP increase could be attributed to the exceedance of the foulant convection towards the membrane over the back-transport velocity of the permeate [97]. *Alginate acid* had the highest TMP growth followed by the *humic acids* and the *BSA*. Charged hydrophilic organic macromolecules such as *alginate acid* possess higher intermolecular bridging (gelation) compared to the hydrophobic *humic acids* used here [98]. The bulky nature and the positive charge of the *BSA* molecules which were fully retained by both PANI and S-PANI membranes would have resulted in deposited foulant cake layer without further pore blocking. The hydrodynamic conditions may have created a continuous shear force to the foulant deposits leading to the least TMP growth in comparison with the *alginate acid* and *humic acids*. The S-PANI membrane demonstrated less TMP increase than PANI which could be explained by the reduced foulant adsorption due to the formation of the hydration layer by the zwitterionic surface [58].

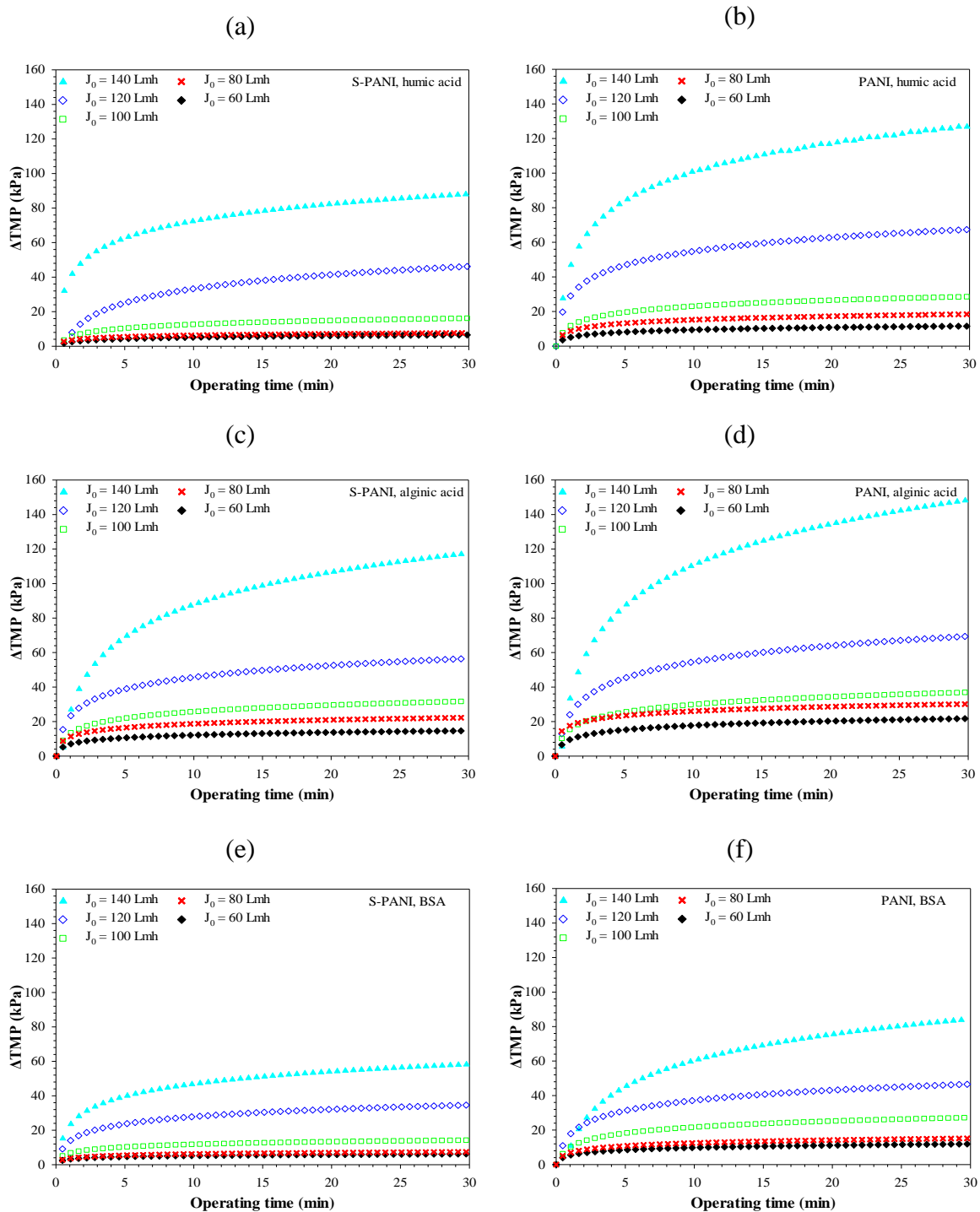


Fig. 2.12 The change in the TMP for S-PANI and PANI membranes while being fouled with *humic acid* (a, b) *alginate acid* (c, d) and *BSA* (e, f), respectively, at different initial flux values (J_0).

Table 2.3 shows the fouling indicators of the PANI and S-PANI membranes. The S-PANI membrane shows excellent antifouling behaviour with lower total fouling rate (F_T) by 44%, 39% and 34% than PANI membranes for *alginate acid*, *humic acid* and *BSA*, respectively. The flux recovery rate (F_r) for

the S-PANI is 84%, 89% and 92% in comparison with 65%, 68%, 77% for the PANI membrane using *alginic acid*, *humic acid* and *BSA*, respectively. Higher Fr% value exhibited intrinsic antifouling properties which could be attributed to the introduction of the sulfonic groups to the polymer backbone [60].

Table 2.3 Fouling indicators for PANI and S-PANI membranes related to the initial cleaning-fouling cycle at equal initial flux.

	Total fouling, F_T %	Reversible fouling, F_{Rev} %	Irreversible fouling, F_{Irr} %
<i>Humic acid</i>			
PANI	51±2	19±1	32±1
S-PANI	20±2	8±1	11±1
<i>Alginic acid</i>			
PANI	56±2	21±1	35±2
S-PANI	25±2	9±1	16±1
<i>BSA</i>			
PANI	41±2	18±2	23±1
S-PANI	14±2	6±1	8±1

Fig. 2.13 shows the fouling behaviour of the PANI and S-PANI membranes with a mixture of model foulant over an extended period of 24 h. Both membranes demonstrated further increase in TMP and flux decline over time in comparison with the use of individual foulants for short test period (30 min). Dramatic performance changes were observed for the first 5 h of operation followed by gradual changes in the next 5 h. However, the performance was stable for the remaining 14 h of the trial period. After the completion of the fouling test, both membranes were flushed with pure water for 30 min and then chemically cleaned with pure water containing 5 ppm of sodium hypochlorite at neutral pH. Chemical cleaning re-established the initial transport properties. S-PANI membranes showed an improved performance demonstrating that sulfonic groups provide intrinsic antifouling properties without the need for additional membrane conditioning.

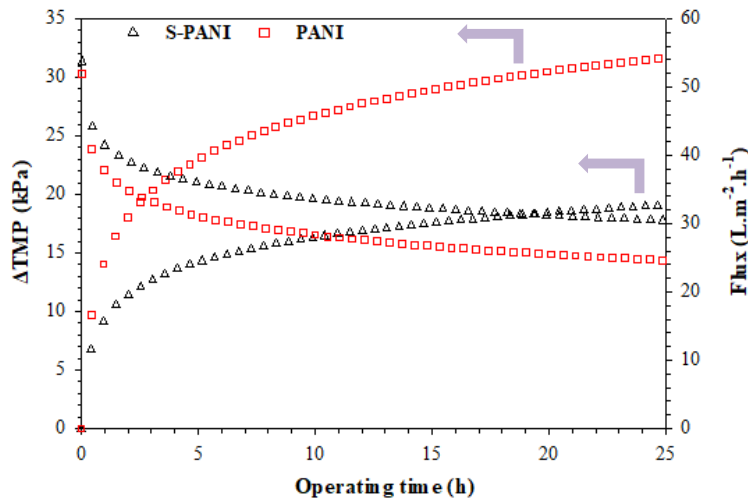


Fig. 2.13 The change in TMP and flux for S-PANI and PANI membranes over a prolonged period of operation using an aqueous solution with a mixture of model foulants (*BSA*, *humic acid* and *alginate*) at feed concentration of 100 mg/L as TOC.

2.4 Conclusions

S-PANI membranes with improved chlorine resistance and enhanced antifouling properties were successfully developed. The S-PANI membranes withstood chlorine exposure at a concentration of 250 ppm of sodium hypochlorite for three consecutive days under different pH values ranging from acidic to basic conditions. S-PANI membrane stability was verified by FTIR spectroscopy, visible inspection, SEM images and, AFM showing no change in membrane polymeric structure on chlorine exposure. Stable S-PANI performance on chlorine exposure was further confirmed by a constant pure water flux and complete rejection of *BSA*. In contrast, PANI membranes suffered critical structural damage and completely lost their ability to reject *BSA*. Furthermore, PES membranes showed 74% increase in pure water permeance and a noticeable change in *BSA* rejection, on chlorine exposure due to the PVP addition to improve the fouling resistance. S-PANI membranes also showed better antifouling properties including a high flux recovery ratio in comparison to the PANI membranes using *alginate*, *humic acid* and *BSA* model foulants. Chemical cleaning by sodium hypochlorite was able to reinstate the initial transport properties of the membranes. SEM, IR spectroscopy, contact angle, and filtration results suggest that the presence of sulfonated groups ($-\text{SO}_3\text{H}$) within the polymer structure is key for enhancing membrane chlorine and fouling resistance. Chlorine resistance and enhanced

antifouling properties make S-PANI a promising material to overcome outstanding challenges, such as, fouling propensity and membrane longevity.

2.5 Acknowledgements

H.A. was funded by a University of Bath for research scholarship (URSA). The authors also thank the technician's team at the Department of Chemical Engineering and the Bio-imaging lab at the University of Bath for support and advice.

2.6 References

- [1] M. Galloway, J. Mahoney, Ultrafiltration for seawater reverse osmosis pretreatment, *Membr. Technol.* (2004) 5–8. [https://doi.org/10.1016/S0958-2118\(04\)00063-1](https://doi.org/10.1016/S0958-2118(04)00063-1).
- [2] E. Gasia-Bruch, P. Sehn, V. García-Molina, M. Busch, O. Raize, M. Negrin, Field experience with a 20,000 m³/d integrated membrane seawater desalination plant in Cyprus, *Desalin. Water Treat.* 31 (2011) 178–189. <https://doi.org/10.5004/dwt.2011.2381>.
- [3] L.K.W. Nazih K. Shammass, *Water Engineering: Hydraulics, Distribution and Treatment*, First, WILEY, 2015.
- [4] J.Z. Leos, A.L. Zydney, *Microfiltration and Ultrafiltration*, Routledge, 2017. <https://doi.org/10.1201/9780203747223>.
- [5] R.W. Baker, Research needs in the membrane separation industry: Looking back, looking forward, *J. Memb. Sci.* 362 (2010) 134–136. <https://doi.org/10.1016/j.memsci.2010.06.028>.
- [6] W. Zhang, N. Grimi, M.Y. Jaffrin, L. Ding, Leaf protein concentration of alfalfa juice by membrane technology, *J. Memb. Sci.* 489 (2015) 183–193. <https://doi.org/10.1016/j.memsci.2015.03.092>.
- [7] F. Knops, S. van Hoof, H. Futselaar, L. Broens, Economic evaluation of a new ultrafiltration membrane for pretreatment of seawater reverse osmosis, *Desalination.* (2007). <https://doi.org/10.1016/j.desal.2006.04.013>.
- [8] J. Suarez, B. Salgado, A. Casanas, J. Carlos Gonzalez, J. Pordomingo, One-year operational experience with ultrafiltration as pretreatment of seawater reverse osmosis desalination system

- (Maspalomas-I Plant), *Desalin. Water Treat.* 55 (2015) 2813–2821. <https://doi.org/10.1080/19443994.2014.959742>.
- [9] S.H. Kim, C.S. Min, J. Cho, Comparison of different pretreatments for seawater desalination, *Desalin. Water Treat.* 32 (2011) 339–344. <https://doi.org/10.5004/dwt.2011.2719>.
- [10] A.R. Guastalli, F.X. Simon, Y. Penru, A. de Kerchove, J. Llorens, S. Baig, Comparison of *DMF* and UF pre-treatments for particulate material and dissolved organic matter removal in SWRO desalination, *Desalination*. 322 (2013) 144–150. <https://doi.org/10.1016/j.desal.2013.05.005>.
- [11] X. Zhao, R. Zhang, Y. Liu, M. He, Y. Su, C. Gao, Antifouling membrane surface construction : Chemistry plays a critical role, *J. Memb. Sci.* 551 (2018) 145–171. <https://doi.org/10.1016/j.memsci.2018.01.039>.
- [12] I.G. Wenten, Khoiruddin, Reverse osmosis applications: Prospect and challenges, *Desalination*. 391 (2016) 112–125. <https://doi.org/10.1016/j.desal.2015.12.011>.
- [13] M.F.A. Goosen, S.S. Sablani, H. Al-Hinai, S. Al-Obeidani, R. Al-Belushi, D. Jackson, Fouling of Reverse Osmosis and Ultrafiltration Membranes: A Critical Review, *Sep. Sci. Technol.* 39 (2005) 2261–2297. <https://doi.org/10.1081/SS-120039343>.
- [14] T. Nguyen, F.A. Roddick, L. Fan, Biofouling of Water Treatment Membranes: A Review of the Underlying Causes, Monitoring Techniques and Control Measures, (2012) 804–840. <https://doi.org/10.3390/membranes2040804>.
- [15] Nidal Hilal; Ahmad Fauzi Ismail; Chris J Wright, *Membrane Fabrication*, CRC Press, 2015. <https://doi.org/10.1201/b18149>.
- [16] S. Rajindar, *Membrane Technology and Engineering for Water Purification - Application, Systems Design and Operation*, (2015) 1–80. <https://doi.org/10.1007/978-1-4613-3135-3>.
- [17] N. Misdan, W.J. Lau, A.F. Ismail, Seawater Reverse Osmosis (SWRO) desalination by thin-film composite membrane—Current development, challenges and future prospects, *Desalination*. 287 (2012) 228–237. <https://doi.org/10.1016/j.desal.2011.11.001>.
- [18] N. Misdan, A.F. Ismail, N. Hilal, Recent advances in the development of (bio)fouling resistant thin film composite membranes for desalination, *Desalination*. 380 (2016) 105–111.

- <https://doi.org/10.1016/j.desal.2015.06.001>.
- [19] N. Hilal, O.O. Ogunbiyi, N.J. Miles, R. Nigmatullin, N. Hilal, O.O. Ogunbiyi, N.J. Miles, R. Nigmatullin, Methods Employed for Control of Fouling in MF and UF Membranes: A Comprehensive Review, 6395 (2007). <https://doi.org/10.1081/SS-200068409>.
- [20] S.F. Anis, R. Hashaikheh, N. Hilal, Reverse osmosis pretreatment technologies and future trends: A comprehensive review, Desalination. 452 (2019) 159–195. <https://doi.org/10.1016/j.desal.2018.11.006>.
- [21] E. Dionisio-Ruiz, J. Pérez, F. Plaza, G. Garralón, A. Garralón, M.A. Gómez, Biofilm evolution in the pretreatment line of a reverse osmosis system, Desalination. 338 (2014) 33–38. <https://doi.org/10.1016/j.desal.2014.01.024>.
- [22] S. Jamaly, N.N. Darwish, I. Ahmed, S.W. Hasan, A short review on reverse osmosis pretreatment technologies, DES. 354 (2014) 30–38. <https://doi.org/10.1016/j.desal.2014.09.017>.
- [23] V. Puspitasari, A. Granville, P. Le-Clech, V. Chen, Cleaning and ageing effect of sodium hypochlorite on polyvinylidene fluoride (PVDF) membrane, Sep. Purif. Technol. 72 (2010) 301–308. <https://doi.org/10.1016/j.seppur.2010.03.001>.
- [24] A. Al-Amoudi, R.W. Lovitt, Fouling strategies and the cleaning system of NF membranes and factors affecting cleaning efficiency, J. Memb. Sci. 303 (2007) 4–28. <https://doi.org/10.1016/j.memsci.2007.06.002>.
- [25] X. Shi, G. Tal, N.P. Hankins, V. Gitis, Fouling and cleaning of ultrafiltration membranes: A review, J. Water Process Eng. 1 (2014) 121–138. <https://doi.org/10.1016/j.jwpe.2014.04.003>.
- [26] J.M. Gohil, A.K. Suresh, Chlorine attack on reverse osmosis membranes: Mechanisms and mitigation strategies, J. Memb. Sci. 541 (2017) 108–126. <https://doi.org/10.1016/j.memsci.2017.06.092>.
- [27] S.Z. Abdullah, P.R. Bérubé, Assessing the effects of sodium hypochlorite exposure on the characteristics of PVDF based membranes, Water Res. 47 (2013) 5392–5399. <https://doi.org/10.1016/j.watres.2013.06.018>.
- [28] Y. Wang, Z. Wang, J. Wang, Lab-scale and pilot-scale fabrication of amine-functional reverse osmosis membrane with improved chlorine resistance and antimicrobial property, J. Memb. Sci.

- 554 (2018) 221–231. <https://doi.org/10.1016/j.memsci.2018.02.062>.
- [29] M. Al-abri, B. Al-ghafri, T. Bora, S. Dobretsov, J. Dutta, S. Castelletto, L. Rosa, A. Boretti, Chlorination disadvantages and alternative routes for biofouling control in reverse osmosis desalination, *Npj Clean Water*. (2019). <https://doi.org/10.1038/s41545-018-0024-8>.
- [30] Ahmadiannamini P., *Encyclopedia of Membranes*, Springer Berlin Heidelberg, Berlin, Heidelberg, 2016. <https://doi.org/10.1007/978-3-662-44324-8>.
- [31] G. Barassi, T. Borrmann, N-chlorination and Orton Rearrangement of Aromatic Polyamides, Revisited, *J. Membr. Sci. Technol.* 02 (2012). <https://doi.org/10.4172/2155-9589.1000115>.
- [32] R. Verbeke, V. Gómez, I.F.J. Vankelecom, Chlorine-resistance of reverse osmosis (RO) polyamide membranes, *Prog. Polym. Sci.* 72 (2017) 1–15. <https://doi.org/10.1016/j.progpolymsci.2017.05.003>.
- [33] H. Huang, S. Lin, L. Zhang, L. Hou, Chlorine-Resistant Polyamide Reverse Osmosis Membrane with Monitorable and Regenerative Sacrificial Layers, *ACS Appl. Mater. Interfaces.* 9 (2017) 10214–10223. <https://doi.org/10.1021/acsami.6b16462>.
- [34] L.F. Greenlee, D.F. Lawler, B.D. Freeman, B. Marrot, P. Moulin, Reverse osmosis desalination: Water sources, technology, and today's challenges, *Water Res.* (2009). <https://doi.org/10.1016/j.watres.2009.03.010>.
- [35] G.M. Geise, H.-S. Lee, D.J. Miller, B.D. Freeman, J.E. McGrath, D.R. Paul, Water purification by membranes: The role of polymer science, *J. Polym. Sci. Part B Polym. Phys.* 48 (2010) 1685–1718. <https://doi.org/10.1002/polb.22037>.
- [36] Y. Yao, W. Zhang, Y. Du, M. Li, L. Wang, X. Zhang, Toward Enhancing the Chlorine Resistance of Reverse Osmosis Membranes: An Effective Strategy via an End-capping Technology, *Environ. Sci. Technol.* 53 (2019) 1296–1304. <https://doi.org/10.1021/acs.est.8b06006>.
- [37] T. Shintani, H. Matsuyama, N. Kurata, Development of a chlorine-resistant polyamide reverse osmosis membrane, *Desalination.* 207 (2007) 340–348. <https://doi.org/10.1016/j.desal.2006.08.009>.

- [38] D. Li, H. Wang, Recent developments in reverse osmosis desalination membranes, *J. Mater. Chem.* 20 (2010) 4551–4566. <https://doi.org/10.1039/b924553g>.
- [39] S. Bhadra, D. Khastgir, N.K. Singha, J. Hee, Progress in Polymer Science Progress in preparation, processing and applications of polyaniline, 34 (2009) 783–810. <https://doi.org/10.1016/j.progpolymsci.2009.04.003>.
- [40] X. Zhang, J. Zhu, N. Haldolaarachchige, J. Ryu, D.P. Young, S. Wei, Z. Guo, Synthetic process engineered polyaniline nanostructures with tunable morphology and physical properties, *Polymer (Guildf)*. 53 (2012) 2109–2120. <https://doi.org/10.1016/j.polymer.2012.02.042>.
- [41] N. Faizah, A. Wahab, N. Hilal, C. Peng, J. Alam, Optimisation of polyethersulfone / polyaniline blended membranes using response surface methodology approach, *DES*. 311 (2013) 182–191. <https://doi.org/10.1016/j.desal.2012.11.033>.
- [42] S.B. Teli, S. Molina, E.G. Calvo, A.E. Lozano, J. De Abajo, Preparation, characterization and antifouling property of polyethersulfone – PANI / PMA ultra filtration membranes, *DES*. 299 (2012) 113–122. <https://doi.org/10.1016/j.desal.2012.05.031>.
- [43] M. Sairam, X.X. Loh, Y. Bhole, I. Sereewatthanawut, K. Li, A. Bismarck, J.H.G. Steinke, A.G. Livingston, Spiral-wound polyaniline membrane modules for organic solvent nanofiltration (OSN), 349 (2010) 123–129. <https://doi.org/10.1016/j.memsci.2009.11.039>.
- [44] X.-L. Wei, Y.Z. Wang, S.M. Long, C. Bobeczko, A.J. Epstein, Synthesis and Physical Properties of Highly Sulfonated Polyaniline, *J. Am. Chem. Soc.* 118 (1996) 2545–2555. <https://doi.org/10.1021/ja952277i>.
- [45] R.P. Parreño, Y.-L. Liu, A.B. Beltran, M.B. Carandang, Effect of a direct sulfonation reaction on the functional properties of thermally-crosslinked electrospun polybenzoxazine (PBz) nanofibers, *RSC Adv.* 10 (2020) 14198–14207. <https://doi.org/10.1039/D0RA01285H>.
- [46] S. Filice, D. D'Angelo, A. Scarangella, D. Iannazzo, G. Compagnini, S. Scalese, Highly effective and reusable sulfonated pentablock copolymer nanocomposites for water purification applications, *RSC Adv.* 7 (2017) 45521–45534. <https://doi.org/10.1039/C7RA08000J>.
- [47] N. Nishad Fathima, R. Aravindhan, D. Lawrence, U. Yugandhar, T.S.R. Moorthy, B. Unni Nair, SPEEK polymeric membranes for fuel cell application and their characterization: A review, *J.*

- Sci. Ind. Res. (India). 66 (2007) 209–219.
- [48] R.M.Q. Mello, R.M. Torresi, S.I. Córdoba De Torresi, E.A. Ticianelli, Ellipsometric, electrogravimetric, and spectroelectrochemical studies of the redox process of sulfonated polyaniline, *Langmuir*. 16 (2000) 7835–7841. <https://doi.org/10.1021/la000391v>.
- [49] M.T. Tsehaye, S. Velizarov, B. Van der Bruggen, Stability of polyethersulfone membranes to oxidative agents: A review, *Polym. Degrad. Stab.* 157 (2018) 15–33. <https://doi.org/10.1016/j.polymdegradstab.2018.09.004>.
- [50] H.M. Colquhoun, D. Chappell, A.L. Lewis, D.F. Lewis, G.T. Finlan, P.J. Williams, Chlorine tolerant, multilayer reverse-osmosis membranes with high permeate flux and high salt rejection, *J. Mater. Chem.* 20 (2010) 4629–4634. <https://doi.org/10.1039/b926352g>.
- [51] J. Glater, S. Hong, M. Elimelech, The search for a chlorine-resistant reverse osmosis membrane, *Desalination*. 95 (1994) 325–345. [https://doi.org/10.1016/0011-9164\(94\)00068-9](https://doi.org/10.1016/0011-9164(94)00068-9).
- [52] C.H. Lee, J. Spano, J.E. McGrath, J. Cook, B.D. Freeman, S. Wi, Solid-state NMR molecular dynamics characterization of a highly chlorine-resistant disulfonated poly(arylene ether sulfone) random copolymer blended with poly(ethylene glycol) oligomers for reverse osmosis applications, *J. Phys. Chem. B*. 115 (2011) 6876–6884. <https://doi.org/10.1021/jp2015148>.
- [53] J. Kučera, F., & Jančář, Homogeneous and heterogeneous sulfonation of polymers: A review, *Polym. Eng. Sci.* 38 (1998) 783–792.
- [54] Pica M, Sulfonation Reaction. In: Drioli E., Giorno L. (eds) *Encyclopedia of Membranes*, Springer Berlin Heidelberg, Berlin, Heidelberg, 2016. <https://doi.org/10.1007/978-3-662-44324-8>.
- [55] G.R. Guillen, T.P. Farrell, R.B. Kaner, E.M.V. Hoek, Pore-structure, hydrophilicity, and particle filtration characteristics of polyaniline-polysulfone ultrafiltration membranes, *J. Mater. Chem.* 20 (2010) 4621–4628. <https://doi.org/10.1039/b925269j>.
- [56] E.L. Sharp, S.A. Parsons, B. Jefferson, Seasonal variations in natural organic matter and its impact on coagulation in water treatment, 363 (2006) 183–194. <https://doi.org/10.1016/j.scitotenv.2005.05.032>.

- [57] B.T. McVerry, J.A.T. Temple, X. Huang, K.L. Marsh, E.M. V. Hoek, R.B. Kaner, Fabrication of Low-Fouling Ultrafiltration Membranes Using a Hydrophilic, Self-Doping Polyaniline Additive, *Chem. Mater.* 25 (2013) 3597–3602. <https://doi.org/10.1021/cm401288r>.
- [58] G. Rong, D. Zhou, J. Pang, Preparation of high-performance antifouling polyphenylsulfone ultrafiltration membrane by the addition of sulfonated polyaniline, *J. Polym. Res.* 25 (2018) 0–8. <https://doi.org/10.1007/s10965-018-1463-0>.
- [59] R.-H. Wu, M.-J. Tsai, K.-S. Ho, T.-E. Wei, T.-H. Hsieh, Y.-K. Han, C.-W. Kuo, P.-H. Tseng, Y.-Z. Wang, Sulfonated polyaniline nanofiber as Pt-catalyst conducting support for proton exchange membrane fuel cell, *Polymer (Guildf)*. 55 (2014) 2035–2043. <https://doi.org/10.1016/j.polymer.2014.02.066>.
- [60] I.F. Amura, S. Shahid, A. Sarihan, J. Shen, D.A. Patterson, E.A.C. Emanuelsson, Fabrication of self-doped sulfonated polyaniline membranes with enhanced antifouling ability and improved solvent resistance, *J. Memb. Sci.* (2019) 117712. <https://doi.org/10.1016/j.memsci.2019.117712>.
- [61] Y. Yang, Y. Min, J. Wu, D.J. Hansford, S.E. Feinberg, A.J. Epstein, Synthesis and Characterization of Cytocompatible Sulfonated Polyanilines a, (2011) 887–892. <https://doi.org/10.1002/marc.201100095>.
- [62] L. Xu, S. Shahid, A.K. Holda, E.A.C. Emanuelsson, D.A. Patterson, Stimuli responsive conductive polyaniline membrane: In-filtration electrical tuneability of flux and MWCO, *J. Memb. Sci.* 552 (2018) 153–166. <https://doi.org/10.1016/j.memsci.2018.01.070>.
- [63] R. Huang, X., Mcverry, B., Marambio-Jones, C., Wong, M., Hoek, E., & Kaner, Novel Chlorine Resistant Low-Fouling Ultrafiltration Membrane Based on a Hydrophilic Polyaniline Derivative, *R. Soc. Chem.* (2012). <https://doi.org/10.1039/C5TA00900F>.
- [64] H.B. Park, B.D. Freeman, Z.B. Zhang, M. Sankir, J.E. McGrath, Highly chlorine-tolerant polymers for desalination, *Angew. Chemie - Int. Ed.* 47 (2008) 6019–6024. <https://doi.org/10.1002/anie.200800454>.
- [65] Y.N. Kwon, S. Hong, H. Choi, T. Tak, Surface modification of a polyamide reverse osmosis membrane for chlorine resistance improvement, *J. Memb. Sci.* 415–416 (2012) 192–198.

- <https://doi.org/10.1016/j.memsci.2012.04.056>.
- [66] S.M.J. Zaidi, K.S. Lakhi, Sulfonated Aromatic Polymer, in: *Encycl. Membr.*, Springer Berlin Heidelberg, Berlin, Heidelberg, 2016: pp. 1842–1844. https://doi.org/10.1007/978-3-662-44324-8_560.
- [67] J. Xue, Z. Jiao, R. Bi, R. Zhang, X. You, F. Wang, L. Zhou, Y. Su, Z. Jiang, Chlorine-resistant polyester thin film composite nanofiltration membranes prepared with B-cyclodextrin, *J. Memb. Sci.* 584 (2019) 282–289. <https://doi.org/10.1016/j.memsci.2019.04.077>.
- [68] Y.J. Kim, K.S. Lee, M.H. Jeong, J.S. Lee, Highly chlorine-resistant end-group crosslinked sulfonated-fluorinated poly(arylene ether) for reverse osmosis membrane, *J. Memb. Sci.* 378 (2011) 512–519. <https://doi.org/10.1016/j.memsci.2011.05.040>.
- [69] L. Xu, S. Shahid, J. Shen, E.A.C. Emanuelsson, D.A. Patterson, A wide range and high resolution one-filtration molecular weight cut-off method for aqueous based nanofiltration and ultrafiltration membranes, *J. Memb. Sci.* 525 (2017) 304–311. <https://doi.org/10.1016/j.memsci.2016.12.004>.
- [70] P. Le Clech, B. Jefferson, I.S. Chang, S.J. Judd, Critical flux determination by the flux-step method in a submerged membrane bioreactor, *J. Memb. Sci.* 227 (2003) 81–93. <https://doi.org/10.1016/j.memsci.2003.07.021>.
- [71] P. van der Marel, A. Zwijnenburg, A. Kemperman, M. Wessling, H. Temmink, W. van der Meer, An improved flux-step method to determine the critical flux and the critical flux for irreversibility in a membrane bioreactor, *J. Memb. Sci.* 332 (2009) 24–29. <https://doi.org/10.1016/j.memsci.2009.01.046>.
- [72] S. Al Aani, C.J. Wright, N. Hilal, Investigation of UF membranes fouling and potentials as pre-treatment step in desalination and surface water applications, *Desalination*. 432 (2018) 115–127. <https://doi.org/10.1016/j.desal.2018.01.017>.
- [73] S. Bhadra, N.H. Kim, J.H. Lee, Synthesis of water soluble sulfonated polyaniline and determination of crystal structure, *J. Appl. Polym. Sci.* 117 (2010) 2025–2035. <https://doi.org/10.1002/app.32152>.

- [74] S.S. An, H.H. Yoon, G. Das, Amperometric urea biosensors based on sulfonated graphene/polyaniline nanocomposite, *Int. J. Nanomedicine*. (2015) 55. <https://doi.org/10.2147/IJN.S88315>.
- [75] L. Li, S. Shahid, D. Alec, E. Anna, C. Emanuelsson, Flexible electro-responsive in-situ polymer acid doped polyaniline membranes for permeation enhancement and membrane fouling removal, *578 (2019) 263–272*. <https://doi.org/10.1016/j.memsci.2018.09.070>.
- [76] L. Wen, N. Kocherginsky, Doping-dependent ion selectivity of polyaniline membranes, *Synth. Met.* 106 (1999) 19–27. [https://doi.org/10.1016/S0379-6779\(99\)00098-3](https://doi.org/10.1016/S0379-6779(99)00098-3).
- [77] P. Chapman, X.X. Loh, A.G. Livingston, K. Li, T.A.C. Oliveira, Polyaniline membranes for the dehydration of *tetrahydrofuran* by pervaporation, 309 (2008) 102–111. <https://doi.org/10.1016/j.memsci.2007.10.016>.
- [78] M. Tohidian, S.R. Ghaffarian, S.E. Shakeri, G. Bahlakeh, Sulfonated Aromatic Polymers and Organically Modified Montmorillonite Nanocomposite Membranes for Fuel Cells Applications, *J. Macromol. Sci. Part B.* 52 (2013) 1578–1590. <https://doi.org/10.1080/00222348.2013.789364>.
- [79] M. Mulder, *Basic Principles of Membrane Technology*, Springer Netherlands, Dordrecht, 1996. <https://doi.org/10.1007/978-94-009-1766-8>.
- [80] E.M. Andrade, Volume Changes of Poly(2-methylaniline) upon Redox Switching Anion and Relaxation Effects, *Electrochem. Solid-State Lett.* 3 (1999) 504. <https://doi.org/10.1149/1.1391192>.
- [81] D.L. Pile, Y. Zhang, A.C. Hillier, Electrochemically Modulated Permeability of Poly(aniline) and Composite Poly(aniline)–Poly(styrenesulfonate) Membranes, *Langmuir*. 22 (2006) 5925–5931. <https://doi.org/10.1021/la060255b>.
- [82] X. Huang, B.T. McVerry, C. Marambio-Jones, M.C.Y. Wong, E.M.V. Hoek, R.B. Kaner, Novel chlorine resistant low-fouling ultrafiltration membrane based on a hydrophilic polyaniline derivative, *J. Mater. Chem. A.* 3 (2015) 8725–8733. <https://doi.org/10.1039/c5ta00900f>.
- [83] S. Ida, PES (Poly(ether sulfone)), Polysulfone, in: *Encycl. Polym. Nanomater.*, Springer Berlin Heidelberg, Berlin, Heidelberg, 2014: pp. 1–8. <https://doi.org/10.1007/978-3-642-36199->

9_238-1.

- [84] Z. Steiner, J. Miao, R. Kasher, Development of an oligoamide coating as a surface mimetic for aromatic polyamide films used in reverse osmosis membranes, *Chem. Commun.* 47 (2011) 2384–2386. <https://doi.org/10.1039/c0cc04379f>.
- [85] Y.J. Tang, Z.L. Xu, S.M. Xue, Y.M. Wei, H. Yang, A chlorine-tolerant nanofiltration membrane prepared by the mixed diamine monomers of PIP and BHTTM, *J. Memb. Sci.* 498 (2016) 374–384. <https://doi.org/10.1016/j.memsci.2015.10.028>.
- [86] Y.-J. Tang, Z.-L. Xu, S.-M. Xue, Y.-M. Wei, H. Yang, Improving the chlorine-tolerant ability of polypiperazine-amide nanofiltration membrane by adding NH₂-PEG-NH₂ in the aqueous phase, *J. Memb. Sci.* 538 (2017) 9–17. <https://doi.org/10.1016/j.memsci.2017.05.049>.
- [87] N. Wang, J. Li, W. Lv, J. Feng, W. Yan, Synthesis of polyaniline/TiO₂ composite with excellent adsorption performance on acid red G, *RSC Adv.* 5 (2015) 21132–21141. <https://doi.org/10.1039/c4ra16910g>.
- [88] T.-H. Le, Y. Kim, H. Yoon, Electrical and Electrochemical Properties of Conducting Polymers, *Polymers (Basel)*. 9 (2017) 150. <https://doi.org/10.3390/polym9040150>.
- [89] R. Li, Z. Wu, Y. Wang, L. Ding, Y. Wang, Role of pH-induced structural change in protein aggregation in foam fractionation of *bovine serum albumin*, *Biotechnol. Reports*. 9 (2016) 46–52. <https://doi.org/10.1016/j.btre.2016.01.002>.
- [90] J. Shen, S. Shahid, A. Sarihan, D.A. Patterson, E.A.C. Emanuelsson, Effect of polyacid dopants on the performance of polyaniline membranes in organic solvent nanofiltration, *Sep. Purif. Technol.* 204 (2018) 336–344. <https://doi.org/10.1016/j.seppur.2018.04.034>.
- [91] Y. Kourde-Hanafi, P. Loulergue, A. Szymczyk, B. Van der Bruggen, M. Nachtnebel, M. Rabiller-Baudry, J.L. Audic, P. Pölt, K. Baddari, Influence of PVP content on degradation of PES/PVP membranes: Insights from characterization of membranes with controlled composition, *J. Memb. Sci.* 533 (2017) 261–269. <https://doi.org/10.1016/j.memsci.2017.03.050>.
- [92] C.. Wienk, I.M., Meuleman, E.E.B., Borneman, Z., van den Boomgaard, T. and Smolders, Chemical treatment of membranes of a polymer blend: Mechanism of the reaction of

- hypochlorite with poly(vinyl pyrrolidone), *Polym. Sci. A Polym. Chem.* 33 (1995).
<https://doi.org/10.1002/pola.1995.080330105>.
- [93] A. Matin, Z. Khan, S.M.J. Zaidi, M.C. Boyce, Biofouling in reverse osmosis membranes for seawater desalination: Phenomena and prevention, *Desalination*. 281 (2011) 1–16.
<https://doi.org/10.1016/j.desal.2011.06.063>.
- [94] D. Norberg, S. Hong, J. Taylor, Y. Zhao, Surface characterization and performance evaluation of commercial fouling resistant low-pressure RO membranes, 202 (2007) 45–52.
<https://doi.org/10.1016/j.desal.2005.12.037>.
- [95] M.J. Liu, K. Tzou, R.V. Gregory, Influence of the doping conditions on the surface energies of conducting polymers, *Synth. Met.* 63 (1994) 67–71. [https://doi.org/10.1016/0379-6779\(94\)90251-8](https://doi.org/10.1016/0379-6779(94)90251-8).
- [96] I. Banerjee, R.C. Pangule, R.S. Kane, Antifouling coatings: Recent developments in the design of surfaces that prevent fouling by proteins, bacteria, and marine organisms, *Adv. Mater.* 23 (2011) 690–718. <https://doi.org/10.1002/adma.201001215>.
- [97] X. Li, J. Li, Critical Flux, in: *Encycl. Membr.*, Springer Berlin Heidelberg, Berlin, Heidelberg, 2015: pp. 1–3. https://doi.org/10.1007/978-3-642-40872-4_2193-1.
- [98] S. Lee, M. Elimelech, Relating Organic Fouling of Reverse Osmosis Membranes to Intermolecular Adhesion Forces, *Environ. Sci. Technol.* 40 (2006) 980–987.
<https://doi.org/10.1021/es051825h>.

Chapter 3

Simplified in-situ tailoring of cross-linked self-doped sulfonated polyaniline (S-PANI) membranes for nanofiltration applications

The work presented in this chapter has been published to Journal of Membrane Science July 2021. H. Alhweij, E.A. Carolina Emanuelsson, S. Shahid, J. Wenk, Simplified in-situ tailoring of cross-linked self-doped sulfonated polyaniline (S-PANI) membranes for nanofiltration applications, J. Memb. Sci. (2021) 119654. <https://doi.org/10.1016/j.memsci.2021.119654>.

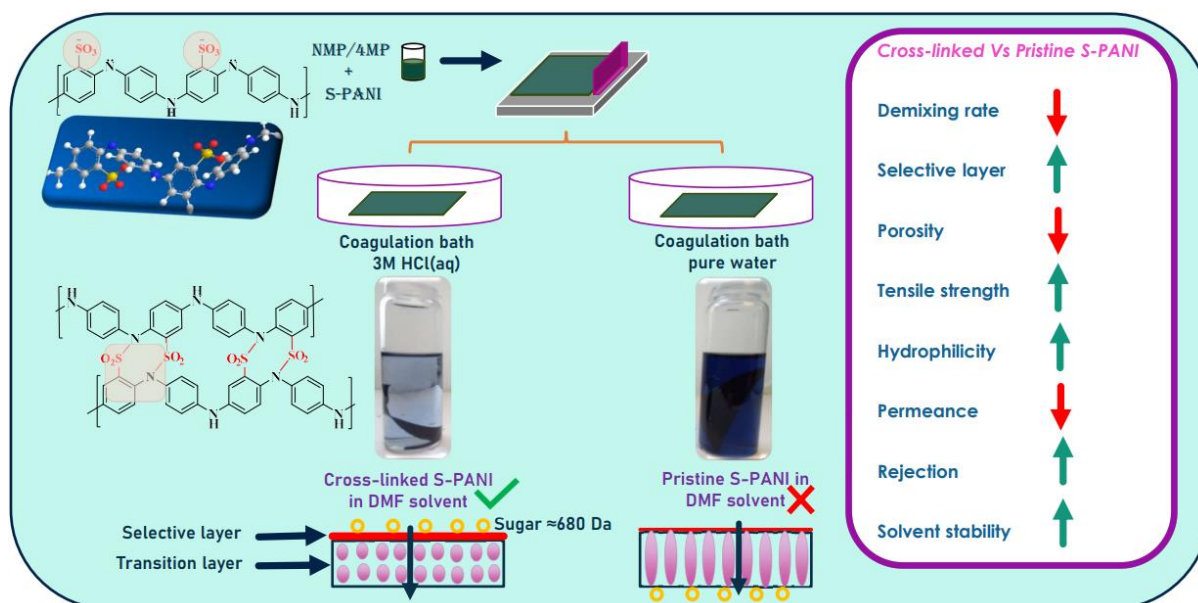
Context:

A simplified and scalable approach for tailoring cross-linked sulfonated polyaniline (S-PANI) membranes at nanofiltration (NF) range could have wide-ranging applications due to their electrical tunability, antifouling behaviour and chlorine resistance. Little work has been done on S-PANI membranes, while recent efforts that are deemed costly, laborious, and complex resulted in tight UF membranes. Developing simple methods for producing cross-linked and solvent stable S-PANI membranes in the NF range is critical for unlocking their full application potential. In this work, the authors systematically investigated, for the first time, the simultaneous cross-linking and coagulation of S-PANI membranes in high acidity solution to produce membranes at the NF range. The proposed procedure is simple, fast, and cost-efficient. Exposing S-PANI casting solution to a high strength acidic coagulation bath could yield cross-linked membranes due to (a) associated acid doping with cross-linking, (b) interaction between sulfonic and amine groups, (c) pH effects on polymer re-assembly and (d) delayed demixing. The chemical analysis indicated a potential interaction between sulfonic groups and nitrogen within S-PANI during the polymer re-assembly process. A loose structure of precipitated polymer particles was observed in pure water compared to a dense and inter-linked structure in an acidic coagulation bath. The simultaneous cross-linking led to an instant formation of a dense skin layer which diminished the solvent/non-solvent exchange rate. This resulted in altered membrane conformation with suppressed macro-voids, reduced porosity, improved tensile strength, enhanced hydrophilicity, and significant improvement in *N,N*-dimethylformamide (*DMF*) solvent stability over an observation time of two weeks. Polyaniline (PANI) membranes formed at the same conditions were dissolved in *DMF*, which reaffirms the sulfonic group's role to facilitate the cross-linking process. In-situ tailored NF S-PANI membranes with $MWCO \approx 680 \text{ g mol}^{-1}$ (sucrose octa-acetate) showed a rejection of 99% for PEG 1000 g mol^{-1} compared to 34% rejection for a commercial membrane with labelled $MWCO 1000 \text{ g mol}^{-1}$. This new simplistic, time, chemical and cost savings scalable approach can be effortlessly applied to design new classes of high-performance S-PANI membranes without the complications of using laborious post modification cross-linking methods.

Contributions:

Hassan Alhweij: Conceptualization, Methodology, Validation, Formal analysis, Investigation, Writing Original Draft, Writing Review & Editing, Visualization; Emma Anna Carolina Emanuelsson: Supervision, Funding acquisition; Salman Shahid: Conceptualization, Methodology, Supervision, Project administration, Writing Review & Editing; Jannis Wenk: Conceptualization, Writing Review & Editing, Visualization, Supervision, Project administration, Funding acquisition.

Graphical Abstract



Simplified in-situ tailoring of cross-linked self-doped sulfonated polyaniline (S-PANI) membranes for nanofiltration applications

Hassan Alhweij^{a,c,d}, Emma Anna Carolina Emanuelsson^{a,b}, Salman Shahid^{a,b,c,*}, Jannis Wenk^{a,c,*}

^a Department of Chemical Engineering, University of Bath, Bath BA2 7AY, United Kingdom

^b Centre for Advanced Separations Engineering, University of Bath, Bath BA2 7AY, United Kingdom

^c Water Innovation and Research Centre (WIRC@Bath), University of Bath, Bath, BA2 7AY, United Kingdom

^d Stantec UK Limited, Dominion House, Warrington, WA3 6GD, United Kingdom

* Corresponding authors

Jannis Wenk: j.h.wenk@bath.ac.uk

Salman Shahid: s.shahid@bath.ac.uk

Abstract

Sulfonated polyaniline (S-PANI) membranes could have wide-ranging applications due to their electrical tunability, antifouling behaviour and chlorine resistance. However, S-PANI membranes below the ultrafiltration (UF) separation range have not been successfully established. This study presents a scalable approach to produce the first in-situ cross-linked S-PANI membranes at nanofiltration (NF) range. S-PANI membranes were produced by non-solvent induced phase separation (NIPS). The presence of sulfonic groups as polymer cross-linking anchors and controlling the coagulation bath's acidic strength resulted in instant stabilisation of the selective layer, which hindered the solvent/non-solvent exchange rate. This enabled the production of a tailored membrane morphology with a dense skin layer, suppressed macro-voids, reduced porosity, enhanced tensile strength, increased hydrophilicity, and solvent stability. S-PANI membranes cast in 3M HCl(aq) with MWCO \approx 680 g mol⁻¹ (sucrose octa-acetate) showed a rejection of 99% for PEG 1000 g mol⁻¹ and 91-100% for dye solution (MW range of 320-1017 g mol⁻¹) compared to 34% and 74-85% rejection for a commercial fluoropolymer membrane (nominal MWCO 1000 g mol⁻¹), respectively. The reported approach is simple and can be applied to design new classes of cross-linked solvent stable S-PANI NF membranes.

Keywords: sulfonated polyaniline, cross-linked, nanofiltration, coagulation bath, acidity

3.1 Introduction

Membrane separation processes are important in numerous industrial applications [1]. Nanofiltration (NF) membranes have been employed in seawater desalination pre-treatment [2], drinking and wastewater treatment [3] and food processing [4]. NF membranes cover a transition region between reverse osmosis (RO) and ultrafiltration (UF) and have a pore size of 1-5 nm with a molecular weight cut off (MWCO) of 200-1000 g mol⁻¹ [5]. Separation by NF membranes is based on three primary mechanisms: size exclusion (sieving), charge interaction (Donnan exclusion effect), and solute-membrane affinity (e.g., hydrophobic attraction, hydrogen bonding) [6,7]. Polymeric membranes are preferred over other materials due to their low cost and processability [8].

Non-solvent induced phase separation (NIPS) is a commonly-used process for producing polymeric membranes with desired morphologies [9]. During NIPS, the membrane material gradually separates from a liquid polymer casting solution by phase inversion in a coagulation bath consisting of a non-solvent, typically water [10]. Phase inversion provides a gradual membrane morphology transitioning from a relative dense selective upper layer to a fully porous bottom structure with large macro-voids [11]. Altering the composition of the coagulation bath can result in simultaneous cross-linking and coagulation [12], while the presence of cross-linkable groups in the chain end or the side-chains of the polymer backbone unit is essential [13]. This eliminates need for additional solvent-based post-treatment for chemically and thermally stable membranes. The cross-linking of polymer chains within a three-dimensional network is the most common way to improve mechanical strength, solvent resistance, and permeate selectivity, while choosing an appropriate cross-linker for a particular polymer may not be straightforward [14].

Both casting solution composition and choice of solvent/non-solvent coagulation bath couples control demixing (instantaneous or delayed) and membrane characteristics, such as morphology, that in turn determine mechanical strength, permeance, rejection and fouling behaviour [14–16]. Cross-linking often diminishes the gap space between the polymer chain segments resulting in limited vibrational freedom [13]. Instant cross-linking may lead to the formation of a dense selective layer which affects the coagulation kinetics by hindering the exchange rate of the solvent/non-solvent. Delayed demixing

may be preferred to produce membranes at the NF range, because it results in a dense top layer with sponge-like substructures while inhibiting the formation of large macro-voids [17]. Contrarily, instantaneous demixing leads to a porous top layer and a finger-like substructure [18].

Polyaniline (PANI) has been explored as a free-standing polymer and blending agent to enhance membrane performance by increasing membrane hydrophilicity [19–22]. Sulfonation of aromatic polymeric membranes increases proton conductivity, mechanical strength, thermal stability, and chemical stability as compared to non-sulfonated polymeric membranes [23]. Integration of covalently-bound sulfonic ($-\text{SO}_3$) groups into a PANI backbone creates sulfonated polyaniline (S-PANI) [24], which was found to improve both antifouling behaviour [25]. S-PANI membranes showed improved chlorine resistance (250 ppm sodium hypochlorite for 3 days under different pH conditions) including a stable performance and solute rejection. In contrast, PANI membranes suffered critical structural damage with complete leakage upon chlorine exposure at the same testing conditions [26].

The production of PANI membranes in the NF range is costly, laborious, and complex, requiring post-treatment cross-linking procedures with organic compounds [27–29]. Little work has been done on NF S-PANI membranes, while recent efforts to condition S-PANI membranes resulted in tight UF membranes (1800 g mol^{-1} MWCO) [25] with improved solvent stability but low permeance. Developing simple methods for producing cross-linked and solvent stable S-PANI membranes in the NF range is critical for unlocking their full application potential.

Exposing the S-PANI casting solution to a high strength acidic coagulation bath could yield cross-linked membranes in the NF range, due to: (a) associated acid doping with cross-linking [27], (b) interaction between sulfonic and amine groups [30], (c) pH effects on polymer re-assembly [31], and, (d) delayed demixing. In this work, simultaneous in-situ cross-linking, and coagulation of S-PANI membranes in a high acidity solution to produce membranes at the NF range was systematically investigated for the first time. The proposed procedure is simple, fast, and cost-efficient.

S-PANI powder was synthesised by free-radical polymerisation. The membrane cast solution was prepared and applied over a non-woven support layer. Membranes were produced by NIPS in pure water, 1 M, and 3 M HCl aqueous coagulation baths, respectively. The polymer molecular weight was

identified by gel permeation chromatography (GPC). Sulfonation of PANI polymer was determined using energy dispersive X-ray (EDX) analysis. Membrane properties were analysed by Fourier transform infrared spectroscopy (FT-IR), X-ray photoelectron spectroscopy (XPS), X-ray diffractometry (XRD), scanning electron microscopy (SEM), gas adsorption-desorption, mechanical analysis, thermal analysis such as thermogravimetric analysis (TGA) and differential scanning calorimetry (DSC), contact angle (CA) and membrane surface charge measurements. Cross-linking is hypothesized to occur at the polymer doping sites (imine and sulfonic groups) and the change in ion exchange capacity was measured by titration. Membrane water uptake, hydrolytic stability and dimensional stability were verified after wetting at different water bath temperatures. Alkaline stability was also confirmed by measuring the weight loss after wetting the membrane in basic aqueous solution. The polymer re-assembly process (precipitation) was explored by transmission electron microscopy (TEM). Precipitation kinetics were determined by measuring the solvent/non-solvent demixing rate [32]. Solvent stability in static condition, swelling degree and gel content were also quantified. Membrane permeance and rejection performances were determined via filtration experiments. Permeance and rejection benchmarking were conducted with a commercial membrane of nominal MWCO 1000 g mol⁻¹.

3.2 Experimental

3.2.1 Materials

Chemicals were obtained from various commercial suppliers and used as received. A list of chemicals is provided in the supporting information (SI), Materials S1. All solutions were prepared with deionised (DI) water produced from an ELGA deioniser (PURELAB Option).

3.2.2 Synthesis of S-PANI polymer

Established methods for sulfonation of aniline monomer before polymerisation (pre-sulfonation) for S-PANI synthesis are described elsewhere [25,33]. Here, a modified S-PANI polymer synthesis was used. A detailed description of the synthesis is provided in SI, S-PANI synthesis S2. In brief, ammonium persulfate aqueous solution was added dropwise to a glass beaker surrounded by ice containing aniline,

metanilic acid (1:1 M ratio) and hydrochloric acid solution (1 M) within controlled time intervals for a prolonged time i.e., 13 h. The resulting S-PANI salt precipitate at $72\pm 1\%$ yield was filtered, washed, dried, sieved in $160\ \mu\text{m}$ and stored until required.

Gel permeation chromatography (GPC) was used to characterise the dried S-PANI powder to identify the weight average and the degree of polymerization dispersity. A detailed description of the molecular weight measurement is provided in SI, Polymer molecular weight determination S3. The average MW was calculated as $46,898\ \text{g mol}^{-1}$ with a polydispersity of 1.93. The incorporation of the sulfonic groups to the polymer backbone and the degree of sulfonation of the S-PANI powder was confirmed by SEM-EDX (details provided in SI, Energy dispersive X-ray S4). The calculated sulfur to nitrogen (S:N) ratio of the synthesised S-PANI is 0.43 (SI, Table S 3.1) corresponding to a fully doped S-PANI [25].

3.2.3 Membrane fabrication

A detailed description of the membrane fabrication is provided in SI, Membrane fabrication S5. In brief, S-PANI membranes were prepared by the NIPS method. The solution (20 wt% SPANI) was used to cast $200\ \mu\text{m}$ membranes (clearance gap) at room temperature at a controlled relative humidity of $\sim 30\%$. Membranes formed after immersion precipitation in the coagulation bath solution at room temperature, considering a consistent evaporation time of 10 seconds before immersing the cast film into the coagulation bath. An overview of sample nomenclature and the conditions applied is provided in Table 3.1. Note M6 and M7 are identical to M2 and M3, respectively, except the latter were dedoped to remove the residual H^+ ions. The former membranes were included in the study to understand if the dedoping process may have an impact on the membrane morphology.

Table 3.1 In-situ and post-treatment conditions of the tested S-PANI membranes.

Membrane	Membrane type	Coagulation solution	Post-treatment
M1	S-PANI	Pure water	-
M2	S-PANI	1M HCl	Stored in pure water for a week
M3	S-PANI	3M HCl	Stored in pure water for a week
M4	S-PANI	Pure water	Doped in 1M HCl overnight
M5	S-PANI	Pure water	Doped in 3M HCl overnight
M6	S-PANI	1M HCl	-
M7	S-PANI	3M HCl	-
M8	Commercial composite fluoropolymer	-	-

3.2.4 Membrane characterisation

A detailed description, including suppliers of analytical equipment, is provided in SI, Membrane characterisation S6. In brief, the chemical properties of S-PANI membranes were determined using an FT-IR spectrometer. The change in the chemical state of the sulfur and nitrogen atoms was analysed by X-ray photoelectron spectroscopy (XPS). The ion exchange capacity was measured using a titrator. The S-PANI membrane water uptake, hydrolytic stability and dimensional stability were verified after wetting at different water bath temperatures. Alkaline stability was also confirmed by measuring the weight loss after wetting the membrane in basic aqueous solution. The polymer structure was analysed by X-ray diffractometry (XRD). The morphological properties, such as membrane surface and cross-sectional area, including the change in the thickness of the selective layer of the membranes, were investigated by SEM. The S-PANI re-assembly process in neutral and acid aqueous solution was investigated by transmission electron microscopy (TEM). The change in membrane porosity was measured by N₂ adsorption-desorption. To understand the effect of the simultaneous cross-linking which resulted in the formation of the dense selective layer, precipitation kinetics were investigated by measuring the change of relative concentration of total organic carbon (TOC) in the coagulation solution at time (t) and at infinite time (∞) defined here as 24 h immersion. Thermal and mechanical analysis was carried out to explore the effect of the cross-linking. Solvent stability was determined by soaking the membranes for two weeks in *N,N*-dimethylformamide (DMF). In parallel, PANI membranes were produced at the same conditions as S-PANI for comparing the role of the sulfonic groups in the cross-

linking process. The swelling degree and the gel content were measured using different polar protic, polar aprotic and nonpolar solvents.

The hydrophilicity of the membranes was measured by sessile dynamic droplet penetration using a contact angle goniometer. Membrane filtration experiments were conducted in dead-end mode with a magnetic stirrer. To ensure that all H^+ ions were leached out during the prolonged rinsing process, the pH measurements of permeates at different filtration stages were conducted and reported as an average of three samples. The solute rejection was carried out using different solutions containing dyes, PEG (1000 g mol⁻¹) and sugar. The membrane surface charge and dye feed solutions' zeta potential were measured to understand the charge interactions between membranes and dye solutes.

3.3 Results and Discussion

3.3.1 FT-IR spectroscopy, XPS and XRD analysis

Fig. 3.1 shows the FT-IR spectra of M1-M3. Characteristic transmittance bands of the S-PANI were observed at 1595 cm⁻¹ (quinoid C = C stretching), 1497 cm⁻¹ (benzenoid C = C stretching) [25]. The presence of aromatic amine C – N stretching was observed at 1295 cm⁻¹ for all samples. C – C bending for all samples was distinct at 816 cm⁻¹ [34,35], and symmetric S = O stretching was detected at 1033 cm⁻¹ and 708 cm⁻¹ [36,37]. Results indicate the introduction of sulfonate groups to PANI structure in agreement with the literature [38]. Nonetheless, M2-M3 exhibited a peak shift from 1168 cm⁻¹ (M1) towards 1148 cm⁻¹. The original peak was assigned to a strong asymmetric stretching vibration of S=O (sulfonate) whereas the new detected peak was linked to S=O stretching of sulfonamide bonds [39]. Similar peak shifts were reported for sulfonamide formation [40–42].

The relative intensity changes of the transmittance band at 1033 cm⁻¹, which is assigned to the stretch vibration of the sulfonic acid group, decreased after cross-linking. This could be attributed to the partial consumption of the sulfonic acid groups (due to the formation of sulfonamide groups) during the cross-linking process. The aromatic imine C = N stretching at transmittance band 1111 cm⁻¹ [29] was only noticed for M1 and disappeared for M2-M3. The imine nitrogen double bond may break on either side of the quinoid ring reacting with the sulfonic group during the polymer re-assembly process. This would

lead to an increased benzoid to quinoid ring ratio which then prevents re-dissolution or dispersion when exposed to aprotic solvents [43]. The pronounced changes in the FT-IR spectra of the M2-M3 samples compared with M1 indicate a potential interaction between sulfonic groups and nitrogen within S-PANI during the polymer re-assembly process.

The cross-linking reaction may involve nucleophilic Sn1 substitution between an electron pair donor (secondary amine) and an electron pair acceptor (sulfonic group). Also, reactions occur between *NMP*/4MP solvents and HCl(aq) in the coagulation bath as reported elsewhere [44]. These reactions involve degradation of *NMP* potentially impacting polymer precipitation during re-assembly and the polymer-polymer bonding.

Cross-linking of M2-M3 takes place during the membrane solidification rather than after. The liquid state of the polymer solution makes the polymer chains more accessible and susceptible for reaction i.e., potential nucleophilic Sn1 substitution or due to the side reaction between the *NMP*/4MP solvents and the HCl(aq), enabling a higher degree of cross-linking of the entire bulk of the membrane. Exploiting the enhanced reactivity of liquid state aromatic polymer solutions for in-situ cross-linking has been previously reported [12]. Post-treatment of S-PANI membranes in their solid-state in acidic solution, conducted with M4-M5, does not interfere with the sulfonic groups because of the absence of polymer mobility. The effect of soaking solidified S-PANI membrane in acidic solution is limited to the introduction or withdrawal of protons at polymer doping sites, as illustrated in SI Fig. S3.15.

Cross-linking of PANI membranes in solid-state requires an organic solvent to swell the polymer and allow contact between the polymer chains and the introduced cross-linker [27]. Alternatively, a heat source could be employed in the presence of the cross-linker to facilitate cross-linking during the condensation process [29].

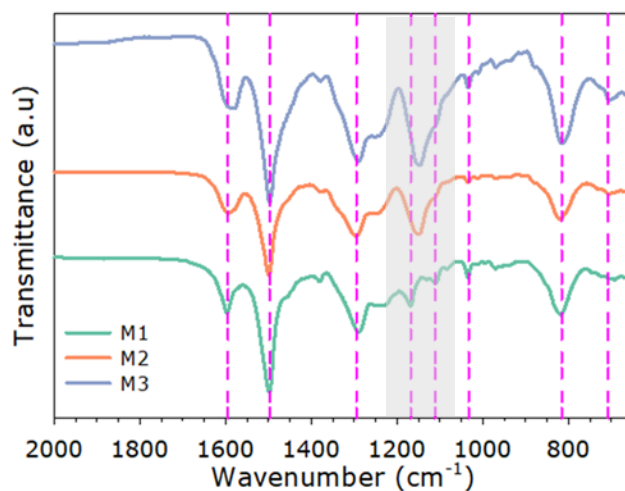


Fig. 3.1 FT-IR spectra of membranes produced in neutral coagulation bath (M1) and acidic coagulation bath (M2-M3).

High-resolution XPS was also used to study M1-M3. The core-level spectra of carbon (C 1s) for all membranes M1-M3 was aligned confirming calibration (XPS spectra S8, Fig. S3.16a), while oxygen peaks were similar (Fig. S3.16b). Core level spectra of sulfur S 2p of M1 were higher compared to M2 and M3 suggesting an increased oxidation state or effective nuclear pull in M1 (Fig. S3.16c). Slight change in core level spectra N 1s was observed between M1 and M2-M3 (Fig. S3.16d). Both XPS and FT-IR results are in agreement suggesting a change in the chemical state of the sulfur and nitrogen bonding following the cross-linking reaction.

XRD was used to investigate changes in polymer crystal structures of M1-M3. PANI and its derivatives have semi-crystalline structures showing three different XRD peaks [45]. Fig. 3.2 provides XRD of M1 with three peaks at $2\Theta=18.4^\circ$, 27° and 42° , as expected. M2 and M3 exhibited two distinctive peaks at $2\Theta=24^\circ$ and 40.4° . M2-M3 showed a broader peak at $2\Theta=40.4^\circ$ compared to M1 while the peak at $2\Theta=18.4^\circ$ disappeared. This suggests that cross-linking of M2 and M3 was less structured than M1 which can be ascribed to shrinkage of the intersegmental distance of polymer chains [25].

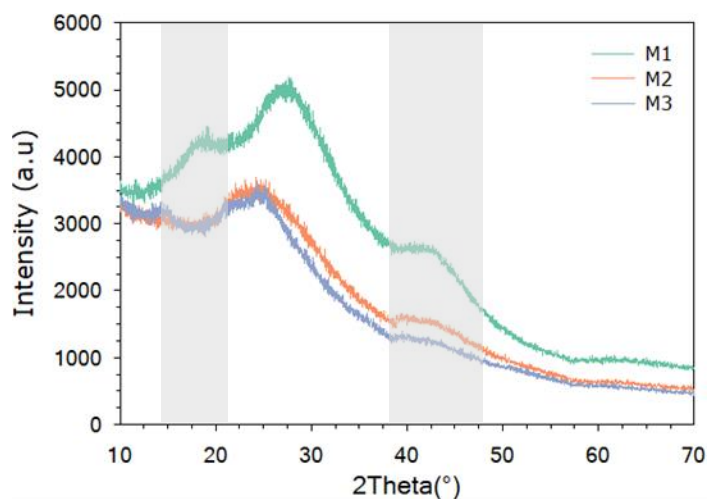


Fig. 3.2 XRD patterns of S-PANI membranes M1-M3.

3.3.2 Ion exchange capacity and water stability

The presence of amine/imine groups and sulfonic cation-exchange functional groups makes the S-PANI a promising material for fuel cell applications [46,47]. Therefore, changes in the chemical state of the ion exchange functional groups are expected to influence the ion exchange capacity. The ion exchange capacity (IEC) of M1 and M2-M3 was measured via titration. A significant reduction of about 86% in the IEC was observed for M2 compared to M1, while a marginal difference was noticed between the cross-linked membranes M2 and M3 (Table 3.2). The change in the IEC could be attributed to the consumption of the amine/imine groups and cation-exchanging sulfonic groups.

Water uptake measurements showed that cross-linking caused about 20-24% suppression of uptake for M2-M3, respectively, compared to M1. The lower water uptake could be attributed to the three-dimensional network of the cross-linked membranes.

Table 3.2 Ion exchange capacity (IEC) and water uptake of S-PANI membranes M1-M3.

Membrane	IEC (meq g ⁻¹)	Water uptake
M1	1.29±0.2	1.94±0.14
M2	0.18±0.03	1.55±0.04
M3	0.16±0.03	1.47±0.03

The water stability test was performed by immersing membrane samples in pure water at 20, 40 and 80°C for 4 h while the dry weight was measured before and after the test. All the tested membranes M1-M3 showed a stable and consistent dry weight as shown in SI, Table S 3.2. Also, the UV absorbance

spectra of the water bath did not show an indication of leaching impurities from the membrane samples. M1-M3 exhibited dimensional stability in a pure water bath at different temperatures 20, 40 and 80°C overnight. Similarly, M1-M3 exhibited dry weight stability before and after soaking in 0.1 NaOH(aq) for 24 h at 20°C. The resulting membranes were alkaline stable, insoluble, and their dimensions were stable even at 80°C deionized water.

3.3.3 Morphology and porosity

Fig. 3.3a-c shows SEM surface images of membranes M1-M3. High magnification SEM images provide no apparent difference between the surface morphologies of different S-PANI membrane samples. This demonstrates that the acidic strength of the coagulation solution and the doping/dedoping process of the S-PANI membranes does not have a noticeable effect on the surface morphology. Fig. 3.3d-f shows SEM images of cross-sectional areas of membranes M1-M3. All membranes exhibited a typical asymmetric morphology of phase inversion, including a dense skin layer, a transition region, and a porous bottom layer [10,48]. Membranes prepared in acidic coagulation solution (M2-M3) had a denser skin layer with suppressed macro-void structure (Fig. 3.3e-f) compared to membranes produced in pure water (M1, Fig. 3.3d). The in-situ cross-linking of the polymer matrix resulted in the formation of a dense skin layer which hindered the demixing rate of solvent/non-solvent and inhibited the formation of large macro-voids. Membranes with dense substructure are favoured over finger-like structures due to the enhanced solute rejection and improved mechanical strength [9,49,50]. The doped sample of the cross-linked membrane (M6-M7) exhibited identical morphological structure to the dedoped samples M2-M3 as shown in the SI, Morphology S10 Fig. S3.17c-d. This emphasizes that HCl doping of the S-PANI membrane was not dominating the conformation and the simultaneous coagulation and crosslinking could be the dominant factor for the changes in membrane morphology as explained in the following sections. Post-treatment doping of M4 and M5 with H⁺ ions (SI, Morphology S10 Fig. S3.17a-b) resulted in similar structures compared to the pristine M1 membrane (Fig. 3.3d), in agreement with a previous study [20]. Morphological differences were more obvious for the cross-

linked membranes while leaching of residual H^+ ions did not induce an apparent change of membrane structure.

The morphological changes were quantified by measuring the thickness of the selective layer and the overall membrane thickness (excluding the support layer). Fig 3.4d-f shows an increase of selective layer thickness from 737 nm to 794 and 1700 nm for M1, M2 and M3, respectively. The overall membrane thickness decreased gradually from 94.8 μm to 66.2 and 47.7 μm for M1, M2 and M3, respectively, due to increasing inhibition of macro-void formation.

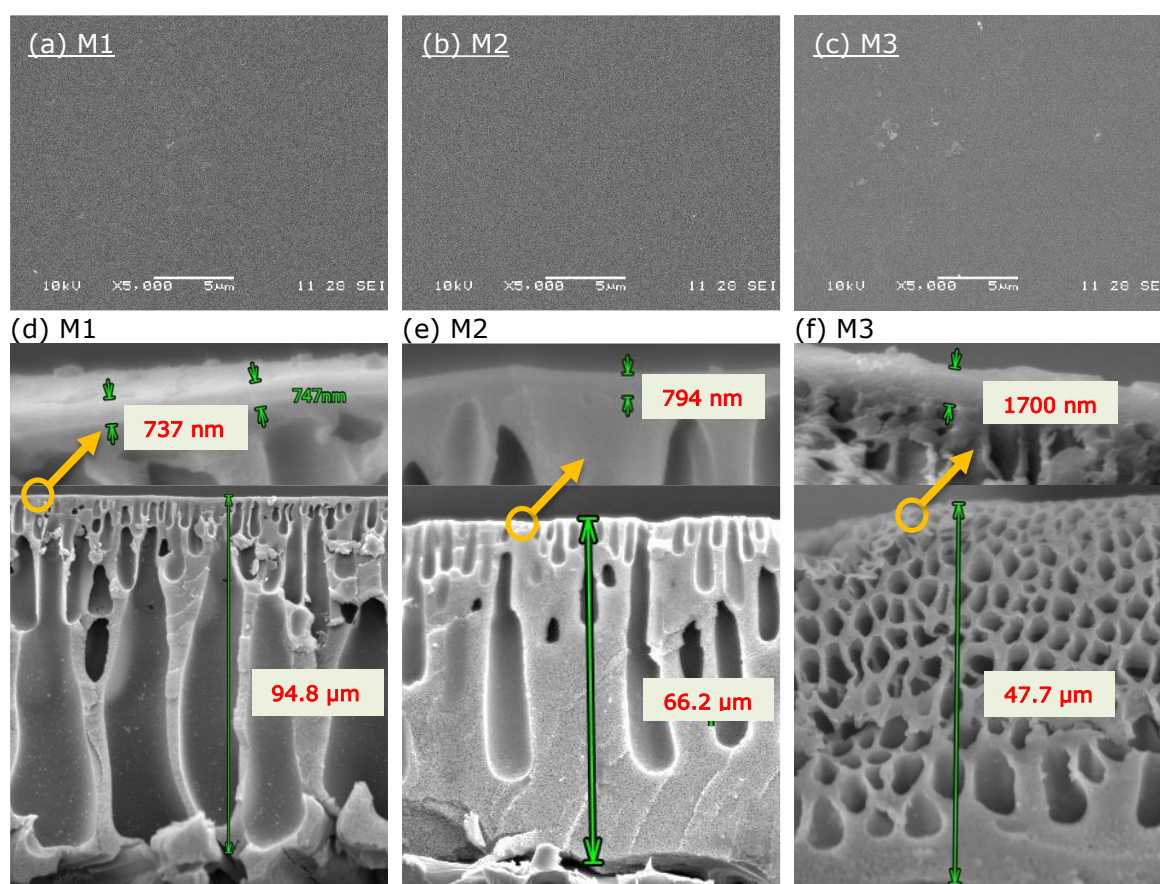


Fig. 3.3 SEM surface and cross-sectional area images of S-PANI membranes prepared in neutral coagulation bath (M1), 1M HCl acidic coagulation bath (M2) and 3M HCl acidic coagulation bath (M3).

To better understand the polymer re-assembly (precipitation) process, 2 mL of S-PANI polymer solution (0.2 wt/wt%) was added to 18 mL of neutral and acidic coagulation bath. The visual observation and TEM images showed different precipitation structures. Immersing the polymer solution in an acidic coagulation bath formed an organised flaky structure whereas the precipitated polymer in a neutral coagulation bath showed a cloudier solution with a fine pin floc-like structure (Fig. 3.4a-c). This was

verified by TEM images showing a loose structure of precipitated polymer particles compared to a dense and inter-linked structure in an acidic coagulation bath (Fig. 3.4d-f).

PANI exhibits a different conformation in low pH coagulation solutions including forming cross-linked networks with fibrillar structure [51]. The morphology changes were attributed to the absence of H-bond interaction between the solvent and the polymer chains due to protonation of the latter. Instead, strong intrinsic interaction between polymer chains causes cross-linkages to form during the polymer re-assembly [31]. Here, the presence of sulfonic groups in S-PANI is believed to significantly affect the polymer re-assembly process and the cross-linking of the polymer matrix due to the potential interaction between the sulfonic groups the nitrogen atom in the doping sites. A solvent stability test of S-PANI and PANI membranes formed in an acidic coagulation is reported in a separate section below to validate this claim.

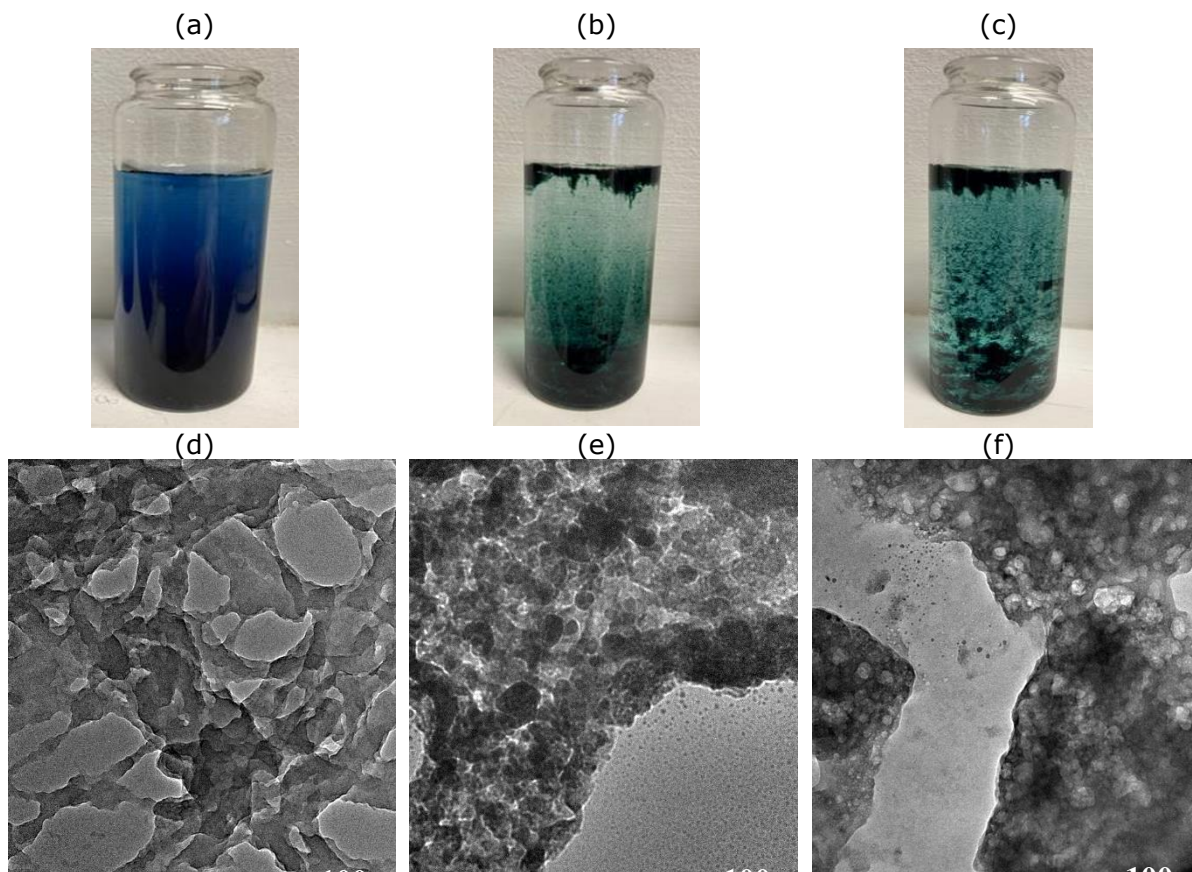


Fig. 3.4 Visual and TEM images of the S-PANI polymer solution in neutral coagulation bath (a, d), 1M coagulation bath (b, e) and 3M coagulation bath (c, f).

The isotherms of the porosity measurements showed a sharp decrease in the surface area of M2 and M3 (37% and 27% of M1 BET surface area, Table. 3.3). The change was also observed for total volume and a total area of pores ≤ 5 nm. The maximum pore volume of M2 and M3 was 26% and 18% of M1, respectively, which corresponds to the observed suppression of the membrane's macro-voids as illustrated in the SEM images.

Table 3.3 Porosity measurements of S-PANI membranes M1-M3.

	Unit	M1	M2	M3
BET surface area	$\text{m}^2 \text{g}^{-1}$	33.6	12.5	8.9
Volume in pores ≤ 5 nm	$\text{cm}^3 \text{g}^{-1}$	8.83E-02	2.41E-02	1.98E-02
Maximum pore volume*	$\text{cm}^3 \text{g}^{-1}$	1.50E-02	5.76E-03	3.68E-03
Area in pores ≤ 5 nm	$\text{m}^2 \text{g}^{-1}$	33.6	8.7	6.2

*At $P/P_0 = 0.144111684$

3.3.4 Demixing kinetics

The demixing rate was measured for the M1-M3 membrane sample as shown in Fig. 3.5. M1 exhibited an abrupt shift in organic solvent concentration within the first hour of polymer precipitation. Subsequently, the concentration stabilised, showing a steady-state profile within 2 h of immersion. The instant demixing explains the formation of the finger-like voids as shown in the SEM images of membrane cross-sections. (Fig. 3.3d) [48]. In contrast, the in-situ cross-linking resulted in a dense selective layer which simultaneously delayed the demixing of the solvent/non-solvent, leading to a gradual release of the organic solvent to the coagulation bath over time. Note that, demixing kinetics for polymer precipitation was obtained by measuring the solvent leaching rate into the coagulation solution [32,52–54]. Light transmittance or microscopy techniques determining demixing kinetics [55–57] could not be employed due to the dark green colour of S-PANI.

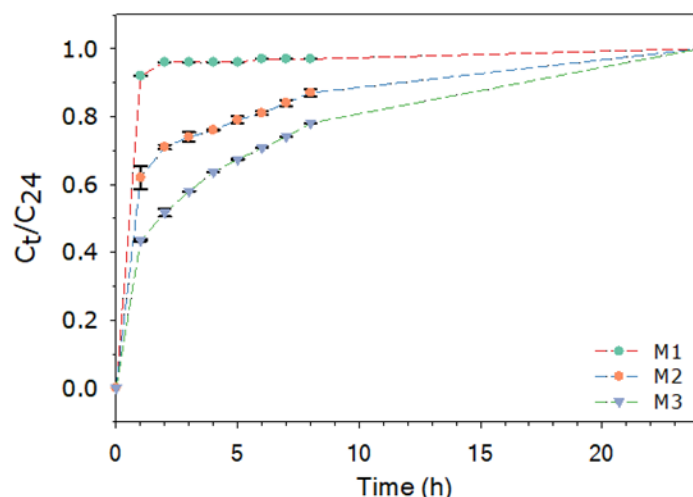


Fig. 3.5 S-PANI solvent demixing kinetics in neutral (M1) and increasingly acidic (M2, 1M HCl; M3, 3M HCl) coagulation solutions.

3.3.5 Thermal and mechanical analysis

Fig. 3.6 shows the TGA results which elucidate the change of weight during controlled heating as a percentage of the initial membrane sample weight and the derivative weight with respect to temperature up to 600°C. Plotting the derivative weight loss showed a first peak in the range of 20–120°C for the pristine M1 (~2.6%) and extended further to 160°C for the cross-linked M2-M3 membrane samples (~12-15%). This was attributed to the evaporation of entrapped water molecules in the polymer matrix and any residual 4-methylpyridine (4MP). The second weight-loss peak of the M1 sample was in the range of 390-590°C. The cross-linked membranes showed different thermal degradation behaviour in the range of 340-410°C for the M2 membrane, followed by the integrated broad and less intense peak to 590°C. M2 showed a more intense reduction in weight than M3 at the second peak. The weight loss at such high-temperature band was assigned to free *N-methyl-2-pyrrolidone* (*NMP*) volatilisation and release of *NMP* molecules, which are hydrogen-bonded to the amine groups of S-PANI [58]. The DSC thermograms also showed that the glass transition temperature of the M1 membrane sample was shifted down from 243°C to 204°C and 187°C for the cross-linked membranes M2 and M3, respectively (SI, Differential scanning calorimetry S12 Fig. S3.24-S3.26). PANI membranes contain considerable amounts of *NMP*, about 18% by weight [58]. The cross-linked membranes might have entrapped a surplus quantity of *NMP* compared to M1 due to the dense structure. *NMP* could have a plasticising

effect at high temperatures resulting in lower glass temperature and a further change in the thermal behaviour.

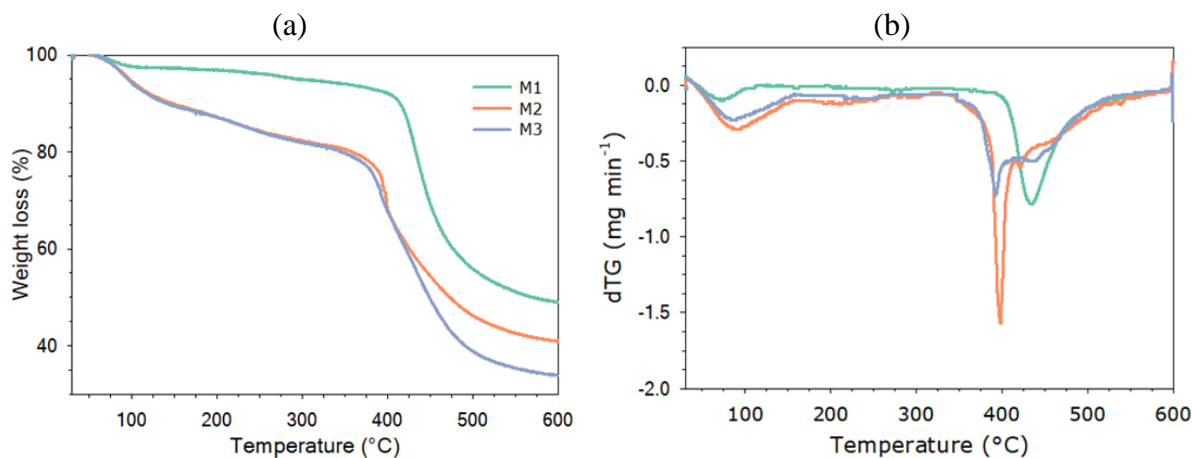


Fig. 3.6 TGA curves for pristine and cross-linked S-PANI membranes (a) weight loss (b) derivative weight loss with respect to temperature from room temperature to 600°C.

Fig. 3.7 shows the mechanical strength and the elongation at the breakage point of the S-PANI membranes, M1-M3 at room temperature. The mechanical strength of the cross-linked membranes M2-M3 is 2.3 times higher than the pristine S-PANI membrane M1, whereas a slight and inconsistent change in the elongation at breakage was observed for all samples. The cross-linked polymer structure exhibits a dense three-dimensional network, with limited freedom for motion by the individual segments of the molecules' steric hindrance to chain movement, which enhanced the mechanical strength.

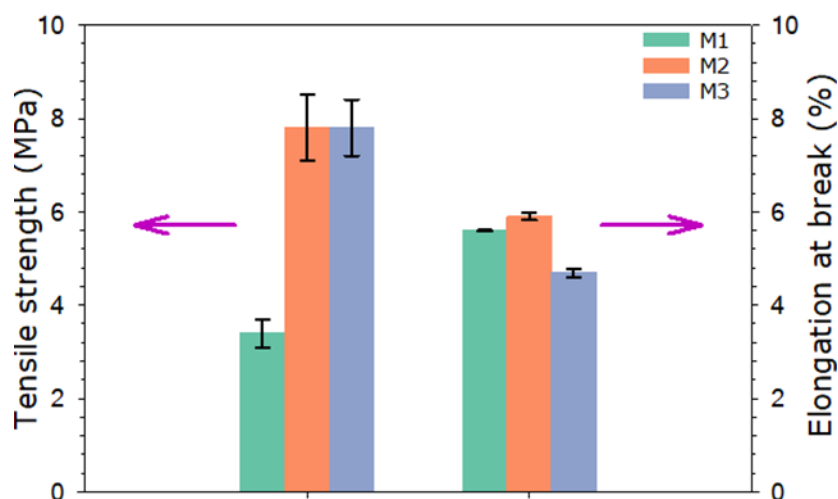


Fig. 3.7 Mechanical properties of the pristine M1 and cross-linked (M2-M3) S-PANI membranes.

The commercial membrane was cast over a support layer which dominates the membrane's tensile strength. As such, the tensile strength of the free-standing S-PANI membrane and commercial membrane values are not comparable.

3.3.6 Solvent stability

Solvent stability in *DMF* as an exemplary solvent was tested. Fig. 8 shows the effect of *DMF* on membranes stability after immersion for two weeks. M1 readily dissolved resulting in a vivid blue solution. M2 and M3 were resistant to *DMF* showing only a slightly discolouring of the solution after 30 minutes without any subsequent changes over the observation time of two weeks. Contrastingly, PANI membranes formed in a pure water and acidic coagulation bath (M1', M2', M3) dissolved in *DMF* (Fig. 3.8b). M2' and M3' were more resistant than M1', while all samples dissolved within one hour. Solvent stability of M2 and M3 may be attributed to the formation of interchain bonds, making the material less vulnerable to solvent attack.



Fig. 3.8 Effect of *DMF* on membrane stability after two weeks.

3.3.7 Mass swelling degree and gel content

Identifying the extent of swelling for polymeric membranes is essential to understand their transport properties and behaviour while being exposed to organic solvents [59]. A set of organic solvents including *Methanol (MeOH)*, *Isopropanol (IPA)*, *Acetone (AC)*, *Toluene (TOL)*, *Tetrahydrofuran (THF)* was used to determine the membrane swelling (Fig. 3.9a) and solvent stability (Fig. 3.9b). The mass swelling degree of M1 increased in the sequence of $TOL < MeOH < AC < IPA < THF$. The maximum swelling was found for *THF* at $88 \pm 8\%$. M1 did not qualify for swelling tests with *DMF* due to instant dissolution. Swelling trends for M2-M3 were different and in the order $AC < THF < MeOH < IPA \approx TOL$. The difference in the swelling degree trend between M1 and M2-M3 could be attributed to the change in the Hansen solubility parameter following the cross-linking reaction. Generally, significant polymer swelling with strong polymer-solvent interaction is anticIPAated for polymers that have similar Hansen

solubility parameters to the surrounding solvent [60]. The highest swelling degree for M2 was about $9 \pm 1\%$ (TOL \approx IPA) while the THF swelling was only $3 \pm 0.2\%$. Marginal difference in the swelling degree was observed between M2 and M3. The decreased swelling degree of M2-M3 could be explained by the reduced porosity due to the inter-linked segments of the polymer. Besides, the top layer of M2-M3 was more hydrophilic than M1 (see also contact angle section), which effectively prevented the dissolution and permeation of organic solvents into the bulk of cross-linked S-PANI matrix.

Fig. 3.9b showed membrane stability static test in organic solvents including DMF over two weeks. M1 was unstable in THF and DMF as the transparent solvent turned blue due to the gradual dissolution of the polymer in THF while being readily dissolved in DMF. The dry mass of the M1 was reduced by $10 \pm 5.6\%$ and $78.5 \pm 3.2\%$ with THF and DMF, respectively. M1 was more stable in MeOH, IPA, AC and TOL than THF and DMF as there was only a slight colour change with maximum decreased mass by 3.5% with MeOH. M2-M3 exhibited stability for all solvents tested providing no change in solvent colour after the two weeks, except a slight discolouring with the DMF in the first 30 minutes. The dry mass of the soaked membrane remained constant while showing weight loss around $4.3 \pm 0.5\%$ (M2) and $0.9 \pm 1\%$ (M3) with DMF.

Functionalising the PANI polymer with sulfonic groups (pre-sulfonation) was proven to be essential for the in-situ cross-linking to take place in an acidic coagulation bath. This test indicates that M2 and M3 may qualify for organic solvent applications, while extended solvent stability tests are part of an ongoing study.

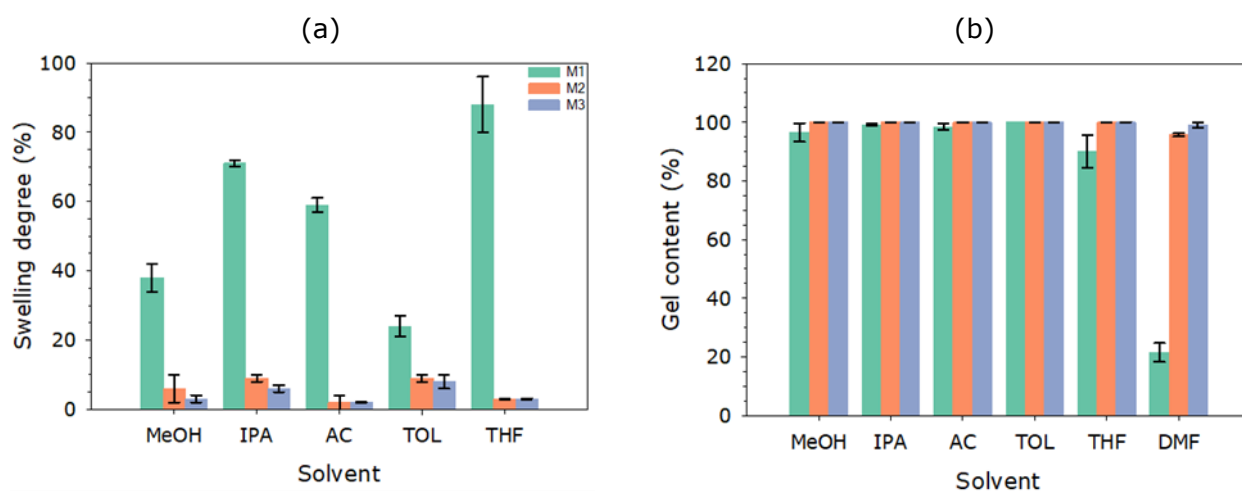


Fig. 3.9 Mass swelling degree and gel content of pristine and crosslinked S-PANI membranes M1-M3 in different polar protic, polar aprotic and nonpolar solvents.

3.3.8 Contact Angle

The hydrophilicity of the pristine and cross-linked S-PANI membranes was estimated by measuring the apparent contact angle of the membrane surface. High affinity to water with a contact angle less than 90° indicates a hydrophilic membrane. As shown in Fig. 3.10 the dynamic CA of M2-M3 showed a continuous and higher decline compared to M1, which provided a relatively constant value. The contact angle of M2 and M3 decreased continuously for 100 s. However, a slightly dynamic decrease was observed after 120 seconds, reaching a steady level ($\sim 28^\circ$) after 140 s. The changes in CA can be rationalised by (a) higher polarity (surface charge) of the membrane surface and therefore stronger intermolecular attraction between water and membrane surface [61–63], and (b) the dense skin layer with less porosity produced a smoother surface which could affect the contact angle and hydrophilicity [18,48]. The hydrophilicity followed the opposite order of the contact angle: $M1 < M2 < M3$ with the marginal difference between M2-M3. A higher hydrophilicity with a smooth and charged surface of M2-M3 could indicate a higher antifouling property [19,29].

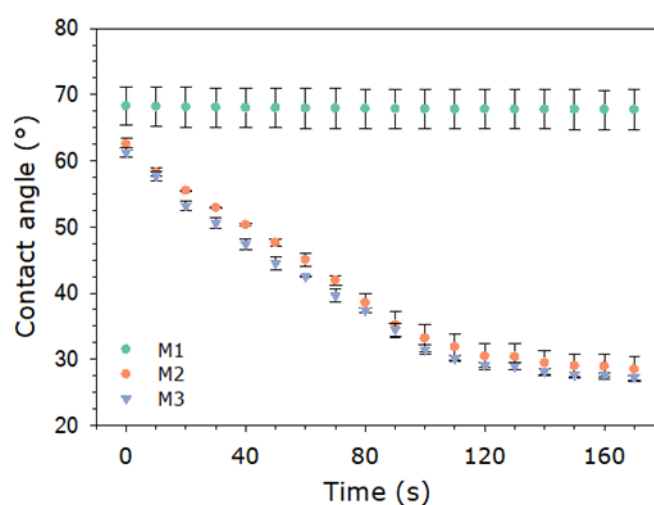


Fig. 3.10 The contact angle of the S-PANI membranes (M1-M3).

3.3.9 Membrane transport properties

The permeance of M1-M5 and the commercial M8 membranes was evaluated using three solutions: pure water (Fig. 3.11), PEG aqueous solution ($MW\ 1000\ g\ mol^{-1}$) (Fig. 3.12a) and aqueous dye solution ($MW\ 320\ to\ 1017\ g\ mol^{-1}$) (Fig. 3.13a). The permeance of M1-M3 and M8 experienced an initial drop

during the preconditioning phase due to the compaction of the membrane under the transmembrane pressure [64]. The permeance became steady (5% difference) after 30 min. A slight increase in the M4-M5 membrane permeance was observed during preconditioning and filtration, therefore, an average permeance value is shown in Fig. 3.11 and Fig. 3.12a. This can be attributed to leached H^+ ions, which increased the membrane's free volume. Soaking M4-M5 in an aqueous solution for a week with a daily change of the solution reinstated the membranes' permeance with stable and neutral permeate pH. Both residual H^+ ions on the polymer chains and the pH variability of feed solution could affect membrane permeance stability, solute rejection, and surface charge [22]. To better understand the in-filtration membrane stability and confirm the absence of residual H^+ ions in the membrane, the pH of the permeate was measured using a feed solution at neutral pH (SI, Transport properties S13 Fig. S3.27). Permeate pH of HCl-doped M4 and M5 decreased during filtration, indicating leaching of H^+ ions. Immersing the M4 and M5 membrane samples for a week in pure water while changing the soaking solution daily helped to de-dope the membranes and reinstate the initial transport properties with stable permeate pH. The permeate pH of M1-M3 remained stable, indicating: (a) the fabrication method of the self-doped S-PANI membrane overcame the acid leaching problem, and (b) rinsing of M2 and M3 for a prolonged time with pure water removed residual H^+ ions. The interwoven and/or double-stranded structure in the S-PANI complex binds the acid more strongly, and thus there is no loss of sulfonated groups during the filtration, which is consistent with the literature [21,36,65]. S-PANI membranes prepared in acidic solution and left in water for one week did not show any leaching of H^+ ions that suggested stable and comparable performance in contrast to the HCl-doped S-PANI membranes that leached H^+ ions and showed unstable performance.

Fig. 3.11 shows that the higher acidic strength of the coagulation bath led to a considerable drop in the pure water permeance by 63-67% and 92-94%, respectively, compared to M1. Transmembrane pressure of M1, M2 and M3 increased from 2 to 3 and 6 bar, respectively, because of the change in density of the selective layer (Fig. 3.3) and porosity (Table. 3.3). The average permeance of M4 and M5 exhibited a decline of around 12-14% compared to M1. The cross-linking resulted in a decrease in the gap space between the polymer chains during the re-arrangement process, explaining the performance change of

M2 and M3 [19,32,66]. Doping the S-PANI membranes in acidic solution resulted in a slight swell [61]. The proposed changes could reduce the pore size of the membrane and create further water transport resistance as illustrated in SI, Transport properties S13 Fig. S3.28. The increase in the doping solution's acidic strength (polymer chains swelling) with reduction of membrane permeance and increase in solute rejection quantitatively confirmed our proposed hypothesis.

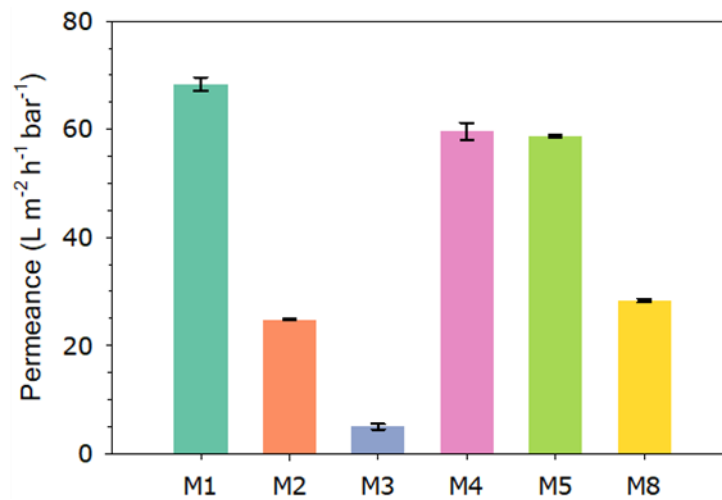


Fig. 3.11 Pure water permeance for the S-PANI membranes (M1-M5) and the commercial membrane (M8).

Fig. 3.12a and Fig. 3.13a show the effect of the solutes' concentration polarisation on the membrane performance. A generic permeance decline of 36-56% and 71-79% was observed for the tested membranes with PEG solution and the dye feed solutions, respectively, compared to pure water permeance. The PEG and dye solution permeance results are in good consistency with the pure water results reflecting the effect of the coagulation bath's acidic strength. NF membranes are known to operate at transmembrane pressure around 2-10 bar with approximate pure water permeance 5-50 L m⁻² h⁻¹ bar⁻¹ [48]. The obtained permeance results of M1, M2, M3 and M8 agree with the literature [67,68]. The permeance and rejection of the dye solution through the HCl-doped M4 and M5 membranes were not evaluated due to the interaction between the dye solutes with the leached H⁺ ions leading to biased UV absorbance and incorrect dye rejection [69].

Fig. 3.12b shows that M1 to M5 and M8 produced distinct MWCO curves with the PEG rejections in the following order: M1<M8<M4<M5<M2<M3. The different PEG rejections between pristine and

HCl-doped M4-M5 membranes were attributed to the contraction of the membrane pore size, because of the different free volumes in the skin layer. The strength of the HCl doping solution enhanced the PEG-1000 g mol^{-1} rejection to 40% and 49% for the M4 and M5 membranes, respectively, in comparison with 29% rejection by M1. A substantial increase in the PEG rejections to 66% and 99% were obtained by M2 and M3, respectively. The higher density of the top skin layer and the change in the membrane conformation to the suppressed macro-void structure with less porosity was directly reflecting the PEG rejections. To evaluate the enhanced performance of S-PANI membranes, the commercial M8 membrane rejection was also acquired. A rejection of around 34% was achieved at 1000 Da in comparison with nominal (labelled) MWCO around 90%. The PEG comprehends a series of water-soluble, linear chain polymers of oxyethylene units, which are mainly present as a helix [70]. The hydrated polymer shows a conformation as an expanded random coil [71], therefore, the wiggling effect of the linear PEG could contribute to the solutes carry-over to the permeate under applied pressure which explains the difference between the measured MWCO and the nominal rejection as found in previous work [72]. The wiggling effect may underestimate the actual MWCO of the tested membranes. Additionally, the measured TOC of the feed PEG solution is high ($\approx 312 \text{ mg L}^{-1}$) which may also underrate the rejection of the tested membranes. To exclude the PEG wiggling effect and identify the exact MWCO of the NF membrane (M3), rejection for sucrose octa-acetate and raffinose was determined at TOC feed of 20 mg L^{-1} . Table. 3.4 shows that the cross-linked M3 membrane has a MWCO around 680 g mol^{-1} compared to 900 g mol^{-1} using the PEG1000 solute.

Table 3.4 The MWCO determination of the NF membrane (M3) using sugar solutes.

Solute	MW (g mol^{-1})	Rejection (%)
Sucrose octa-acetate	678.6	90.0 \pm 2
Raffinose	504.4	60.0 \pm 3

The nominal MWCO of M8 (charged membrane), as presented by the supplier, might have been measured based on the different dye solutions. The Donnan effect could have resulted in such higher dye rejection and apparently lower MWCO. On the other hand, PEG is electrically neutral, and its rejection will not be influenced by the Donnan effect, thus resulting in lower rejection of M8 for PEG

solution and higher MWCO [72]. The overall outcome shows coherence between the permeance and the rejection results. The results also suggest that M3 was the only one to be classified as an NF membrane. The specific MWCO values of the other membranes can be determined using solutes that are larger than the maximum MW of 1074 g mol^{-1} used in this work.

To have an accurate evaluation of the membrane rejection because of the adopted modifications, the rejection test of four different dyes was implemented for the M1-M3 and the commercial M8 membrane. Fig. 3.13b shows the rejection values from 50-84% to 72-96% and 91-100% for the M1-M3 membranes at a molecular weight range from 320 to 1017 g mol^{-1} . Also, M8 exhibited a high dye rejection between 74 to 85%. The membrane surface charge and the dye feed solution's zeta potential measurements were undertaken to evaluate membrane-solute charge interaction, which could influence the dye exclusion and show higher apparent rejection of dye [73]. Fig. 3.14a shows the surface charge of M1-M5 and the commercial M8 membrane. The reported surface charge of the S-PANI membrane doped in acidic solution at pH 4.5 was around 20 mV [26,74], which falls within the same range as the HCl-doped M4 membrane. It can be observed that the higher acidic strength enhanced the surface charge of the doped M5 membrane to 25 mV. This can be attributed to the abundance of H^+ ions which protonated the polymer chains and therefore implied an increase of membrane surface charge. M2 and M3 membranes exhibited a significant step-change (74%) in surface charge even after leaching of all residual H^+ ions compared to the M1 membrane. Compared to the S-PANI membrane, the surface charge of the M8 was obtained ($-11.7 \pm 3.4 \text{ mV}$) and the negative surface charge agreed with the literature values [75]. The zeta potential of the four tested dye feed solutions was measured, as shown in Fig. 3.14b. All dye solutions were negatively charged with zeta potential ranging from -1.6 to -27.4 mV. The difference between the S-PANI membrane surface charge and the zeta potential of the dye solutes could underestimate the membranes' rejection, in contrast with the commercial membrane, where the actual rejection rate could be overestimated.

The anionic charge of the aqueous dye feed solution and the negative surface charge of the commercial M8 membrane appeared to have a contribution to the solute repulsion leading to higher rejection due to the Donnan effect [72]. However, all tested S-PANI membranes (M1-M3) which had an opposite charge

to the retained dye solutes, also demonstrated a higher rejection than the PEG solutes. To differentiate the S-PANI membrane's dye rejection mechanism, i.e., size-exclusion versus adsorption, as there would not be any Donnan exclusion in the cationic membrane for anionic molecules, the adsorbed dye mass was quantified for the M1 membrane based on the mass balance of the feed, concentrate and the permeate, (SI, Table. S3.3). The mass of the adsorbed dye to the M1 membrane was in the following order Indigo carmine>Rose bengal>Methylene blue. The dye mass adsorption follows similar order to the dye's zeta potential -27.4, -6.1 and -1.5 mV, respectively. The significant difference in the membrane surface charge and the Indigo carmine solution's zeta potential ($\Delta V \approx 38.9$ mV) resulted in the highest mass adsorption ($\approx 42\%$) compared with the methylene blue dye solution where the adsorbed mass $\approx 16\%$. This means that the size exclusion is the dominant rejection mechanism for the methylene blue dye solutes for the S-PANI membranes. The bulky nature of the dye molecule showed a higher rejection compared to the flexible PEG molecule for the same MW of PEG and dye solution, as the PEG chain allows it to wiggle through the small size pore while the dye molecule clogs the pore [76,77].

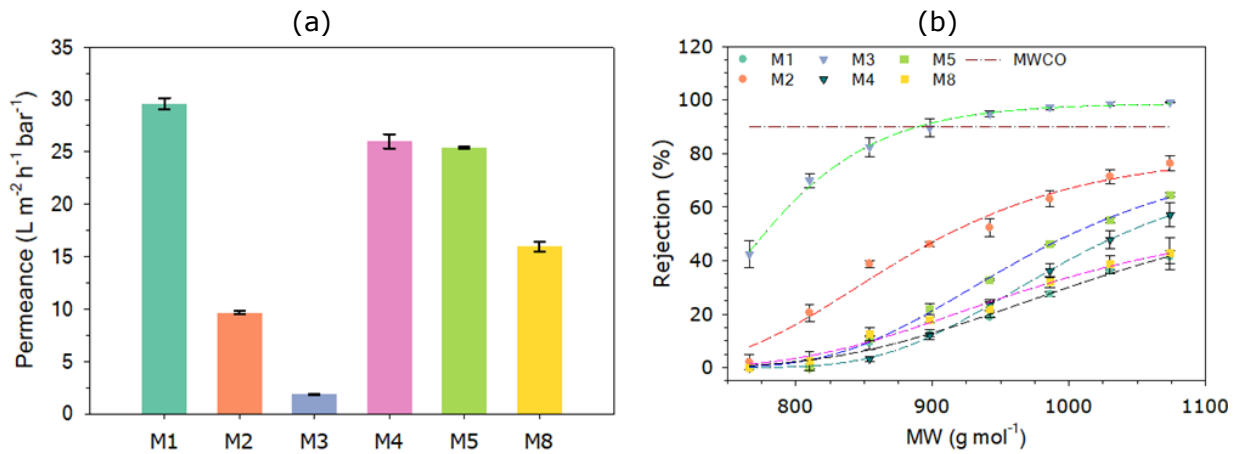


Fig. 3.12 (a) PEG permeance and (b) rejection of the S-PANI membranes (M1-M5) and the commercial membrane (M8).

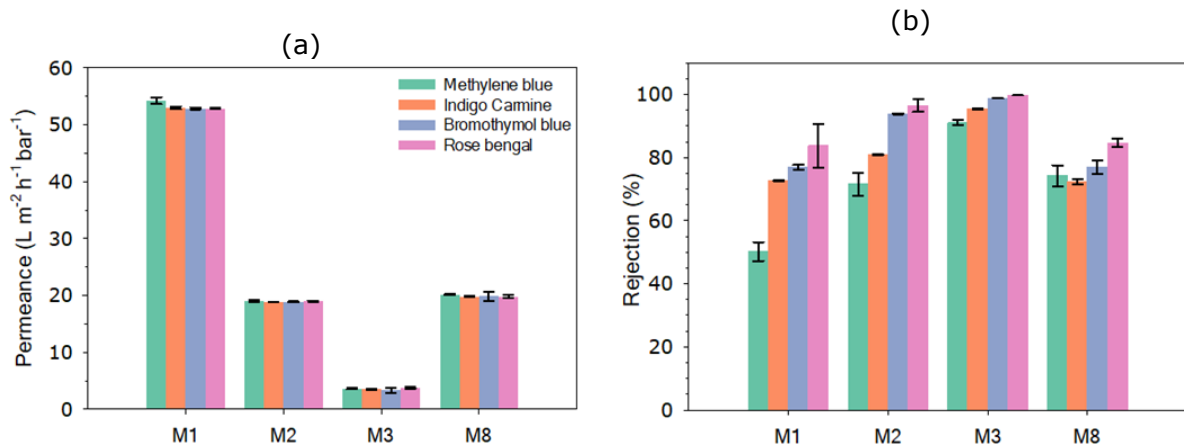


Fig. 3.13 (a) dye feed solution (methylene blue, indigo carmine, bromothymol blue and rose bengal) permeance and (b) rejection for of the S-PANI membranes (M1-M3) and the commercial membrane (M8).

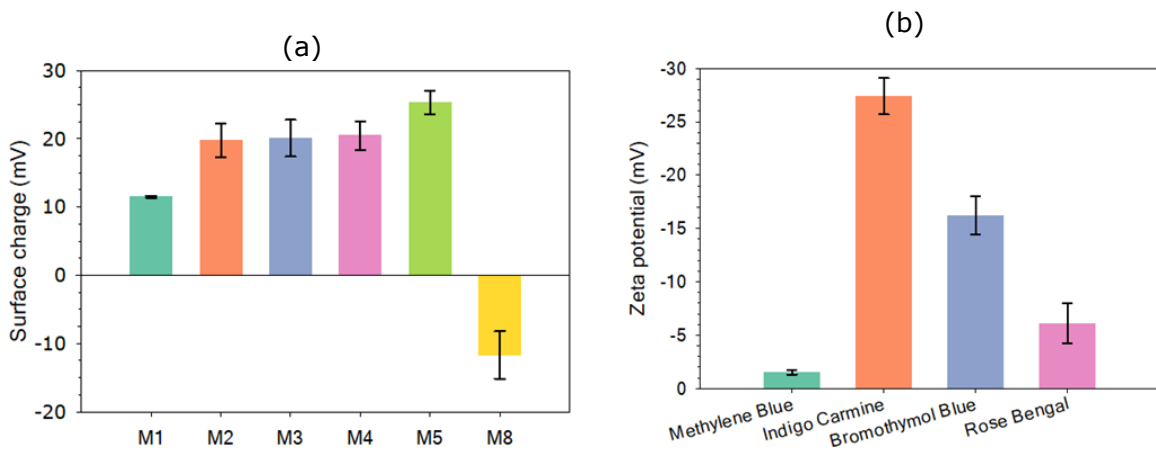


Fig. 3.14 (a) The surface charge of M1-M5 membranes and the commercial M8 membrane and (b) The zeta potential of dye feed solutions (methylene blue 10 mg L⁻¹, indigo carmine 10 mg L⁻¹, bromothymol blue 50 mg L⁻¹ and rose bengal 10 mg L⁻¹).

3.4 Conclusions

S-PANI powder was synthesised by oxidation polymerisation and subsequently, integrally skinned asymmetric membranes were prepared using the NIPS technique. The presence of sulfonic groups in the polymer backbone provides the anchor to cross-link the polymer while precipitating in an acidic aqueous coagulation bath. FT-IR, XPS and XRD spectra of the SPANI membranes produced in 1 M and 3 M HCl(aq) coagulation bath (M2-M3) indicates a potential interaction between the sulfonic groups and the nitrogen resulting in a more amorphous matrix compared to the pristine S-PANI produced in pure water coagulation bath (M1). TEM images showed a loose structure of precipitated polymer particles in pure water, compared to a dense and inter-linked structure in an acidic coagulation bath. The simultaneous cross-linking led to an instant formation of a dense selective layer, which diminished the demixing rate. This resulted in an altered membrane conformation with suppressed macro-voids, reduced porosity, improved tensile strength, enhanced hydrophilicity, and a significant improvement in *DMF* solvent stability over an observation time of two weeks. The TGA of the cross-linked membranes also showed a broad and extended peak at high temperature whereas the glass transition temperature was decreased. In-situ tailored NF S-PANI membranes (M3) with MWCO \approx 680 g mol⁻¹ (sucrose octa-acetate) showed a rejection of 99% for PEG 1000 g mol⁻¹ and 91-100% for dye solutes (MW range of 320-1017 g mol⁻¹) compared to 34% and 74-85% rejection for a commercial membrane with nominal (labelled) MWCO 1000 g mol⁻¹, respectively. In summary, high-performance S-PANI membranes were prepared in-situ by exploiting cross-linkable sulfonic groups, while tailoring the coagulation bath conditions. This new simplistic, time, chemical and cost savings scalable approach can be effortlessly applied to design new classes of S-PANI membranes in NF range without the complications of using laborious post modification cross-linking methods.

3.5 Acknowledgements

H.A. was supported by a University of Bath research scholarship. The authors thank Matthew Jones and Simon Lewis for valuable discussion and the technicians' team at the Department of Chemical Engineering and the Bio-imaging lab at the University of Bath for support and advice. The X-ray

photoelectron (XPS) data collection was performed at the EPSRC National Facility for XPS (“HarwellXPS”), operated by Cardiff University and UCL, under Contract No. PR16195.

3.6 References

- [1] L.K. Wang, J.P. Chen, Y.-T. Hung, N.K. Shammass, eds., *Membrane and Desalination Technologies*, Humana Press, Totowa, NJ, 2011. <https://doi.org/10.1007/978-1-59745-278-6>.
- [2] L. Llenas, G. Ribera, X. Martínez-Lladó, M. Rovira, J. de Pablo, Selection of nanofiltration membranes as pretreatment for scaling prevention in SWRO using real seawater, *Desalin. Water Treat.* 51 (2013) 930–935. <https://doi.org/10.1080/19443994.2012.714578>.
- [3] V. Yangali-Quintanilla, S.K. Maeng, T. Fujioka, M. Kennedy, G. Amy, Proposing nanofiltration as acceptable barrier for organic contaminants in water reuse, *J. Memb. Sci.* 362 (2010) 334–345. <https://doi.org/10.1016/j.memsci.2010.06.058>.
- [4] O. Akin, F. Temelli, S. Köseoğlu, *Membrane Applications in Functional Foods and Nutraceuticals*, *Crit. Rev. Food Sci. Nutr.* 52 (2012) 347–371. <https://doi.org/10.1080/10408398.2010.500240>.
- [5] A.F. Ismail, *Membrane Technology for Water and Wastewater Treatment, Energy and Environment*, 2016. <https://doi.org/10.1201/b19702>.
- [6] A.I. Schäfer, *Natural Organics Removal Using Membranes*, CRC Press, 1999. <https://doi.org/10.1201/9781420031638>.
- [7] P. Marchetti, M.F. Jimenez Solomon, G. Szekely, A.G. Livingston, Molecular Separation with Organic Solvent Nanofiltration: A Critical Review, *Chem. Rev.* 114 (2014) 10735–10806. <https://doi.org/10.1021/cr500006j>.
- [8] I. Koyuncu, R. Sengur, T. Turken, S. Guclu, M.E. Pasaoglu, Advances in water treatment by microfiltration, ultrafiltration, and nanofiltration, in: *Adv. Membr. Technol. Water Treat.*, Elsevier, 2015: pp. 83–128. <https://doi.org/10.1016/B978-1-78242-121-4.00003-4>.
- [9] G.R. Guillen, Y. Pan, M. Li, E.M.V. Hoek, Preparation and characterization of membranes formed by nonsolvent induced phase separation: A review, *Ind. Eng. Chem. Res.* 50 (2011)

- 3798–3817. <https://doi.org/10.1021/ie101928r>.
- [10] M. Mulder, *Basic Principles of Membrane Technology*, Springer Netherlands, Dordrecht, 1996. <https://doi.org/10.1007/978-94-009-1766-8>.
- [11] B. Singh, V. Kochkodan, R. Hashaikeh, N. Hilal, A review on membrane fabrication : Structure, properties and performance relationship, *Desalination*. 326 (2013) 77–95. <https://doi.org/http://dx.doi.org/10.1016/j.desal.2013.06.016>.
- [12] K. Vanherck, A. Cano-Odena, G. Koeckelberghs, T. Dedroog, I. Vankelecom, A simplified diamine crosslinking method for PI nanofiltration membranes, *J. Memb. Sci.* 353 (2010) 135–143. <https://doi.org/10.1016/j.memsci.2010.02.046>.
- [13] Z. Wang, Cross-Link, in: *Encycl. Membr.*, Springer Berlin Heidelberg, Berlin, Heidelberg, 2016: pp. 479–480. https://doi.org/10.1007/978-3-662-44324-8_1809.
- [14] A. Asadi Tashvigh, Y. Feng, M. Weber, C. Maletzko, T.-S. Chung, 110th Anniversary: Selection of Cross-Linkers and Cross-Linking Procedures for the Fabrication of Solvent-Resistant Nanofiltration Membranes: A Review, *Ind. Eng. Chem. Res.* 58 (2019) 10678–10691. <https://doi.org/10.1021/acs.iecr.9b02408>.
- [15] A.L. Zydney, C. Ho, Effect of Membrane Morphology on System Capacity During Normal Flow Microfiltration, (2003). <https://doi.org/10.1002/bit.10699>.
- [16] M. Elimelech, Xiaohua Zhu, A.E. Childress, Seungkwan Hong, Role of membrane surface morphology in colloidal fouling of cellulose acetate and composite aromatic polyamide reverse osmosis membranes, *J. Memb. Sci.* 127 (1997) 101–109. [https://doi.org/10.1016/S0376-7388\(96\)00351-1](https://doi.org/10.1016/S0376-7388(96)00351-1).
- [17] K. Scott, Membrane materials, preparation and characterisation, in: *Handb. Ind. Membr.*, Elsevier, 1995: pp. 187–269. <https://doi.org/10.1016/B978-185617233-2/50005-2>.
- [18] C.J.W. Nidal Hilal, Mohamed Khayet, *Membrane Modification*, CRC Press, 2016. <https://doi.org/10.1201/b12160>.
- [19] H. Deligöz, Preparation of self-standing polyaniline-based membranes: Doping effect on the selective ion separation and reverse osmosis properties, *J. Appl. Polym. Sci.* 105 (2007) 2640–

2645. <https://doi.org/10.1002/app.26377>.
- [20] L.L. Xu, S. Shahid, D.A. Patterson, E.A.C. Emanuelsson, Flexible electro-responsive in-situ polymer acid doped polyaniline membranes for permeation enhancement and membrane fouling removal, *J. Memb. Sci.* 578 (2019) 263–272. <https://doi.org/10.1016/j.memsci.2018.09.070>.
- [21] H. Hu, J.M. Saniger, J.G. Bañuelos, Thin films of polyaniline-polyacrylic acid composite by chemical bath deposition, *Thin Solid Films.* 347 (1999) 241–247. [https://doi.org/10.1016/S0040-6090\(99\)00039-5](https://doi.org/10.1016/S0040-6090(99)00039-5).
- [22] N.F. Razali, A.W. Mohammad, N. Hilal, Effects of polyaniline nanoparticles in polyethersulfone ultrafiltration membranes: Fouling behaviours by different types of foulant, *J. Ind. Eng. Chem.* 20 (2014) 3134–3140. <https://doi.org/10.1016/j.jiec.2013.11.056>.
- [23] S.M.J. Zaidi, K.S. Lakhi, Sulfonated Block Copolymer Membrane, in: *Encycl. Membr.*, Springer Berlin Heidelberg, Berlin, Heidelberg, 2016: pp. 1844–1845. https://doi.org/10.1007/978-3-662-44324-8_561.
- [24] J. Yue, Z.H. Wang, K.R. Cromack, A.J. Epstein, A.G. MacDiarmid, Effect of sulfonic acid group on polyaniline backbone, *J. Am. Chem. Soc.* 113 (1991) 2665–2671. <https://doi.org/10.1021/ja00007a046>.
- [25] I.F. Amura, S. Shahid, A. Sarihan, J. Shen, D.A. Patterson, E.A.C. Emanuelsson, Fabrication of self-doped sulfonated polyaniline membranes with enhanced antifouling ability and improved solvent resistance, *J. Memb. Sci.* (2019) 117712. <https://doi.org/10.1016/j.memsci.2019.117712>.
- [26] H. Alhweij, I. Amura, J. Wenk, E.A.C. Emanuelsson, S. Shahid, Self-doped sulfonated polyaniline ultrafiltration membranes with enhanced chlorine resistance and antifouling properties, *J. Appl. Polym. Sci.* (2021) 50756. <https://doi.org/10.1002/app.50756>.
- [27] X.X. Loh, M. Sairam, A. Bismarck, J.H.G. Steinke, A.G. Livingston, K. Li, Crosslinked integrally skinned asymmetric polyaniline membranes for use in organic solvents, 326 (2009) 635–642. <https://doi.org/10.1016/j.memsci.2008.10.045>.
- [28] M. Sairam, X. Xing, K. Li, A. Bismarck, J. Hans, G. Steinke, A. Guy, Nanoporous asymmetric polyaniline films for filtration of organic solvents, 330 (2009) 166–174.

- <https://doi.org/10.1016/j.memsci.2008.12.067>.
- [29] J. Shen, S. Shahid, A. Sarihan, D.A. Patterson, E.A.C. Emanuelsson, Effect of polyacid dopants on the performance of polyaniline membranes in organic solvent nanofiltration, *Sep. Purif. Technol.* 204 (2018) 336–344. <https://doi.org/10.1016/j.seppur.2018.04.034>.
- [30] V. Vijayalekshmi, D. Khastgir, Eco-friendly methanesulfonic acid and sodium salt of dodecylbenzene sulfonic acid doped cross-linked chitosan based green polymer electrolyte membranes for fuel cell applications, *J. Memb. Sci.* 523 (2017) 45–59. <https://doi.org/10.1016/j.memsci.2016.09.058>.
- [31] S. Zhao, Z. Wang, J. Wang, S. Wang, The effect of pH of coagulation bath on tailoring the morphology and separation performance of polysulfone/polyaniline ultrafiltration membrane, *J. Memb. Sci.* 469 (2014) 316–325. <https://doi.org/10.1016/j.memsci.2014.06.054>.
- [32] K. V. Kurada, S. De, Polyaniline doped ultrafiltration membranes: Mechanism of membrane formation and pH response characteristics, *Polymer (Guildf)*. 153 (2018) 201–213. <https://doi.org/10.1016/j.polymer.2018.08.032>.
- [33] I. Mav, M. Žigon, A. Šebenik, Sulfonated polyaniline, *Synth. Met.* 101 (1999) 717–718. [https://doi.org/10.1016/S0379-6779\(98\)01166-7](https://doi.org/10.1016/S0379-6779(98)01166-7).
- [34] S. Bhadra, N.H. Kim, J.H. Lee, Synthesis of water soluble sulfonated polyaniline and determination of crystal structure, *J. Appl. Polym. Sci.* 117 (2010) 2025–2035. <https://doi.org/10.1002/app.32152>.
- [35] S.S. An, H.H. Yoon, G. Das, Amperometric urea biosensors based on sulfonated graphene/polyaniline nanocomposite, *Int.J. Nanomedicine*.(2015)55. <https://doi.org/10.2147/IJN.S88315>.
- [36] L. Li, S. Shahid, D. Alec, E. Anna, C. Emanuelsson, Flexible electro-responsive in-situ polymer acid doped polyaniline membranes for permeation enhancement and membrane fouling removal, 578 (2019) 263–272. <https://doi.org/10.1016/j.memsci.2018.09.070>.
- [37] J. Jang, J. Ha, J. Cho, Fabrication of Water-Dispersible Polyaniline-Poly(4-styrenesulfonate) Nanoparticles For Inkjet-Printed Chemical-Sensor Applications, *Adv. Mater.* 19 (2007) 1772–

1775. <https://doi.org/10.1002/adma.200602127>.
- [38] B.T. McVerry, J.A.T. Temple, X. Huang, K.L. Marsh, E.M. V. Hoek, R.B. Kaner, Fabrication of Low-Fouling Ultrafiltration Membranes Using a Hydrophilic, Self-Doping Polyaniline Additive, *Chem. Mater.* 25 (2013) 3597–3602. <https://doi.org/10.1021/cm401288r>.
- [39] C. Topaçli, A. Topaçli, Infrared spectra simulation for some sulfonamides by using semi-empirical methods, *Spectrosc. Lett.* 35 (2002) 207–217. <https://doi.org/10.1081/SL-120003806>.
- [40] T. Sata, Ion exchange membranes and separation processes with chemical reactions, *J. Appl. Electrochem.* 21 (1991) 283–294. <https://doi.org/10.1007/BF01020210>.
- [41] G. Chamoulaud, D. Bélanger, Chemical Modification of the Surface of a Sulfonated Membrane by Formation of a Sulfonamide Bond, *Langmuir.* 20 (2004) 4989–4995. <https://doi.org/10.1021/la0362851>.
- [42] B.P. TriPathi, T. Chakrabarty, V.K. Shahi, Highly charged and stable cross-linked 4,4'-bis(4-aminophenoxy)biphenyl-3,3'-disulfonic acid (BAPBDS)-sulfonated poly(ether sulfone) polymer electrolyte membranes impervious to *Methanol*, *J. Mater. Chem.* 20 (2010) 8036. <https://doi.org/10.1039/c0jm01183e>.
- [43] P. Chapman, X.X. Loh, A.G. Livingston, K. Li, T.A.C. Oliveira, Polyaniline membranes for the dehydration of *tetrahydrofuran* by pervaporation, 309 (2008) 102–111. <https://doi.org/10.1016/j.memsci.2007.10.016>.
- [44] Westerhof HP, Picken SJ, On the structure and dissolution properties of poly(p-phenylene terephthalamide) effect of solvent composition, Delft University of Technology, 2009.
- [45] S. Bhadra, D. Khastgir, Determination of crystal structure of polyaniline and substituted polyanilines through powder X-ray diffraction analysis, *Polym. Test.* 27 (2008) 851–857. <https://doi.org/10.1016/j.polymertesting.2008.07.002>.
- [46] S. Tan, A. Laforgue, D. Bélanger, Characterization of a Cation-Exchange/Polyaniline Composite Membrane, *Langmuir.* 19 (2003) 744–751. <https://doi.org/10.1021/la0263054>.
- [47] P. Sivaraman, J.G. Chavan, A.P. Thakur, V.R. Hande, A.B. Samui, Electrochemical modification of cation exchange membrane with polyaniline for improvement in

- permselectivity, *Electrochim. Acta.* 52 (2007) 5046–5052.
<https://doi.org/10.1016/j.electacta.2007.02.016>.
- [48] Nidal Hilal; Ahmad Fauzi Ismail; Chris J Wright, *Membrane Fabrication*, CRC Press, 2015.
<https://doi.org/10.1201/b18149>.
- [49] P. Sukitpaneenit, T. Chung, Molecular elucidation of morphology and mechanical properties of PVDF hollow fiber membranes from aspects of phase inversion , crystallization and rheology, 340 (2009) 192–205. <https://doi.org/10.1016/j.memsci.2009.05.029>.
- [50] D. Wang, K. Li, W.K. Teo, Porous PVDF asymmetric hollow fiber membranes prepared with the use of small molecular additives, 178 (2000) 13–23. [https://doi.org/10.1016/S0376-7388\(00\)00460-9](https://doi.org/10.1016/S0376-7388(00)00460-9).
- [51] J. Huang, R.B. Kaner, The intrinsic nanofibrillar morphology of polyaniline, (2006) 367–376.
<https://doi.org/10.1039/b510956f>.
- [52] M. Sadrzadeh, S. Bhattacharjee, Rational design of phase inversion membranes by tailoring thermodynamics and kinetics of casting solution using polymer additives, *J. Memb. Sci.* 441 (2013) 31–44. <https://doi.org/10.1016/j.memsci.2013.04.009>.
- [53] C. Sun, Poly(vinylidene fluoride) membranes: Preparation, modification, characterization and applications, *Chem. Eng.* (2009) 193. <https://doi.org/10.1016/j.actbio.2008.09.016>.
- [54] U. Rosenthal, J. Nechushtan, A. Kedem, D. Lancet, M.A. Frommer, An apparatus for studying the mechanism of membrane formation, *Desalination.* 9 (1971) 193–200.
[https://doi.org/10.1016/S0011-9164\(00\)80029-6](https://doi.org/10.1016/S0011-9164(00)80029-6).
- [55] H. Strathmann, K. Kock, P. Amar, R.W. Baker, The formation mechanism of asymmetric membranes, *Desalination.* 16 (1975) 179–203. [https://doi.org/10.1016/S0011-9164\(00\)82092-5](https://doi.org/10.1016/S0011-9164(00)82092-5).
- [56] H.J. Kim, R.K. Tyagi, A.E. Fouda, K. Jonasson, The kinetic study for asymmetric membrane formation via phase-inversion process, *J. Appl. Polym. Sci.* 62 (1996) 621–629.
[https://doi.org/10.1002/\(SICI\)1097-4628\(19961024\)62:4<621::AID-APP5>3.0.CO;2-V](https://doi.org/10.1002/(SICI)1097-4628(19961024)62:4<621::AID-APP5>3.0.CO;2-V).
- [57] J.H. Kim, K.H. Lee, Effect of PEG additive on membrane formation by phase inversion, *J.*

- Memb. Sci. 138 (1998) 153–163. [https://doi.org/10.1016/S0376-7388\(97\)00224-X](https://doi.org/10.1016/S0376-7388(97)00224-X).
- [58] P.C. Rodrigues, G.P. De Souza, J.D. Da Motta Neto, L. Akcelrud, Thermal treatment and dynamic mechanical thermal properties of polyaniline, *Polymer (Guildf)*. 43 (2002) 5493–5499. [https://doi.org/10.1016/S0032-3861\(02\)00401-9](https://doi.org/10.1016/S0032-3861(02)00401-9).
- [59] E. Tarleton, J. Robinson, S. Smith, J. NA, New experimental measurements of solvent induced swelling in nanofiltration membranes, *J. Memb. Sci.* 261 (2005) 129–135. <https://doi.org/10.1016/j.memsci.2005.02.037>.
- [60] A.F.M. Barton, *Handbook of Solubility Parameters and Other Cohesion Parameters.*, CRC Press, 1983.
- [61] L. Xu, S. Shahid, A.K. Holda, E.A.C. Emanuelsson, D.A. Patterson, Stimuli responsive conductive polyaniline membrane: In-filtration electrical tuneability of flux and MWCO, *J. Memb. Sci.* 552 (2018) 153–166. <https://doi.org/10.1016/j.memsci.2018.01.070>.
- [62] M.J. Liu, K. Tzou, R.V. Gregory, Influence of the doping conditions on the surface energies of conducting polymers, *Synth. Met.* 63 (1994) 67–71. [https://doi.org/10.1016/0379-6779\(94\)90251-8](https://doi.org/10.1016/0379-6779(94)90251-8).
- [63] M. Mänttari, A. Pihlajamäki, M. Nyström, Effect of pH on hydrophilicity and charge and their effect on the filtration efficiency of NF membranes at different pH, *J. Memb. Sci.* 280 (2006) 311–320. <https://doi.org/10.1016/j.memsci.2006.01.034>.
- [64] I.F. Vankelecom, K. De Smet, L.E. Gevers, A. Livingston, D. Nair, S. Aerts, S. Kuypers, P.A. Jacobs, Physico-chemical interpretation of the SRNF transport mechanism for solvents through dense silicone membranes, *J. Memb. Sci.* 231 (2004) 99–108. <https://doi.org/10.1016/j.memsci.2003.11.007>.
- [65] L. Sun, H. Liu, R. Clark, S.C. Yang, Double-strand polyaniline, *Synth. Met.* 84 (1997) 67–68. [https://doi.org/10.1016/s0379-6779\(96\)03839-8](https://doi.org/10.1016/s0379-6779(96)03839-8).
- [66] M.A. Alaei Shahmirzadi, S.S. Hosseini, G. Ruan, N.R. Tan, Tailoring PES nanofiltration membranes through systematic investigations of prominent design, fabrication and operational parameters, *RSC Adv.* 5 (2015) 49080–49097. <https://doi.org/10.1039/c5ra05985b>.

- [67] R.W. Baker, *Membrane Technology and Applications*, John Wiley & Sons, Ltd, Chichester, UK, 2004. <https://doi.org/10.1002/0470020393>.
- [68] American Water Works Association, *Microfiltration and Ultrafiltration Membranes for Drinking Water - Manual of Water Supply Practices*, 2nd Editio, 2016.
- [69] J. Shen, S. Shahid, I. Amura, A. Sarihan, M. Tian, Enhanced adsorption of cationic and anionic dyes from aqueous solutions by polyacid doped polyaniline, *Synth. Met.* 245 (2018) 151–159. <https://doi.org/10.1016/j.synthmet.2018.08.015>.
- [70] 2001 Huang, L. & Nishinari, K., Interaction between poly(ethylene glycol) and water as studied by differential scanning calorimetry, *J. Polym. Sci.* 5 (2001) 496–50. [https://doi.org/https://doi-org.ezproxy1.bath.ac.uk/10.1002/1099-0488\(20010301\)39:5<496::AID-POLB1023>3.0.CO;2-H](https://doi.org/https://doi-org.ezproxy1.bath.ac.uk/10.1002/1099-0488(20010301)39:5<496::AID-POLB1023>3.0.CO;2-H).
- [71] E. Sabadini, E.M. Assano, T.D.Z. Atvars, Molecular weight of polyethylene glycols by vapor pressure osmometry: An alternative data treatment, *J. Appl. Polym. Sci.* 65 (1997) 595–600. [https://doi.org/10.1002/\(SICI\)1097-4628\(19970718\)65:3<595::AID-APP19>3.0.CO;2-W](https://doi.org/10.1002/(SICI)1097-4628(19970718)65:3<595::AID-APP19>3.0.CO;2-W).
- [72] L. Xu, S. Shahid, J. Shen, E.A.C. Emanuelsson, D.A. Patterson, A wide range and high resolution one-filtration molecular weight cut-off method for aqueous based nanofiltration and ultrafiltration membranes, *J. Memb. Sci.* 525 (2017) 304–311. <https://doi.org/10.1016/j.memsci.2016.12.004>.
- [73] Y.H.S. Toh, X.X. Loh, K. Li, A. Bismarck, A.G. Livingston, In search of a standard method for the characterisation of organic solvent nanofiltration membranes, 291 (2007) 120–125. <https://doi.org/10.1016/j.memsci.2006.12.053>.
- [74] N. Wang, J. Li, W. Lv, J. Feng, W. Yan, Synthesis of polyaniline/TiO₂ composite with excellent adsorption performance on acid red G, *RSC Adv.* 5 (2015) 21132–21141. <https://doi.org/10.1039/c4ra16910g>.
- [75] & B.E. Lunkwitz; Klaus, U., Buchhammer; Heide-Marie, *Permanent hydrophilic modification of fluoropolymers*, 1996.
- [76] X. Yang, Experimental observations of nanofiltration with organic solvents, *J. Memb. Sci.* 190

(2001) 45–55. [https://doi.org/10.1016/S0376-7388\(01\)00392-1](https://doi.org/10.1016/S0376-7388(01)00392-1).

- [77] R. Levenstein, D. Hasson, R. Semiat, Utilization of the Donnan effect for improving electrolyte separation with nanofiltration membranes, *J. Memb. Sci.* 116 (1996) 77–92. [https://doi.org/10.1016/0376-7388\(96\)00029-4](https://doi.org/10.1016/0376-7388(96)00029-4).

Supporting Information

Simplified in-situ tailoring of cross-linked self-doped sulfonated polyaniline (S-PANI) membranes for nanofiltration applications

Hassan Alhweij^{a,c,d}, Emma Anna Carolina Emanuelsson^{a,b}, Salman Shahid^{a,b,c*}, Jannis Wenk^{a,c*}

^a Department of Chemical Engineering, University of Bath, Bath BA2 7AY, United Kingdom

^b Centre for Advanced Separations Engineering, University of Bath, Bath BA2 7AY, United Kingdom

^c Water Innovation and Research Centre (WIRC@Bath), University of Bath, Bath, BA2 7AY, United Kingdom

^d Stantec UK Limited, Dominion House, Warrington, WA3 6GD, United Kingdom

* Corresponding authors

Jannis Wenk: j.h.wenk@bath.ac.uk

Salman Shahid: s.shahid@bath.ac.uk

Materials S1

Aniline, ammonium persulfate (APS), 4-methylpyridine (4MP), *N*-methyl-2-pyrrolidone (NMP), ammonium hydroxide solution, *acetonitrile* (ACN) HPLC grade, *N,N*-dimethylformamide (DMF), raffinose (MW 504.5 g mol⁻¹), sucrose octa-acetate (MW 678.6 g mol⁻¹), methylene blue (MW 319.8 g mol⁻¹), indigo carmine (MW 466.4 g mol⁻¹), bromothymol blue (MW 624.4 g mol⁻¹) and rose bengal (MW 1017.6 g mol⁻¹) were obtained from Sigma-Aldrich, UK. *Methanol*, 3-aminobenzene sulfonic acid (metanilic acid), sodium hydroxide and hydrochloric acid (HCl) aqueous solution were obtained from VWR, UK. Polyethylene glycol (PEG) 1000 g mol⁻¹ was obtained from Fisher, UK. Commercial composite fluoropolymer flat sheet membrane (nominal MWCO 1000 g mol⁻¹) was obtained from Alfa Laval, UK.

S-PANI synthesis S2

S-PANI was synthesised by radical polymerisation of aniline and metanilic acid in the presence of ammonium persulfate in an acidic medium. During a typical synthesis, aniline was added to HCl solution (1.0 M). The mixture was then poured into a glass beaker surrounded by ice for cooling. Metanilic acid was added to the aniline-hydrochloric acid mixture and then stirred for 5 minutes using an overhead mechanical mixer fitted with a Teflon coated impeller. In a separate beaker, ammonium persulfate (APS) was dissolved in HCl solution (1.0 M). The APS-HCl solution was then added into the aniline flask drop by drop using a Watson Marlow peristaltic pump to allow control over the reaction temperature and formation of a reasonably long-chain polymer. The aniline, metanilic acid and APS were 1:1 M ratio. The total APS-HCl solution addition period was around 13 h. After a reaction period of 24 h which involves APS addition and extended stirring, the solution was filtered (Whatman paper) and washed multiple times with pure water and then *Methanol* until a neutral pH of the washing solution was reached. Subsequently, the powder was added to ammonium hydroxide solution (1.0 M) and left to mix using a magnetic stirrer for 1 h at room temperature to deprotonate the polymer salt to its base form. The powder was then washed down with pure water (1 L), followed by 200 mL of *Methanol* (50%, w/v) and finally 1 L of pure water. The filtered polymer powder was dried under a vacuum for

24 h at 60°C. The dry S-PANI powder was grounded by ceramic mortar and pestle, then passed through a 160 µm mesh sieve to remove any remaining clusters, leaving a fine powder with 72±1% yield based on the aniline monomer. This powder was then stored in plastic vials until required.

Fig. S3.1 shows the chemical structure of the formed S-PANI salt with the sulfonate functional group bonded with the aromatic benzene ring. The obtained powder was analysed by FT-IR to confirm that sulfonation had occurred.

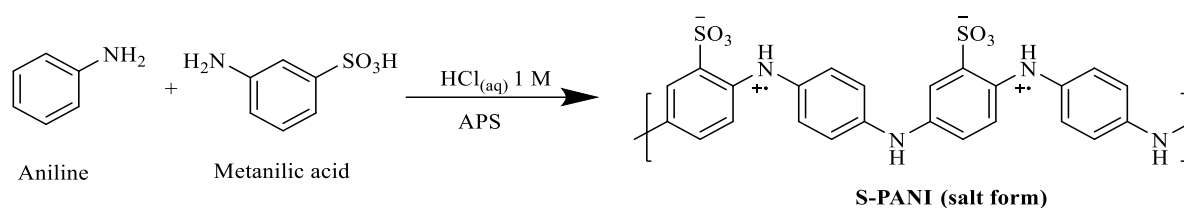


Fig. S3.1 Polymerisation scheme for S-PANI.

S-PANI molecular weight determination S3

All analysis was performed on an Agilent Infinity II MDS instrument equipped with differential refractive index (DRI), viscometry (VS), dual-angle light scatters (LS) and variable wavelength UV detectors. The system was equipped with 2 x PLgel Mixed D columns (300 x 7.5 mm) and a PLgel 5 µm guard column. The eluent is *DMF* with a 5 mmol NH_4BF_4 additive. Samples were solubilised overnight before filtration through a nylon membrane with 0.22 µm pore size before injection. Samples were run at 1 mL min^{-1} at 50°C. Poly(methyl methacrylate) standards (Agilent EasiVials) were used for calibration between 955,000–550 g mol^{-1} . Respectively, experimental molar mass (M_n , SEC) and dispersity (\mathcal{D}) values of synthesized polymers were determined by conventional calibration using Agilent GPC/SEC software.

Energy dispersive X-ray S4

The element analysis of the S-PANI powder was studied via Scanning electron microscope- energy dispersive X-ray (SEM-EDX) using an FSEM (JSM-6301F, JEOL, Germany). The element analysis is shown in Table S 3.1.

Table. S3.1 Element analysis (Atomic % and weight%) of S-PANI powder.

Element	Weight %	Atomic %
C	67.6±0.3	76.8±0.5
N	11.4±0.2	10.3±0.1
O	9.8±0.4	7.2±0.1
S	9.3±0.1	4.4±0.1
Cl	1.9±1.1	1.3±0.3

Membrane fabrication S5

For the cast film solution, S-PANI powder (20 wt%) was added in small portions to a mixture of *NMP* (74 wt%) and an anti-gelling agent 4MP (6 wt%). The mixture was stirred at 100 rpm for 2 h until a homogeneous solution was obtained and then left stirring at 50 rpm overnight. Afterwards, the polymer solution was left unstirred for 12 h for deaeration. A PET/PBT non-woven support layer (Novatexx 2484, 120 μm , Freudenberg Filter Technologies, Germany) was placed on a flat glass plate before casting. Elcometer 3540 film applicator was used to cast 200 μm membranes (clearance gap) at room temperature at a controlled relative humidity of ~30%. Membranes formed after immersion precipitation in the coagulation bath solution at room temperature, considering a consistent evaporation time of 10 seconds, before immersing the polymer solution into the coagulation bath. Different acidic strengths of coagulation solution (pure water, 1 M HCl and 3 M HCl) were used to produce membrane samples. After 24 h, some of the resulting membrane sheets were rinsed and stored at room temperature in pure water for a week, while the others were used freshly to understand the effect of H^+ ion leaching on membrane morphology and transport properties. The rinsing water was changed daily to ensure complete H^+ ion removal from the membranes. A set of S-PANI membrane control samples was produced in a pure water coagulation bath and subsequently doped in acidic aqueous solutions (1 M and 3 M HCl) overnight to understand the effect of doping as a post-treatment of the membrane transport properties. The H^+ doped S-PANI membranes were rinsed with water for 5 min before use. In parallel, a set of the post-treated (doped) membranes was also rinsed in water for a week to assess the membrane performance after dedoping.

Membrane characterisation S6

FT-IR, XPS and XRD analysis

The chemical composition of S-PANI membranes was determined using an FT-IR spectrometer (PIKE Technologies Inc, USA) fitted with an attenuated total reflectance (ATR) accessory. Each FT-IR spectrum had 32 scans with 4 cm^{-1} resolution.

XPS data were acquired using a Kratos Axis SUPRA using monochromated Al $K\alpha$ (1486.69 eV) X-rays at 15 mA emission and 12 kV HT (180W) and a spot size/analysis area of $700 \times 300\ \mu\text{m}$. The instrument was calibrated to gold metal Au 4f (83.95 eV) and dispersion adjusted to give a binding energy (BE) of 932.6 eV for the Cu 2p_{3/2} line of metallic copper. Ag 3d_{5/2} line FWHM at 10 eV pass energy was 0.544 eV. Source resolution for monochromatic Al $K\alpha$ X-rays is ~ 0.3 eV. The instrumental resolution was determined to be 0.29 eV at 10 eV pass energy using the Fermi edge of the valence band for metallic silver. Resolution with charge compensation system on < 1.33 eV FWHM on PTFE. High-resolution spectra were obtained using a pass energy of 20 eV, step size of 0.1 eV and sweep time of 60 seconds, resulting in a line width of 0.696 eV for Au 4f_{7/2}. Survey spectra were obtained using a pass energy of 160 eV. Charge neutralisation was achieved using an electron flood gun with filament current = 0.38 A, charge balance = 2 V, filament bias = 4.2 V. Successful neutralisation was adjudged by analysing the C 1s region wherein a sharp peak with no lower BE structure was obtained. Spectra have been charge corrected to the mainline of the carbon 1s spectrum (adventitious carbon) set to 284.8 eV. All data was recorded at a base pressure of below 9×10^{-9} Torr and a room temperature of 294 K. Data was analysed using CasaXPS v2.3.19PR1.0. Peaks were fit with a Shirley background before component analysis.

X-ray diffractometry (XRD) was used to characterise M1, M2 and M3. XRD spectra were scanned on a STOE STADI P double setup, equipped with mythen detectors, using pure Cu- $K\alpha 1$ radiation ($\lambda = 1.54060\ \text{\AA}$).

Ion exchange capacity (IEC), Water uptake (WU), hydrolytic and alkalinity stability

After immersion in pure water for one day, membrane samples were subsequently immersed for one day in 100 mL of HCl(aq) solution to fully protonate the polymeric structure. The membrane was then washed and equilibrated for 4 h with distilled water, while the distilled was changed several times to remove the last traces of acid. The membrane was then equilibrated with 50 mL of 0.01 M NaOH(aq) solution for 24 h and the cation exchange capacity was determined from the reduction in alkalinity determined by back titration. The ion exchange capacity of the cation exchange membrane was calculated using equation:

$$IEC = \frac{V_{NaOH} \times S_{NaOH}}{m_{dry}} \quad \text{Equation S 3.1}$$

where, V_{NaOH} is the volume of NaOH used in the titration, m_{dry} is the dry weight of the membrane in g, and S_{NaOH} is the strength of NaOH used for the determination of IEC (meq g^{-1}).

Water uptake was measured by first drying all membranes at 40°C for 24 h and the dry mass of individual membrane strips was recorded. The membrane strips were then immersed individually in pure water at room temperature for 24 h. The water remaining on the surface of the wetted membrane was carefully dried utilizing absorbent paper before weighing. The water uptake was calculated as:

$$WU = \left(\frac{m_{wet} - m_{dry}}{m_{dry}} \right) \times 100 \quad \text{Equation S 3.2}$$

Where m_{wet} is the mass of the swollen membrane after equilibrium and m_{dry} is the mass of the dry membrane.

The hydrolytic stability test of the membranes was explored by weighing the dried samples before and after wetting at different water bath temperatures 20, 40, 80°C for 4 h. UV spectroscopy was also used to look for small changes in the absorption of the solution.

The S-PANI membranes M1-M3 were cut into strips with approximate dimensions of 75 x 5.5 mm. The samples were dried in a vacuum oven overnight and then the dimensions of the dried samples were

measured. Afterwards, the membranes were soaked in pure water at 20, 40 and 80°C overnight. Afterwards, the samples were dried in a vacuum oven and the final dimensions were measured. The membrane stability in alkaline solution was tested by weighing the dried samples before and after wetting in the alkaline solution (0.1 NaOH(aq)) at 20°C for 24 h.

Morphology and porosity

The morphological properties of the membranes were investigated by SEM (SU3900, Hitachi, Japan). To analyse membrane morphology, SEM images on both the surface and the cross-section of membranes were captured at an acceleration voltage of 10 kV. A representative cross-section was obtained by fracturing membranes in liquid nitrogen. Samples were mounted onto SEM stubs and coated with gold using a sputter coater (S150B, Edwards, USA). Change of skin layer thickness was determined for different coagulation bath conditions.

Also, the re-assembly (precipitation) process of S-PANI polymer solution in neutral and acid aqueous solution was investigated by dissolving 0.2 wt% of S-PANI powder into *NMP* and adding 2 mL of the solution to either 18 mL of pure water, 1 M, and 3 M HCl, respectively. The precipitated polymer was dipped into a copper grid and submitted to transmission electron microscopy (TEM), JEOL JSM-2100Plus .

Adsorption isotherms, combined with the Brunauer-Emmet-Teller (BET) theory for multilayer adsorption, allowed the determination of the internal surface area of the membrane. Although the use of gas adsorption isotherm is more common for characterisation of porous media, its application in membrane research was reported elsewhere [1]. The application of this method was seen as complementary to other methods due to the low membrane porosities as well as difficulties in correctly interpreting these results [2]. N₂ adsorption-desorption measurements were performed with a Micromeritics; model 3 Flex 3500, USA. For porosity measurements, separate batches of M1-M3 were prepared without a support layer. Membrane samples were first dried at ambient laboratory conditions. Afterwards, each sample was placed in a sample tube to ensure complete drying and degassing at 40°C for 24 h. The specific surface area and pore size distribution measurements were completed within 24 h in a liquid nitrogen bath.

Demixing kinetics

Polymer films along with the glass plate were immersed in coagulation solution to produce membranes M1 to M3. Samples of the coagulation solution were taken at hourly intervals over 8 h and after 24 h at 6 mm distance to the cast film. Change of organic (solvent) concentration was measured using a total organic carbon analyser (TOC-L CPH, Shimadzu, Japan). The demixing rate was determined by plotting the change of relative concentration of TOC in the coagulation solution at time (t) and at infinite time (∞) defined here as 24 h immersion.

Thermal and mechanical analysis

The thermal degradation property of the S-PANI was studied by thermogravimetric analysis (TGA, TA instruments Q-500). All S-PANI membrane samples were heated from 30 to 600°C with an airflow rate of 60 mL min⁻¹ and a heating rate of 10°C min⁻¹. Differential scanning calorimeter (DSC, TA Instruments Q2000) measurements were implemented under a nitrogen flow rate of approximately 20 mL min⁻¹ at a heating rate of 10°C min⁻¹ from 30 to 300°C.

Tensile strength and % elongation at breakage of the S-PANI membranes were measured to assess the effect of the cross-linking on the membranes' mechanical properties. An Instron 3369 mechanical tester was used and dried membrane casts without a support layer were cut into rectangular strips of approximately 70 × 6 mm for testing. All tests were conducted with a pull speed of 2 mm min⁻¹ at room temperature. The membrane thickness was measured using standard Vernier callipers. The reported mechanical data is an average of three different membrane samples.

Solvent stability

Solvent stability of M1-M3 was determined by immersion for two weeks in DMA solvent. To understand the role of sulfonic groups in the cross-linking process, PANI powder was prepared following the protocol described in section S-PANI synthesis S2 but without metanilic acid. Afterwards, PANI membranes were prepared while mimicking the coagulation bath conditions as used for M1-M3. The obtained PANI membranes were also immersed in DMA for two weeks and labelled as M1'-M3'.

Mass swelling degree and gel content

A set of organic solvents such as *Methanol (MeOH)*, *Isopropanol (IPA)*, *Acetone (AC)*, *Toluene (TOL)*, *Tetrahydrofuran (THF)* were used to determine the membrane swelling and stability. In terms of polarity, *MeOH* and *IPA* are polar protic solvents, *AC* and *THF* are polar aprotic solvents, and *TOL* is a nonpolar solvent. M1-M3 were cut into small samples (2×2 cm) and dried in the vacuum oven. The dried membrane samples (of known mass) were allowed to equilibrate with an excess of the solvent in a sealed flask at 25°C for 1 h. The swollen membranes were taken from the solvent and quickly dried with filter paper to remove solvent from the external surface. The mass of the swollen membranes was then determined. The mass swelling degree (SD) was calculated using the following equation:

$$SD = (m_{wet} - m_{dry})/m_{dry} \quad \text{Equation S 3.3}$$

where m_{wet} is the mass of the swollen membrane after equilibrium and m_{dry} is the mass of the dry membrane.

The stability of the S-PANI membranes in the solvents was determined by immersing the membrane sample in the solvent for two weeks (same conditions as per swelling test) including for *DMF*. After two weeks, the membrane samples were removed from the solvent and dried in the vacuum oven. The mass change of the dry membrane before and after soaking in the solvent indicates membrane dissolution. The gel content is a parameter that is used to define the polymer stability in different solvent was calculated by using the following equation:

$$Gel\ content\ \% = (W_a/W_b) \times 100 \quad \text{Equation S 3.4}$$

where W_b and W_a is the dry weight of the membrane sample before and after solvent soaking, respectively. Partially or fully dissolved membranes are designated as dissolved (for *DMF*). Moderately swollen membranes or those with gel content below 90% are designated as swollen. Membranes that showed no swelling or dissolution in *DMF* and had a gel content higher than 90%, are designated crosslinked [3].

Contact Angle

The hydrophilicity of the membranes was measured (3 times per sample) by sessile dynamic droplet penetration using a contact angle goniometer (Contact Angle System OCA 15Pro, Dataphysics, Germany). A small droplet of water (2.0 μL) was placed onto the membrane surface at a dosing rate of 1.0 $\mu\text{L s}^{-1}$ using a Hamilton syringe. The software SCA20 was used to calculate the dynamic effective contact angle (CA).

Membrane transport properties

Membrane filtration experiments were conducted in dead-end mode using a stainless steel chemically resistant dead-end cell (Sterlitech HP4750) with an active membrane area of 14.6 cm^2 . The schematic of the experimental set-up is illustrated in Fig. S3.2. Permeate flow rates were measured using a digital scale connected to a computer. The software programme LabVIEW 2011 was used to calculate the membrane permeance J_p ($\text{L m}^{-2} \text{hr}^{-1} \text{bar}^{-1}$) by using the following equation:

$$J_p = \frac{\Delta W}{A \cdot \Delta P \cdot t \cdot \rho_p} \quad \text{Equation S 3.5}$$

Where ΔW (kg) is the obtained permeate weight during a fixed time slot, ρ_s (kg m^{-3}) is the permeate density at room temperature, A (m^2) is the membrane coupon active surface area (filtration area), t is the time intervals between each measurement and ΔP (bar) represents the differential pressure at the membrane, which is maintained by the inline N_2 cylinder. For M1-M5 stability and performance changes related to the membrane, doping was assessed via pH measurements of permeates at different filtration stages, reported as an average of three membrane samples.

To define the effect on the membranes' solutes' retention, different batches of dye feed solutions ranging from 320 to 1017 g mol^{-1} were used sequentially. Methylene blue, indigo carmine, bromothymol blue and rose bengal dye powder were separately dissolved in pure water. For a typical dye solution, 10 mg of dye powder was added to 1 L of pure water at room temperature except for bromothymol blue where 50 mg were added instead. The dye powder was dissolved and stirred using a magnetic stirrer at 200 rpm until the dye powder was completely dissolved.

Dye rejection was measured by filtering 50 mL of the fresh dye feed solution using a dead-end cell set-up. The dye concentration in the feed and permeate samples were measured via UV absorbance using an Agilent Carry 100 UV-Vis spectrometer (Agilent Corporation). For calibrations curves see Fig. S3.3-S3.6. The adsorbed dye mass on the membrane surface was quantified by conducting a mass balance for the M1 membrane sample. The dye rejection was calculated using the following equation:

$$R\% = \left(1 - \frac{C_p}{C_f}\right) \times 100 \quad \text{Equation S 3.6}$$

Where C_p is the dye solution concentration in the permeate and C_f is that in the feed.

The membrane surface charge and the dye feed solutions were measured (3 times per sample) to understand the charge interactions between the membranes and the dye solutes. The surface charge of M1-M5 and M8 was measured by using Zetasizer nano series model ZS, Malvern-Panalytical, UK. Zeta potential planar cell (ZEN 1020) along with tracer particles (Latex beads, polystyrene 0.3 μm mean particle size) were used to measure the electrophoretic mobility of the particles at varying distances from the planar surface at neutral pH. The zeta potential of the dye solution feed was measured with a Zetasizer (Malvern-Panalytical Instruments, UK) at 20°C.

The MWCO of membranes, defined as the MW weight at 90% solute retention [4], was obtained using the 90% retention value for rejection curves recorded with PEG and two sugars of a defined MW, as described in detail in SI, Materials S1.

To prepare PEG feed solution, 600 mg of PEG 1000 g mol^{-1} was added to 1 L of pure water and continuously stirred at 200 rpm until complete dissolution. The PEG feed solution (50 mL) was filtered through the dead-end cell to obtain 25 mL permeate. The PEG concentrations were analysed by an Agilent 1260 infinity series high-performance liquid chromatography (HPLC) machine equipped with an evaporative light scattering (ELSD) detector. A flow rate of 1.0 mL min^{-1} was used with mobile phase *acetonitrile*/water (15/85). Analytic peaks were analysed using an established method for MWCO determination by using 1000 g mol^{-1} PEG exclusively [5]. Calibration curves are provided in Fig S 3.7-S 3.14. Raffinose and sucrose octa-acetate aqueous solutions (20 mg L^{-1} as TOC) were also used to verify the MWCO of the obtained NF membrane.

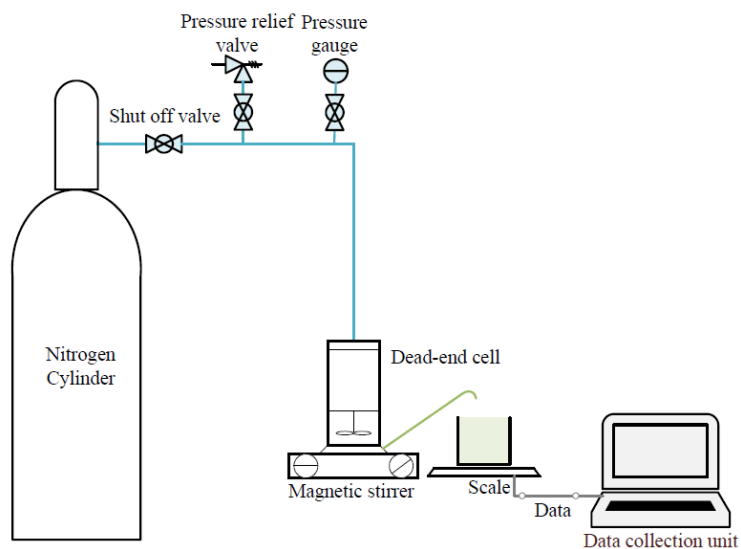


Fig. S3.2 Schematic diagram of the dead-end cell filtration.

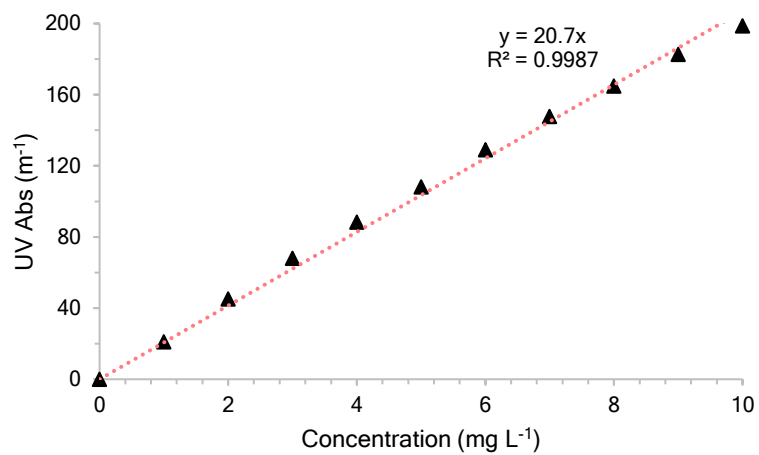


Fig. S3.3 The calibration curve of methylene blue dye aqueous solution as a relation between the feed solution concentration and the UV absorbance (peak absorption at wavelength 661 nm).

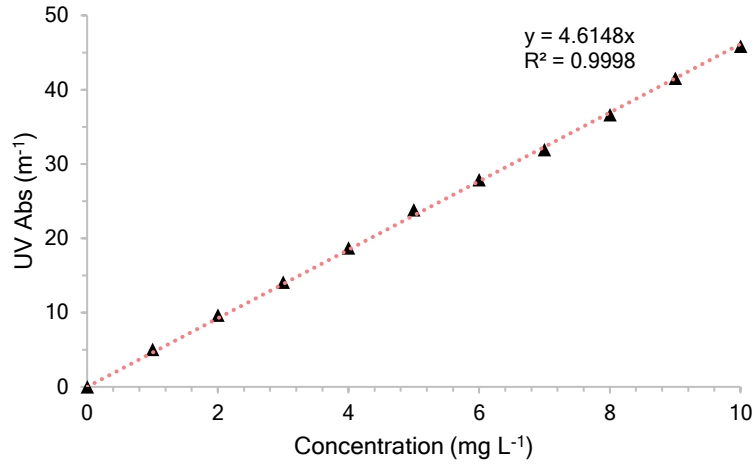


Fig. S3.4 The calibration curve of indigo carmine dye aqueous solution as a relation between the feed solution concentration and the UV absorbance (peak absorption at wavelength 612 nm).

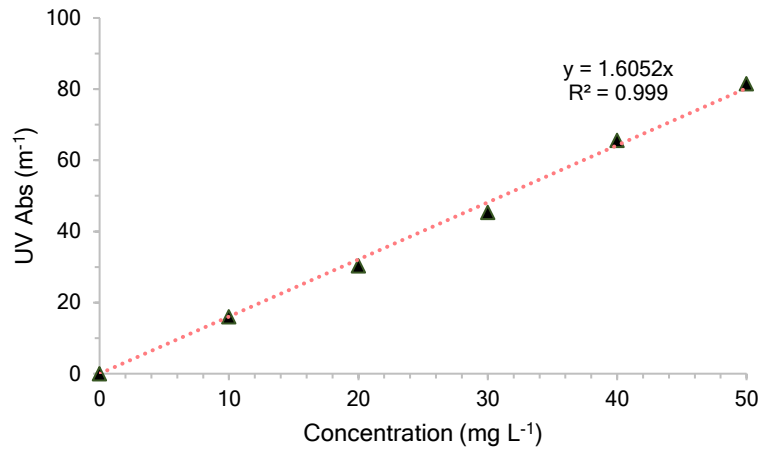


Fig. S3.5 The calibration curve of bromothymol blue dye aqueous solution as a relation between the feed solution concentration and the UV absorbance (peak absorption at wavelength 430 nm).

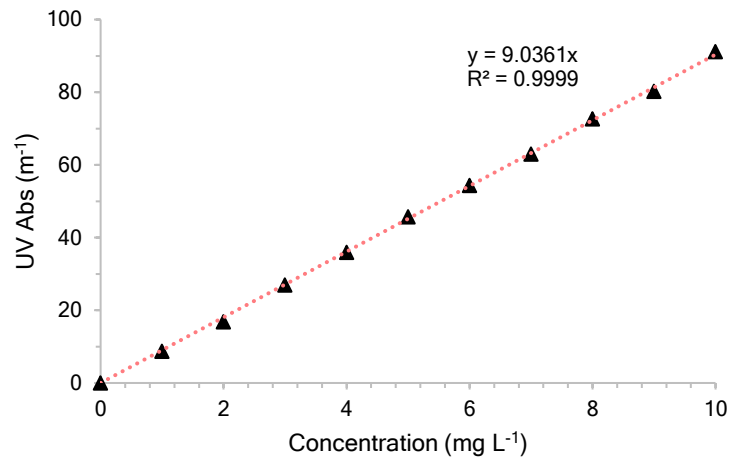


Fig. S3.6 The calibration curve of rose bengal dye aqueous solution as a relation between the feed solution concentration and the UV absorbance (peak absorption at wavelength 549 nm).

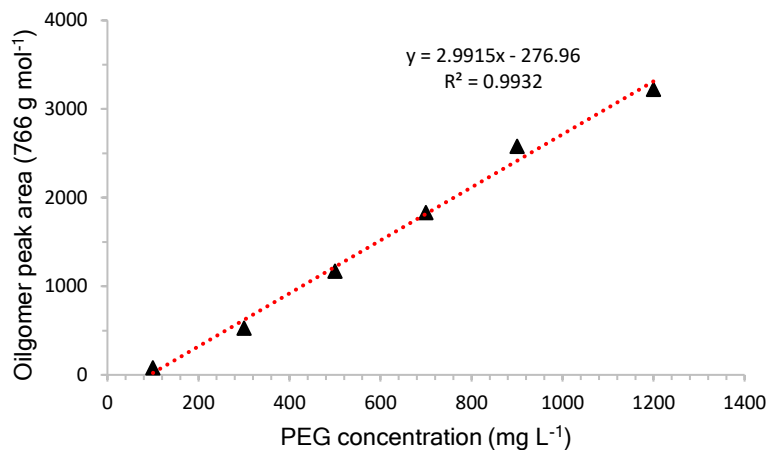


Fig. S3.7 The calibration curve of the PEG oligomer MW 766 g mol⁻¹ at different concentrations.

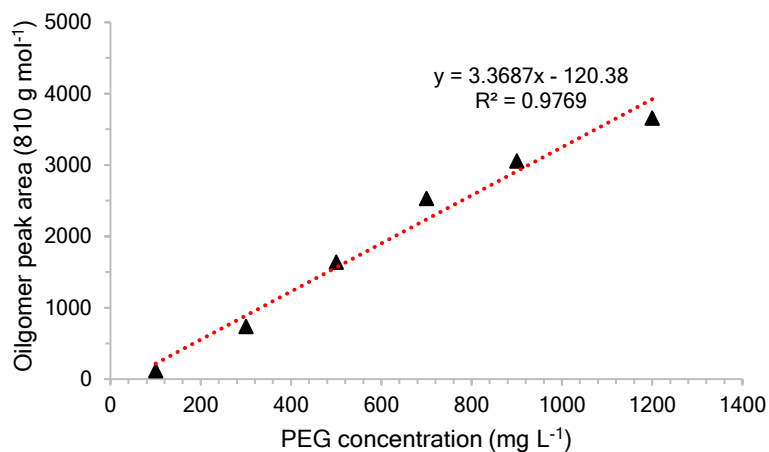


Fig. S3.8 The calibration curve of the PEG oligomer MW 810 g mol⁻¹ at different concentrations.

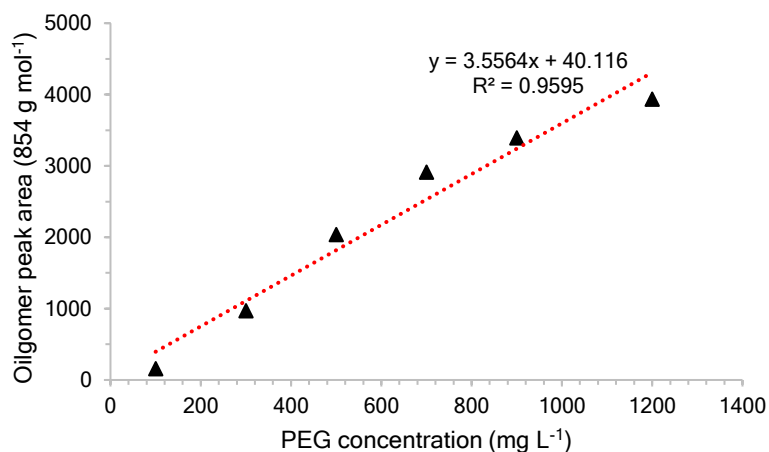


Fig. S3.9 The calibration curve of the PEG oligomer MW 854 g mol⁻¹ at different concentrations.

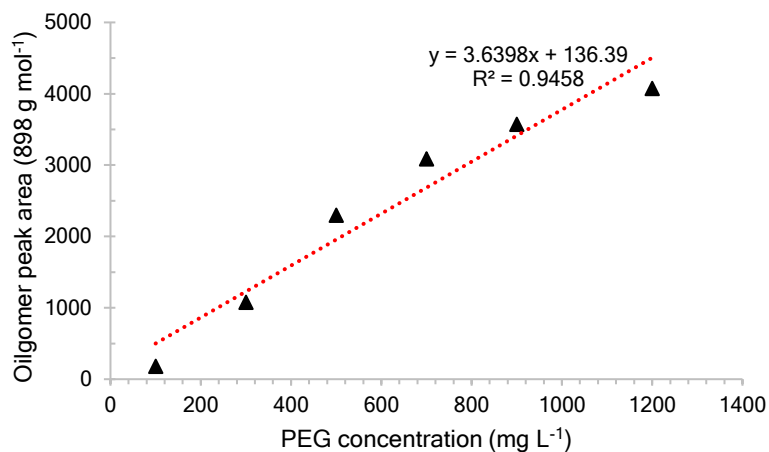


Fig. S3.10 The calibration curve of the PEG oligomer MW 898 g mol⁻¹ at different concentrations.

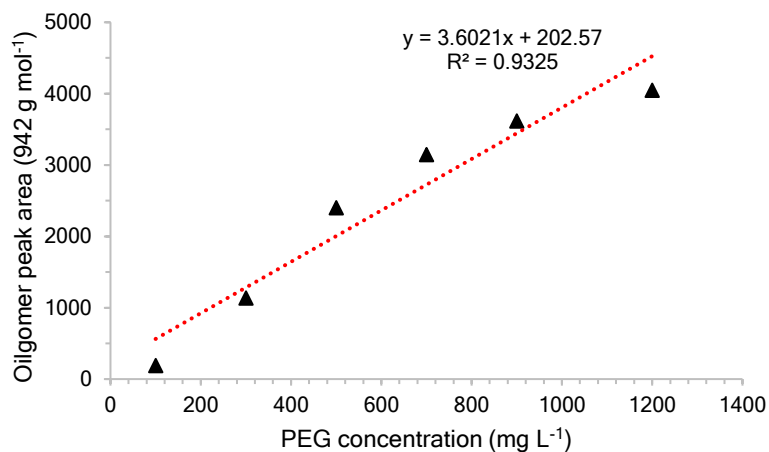


Fig. S3.11 The calibration curve of the PEG oligomer MW 942 g mol⁻¹ at different concentrations.

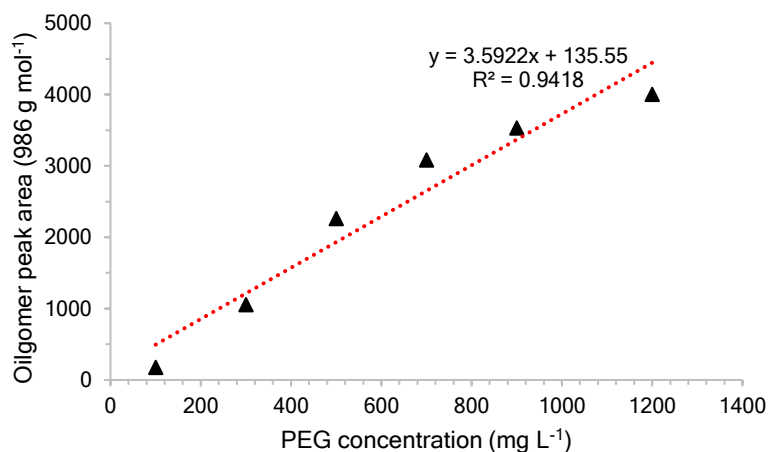


Fig. S3.12 The calibration curve of the PEG oligomer MW 986 g mol⁻¹ at different concentrations.

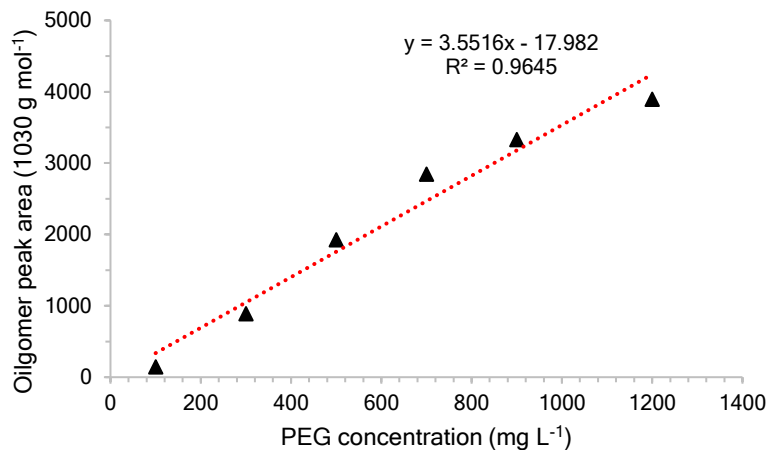


Fig. S3.13 The calibration curve of the PEG oligomer MW 1030 g mol⁻¹ at different concentrations.

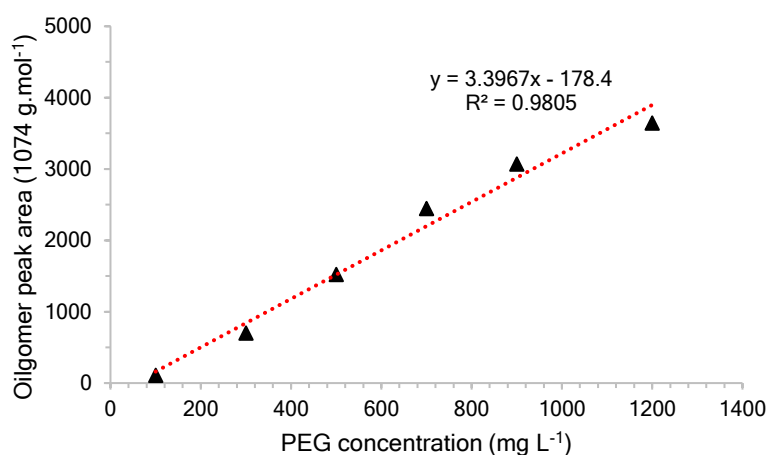


Fig. S3.14 The calibration curve of the PEG oligomer MW 1074 g mol⁻¹ at different concentrations.

S-PANI doping S7

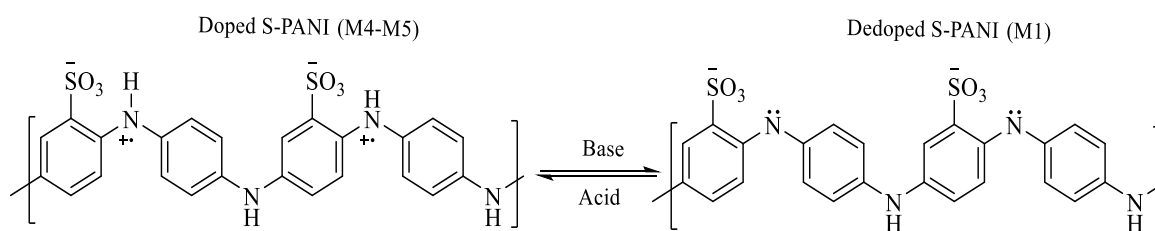


Fig. S3.15 pictorial representation of both doped/dedoped M4-M5 and M1 membranes.

XPS spectra S8

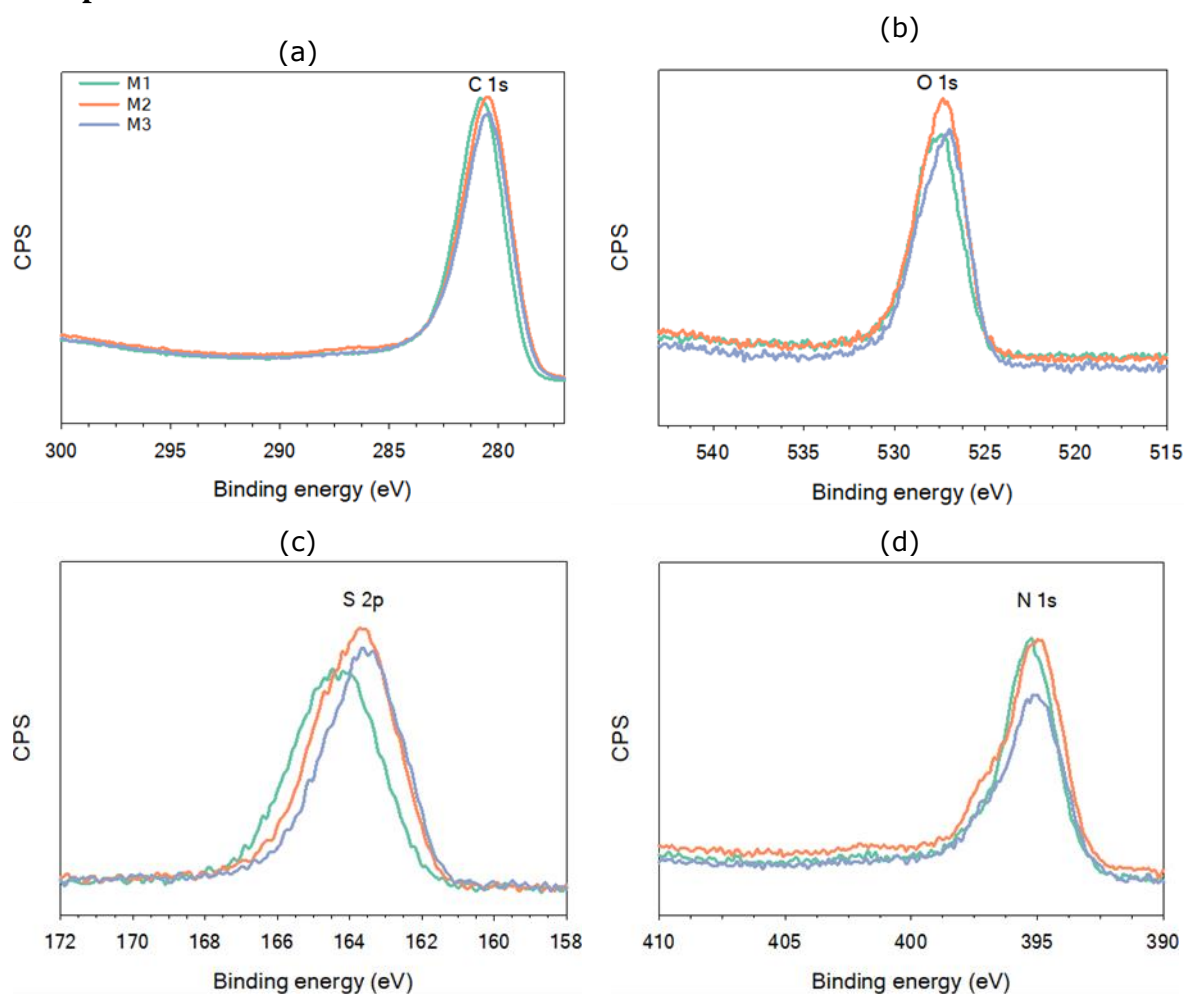


Fig. S3.16 Core-level spectra of S-PANI membranes M1-M3 (a) C 1s (b) O 1s (c) S 2p (d) N 1s.

Water stability S9

Table. S3.2 Hydrolytic and alkalinity stability of S-PANI membranes M1-M3.

Membrane	Weight loss in DI water (%)			Weight loss in 0.1 NaOH(aq)
	20°C	40°C	80°C	20°C
M1	None	None	None	None
M2	None	None	None	None
M3	None	None	None	None

Morphology S10

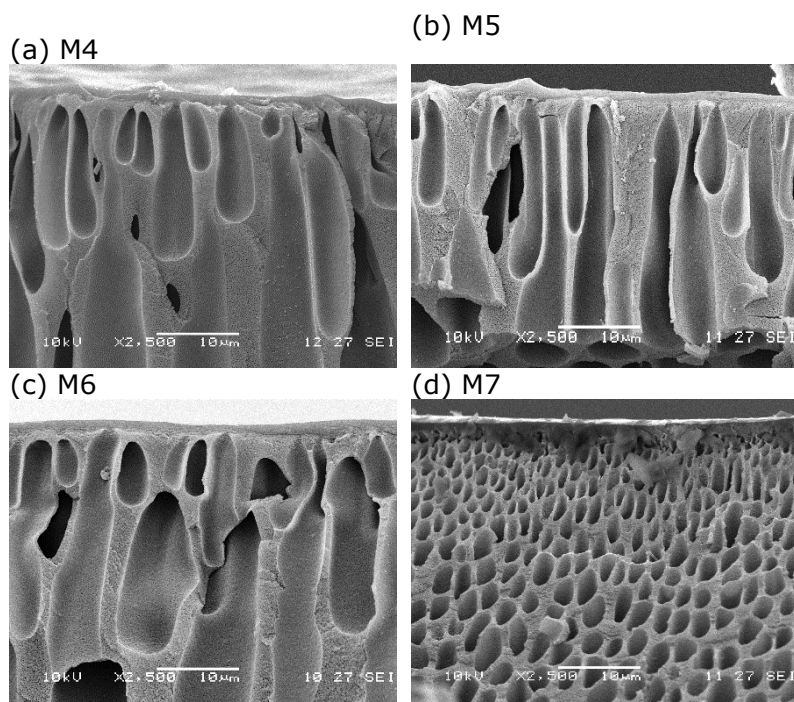


Fig. S3.17. SEM surface and cross-sectional area images of HCl doped S-PANI membranes prepared in neutral coagulation bath (M4-M5), 1M HCl acidic coagulation bath (M6) and 3M HCl acidic coagulation bath (M7).

Porosity S11

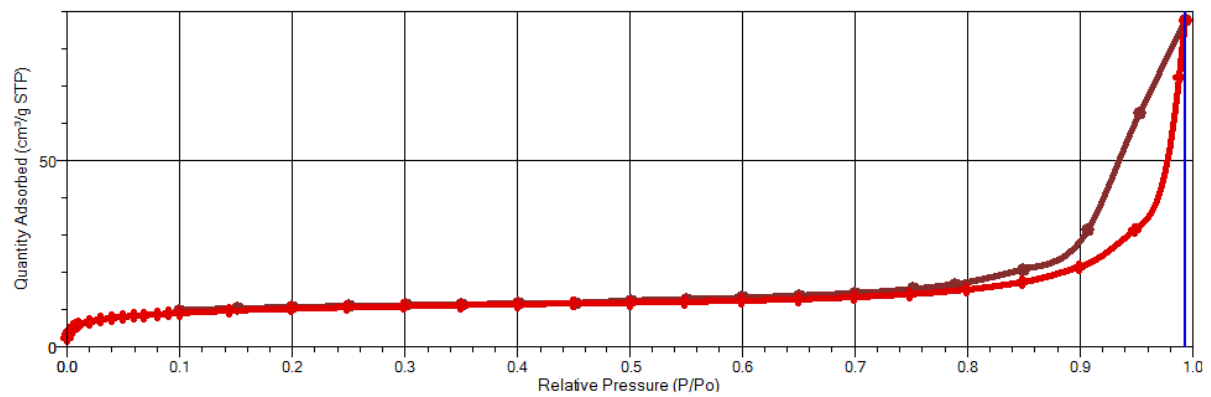


Fig. S3.18 The isotherm of the S-PANI membrane produced in pure water coagulation bath (M1).

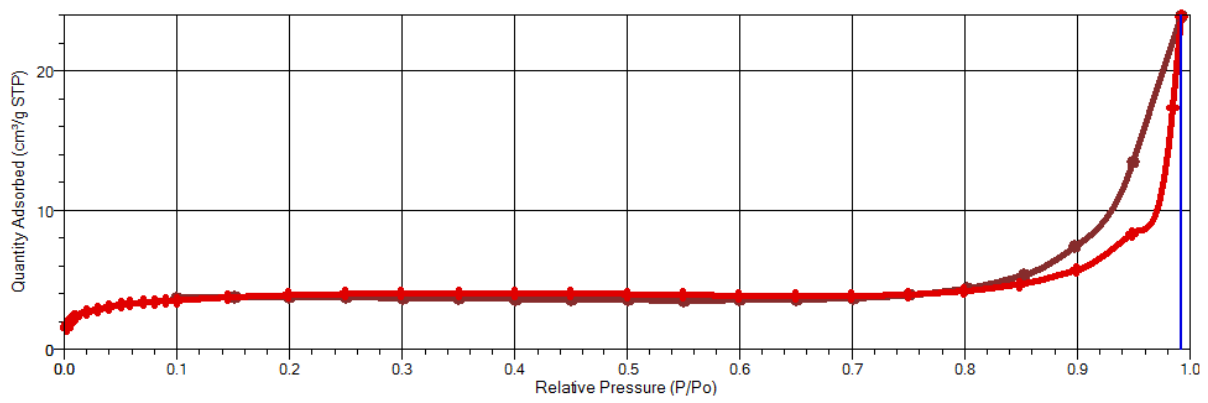


Fig. S3.19 The isotherm of the S-PANI membrane produced in 1M HCl(aq) coagulation bath (M2).

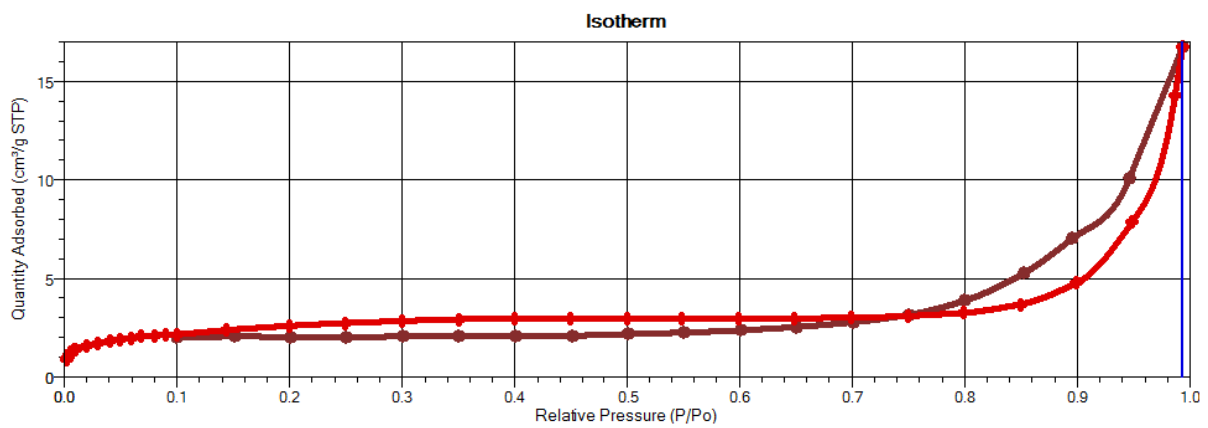


Fig. S3.20 The isotherm of the S-PANI membrane produced in 3M HCl(aq) coagulation bath (M3).

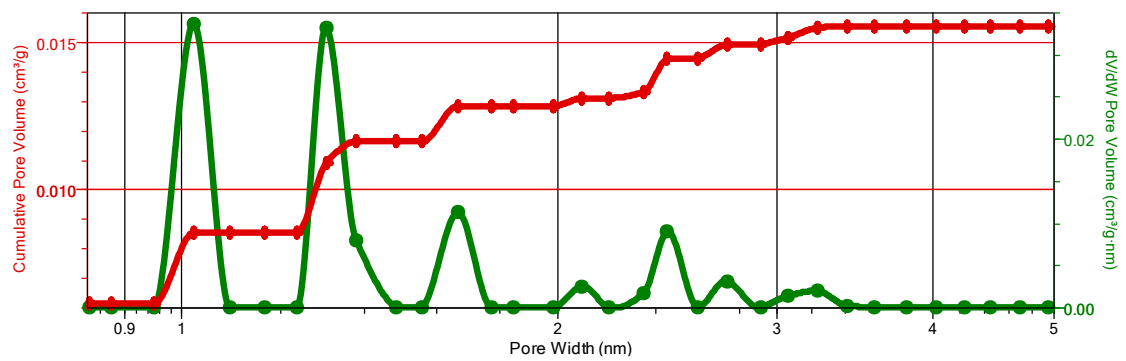


Fig. S3.21 The cumulative pore volume versus the pore width of the S-PANI membranes prepared in a neutral coagulation bath (M1) without a support layer.

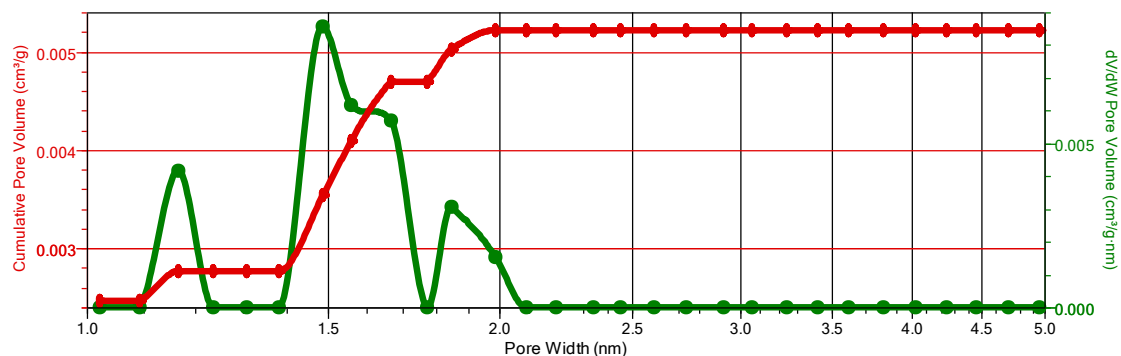


Fig. S3.22 The cumulative pore volume versus the pore width of the S-PANI membranes prepared in 1M HCl acidic coagulation bath (M2) without a support layer.

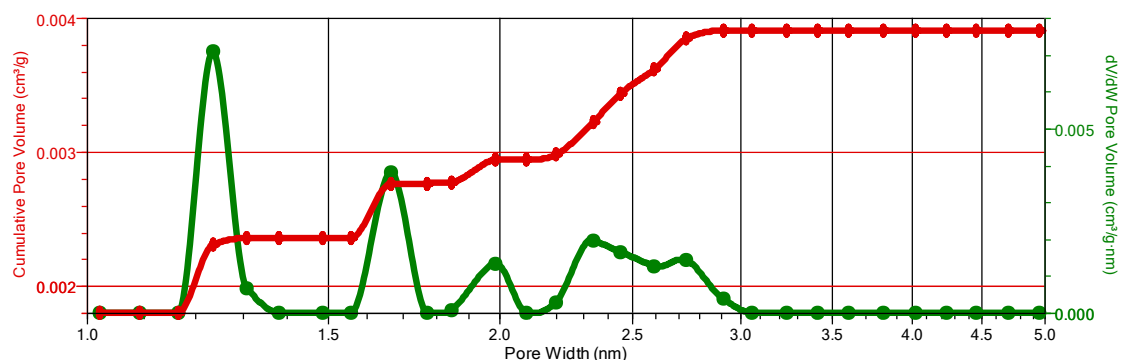


Fig. S3.23 The cumulative pore volume versus the pore width of the S-PANI membranes prepared in 3M HCl acidic coagulation bath (M3) without a support layer.

Differential scanning calorimetry S12

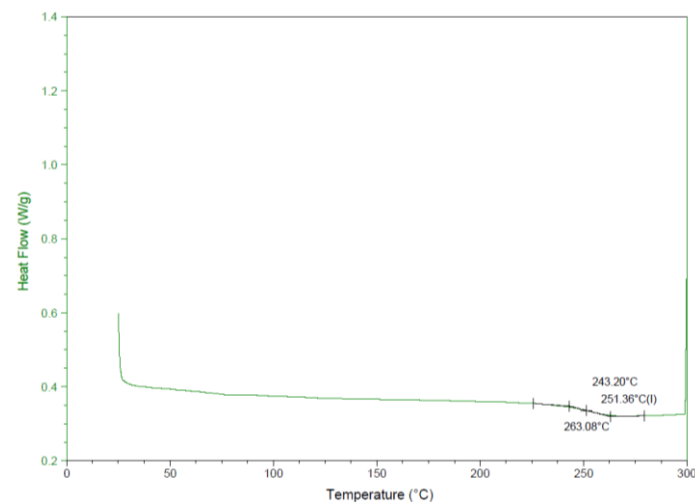


Fig. S3.24 DSC thermogram register from 20 to 300°C of M1 S-PANI membrane produced in DI water coagulation bath.

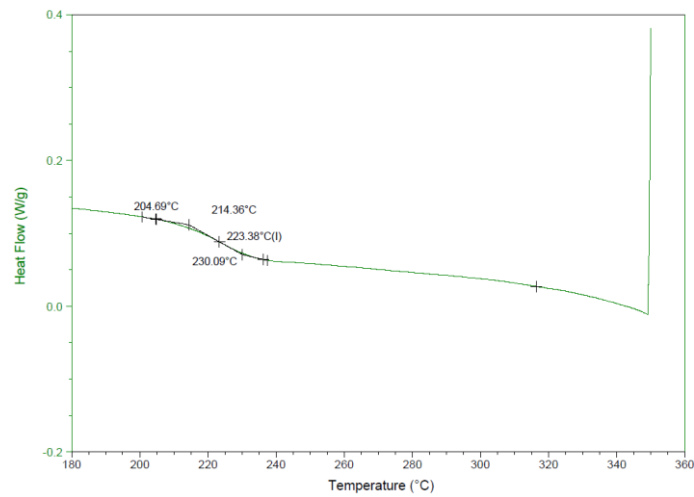


Fig. S3.25 DSC thermogram register from 150 to 350°C of M1 S-PANI membrane produced in 1M HCl coagulation bath.

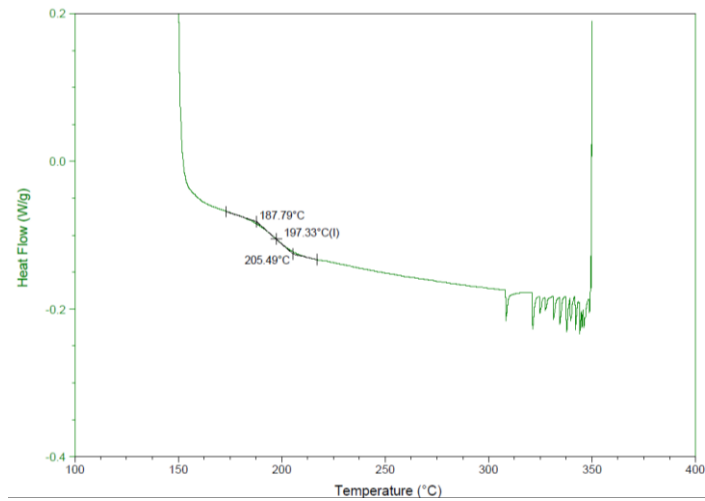


Fig. S3.26 DSC thermogram register from 150 to 350°C of M1 S-PANI membrane produced in 3M HCl coagulation bath.

Transport properties S13

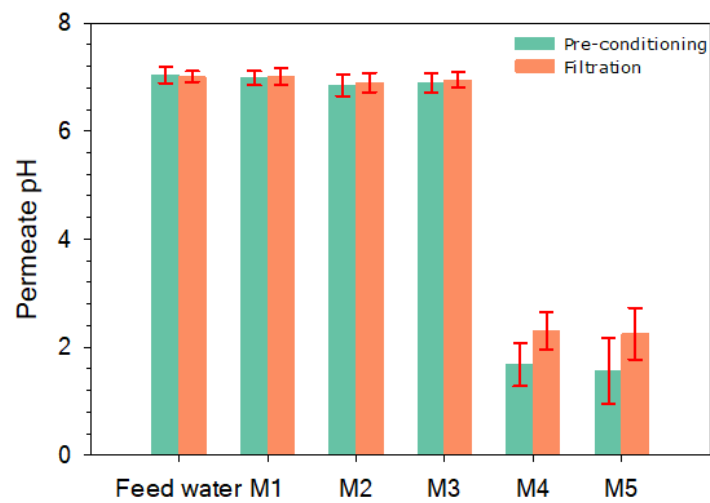


Fig. S3.27 pH change of the M1-M5 membranes' permeate after preconditioning and filtration.

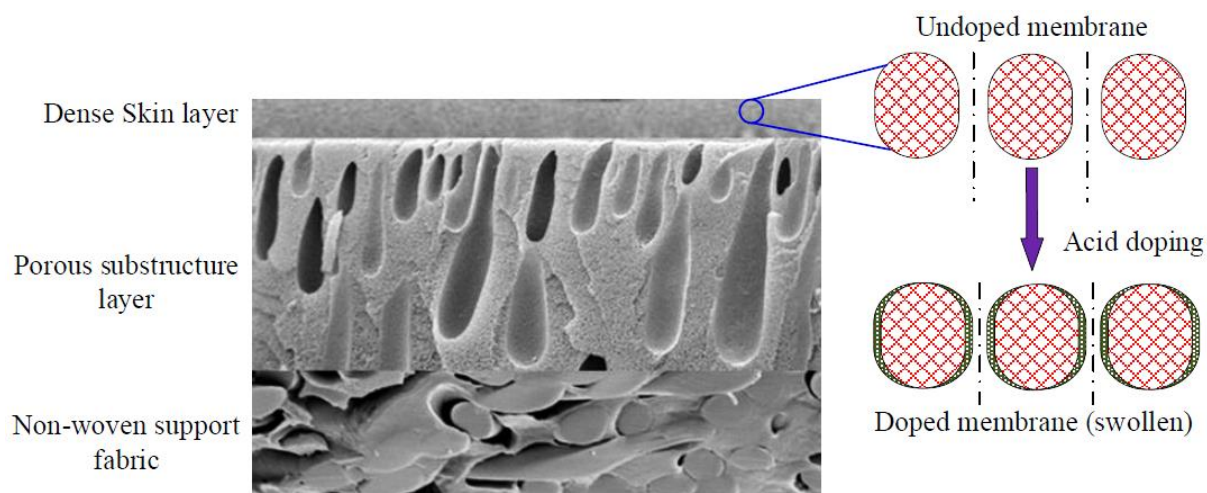


Fig. S3.28 A schematic representation of asymmetric S-PANI membrane and matrix swelling and pore contraction of the membrane after HCl(aq) acid doping.

Table. S3.3 The dye removal mechanism of the S-PANI M1 membrane.

Dye	MW (g mol⁻¹)	Total rejection (%)	Size exclusion (%)	Adsorption (%)
Rose bengal	1017.6	84±6.9	74±0.1	26±0.1
Indigo carmine	466.4	73±0.1	58±0.5	42±0.5
Methylene blue	319.8	50±3	84±0.2	16±0.2

References S14

- [1] T. Virtanen, G. Rudolph, A. Lopatina, B. Al-Rudainy, H. Schagerlöf, L. Puro, M. Kallioinen, F. Lipnizki, Analysis of membrane fouling by Brunauer-Emmet-Teller nitrogen adsorption/desorption technique, *Sci. Rep.* 10 (2020) 3427. doi:10.1038/s41598-020-59994-1.
- [2] J.I. Calvo, P. Prádanos, A. Hernández, W.R. Bowen, N. Hilal, R.W. Lovitt, P.M. Williams, Bulk and surface characterization of composite UF membranes Atomic force microscopy, gas adsorption-desorption and liquid displacement techniques, *J. Memb. Sci.* 128 (1997) 7–21. doi:10.1016/S0376-7388(96)00304-3.
- [3] K. Vanherck, A. Cano-Odena, G. Koeckelberghs, T. Dedroog, I. Vankelecom, A simplified diamine crosslinking method for PI nanofiltration membranes, *J. Memb. Sci.* 353 (2010) 135–143. doi:10.1016/j.memsci.2010.02.046.
- [4] D.A. Rohani, Rosiah, Hyland, Margaret & Patterson, A Refined One-Filtration Method for Aqueous Based Nanofiltration and UltraFiltration Membrane Molecular Weight Cut-Off Determination using Polyethylene Glycols, 382 (2011) 278–290. doi:https://doi.org/10.1016/j.memsci.2011.08.023.
- [5] L. Xu, S. Shahid, J. Shen, E.A.C. Emanuelsson, D.A. Patterson, A wide range and high resolution one-filtration molecular weight cut-off method for aqueous based nanofiltration and ultrafiltration membranes, *J. Memb. Sci.* 525 (2017) 304–311. doi:10.1016/j.memsci.2016.12.004.

Chapter 4

Organic matter removal and antifouling performance of sulfonated polyaniline nanofiltration (S-PANI NF) membranes

The work presented in this chapter has been published to Journal of Environmental Chemical Engineering Jun 2022. H. Alhweij, E.A. Carolina Emanuelsson, S. Shahid, J. Wenk, Organic matter removal and antifouling performance of sulfonated polyaniline nanofiltration (S-PANI NF) membranes.

Context:

In this study we investigate the removal performance of natural organic matter (NOM) of a newly developed sulfonated polyaniline nanofiltration (S-PANI NF) membrane. We used three different types of water, namely artificial surface water, artificial seawater, and a stabilised landfill leachate as test solutions to determine membrane separation performance. NOM removal across five different size fractions of the NOM and at different NOM concentrations was measured. In addition, for the landfill leachate we also investigated chemical oxygen demand (COD) removal efficiency. Test solutions at higher NOM concentrations were used for long term fouling experiments, followed by performance recovery measurements after cleaning and microscopic investigation of the membrane surface. Test results for the newly developed membrane were compared with the performance of a commercial hydrophilic polyimide membrane, that had similar properties to our membrane and a conventional flocculation – coagulation treatment process optimised for organic matter removal.

This work has significant novelty as it is the first study of S-PANI membranes for water treatment applications and under high fouling conditions. In addition, we believe that the inter-process comparison between a conventional treatment process and membrane processes across highly different water matrices, including results for NOM fractionated into five size range provides interesting and important results for drinking water, seawater desalination and landfill leachate treatment research communities and engineers for the efficiency of NOM removal and how this could affect downstream treatment processes.

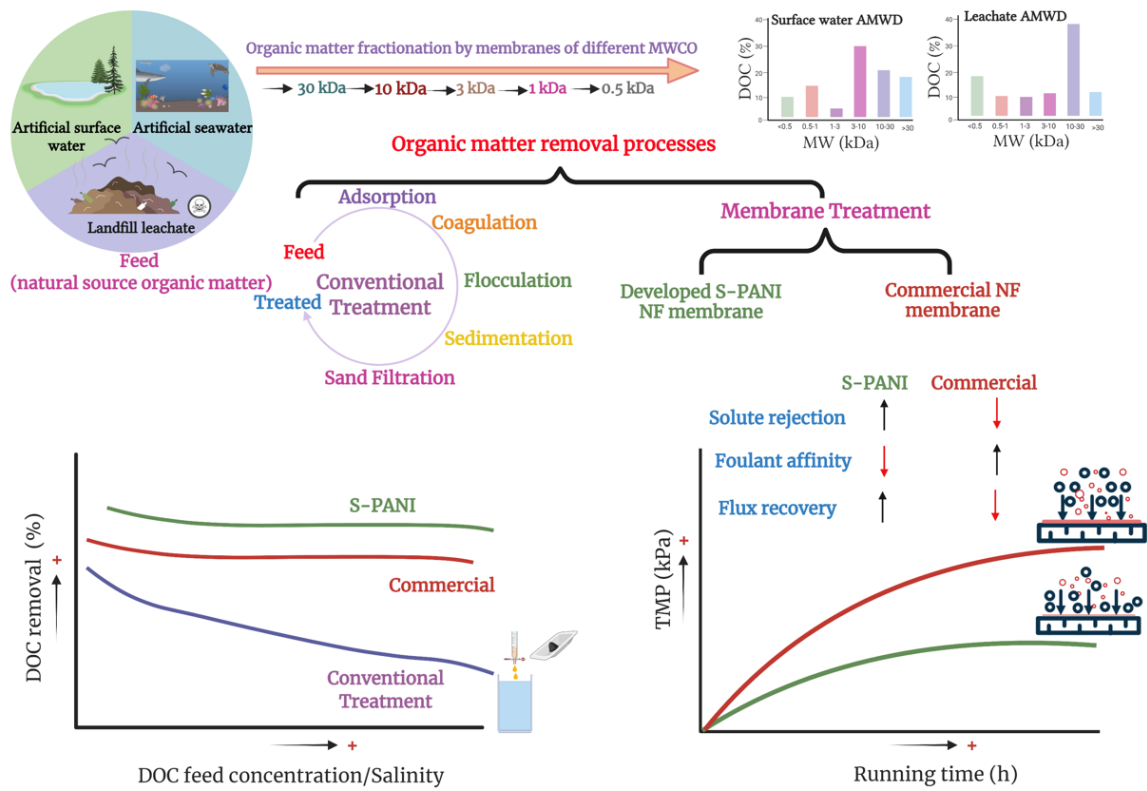
Our study is part of a series of recently published studies on developing a novel type of polyaniline-based sulfonated membranes, with superior properties over other types of polymeric membranes, including separation performance, fouling resistance and longevity. Specifically, we modified regular polyaniline (PANI) membranes to achieve better antifouling behaviour and chlorine resistance by introducing sulfonic acid groups ($-\text{SO}_3\text{H}$) resulting in synthesized sulfonated polyaniline (S-PANI) membranes at the ultrafiltration (UF) separation range (chapter 2, <https://doi.org/10.1002/app.50756>).

Subsequently, S-PANI membranes were tailored into the nanofiltration (NF) separation range (molecular weight cut off (MWCO) $\approx 680 \text{ g mol}^{-1}$) with a densified selective layer via refining the membrane production procedures (chapter 3, <https://doi.org/10.1016/j.memsci.2021.119654>). This technique was adopted for the preparation of in-situ tuneable high performance organic stable NF S-PANI membranes which endured organic solvent ageing tests without physical or chemical deterioration (chapter 5, <https://doi.org/10.1016/j.polymer.2022.124682>). Here, we expand the application of the newly developed S-PANI NF membranes towards water treatment with very promising results pointing out the potential of this membrane material for water treatment. S-PANI membranes show high and consistent organic matter removal efficiencies at variable organic loads at highly different water matrices that are either better or similar when compared to conventional treatment and the commercial membrane, including fouling behaviour and recovery.

Contributions:

Hassan Alhweij: Conceptualization, Methodology, Validation, Formal analysis, Investigation, Writing - Original Draft, Writing - Review & Editing, Visualization; Emma Anna Carolina Emanuelsson: Supervision, Funding acquisition; Salman Shahid: Writing - Review & Editing; Jannis Wenk: Conceptualization, Writing - Original Draft, Writing - Review & Editing, Visualization, Supervision, Project administration, Funding acquisition.

GRAPHICAL ABSTRACT



Organic matter removal and antifouling performance of sulfonated polyaniline nanofiltration (S-PANI NF) membranes

Hassan Alhweij^{a,c,d}, Emma Anna Carolina Emanuelsson^{a,b}, Salman Shahid^{a,b,c}, Jannis Wenk^{a,c,*}

^a Department of Chemical Engineering, University of Bath, Bath BA2 7AY, United Kingdom

^b Centre for Advanced Separations Engineering, University of Bath, Bath BA2 7AY, United Kingdom

^c Water Innovation and Research Centre (WIRC@Bath), University of Bath, Bath, BA2 7AY, United Kingdom

^d Stantec UK Limited, Dominion House, Warrington, WA3 6GD, United Kingdom

Abstract

Natural organic matter (NOM) removal from water prior to other treatment processes can improve treatment efficiency and final water quality. Here, NOM removal across five size fractions by newly developed sulfonated polyaniline nanofiltration (S-PANI NF) membranes was compared with a commercial membrane and conventional adsorption-coagulation-flocculation, optimised for NOM removal. Artificially prepared surface water and seawater containing 10 – 100 mg C L⁻¹ NOM extract and a stabilised landfill leachate served as test solutions. S-PANI NF membranes showed best NOM separation performance for both surface and seawater followed by the commercial membrane and conventional treatment. For landfill leachate conventional treatment had the best performance followed by S-PANI NF membranes. S-PANI performed slightly better in removal of chemical oxygen demand (COD) (74%) compared to the commercial membrane (70%) and conventional treatment (70%). Both membranes performed consistent with increasing salinity and NOM concentration, while experiencing a modest carryover at higher salinity. During long-term fouling S-PANI exhibited slower growth in transmembrane pressure (TMP), less affinity towards organic matter and higher flux recovery compared to the commercial membrane, particularly at high NOM concentration. This is the first study to investigate S-PANI membranes for water treatment applications and under high-fouling conditions. Results indicate S-PANI NF membranes are promising for such applications. In addition, this study also provides an inter-process comparison for NOM removal over an extreme range of water matrix conditions.

Keywords: Nanofiltration, sulfonated polyaniline, NOM removal, antifouling, conventional

4.1 Introduction

Aqueous organic matter is ubiquitous in natural waters and comprises a complex mixture of organic compounds derived from biological and chemical degradation processes of plants and animals [1]. Natural organic matter (NOM) significantly affects water treatment, for example due to its interference with treatment processes such as coagulation and chemical oxidation [2], as membrane foulant, ligand for metal ions [3], sorbent of hydrophobic organic chemicals, substrate for bacterial growth in distribution systems, cause of colour, taste, and odour issues and as disinfection by-product precursor [4–7]. Organic matter in landfill leachate is critical for mobilization of pollutants [8,9]. To address NOM-induced water treatment performance issues and water quality problems organic matter can be fully or partially removed via ion exchange [10], advanced oxidation [11] and conventional treatment including coagulation, flocculation, clarification, sand filtration, adsorption, and biodegradation [12]. Seasonal or temporal variability in source water quality, organic matter concentration and characteristics require careful control and frequent adjustments of such processes [13,14].

Microfiltration (MF) in combination with ultrafiltration (UF) as alternative to conventional water treatment allows removal of suspended solids and reduction of microbial load [15]. MF/UF provides limited organic matter removal, between 5-10% and 6-56% for MF and UF membranes, respectively [16–19]. Integration of conventional (pre)treatment with MF/UF membranes or nanofiltration (NF) results in higher organic matter removal [20,21]. NF membranes are increasingly used for removal of organic contaminants in drinking water [22], for leachate treatment, wastewater reuse [23,24], and seawater pre-treatment [25]. Challenges persist due to membrane (bio)fouling requiring frequent physical and chemical cleaning, while decreasing membrane lifetime [26,27].

Altering commercially available hydrophobic membranes towards hydrophilicity and smoother surfaces for less fouling may overcome this challenge [27–31]. Physical or chemical membrane modification processes such as graft polymerization, plasma treatment, preadsorption of hydrophilic components and incorporation of hydrophilic additives by sulfonation, carboxylation, and nitration in the membrane matrix during membrane synthesis have been used to create more hydrophilic surfaces

to enhance membrane fouling resistance [32]. Surface modification by graft copolymers using additives that chemically attach to the polymer such as polyethylene glycol (PEG) were extensively studied to enhanced hydrophilicity of the hydrophobic polymeric backbones [33]. The incorporation of tailor-made surface-active macromolecules and polymers into membrane casting solution to manufacture surface modified membranes via a single-step casting has been an attractive approach to decrease flux reductions and NOM accumulation of polyethersulfone (PES) membranes for environmental applications [34,35]. A combination of a high-throughput platform approach together with photoinduced graft polymerization (PGP) was also reported for facile modification of commercial membranes to control NOM fouling [36]. Two step surface grafting was investigated to introduce hydrophilic and low surface energy sites to minimize the intermolecular forces between the NOM and membrane surfaces leading to easily removable foulants via modest hydrodynamic shear forces at mechanical cleaning [37]. Membrane charge modification, for example by covalent attachment of negatively charged sulfonic acid groups to the membrane surface was an effective way to improve removal of *humic acids* and reduce membrane fouling [38]. Incorporation of hydrophilic inorganic nanoparticles such as TiO₂, graphene oxide (GO) and silica into polymeric membranes can improve antifouling behaviour and permselective properties of NF membranes for NOM removal [39–42]. However, nanoparticles may negatively affect membrane performance, while potentially toxic properties of nanoparticles, especially in drinking water applications, need to be considered [43]. Also, inorganic nanoparticles such as GO exhibit poor compatibility with the organic polymer matrix leading to weak interfacial interactions and resulting in unfavourable effects on membrane stability and mechanical properties [42,44]. Achieving uniform mixed matrix membranes with long shelf life and long-term stability during operation without leaching of grafting compounds remains challenging despite numerous modification strategies [45].

Polyaniline (PANI) is a hydrophilic polymer membrane material with high compatibility towards other polymers, exhibiting favourable transport properties including antifouling behaviour and tuneable separation characteristics [46–50]. PANI membranes are straightforward to produce, while tuning e.g., to increase permselectivity or chemical durability, is simple via low-cost doping/dedoping chemistry [51,52]. Previously, we have modified PANI membranes to improve both antifouling behaviour and

chlorine resistance by introducing sulfonic acid groups ($-\text{SO}_3\text{H}$) resulting in sulfonated polyaniline (S-PANI) UF membranes [53]. Subsequently, S-PANI membranes were tailored into the NF separation range (molecular weight cut off (MWCO) $\approx 600\text{-}680 \text{ g mol}^{-1}$) [54]. Simultaneously, this increased tensile strength and solvent stability as static long-term 30-day ageing tests in harsh solvents showed [55]. We anticipate that the newly developed hydrophilic NF S-PANI membranes may also strongly perform for organic matter removal applications in water, wastewater treatment and aqueous leachate treatment. Therefore, the goal of this work was to determine the suitability of S-PANI NF membranes for organic matter separation and compare with both a commercial membrane and a conventional treatment option. This included determining the removal of dissolved organic carbon (DOC) as NOM surrogate and individual organic fractions at different DOC concentration [DOC] and different water matrices for membranes and the conventional treatment process. Fouling behaviour of S-PANI NF membranes was characterized in comparison with the commercial membrane. To our knowledge, this is the first study to investigate aqueous organic matter separation and fouling behaviour of S-PANI NF membranes. S-PANI NF performance was benchmarked against a comparable commercial modified hydrophilic NF membrane (nominal MWCO $\approx 500 \text{ g mol}^{-1}$) and against an optimized conventional treatment for organic matter removal consisting of adsorption / coagulation / flocculation / clarification / filtration [56]. For this study a batch of new S-PANI NF membranes was synthesized [54]. S-PANI and commercial membrane performance tests were conducted in artificial surface water, seawater at different [DOC] ranging from 10-100 mg C L^{-1} and stabilized landfill leachate sampled from a nearby treatment site. Organic matter was characterized via optical and size-separation methods. Membrane fouling was determined measuring transmembrane pressure (TMP), foulant mass and optically via scanning electron microscopy (SEM).

4.2 Experimental

4.2.1 Materials

A list of chemicals obtained from various commercial suppliers is provided in the supporting information (SI), Materials S1. All solutions were prepared with deionized (DI) water produced from

an ELGA deionizer (PURELAB Option).

4.2.2 Artificially prepared waters and leachate characterization

Artificially prepared surface water and seawater were used as feed solutions containing NOM as probe foulant. The employed natural source NOM solution (Fulvic 25, Solufeed, UK) is a by-product of a commercial scale potable water purification process and was used as a more realistic approach in comparison to model foulants reported elsewhere [53]. NOM concentrations (measured as dissolved organic carbon [DOC]) of 10 and 20 mg C L⁻¹ were used to mimic real-life conditions (at the upper end of concentrations normally expected in most natural waters) whereas high concentration of 100 mg C L⁻¹ was applied to reveal the membrane performance at accelerated fouling [57]. NOM concentrations in natural surface waters are mostly in the range of 1 to 20 mg C L⁻¹ [10,58], while seawater [DOC] is in the range of 1 mg C L⁻¹ [7] (note, in case of algal blooms [DOC] can be higher [7]). A stabilized landfill leachate sample after primary treatment was used as wastewater probe solution and was obtained from an aerated lagoon in Southwest England, Wiltshire, UK. All feed solutions were initially filtered through 0.45 µm Whatman™ filter paper. The effect of suspended solids was not investigated in this work as NF membrane feed streams are typically polished to avoid accumulation and build-up of suspended solids at the membrane surface [59].

The artificially prepared waters and leachate were characterized via various standard methods. The [DOC] was measured using TOC-L CPH analyser, Shimadzu, Japan. Ultraviolet absorption at 254 nm (UV₂₅₄) using quartz glass cuvettes was measured with an Agilent Carry 100 UV-Vis as a simple means to observe changes in NOM composition. The specific ultraviolet absorption (SUVA) was calculated (Equation 4.1).

$$\text{SUVA} = \left(\frac{\text{UV}_{254}}{C_f} \right) \times 100 \quad \text{Equation 4.1}$$

Where UV₂₅₄ and C_f represent the UV₂₅₄ absorbance and [DOC] in the feed stream.

The conductivity was measured using a portable Hach, HQ14D conductivity meter. Total hardness was measured using an AT1000 titration bundle, Hach, UK. The Turbidity was measured via 2100Q portable turbidimeter, Hach, UK. The feed solutions' zeta potential was measured with a Zetasizer (Malvern-Panalytical Instruments, UK) at 20°C to understand the effect of the charge interaction

between the solutes and the membrane to the rejection and fouling behaviour. The leachate's phosphate, chemical oxygen demand (COD), nitrite, nitrate, ammonium, and chloride were analysed using DR3900 Laboratory Spectrophotometer, Hach, UK. Table. 4.1 summarizes the properties of the artificially prepared surface water and seawater.

Table 4.1 Properties of artificially prepared surface water and seawater at different natural source [DOC].

Parameter	Unit	Artificial surface water	Artificial seawater
DOC	mg L ⁻¹	10.0/20.0/100.0	10.0/20.0/100.0
UV ₂₅₄	m ⁻¹	4.5/9.6/50.9	4.5/9.6/50.9
SUVA ₂₅₄	L mg ⁻¹ m ⁻¹	0.5	0.5
Conductivity 20 °C	µS cm ⁻¹	350.0	55,000.0
Total hardness	mg CaCO ₃ L ⁻¹	170.0	7,210.0
Turbidity	NTU	0.1	0.1
pH	-	7.2	7.2
Zeta Potential	mV	-19.7±1.0	-6.9±0.6
Orthophosphate	mg L ⁻¹	<0.03	<0.03

Table. 4.2 illustrates the leachate characteristics. The analytical results showed a high fraction of recalcitrant organic matter based on a chemical oxygen demand (COD) to biological oxygen demand (BOD) ratio of approximately 31:1 which is considered difficult to treat at a conventional sewage treatment works [60,61]. The COD/DOC ratio is 1.86 which indicates that 86% of the COD is organic origin.

Table 4.2 Characterization of a stabilized solid waste landfill leachate.

Parameter	Unit	Landfill leachate
BOD (ATU)	mg L ⁻¹	22.0
Total COD	mg L ⁻¹	688.0
DOC	mg L ⁻¹	368.8
pH	-	8.0
Ammonia as N	mg L ⁻¹	4.0
Total oxidized N	mg L ⁻¹	712.3
Nitrite as N	mg L ⁻¹	0.4
Nitrate as N	mg L ⁻¹	712.0

Orthophosphate	mg L ⁻¹	13.5
Chloride	mg L ⁻¹	608.0

A tangential (crossflow) flow filtration, custom-made, bench scale membrane unit equipped with five different commercially available membranes with different MWCO ranging from 0.5 kg mol⁻¹ to 30 kg mol⁻¹ (SI, Solute fractionation S2, Table S4.1) was used for separation of NOM and leachate fractions. The DOC and COD of each membrane permeate was measured to quantify the apparent molecular weight distribution (AMWD) of the solute.

4.2.3 Conventional treatment

Fig. 4.1 shows the schematic diagram of the lab-scale simulated conventional treatment for both artificially prepared water and leachate. The process consisted of powder activated carbon (PAC) adsorption, coagulation, flocculation, clarification by sedimentation, and sand filtration and was optimised for DOC removal in an iterative process. PAC optimised dose of 300, 400 and 700 mg L⁻¹ was applied for 20 minutes followed by optimized coagulant (ferric chloride) addition of 8, 12 and 32 mg L⁻¹ as Fe⁺³ to treat artificially prepared water containing 10, 20 and 100 mg C L⁻¹ [DOC], respectively, at dosed sample optimized pH \approx 5.5. To enhance settlement and avoid floc breakage resulting in NOM carryover into the sand filter column, BASF Magnafloc[®] LT22S flocculant additive was supplemented at 0.1, 0.15 and 0.2 mg L⁻¹ with increasing [DOC]. Details of the process set up and optimisation are available in supporting information (SI), conventional treatment S3. Conventional treatment of landfill leachate was similar except that no flocculant aid had to be added. Due to the high [DOC] of \approx 370 mg C L⁻¹ of the leachate sample used, both optimal ferric chloride and PAC doses were relatively high using 100 mg L⁻¹ as Fe⁺³ and 1,000 mg L⁻¹ of PAC, respectively, at dosed water pH of \approx 6.0.

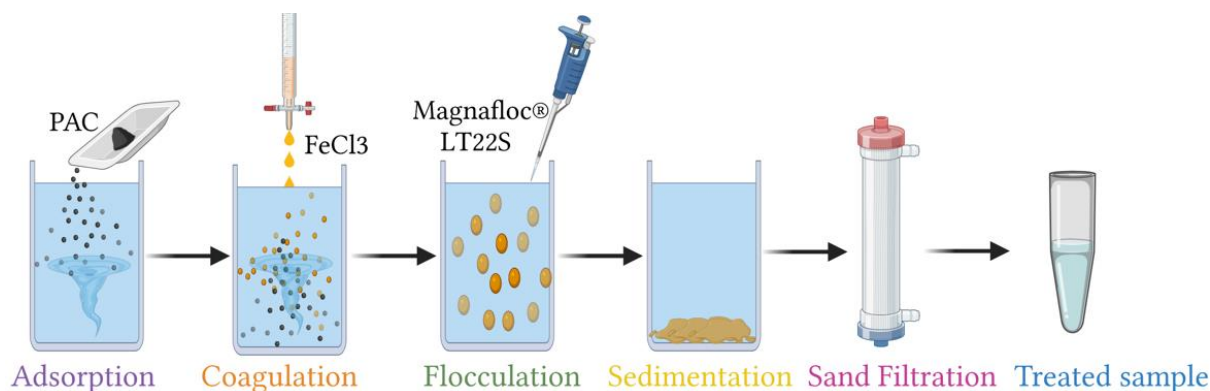


Fig. 4.1 Schematic diagram for the sequence of the applied conventional treatment for artificially prepared surface water and seawater solutions.

4.2.4 Membrane treatment and fouling behaviour

S-PANI membrane fabrication

S-PANI polymerisation and membrane preparation including cross-linking via a NIPS protocol was conducted as previously described [53,54]. In brief, S-PANI powder was prepared by pre-sulfonation of aniline monomers followed by radical polymerization. For membrane preparation, a fixed amount (20 wt%) of S-PANI was gradually added in small portions and dissolved in a mixture of 74 wt% *N*-methyl-2-pyrrolidone (NMP) and 6 wt% anti-gelling agent 4-methylpiperidine (4MP) using a funnel within 1 h. The mixture was stirred until a homogeneous solution was achieved and then left unstirred for deaeration. Subsequently, the mixture was cast at room temperature and controlled relative humidity of 30% on a flat glass plate using a polyethylene terephthalate/ polybutylene terephthalate (PET/PBT) support layer (Novatexx 2484) and spread with an Elcometer 3540 film applicator to produce 200 μm (clearance gap) sheets. Membrane sheets were in-situ formed and cross-linked through immersion precipitation in a 3 M HCl(aq) coagulation bath. After 24 h, the finished membrane sheets were rinsed with 0.01 M NaOH solution to remove residual H^+ ions and then stored at room temperature in pure water until further use.

Membrane transport properties

Permselective properties of S-PANI and the commercial DuraMem[®]500 (Evonik, UK) membranes were evaluated using a crossflow setup following a procedure illustrated in previous work [53]. Permeate flow rates were measured using a digital scale connected to a computer. LabVIEW 2011 software was

used to calculate the normalized membrane permeance. DuraMem[®]500 membranes are made of modified hydrophilic polyimide [62] and are therefore considered as suitable benchmarking membrane for S-PANI. DuraMem[®]500 hydrophilic properties provide a water contact angle of 67° [63] with a measured MWCO around 600 g mol⁻¹ [55]. This compares to a water contact angle of 61° and MWCO ≈ 680 for S-PANI [54]. The [DOC] and [COD] were measured at the feed, concentrate, and permeate to quantify the solute rejection for both membrane samples after prolonged operation period of 24 h.

Fouling behaviour

Real-time monitoring of TMP was conducted using a pressure transducer (model PXM309-007-GI, OEMGA Engineering) connected to a Pico data logging system 1000 Series, Pico Technology. Note, foulant solution application time was 24 h rather than 30 minutes as employed previously [53] to obtain a more realistic understanding of the membrane antifouling behaviour.

Membrane-Foulant affinity

Solute mass balance in the feed, permeate and retentate was derived to obtain the accumulated foulant mass in the membrane coupon (equation 4.2).

$$M = (V_F \cdot C_F) - (V_P \cdot C_P) - (V_R \cdot C_R)/1000 \quad \text{Equation 4.2}$$

Where V_F , V_P , V_R are the volume of feed, permeate and retentate in mL, respectively. C_F , C_P and C_R are the feed, permeate and retentate [DOC] in mg C L⁻¹.

Foulant accumulation on membranes was also measured via recovery of organic matter from the membranes during chemical cleaning. For cleaning, fouled membrane coupons were placed in clean stainless steel dead-end cells (Sterlitech HP4750) with an active membrane area of 14.6 cm² and cleaned twice with 3.2 mM sodium hydroxide solution (around pH 11.5) provided as feed, followed by mild acidic cleaning (HCl) at pH 5.0 and rinsing with pure water until a stable permeate flux baseline was re-established. Subsequently, the DOC of the pooled cleaning solution was analysed. Remaining foulant NOM on membranes was assumed negligible as indicated by full recovery of membrane permeability after cleaning. The specific foulant mass accumulation (m , μg cm⁻²) was calculated using equation 4.3:

$$m = M \times 10^4 / A$$

Equation 4.3

Where M is the mass of deposited organic matter (μg), and m is the specific accumulated mass per active filtration surface area (A , cm^2).

Membrane-foulant affinity was also investigated using SEM (SU3900, Hitachi, Japan). SEM surface images of membranes were captured at an acceleration voltage of 10 kV. Samples were mounted onto SEM stubs and coated with gold using a sputter coater (S150B, Edwards, USA).

The surface charge of the S-PANI and DuraMem[®]500 was measured by using Zetasizer nano series model ZS, Malvern-Panalytical, UK. Zeta potential planar cell (ZEN 1020) along with tracer particles (Latex beads, polystyrene 0.3 μm mean particle size) were used to measure the electrophoretic mobility of the particles at varying distances from the planar surface at neutral pH. The properties for both S-PANI and DuraMem[®]500 membranes are shown in Table 4.3.

Table 4.3 Characterization of the S-PANI and DuraMem[®]500 membranes.

Parameter	Unit	Membrane	
		S-PANI	DuraMem [®] 500
Polymer	—	Sulfonated polyaniline	P84 [®] Modified Polyimide
MWCO	g mol^{-1}	≈ 680.0 [39] ^{α}	≈ 600.0 [192] ^{β}
Water contact angle	$^\circ$	61.0 [39]	67.0 [193]
Surface charge (pH 7.0)	mV	+20.0 \pm 1.2	-16.3 \pm 1.5
Mean surface roughness, R_a	nm	11.8	8.4
Root mean square surface roughness, R_q	nm	9.1	6.5
Recommended maximum pressure	bar	30	20
Recommended pH range (25 $^\circ\text{C}$)	—	4.0-12.0	7.0
Permeance ^{γ}	$\text{L m}^{-2} \text{h}^{-1} \text{bar}^{-1}$	5.0 [39]	9.5 [74]
Configuration	—	Flat sheet membrane	Flat sheet membrane

α) Probe solute sucrose octa-acetate MW 678.6 g mol^{-1} .

β) Probe solute polystyrene.

γ) To obtain comparable results, the initial permeance at this work as adjusted to 7.0 $\text{L m}^{-2} \text{h}^{-1} \text{bar}^{-1}$.

4.3 Results and Discussion

4.3.1 Apparent molecular weight distribution (AMWD) of artificially prepared waters and leachate

Discrete size distributions of aquatic DOC and leachate COD were determined using a series of pressurized UF membranes with MWCO from 0.5 to 30 kg mol⁻¹ in crossflow mode. The size distribution was calculated as a difference in mass concentration between permeates from cells containing membranes with different nominal MWCOs. The sizes of dissolved organics are referred to as apparent molecular weights, since separations are calibrated with compounds of known molecular weight, not size. Fig. 2a shows the AMWD of the NOM solute fractions in the artificially prepared surface water and seawater as percentage of the measured [DOC]. As both artificially prepared waters contain the same mass of organic substances in stock solution, AMWDs for both waters were similar. A moderate shift towards smaller molecular weight was observed for artificial seawater, especially for the upper (>30 kg mol⁻¹) and lower MW fractions (<0.5 kg mol⁻¹) exhibiting decreases and increases of approximately 5 to 7% in their contribution to [DOC], respectively. A considerable increase in the solutes fraction from 12% to 18% was observed for MWs below 0.5 kg mol⁻¹. The shifts in AMWD in the artificial seawater stream can be attributed to the compaction of the humic substances at high ionic strength [65]. Small MW aquatic organic fractions contribute to 12% (<0.5 kg mol⁻¹), 14% (<0.5-1 kg mol⁻¹) and 6% (<1-3 kg mol⁻¹) of the measured [DOC]. A reasonable fraction of the NOM accounting to 30% of the [DOC] falls in the range of 3-10 kg mol⁻¹ compared to 20% and 18% for MW range 10 - 30 kg mol⁻¹ and > 30 kg mol⁻¹, respectively.

Fig. 4.2b shows the solute MW fraction in the leachate as a percentage of measured [DOC] and [COD]. A considerable portion of the solutes around 22% as [DOC] and 30% as [COD] falls below 0.5 kg mol⁻¹. In contrast, around 8-12% of [DOC] and 8-15% of [COD] fractions are individually available within apparent MW range of 0.5-1, 1-3, 3-10 and > 30 kg mol⁻¹. A substantial organic fraction around 41% as [DOC] and 23% [COD] is in the range of 10-30 kg mol⁻¹. Stabilized leachate was reported to possess substantial portion (around 30%) of organic compounds contributing to COD with apparent MW < 0.5 kg mol⁻¹ [66]. This indicates the presence of small MW organics in the leachate resulting from decomposition and microbial degradation of organic waste at the landfill site [67]. Leachate organic

matter analysis at different sites was reported to exhibit higher MW fractions in the range 11-13 kg mol⁻¹ compared to low MW fractions \approx 0.2-3 kg mol⁻¹ [68].

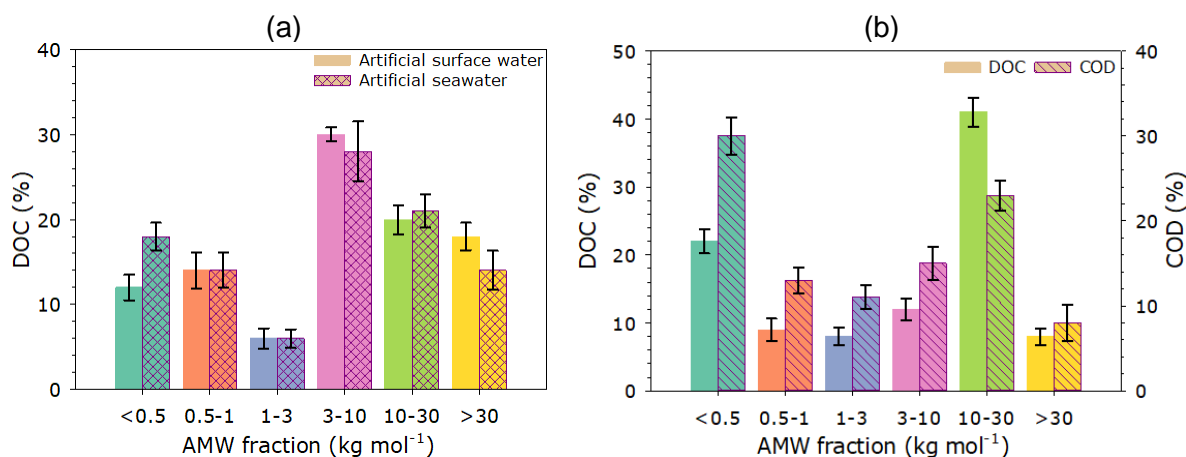


Fig. 4.2 Apparent molecular weight distribution of a) NOM (measured as [DOC] of 20 mg C L⁻¹) in feed aqueous solution for artificial surface water and seawater and b) COD and DOC in landfill leachate with error bars representing one standard deviation calculated from the results of triplicate runs at the specific experimental conditions.

4.3.2 Treatment of artificially prepared water

Conventional treatment

Fig. 4.3a shows results for the optimized performance of the integrated conventional treatment in terms of DOC removal via at three different feed concentrations 10, 20 and 100 mg C L⁻¹. The highest DOC removal was $74 \pm 4\%$ and $63 \pm 5\%$ for artificially prepared surface water and seawater, respectively, at an initial [DOC] of 10 mg C L⁻¹. Removal efficiency gradually declined with increasing [DOC] to $71 \pm 5\%$ and $61 \pm 5\%$ for artificially prepared surface water compared to $59 \pm 5\%$ and $50 \pm 5\%$ for artificially prepared seawater at [DOC] of 20 and 100 mg C L⁻¹, respectively.

Combined mechanisms for NOM removal via coagulation include charge neutralization, adsorption, complexation with metal ions of the dosed inorganic coagulant into insoluble particulate aggregates and entrapment [69]. Changes in the artificial surface water zeta potential from -19.7 mV at neutral pH to -4.3 mV (Table S4.2) at dosed water pH 5.5 were observed before and after acid and coagulant dosing, respectively. At dosed water pH <6.0 complexation of negatively charged NOM with positively charged soluble metal species onto insoluble precipitates is the main NOM removal mechanism [70,71]. Further NOM adsorption onto metal-NOM precipitates accounts for additional removal [72]. Charge

neutralization also occurred at acidic conditions [73]. Medium and small MW species are likely to be removed by complexation, charge neutralization, adsorption, or co-precipitation whereas removal of high MW species has been attributed to bridging or sweep flocculation [74]. More hydrophobic and high MW fractions of NOM are readily removed by coagulation [75]. However, the artificial surface water SUVA₂₅₄ of 0.5 L mg⁻¹ m⁻¹ suggests that low MW hydrophilic organic matter is dominant [56,76]. The NOM fractionation (section 4.3.1) shows that around 33% of the feed NOM molecules are below 3 kg mol⁻¹. Therefore, the principal removal mechanism is expected to be adsorption onto metal hydroxide surfaces due to the high representation of low MW and non-humic substances, leading to much higher optimal coagulant dose [56]. The solubility curves for amorphous ferric hydroxide in seawater are reported elsewhere showing high fractions (around 99% at pH 5.5) of positively charged Fe as $Fe(OH)_2^+$ available for adsorption and charge neutralization coagulation reactions [77].

DOC removal efficiency was consistently smaller across the different [DOC] in artificial seawater, partially due to the salinity-induced reduction of interfacial charge of the *humic acid* [65] leading to electrodynamic instability of colloids [78]. This change might be attributed by either double layer compression, caused by the concentration of high ionic strength of the artificial seawater, or by adsorption/interaction of specific ions (such as Ca⁺² and Mg⁺²) with the *humic acid* molecules giving likelihood that double layer compression effects are more significant [79]. More generally, increased ionic strength and shifts in individual anion and cation concentration in saline water affect coagulation mechanisms, colloid destabilization, and colloidal removal in various ways [80]. At high salinity the solubility of ferric salt coagulants is low over a wide range of pH and temperature conditions, which makes equilibrium conditions and speciation of amorphous ferric hydroxide in seawater different from those in surface and other freshwaters [77]. In addition, the increased total hardness in seawater promotes formation of less stable flocs prone to inferior settling [81]. Flocculation takes place under appropriate conditions where agglomeration of micro flocs enforced by Van der Waals and electrostatic forces lead to formation of larger flocs or aggregates [82]. Poor floc settlement was observed during jar testing as a result of weaker attractive forces bonding the floc together due to the increased separation distance and steric repulsion from adsorbed NOM [83]. As such, flocculant aid (Magnafloc® LT22S, potable water grade) cationic polyelectrolyte copolymer of acrylamide and quaternized cationic

monomer was applied. The developed electrostatic attraction by the counterions promotes adsorption and charge neutralization reducing the colloid stability leading to the formation of dense flocs with high strength and improved settling process [84]. Note, that despite the overall decrease in conventional process performance with increasing salinity, PAC treatment had a more noticeable effect in artificial seawater showing 4.3% surplus NOM adsorption to PAC compared to the artificially prepared surface water (Table S4.2). The presence of Ca^{+2} and Mg^{+2} in seawater leads to alternation in adsorption affinity due to the organic ligands associated with divalent ions [85]. The increased adsorption of NOM to PAC in seawater has been explained by a combination of decreased electrostatic repulsion and increased chemisorption between NOM and PAC at high salt concentrations [86]. Aquatic organic matter adsorption by PAC is governed by many aspects such as NOM molecular weight distribution, zeta potential, solution pH, salinity, degree of hydrophobicity and the hydrogen bonding formation ability between the PAC surface and NOM [87]. Although the high MW fraction of the NOM ($> 10 \text{ kg mol}^{-1}$) does not readily adsorb to PAC due to size exclusion effects [88], it is generally removed by coagulation [89]. In comparison, the intermediate MW fractions ($0.5\text{-}4 \text{ kg mol}^{-1}$) are well removed by activated carbon whereas the low MW NOM fractions which benefits from access to a large percentage of the activated carbon pore volume might be removed based on size considerations alone or could be less adsorbable if they are more hydrophilic [88,90].

Fig. 4.3b shows the shifts in the AMWD of the NOM in the feed and the conventionally treated artificial water. A noticeable shift in the NOM AMWD ($11 \pm 2 \%$ to $15 \pm 2 \%$) took place particularly for intermediate and low MW fractions (0.5 to 3 kg mol^{-1}) following the conventional treatment. In contrast, the representation of the higher MW organic fractions ($3\text{-}30 \text{ kg mol}^{-1}$) was diminished by $16 \pm 1 \%$ to $24 \pm 2 \%$. Similarly, the AMWD of the organic fractions $> 30 \text{ kg mol}^{-1}$ was decreased by $6 \pm 1 \%$ and $1 \pm 2 \%$ for the artificially prepared surface water and seawater, respectively. The results suggests that conventional treatment processes possess higher efficiency for NOM removal of high MW organic matter while having limitations to tackle intermediate to low MW fractions which agrees with studies reported elsewhere [91]. Ineffective removal of the low MW organic fractions is believed to be

problematic due to their increased tendency for DBP formation [92], and enhanced biofouling activity in distribution networks and downstream membrane processes [93,94].

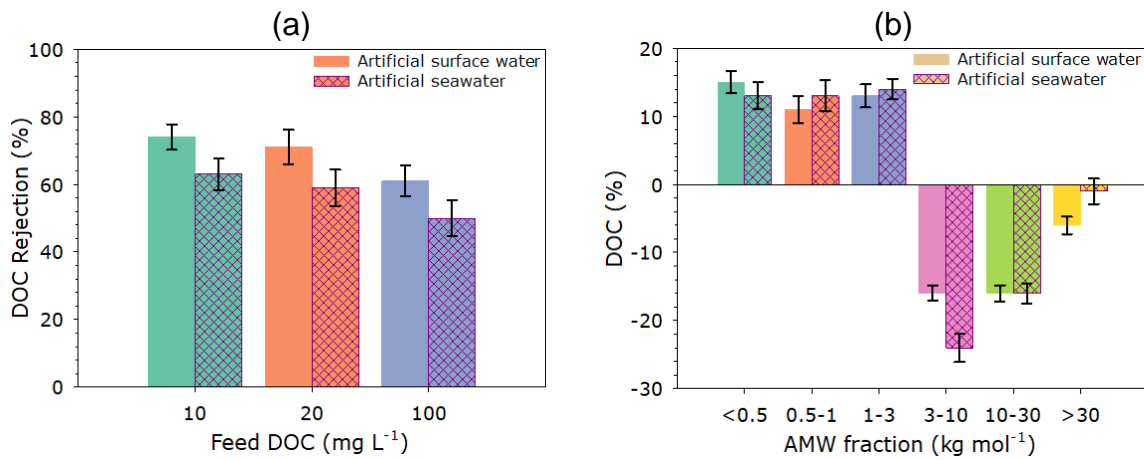


Fig. 4.3 a) NOM (measured [DOC]) removal for artificially prepared surface water and seawater feed containing different DOC concentrations using conventional treatment with error bars representing one standard deviation calculated from the results of triplicate runs at the specific experimental conditions, b) Shift in apparent molecular weight distribution of the NOM for conventionally treated artificial surface water and artificial seawater at [DOC] 20 mg C L⁻¹ with error bars represent one standard deviation calculated from the results of triplicate runs at the specific experimental conditions.

Membrane treatment

Fig. 4.4 shows solution permeance and DOC rejection for S-PANI and DuraMem[®]500 membranes. The reported pure water permeance for S-PANI and the DuraMem[®]500 membrane were 5.0 and 9.5 L m⁻² h⁻¹ bar⁻¹, respectively [54,55]. However, S-PANI membranes were tested here at higher permeance to allow inter-membrane comparison. The applied pressure was adjusted to achieve initial permeance of 7.0 L m⁻² h⁻¹ bar⁻¹ for both membranes. For S-PANI, increasing [DOC] from 10 to 100 mg C L⁻¹ decreased permeance by 7% and 12%, respectively, for artificial surface water compared to 4% and 10% decrease for artificial seawater (Fig 4.4a). At same [DOC], permeance for both artificial surface water and seawater was comparable and only slightly lower (4%) for seawater at [DOC] 10 mg C L⁻¹. Similarly, with increasing [DOC] permeance of DuraMem[®]500 membranes decreased between 6% to 14% for artificial surface water and 1% to 11% for seawater, respectively. Increased permeate flux decline was associated with step increase in NOM feed concentration and increased ionic strength. This could be to corresponding to cake formation and concentration polarization, respectively [95]. Changes in the NOM concentrations from 10 mg C L⁻¹ to 100 mg C L⁻¹ could alter the fouling mechanisms from pore blocking/pore constriction to cake formation as a result of NOM accumulation at the membrane

surface [96]. Despite operating beyond higher permeance settings than usual, the S-PANI membrane permeance was slightly above that of the commercial membrane across different [DOC]. The slight change in the productivity decline, decrements in flux over time of operation, could be attributed to the increment of hydraulic resistance as a result of both reversible and irreversible fouling development [97]. Enhanced flux reduction of the DuraMem[®]500 at high ionic strength could be explained by the reduced charge repulsion by electrostatic interaction between the negatively charged membrane (-16.3 mV) and the positively charged Na⁺ [98]. However, higher permeance rates may affect fouling rates of membranes [99]. The fouling behaviour of both membranes are addressed in the fouling section of this study, following below where TMP and membrane-foulant affinity were investigated to understand and monitor the fouling behaviour of both membranes. DOC removal for S-PANI was consistently 8 to 10% above that for the commercial membrane for both waters tested and at different [DOC] (Fig 4.4b). For artificial surface water DOC removal across different initial [DOC] was consistent for both membranes. The NOM could be removed by both NF membranes via a combination of convection, diffusion, and electrostatic repulsion mechanisms [100]. The size distribution of solutes and pores as well as the surface charge might have contributed to slight changes in the transport mechanisms of NOM through the membranes [101]. Table S4.2 shows that the zeta potential of the membrane filtrate for the artificial surface water feed was almost neutrally charged (-0.9 mV, S-PANI and -1.2 mV DuraMem[®]500) which suggests that the carried over solute pores are either smaller than the membranes pores or neutrally charged which diminished their rejection by size exclusion or electrostatic repulsion. However, both membranes exhibited lower DOC removal efficiency with artificial seawater, between 2% and 9%, with increasing initial [DOC]. This can be partially explained by the compaction of NOM in high salinity environments, as discussed above, affecting their retention by a given membrane.[102]. In addition, the increase in ionic strength may reduce charge repulsion between ionized functional groups on single NOM molecules, allowing NOM to adopt a more compact configuration. However, both increasing NOM concentration and solution ionic strength was reported to cause permeate flux decline and NOM rejection of hydrophobic membranes (Polysulfone) due to the enhanced accumulation of NOM on membrane surface [96]. This was explained by the interaction between positively charged Na⁺ and

negatively charged NOM functional groups, causing NOM accumulation on the membrane surface [103]. Increasing ionic strength had little effect on the mass of NOM deposited, but significantly increased the compactness and specific resistance of the NOM [95,104]. Both membranes tested in this work have hydrophilic surfaces with lower affinity towards foulants. The hydrophilicity of the membrane surfaces was characterized by measuring the contact angle of water droplets. Hydrophobic membranes have higher tendency towards foulants in contrast with hydrophilic counterparts which do not tend to form hydrogen bonding interactions between the membrane interfaces and water. This spontaneous process leads to an increased entropy and foulant adsorption which dominates the boundary layer [27,31,105]. Membrane hydrophilicity is indicated by contact angles below 90° and contact angles decrease with increasing hydrophilicity [106]. S-PANI and DuraMem[®]500 showed water contact angles of 61° and 67° , respectively (Table 4.3). Therefore, S-PANI has a slightly higher hydrophilicity than DuraMem[®]500. This potentially diminished the effect of cake layer formation which favours flux decline on the account of NOM macromolecule rejection at high ionic strength.

In comparison to the optimized conventional coagulation – flocculation treatment (previous section) membranes performed between 23-36% and 32-41% (S-PANI), and 16-31% and 25-33% (DuraMem[®]500) better in DOC removal for artificial surface water and seawater, respectively. Membranes exhibited consistent performance across the significant water matrix changes induced by the increased salinity tested here without need for process optimization. Note that pH adjustment towards acidic pH for S-PANI could provide further modest improvements of DOC rejection due to the responsiveness of the membrane material to pH changes [53] and changes in NOM conformation (coiled vs linear) at lower pH [67]. The AMWD for the membrane permeate sample was not determined because a) the NOM fractions were isolated into various MW components using membrane fractionation technique filtration protocol by employing a series of UF and NF membranes of predefined MWCO and b) the probe commercial membrane DuraMem[®]500 was already used for NOM fractionation as shown in SI, Table. S4.1. The MWCO of the S-PANI membrane is near that of DuraMem[®]500 and it can be assumed that size exclusion is the dominating retention mechanism for the prolonged operating period of 24 h in dynamic crossflow filtration mode.

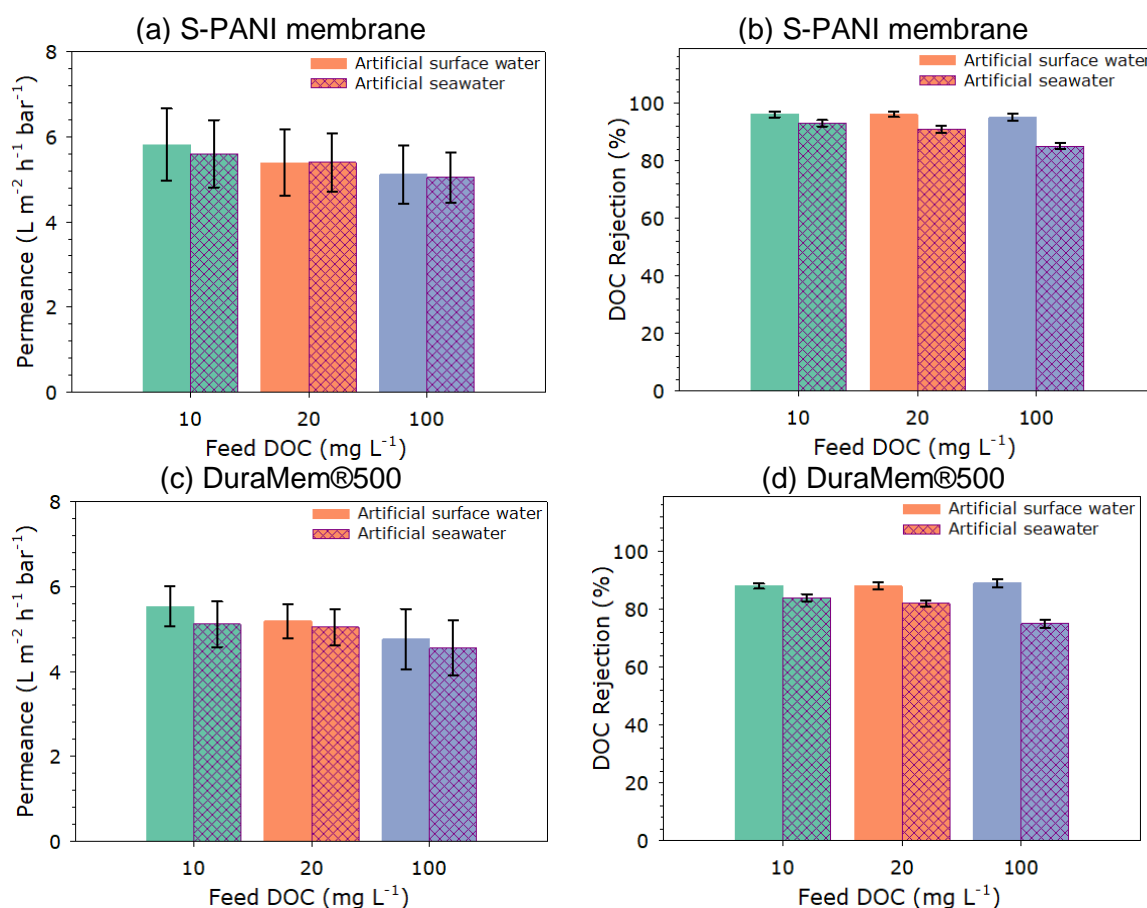


Fig. 4.4 Permeance and DOC rejection for artificially prepared surface water and seawater solutions containing different [DOC] using S-PANI membranes (a, b) and DuraMem®500 membranes (c, d) with error bars representing one standard deviation calculated from the results of triplicate runs at the specific experimental conditions.

4.3.3 Landfill leachate treatment

Conventional and membrane treatment

Fig. 4.5a shows the DOC and COD removal efficiency of conventional and membrane treatment for the leachate feed solution. The DOC removal was in the following order: conventional treatment (91 ± 7 %) > S-PANI membrane (85 ± 3 %) > DuraMem®500 (78 ± 3 %). In contrast, the COD removal efficiency followed different order: S-PANI membrane (74 ± 3 %) > DuraMem®500 (70 ± 3 %) \approx conventional treatment (70 ± 5 %). Humic substances comprise a substantial fraction of the organic content in stabilized leachate [107]. Refractory humic substances, mainly in the form of *humic acids* (moderate MW 10 kg mol^{-1}) and *fulvic acids* (moderate MW 1 kg mol^{-1}) alter the biodegradable fraction of organic compounds during the stabilization process in landfill sites [108,109]. The repulsion of the negatively charged leachate colloidal particles (pH range ≈ 5 -9) inhibits self-coagulation and settlement

[110]. The coagulation and flocculation process helped to neutralize and destabilize the negatively charged leachate colloidal particles leading to settleable aggregated flocs [111]. Ferric chloride has been reported as a more effective coagulant than aluminium-based coagulants for landfill leachate treatment [112,113]. A comparable conventional treatment system was reported to achieve optimal COD removal of 70-77% [113,114] and DOC removal > 80% DOC [115]. The high *humic acid* content explains the high removal efficiency of the tested conventional system. The combined process of coagulation/flocculation and adsorption ameliorated the drawbacks of each single process. Although conventional treatment can achieve high DOC removal and moderate COD removal, excess sludge production including high chemical demand can be an issue [116].

PAC adsorption is a common and attractive method for the removal of recalcitrant organic compounds in leachate given its high reduction in COD unaffected by initially high organic matter concentrations [117,118]. The DOC and COD low MW fractions ($< 0.5 \text{ kg mol}^{-1}$) in the leachate feed was around 22% and 30%, respectively, (Fig. 4.2b) which explains the threshold removal efficiency of the NF membrane treatment. COD removal for a comparable stabilized leachate via NF membranes was 70-80% with MWCOs similar to the membranes used here [116]. For the investigated works, tight UF membranes (MWCO $\approx 1 \text{ kg mol}^{-1}$) are required for COD and DOC removal targets over 70%. The abundance of small MW compounds below 1 kg mol^{-1} raises the concern over the applicability of the NF membrane treatment due to the increased risk of pore plugging. There is also a substantial segment of organic species (41% DOC) in the MW range of $10\text{-}30 \text{ kg mol}^{-1}$ which expose the membrane to fouling by surface deposition and cake formation of organic segments. The prospective high fouling risk emphasizes the importance of investigating the fouling behaviour of the developed S-PANI membranes and their potential for full-scale applications with realistic feed streams in comparison to the commercial membranes.

Fig. 4.5b shows the shifts in the AMWD for the conventionally treated leachate. The AMWD for the membrane permeate sample is not determined (see membrane treatment section). Low MW DOC and COD fractions ($< 0.5 \text{ kg mol}^{-1}$) were increased by $19 \pm 3 \%$ compared to slight increases by $7 \pm 2 \%$ and $4 \pm 2 \%$ for the MW fractions $0.5\text{-}1 \text{ kg mol}^{-1}$. An equally marginal increase in DOC and COD ($2 \pm 2 \%$) was observed for the MW fractions $1\text{-}3 \text{ kg mol}^{-1}$. In contrary to the increase in organic fraction (3

$\pm 2\%$) for the MW range 3-10 kg mol⁻¹, the COD fraction was diminished by $7 \pm 2\%$. The conventional treatment markedly removed organic fractions in the 10-30 kg mol⁻¹ MW range reflected by a decrease in measured COD by $13 \pm 2\%$ whereas a slight decrease ($2 \pm 2\%$ for DOC and $5 \pm 2\%$ COD) was observed for MW fractions > 30 kg mol⁻¹. The limited removal rate of the intermediate and low MW organic fractions could be explained by the limited capacity of coagulation for the removal of organic fractions < 4 kg mol⁻¹, reported elsewhere [119]. The removal efficiency of the coagulation and adsorption process is also dependent on the hydrophobic nature of the solutes, while hydrophobic fractions are more readily removed than hydrophilic fractions [66,88]. The hydrophilic aquatic organic fractions possess negligible charge density in contrast with the hydrophobic NOM fractions which exert greater dominance on coagulation control [92]. The AMWD of the COD followed the same order for MW range < 3 kg mol⁻¹. However, the COD fraction was decreased at the 3-10 kg mol⁻¹ MW range in contrast to overall DOC. This could be attributed to the removal of inorganic fractions which might be removed by sweep flocculation [120,121] or PAC adsorption [122].

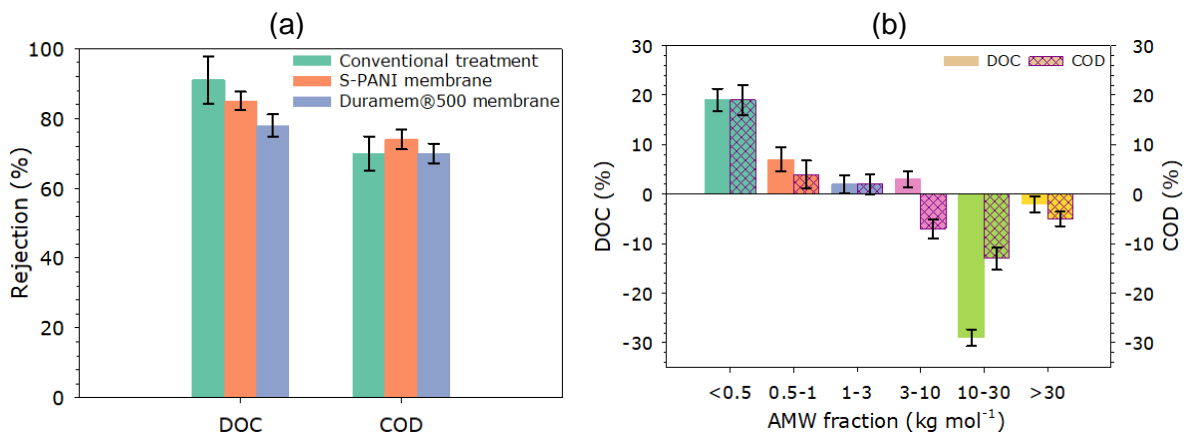


Fig. 4.5 a) Solute removal efficiency in terms of measured DOC and COD by conventional and membrane treatment and b) Shift in apparent molecular weight distribution of the DOC and COD for conventionally treated leachate at $[\text{DOC}] \approx 370 \text{ mg C L}^{-1}$ with error bars representing one standard deviation calculated from the results of triplicate runs at the specific experimental conditions.

4.3.4 Membrane fouling behaviour

Artificially prepared water

Fouling behavior of S-PANI and DuraMem[®]500 membranes during treatment of artificial surface water and seawater was recorded by measuring the TMP development over time at different $[\text{DOC}]$ at initial permeance of $7.0 \text{ L m}^{-2} \text{ h}^{-1} \text{ bar}^{-1}$ (Fig. 4.6). Both turbidity and the orthophosphate of the feed solution

were low, therefore dominance of the NOM induced fouling can be expected [6]. The measured SUVA₂₅₄ of the feed solution was in the lower range ($0.5 \text{ L mg}^{-1} \text{ m}^{-1}$) compared to SUVA₂₅₄ values typical for surface water ranging from 1.0 to $6.0 \text{ L mg}^{-1} \text{ m}^{-1}$ [123]. High SUVA₂₅₄ values (> 4.0) indicate that the NOM is mostly composed of high MW hydrophobic material whereas low SUVA₂₅₄ (< 2.0) suggests that low MW hydrophilic organic matter is dominant [56,76]. The results revealed that fulvic acids (hydrophilic fraction) are dominating the NOM sample which agrees with the supplier datasheet. SUVA₂₅₄ of ocean NOM is usually smaller than 1.0 [77,124] which makes the NOM stock solution of this experiment a good representative sample in terms of SUVA. Under the experimental conditions, TMP can be assumed to vary only due to fouling. TMP of both membranes increased gradually for 5-10 h for different [DOC] and for both types of water, with the fastest increase at the highest [DOC] of 100 mg C L^{-1} , and then either continued to increase at a slower rate or remaining stable until the end of the test period of 24 h. Maximum TMP increased with increasing [DOC] and was 14 and 19 kPa for of S-PANI and 25 and 35 kPa for the DuraMem[®]500 membrane of artificially prepared surface water and seawater, respectively, as indicated in Fig 4.6. For both membranes maximum TMP at given [DOC] was consistently higher for artificial seawater with 30-37% higher values for S-PANI and 30-47% higher values for the DuraMem[®]500 membrane, respectively. The higher fouling rate of the saline environment is in agreement with both the observed decrease in permeance (Figure 4.4) and shifts in AMWD (Figure 4.2b), discussed above. Binding of divalent ions (Ca^{+2} , Mg^{+2}) to NOM was one of the major causes for the accumulation and growth of a densely compacted fouling layer on the membrane surface, which leads to severe flux decline. The ability of the NF membranes to retain divalent ions leads to an increase in concentration of rejected Ca^{+2} , for instance, at the membrane surface leading to concentration polarization and hence enhanced fouling by Ca-NOM complexing and aggregate formation [125]. As such, the enhanced adsorption and deposition of NOM at high salinity leads to changes in the NF membrane surface characteristics due to the increase in surface hydrophobicity. This development of foulant growth makes the membrane gradually more vulnerable to fouling [126]. It is likely that the morphological changes of NOM induced at high salinity lead increased pore clogging of membranes and higher fouling indicated by TMP [102]. Non-proportional effects at increased foulant concentration are well known and have been ascribed to the

porous nature of the formed foulant cake layer as compared to the membrane porosity [127]. In addition, hydrodynamic conditions may have created shear forces that prevented continued growth of foulant deposits alongside increasing TMP [125]. TMP increase was generally lower for the S-PANI membrane compared to the DuraMem®500 membrane, with TMP values 3-9 and 7-15 kPa (S-PANI) and 7-12 and 11-20 kPa (DuraMem®500) at different [DOC] concentrations during the first 4 h of crossflow filtration. The better fouling performance of the S-PANI membrane can be explained by the formation of a hydration layer by the zwitterionic surface of S-PANI which decrease the membrane affinity towards hydrophobic foulants [128].

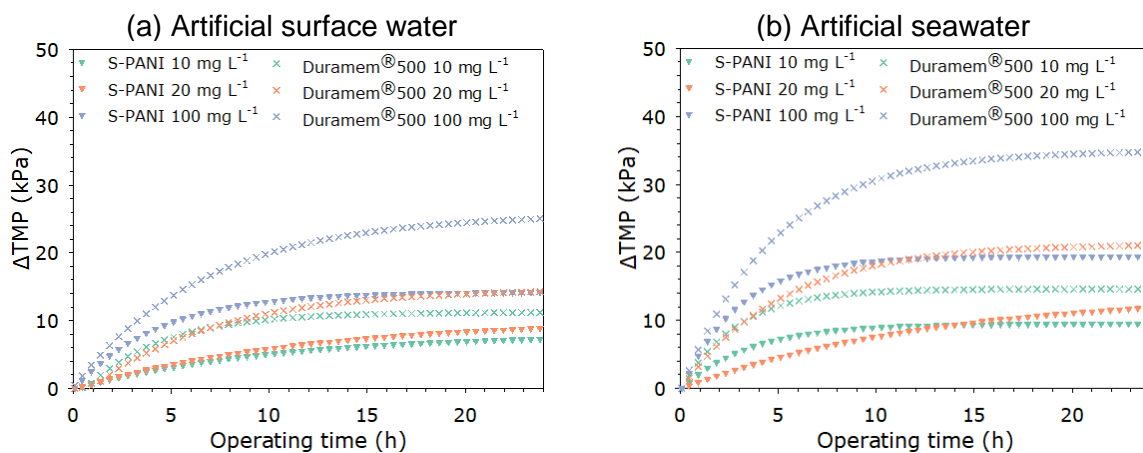


Fig. 4.6 The change in the transmembrane pressure (TMP) for fouled S-PANI and DuraMem®500 membranes at different [DOC] obtained from natural source (a) artificial surface water, (b) artificial seawater, at identical initial permeance values ($\approx 7.0 \text{ L m}^{-2} \text{ h}^{-1} \text{ bar}^{-1}$).

Fig. 4.7 shows the foulant mass accumulation per membrane unit area. The foulant mass was obtained via two approaches using either derived from mass balance calculations of the filtration system or determining the chemically recovered organic matter from each membrane coupon. Results obtained via the solution mass balance were between 1.2-1.6 times higher than the chemically determined mass likely representing an over estimation of foulant accumulation. However, trends observed when comparing both approaches were similar. The DuraMem®500 accumulated more mass per unit area than the S-PANI membrane. The mass balance, for instance, displays surplus organic matter deposition over the DuraMem®500 membrane compared to S-PANI membrane by 26%, 39% and 43% at 10, 20 and 100 mg C L⁻¹, respectively, compared to 35%, 46% and 42% in artificially prepared surface water

and seawater, respectively. The accumulated mass data suggest that the S-PANI membrane has less foulant affinity towards NOM foulants than the tested DuraMem[®]500 membrane.

The order of fouling potential of NOM fraction as hydrophilic neutral > hydrophobic acids > transphilic acids > hydrophilic charged [129]. The SUVA₂₅₄ of the artificial surface water indicates that the hydrophilic fractions dominate the NOM composition. The nature of membrane materials affects the rate of accumulation of carbohydrate-like substances (hydroxyl and carboxyl groups) which represents the hydrophilic fractions of NOM [130]. Hydroxyl groups have stronger adhesion towards the membrane surface than carboxylic groups which can be explained by strong hydrogen bond generated with the membrane material. Electronegative polymeric membranes may exhibit strong adhesion with the NOM hydrophilic fractions that are associated with hydroxyl groups [131]. Albeit hydrophobicity and electrostatic interactions between solute and membrane are *princIPAL* factors affecting the extent of NOM fouling [97], the negative surface charge of the DuraMem[®]500 (-16.3 mV as shown in Table 4.3) and the nature of NOM hydrophilic fractions in this instance could explain the higher foulant affinity compared to the positively charged S-PANI (+20 mV). The adsorption of the negatively charged NOM to the positively charged S-PANI surface might take place during the filtration process, the charged adsorption sites are expected to form a “dynamic membrane” due to the selective (reversible) adsorption of the NOM charged molecules on the membrane [132]. The S-PANI material also benefits from low surface energy which offer a self-cleaning ability at certain hydrodynamic conditions [128]. Both membranes possess smooth surfaces (Table 4.3) with marginal difference in mean surface roughness. As such, the roughness may not account for fouling affinity of either membrane. In common, both membranes experienced higher foulant affinity in seawater. Increased fouling tendency of polymeric membranes was reported elsewhere and explained by the presence of calcium ions in seawater [133]. Also, the polymeric membrane materials were observed to behave differently in seawater environments showing increased contact angles (higher hydrophobicity) and surface roughness leading to higher fouling rate [134].

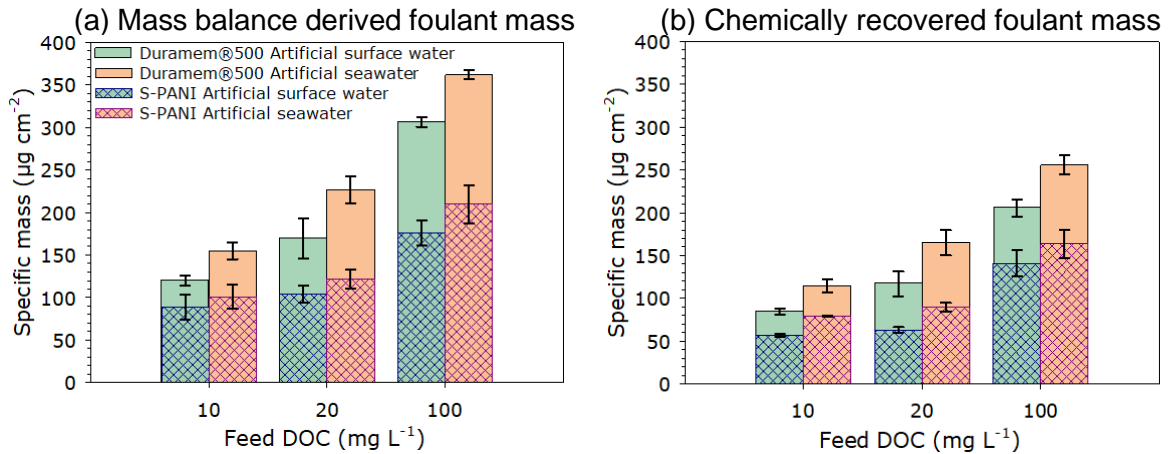


Fig. 4.7 The accumulated foulant mass per unit membrane surface area for SPANI and DuraMem®500 membranes (a) mass balance derived foulant mass and (b) chemically recovered foulant mass, with error bars represent one standard deviation calculated from the results of triple runs at the specific experimental conditions.

Landfill leachate

Fig. 4.8a shows the change in the TMP for both membranes for leachate [DOC] ≈ 370 mg C L⁻¹. The high organic content, different chemistry and AMWD of the leachate compared to the NOM used in the artificial water experiments resulted in extensive and continued TMP growth for both membranes during the test period of 24 h of up to 23 kPa for S-PANI and up to 47 kPa for the DuraMem®500 membrane. Fig 4.8b shows accumulated foulant mass for the leachate with similar differences between mass balance derived and chemically recovered mass (see previous section). The S-PANI membrane had lower affinity towards foulants accumulating between 182-232 µg per cm⁻² of membrane surface area for the chemically recovered and mass balance derived organic foulant mass compared to 332-481 µg per cm⁻² for the DuraMem®500, respectively. Leachate fouling results suggests the need for preliminary treatment of the leachate stream prior to NF treatment (for instance, UF membrane of MWCO ≈ 10 kg mol⁻¹ or an integrated conventional treatment such as coagulation or adsorption) to diminish the impact of bulky foulants to NF membranes.

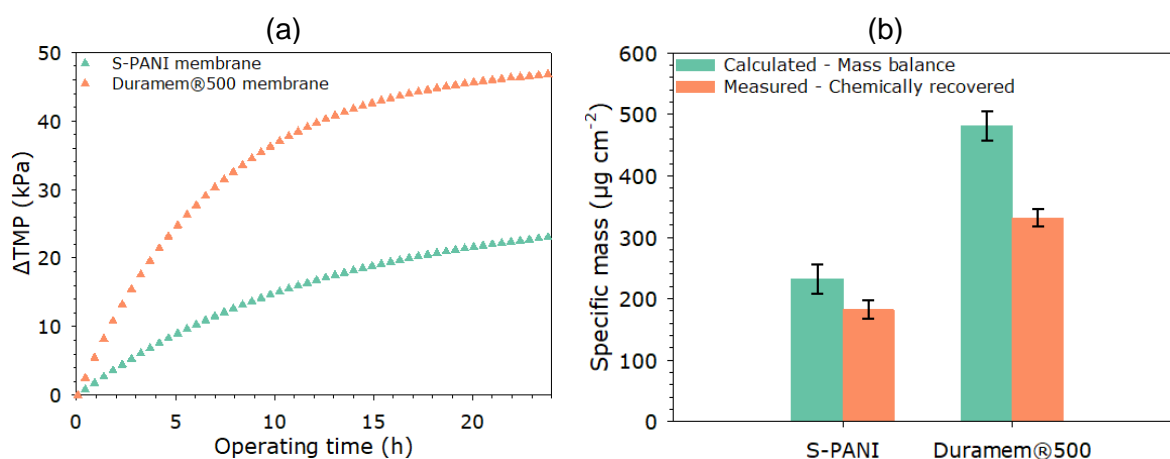


Fig. 4.8 a) Development of transmembrane pressure (TMP) for fouled membranes with landfill leachate for S-PANI and DuraMem®500 at identical initial permeance values ($\approx 7.0 \text{ L m}^{-2} \text{ h}^{-1} \text{ bar}^{-1}$) and (b) Mass balance derived and chemically recovered accumulated foulant mass per unit membrane surface area for SPANI and DuraMem®500 membranes, respectively. Error bars represent one standard deviation calculated from the results of triplicate runs at the specific experimental conditions.

Fouling indicators

Membrane fouling is an inevitable phenomenon during filtration processes. As such, artificial surface water, artificial seawater and the landfill leachate were distinctly used to assess the antifouling property by quantifying the total fouling, reversible fouling, irreversible fouling, and flux recovery ratio. Reversible fouling is defined following the removal of loosely bound deposits and concentration polarization layers solely by water rinsing in contrast with the irreversible fouling [135]. Table 4.4 shows the fouling indicators of the S-PANI and the DuraMem®500 membrane. The S-PANI membrane shows excellent antifouling behaviour with lower total fouling rate (FT) by 24%, 13% and 19% at [DOC] of 10, 20 and 100 mg C L⁻¹, respectively, in artificial surface water feed compared to the DuraMem®500. Likewise, the total fouling of the S-PANI in artificial seawater was less than the DuraMem®500 by 19%, 35% and 27%, respectively. The S-PANI membrane also exhibited less fouling rate in leachate feed by 24% compared to the DuraMem®500. The flux recovery rate (Fr) for the S-PANI is higher than the DuraMem®500 membrane by 4% to 10% using different organic concentration of artificial surface water, artificial seawater, and 12% using a constant feed of landfill leachate. The total fouling of both membranes was only increased by 52-58% and 30-40% for the artificial surface water and the artificial seawater feed, respectively, despite 10-fold increase in the feed DOC concentration. The experimental data show that both membranes provide high flux recovery ratio and relatively low irreversible fouling ratio even at high foulant concentration and prolonged running time

for each dynamic filtration stage. Long running time (24 h) allowed for large amounts of water to pass through the membrane and thus was more vulnerable to fouling leading to higher flux decline. The high antifouling property is attributed to the formation of the hydration layer which forms a boundary limiting foulants' deposition and adsorption over the membrane surface. Nevertheless, the reversible fouling data show that S-PANI has better self-cleansing property and less foulant affinity than DuraMem®500. The reversible fouling forms about 59-78% and 54-59% of the total fouling for S-PANI compared to 19-54% and 14-33% for DuraMem®500 using artificial surface water and artificial seawater, respectively, at feed DOC 10-100 mg C L⁻¹. The elevated irreversible fouling rate of DuraMem®500 agrees with the fouling affinity findings (Figure 4.7) which was ascribed to the higher binding propensity of the foulant's hydroxyl functional groups and the negatively charged DuraMem®500 membrane surface. While both membranes have relatively comparable hydrophilic property and smooth surface, there was also no clear trend between membrane surface hydrophilicity and membrane fouling propensity.

Table 4.4 Fouling indicators for S-PANI and commercial DuraMem®500 membranes related to the initial cleaning-fouling cycle at equal initial permeance.

	Artificial surface water			Artificial seawater			Landfill leachate
	10.0	20.0	100.0	10.0	20.0	100.0	368.8
S-PANI							
Total fouling, F_T %	17±1.5	23±1.1	27±1.6	20±1.2	22±1.2	28±1.3	34±1.3
Reversible fouling, F_{Rev} %	13±1.0	18±1.5	16±1.2	11±1.1	13±1.3	15±1.1	14±1.1
Irreversible fouling, F_{Irr} %	4±1.0	5±1.4	11±1.0	9±1.0	10±1.3	13±2.0	20±1.0
DuraMem®500							
Total fouling, F_T %	21±1.6	26±1.4	32±1.5	27±1.1	28±1.3	35±1.9	42±2.1
Reversible fouling, F_{Rev} %	8±1.1	14±1.0	6±2.2	9±1.2	9±1.8	5±1.7	10±1.8
Irreversible fouling, F_{Irr} %	13±1.7	12±1.1	26±1.4	17±1.3	19±2.0	30±1.9	32±1.5

Membrane surface morphology

SEM analysis was carried out to further examine the cleaning efficiency and evaluate the affinity of solutes towards the membrane surface for artificial water and leachate streams as shown in Fig. 4.9 and

Fig. 4.10, respectively. The SEM images shows a clear and evident foulant depositions for both membranes. The S-PANI revealed less foulant deposits compared to the DuraMem®500 based on a holistic scan of the analysed samples at different magnifications. Cleaning the membrane at high shear velocity was effective for both membranes. The DuraMem®500 exhibited more residual deposits following the flushing cycle compared to the S-PANI membrane which is in line with the fouling indicator investigation in Table. 4.4. Chemical cleaning in place (CIP) (protocol explained in SI, membrane chemical cleaning procedure S4) succeeded to almost fully recover both fouled membranes in artificial waters to its pristine status, SI, Fig. S4.4. Nonetheless, both membranes showed dispersed foulant deposits following the CIP process of the leachate fouled samples. Fouling deposit leftovers were more obvious for the DuraMem®500 sample. This result confirms that the developed S-PANI in NF separation range has promising antifouling properties even under relatively harsh test conditions of heterogeneous NOM solution [DOC] 100 mg C L⁻¹ and stabilized landfill leachate solution [DOC] ≈ 370 mg C L⁻¹.

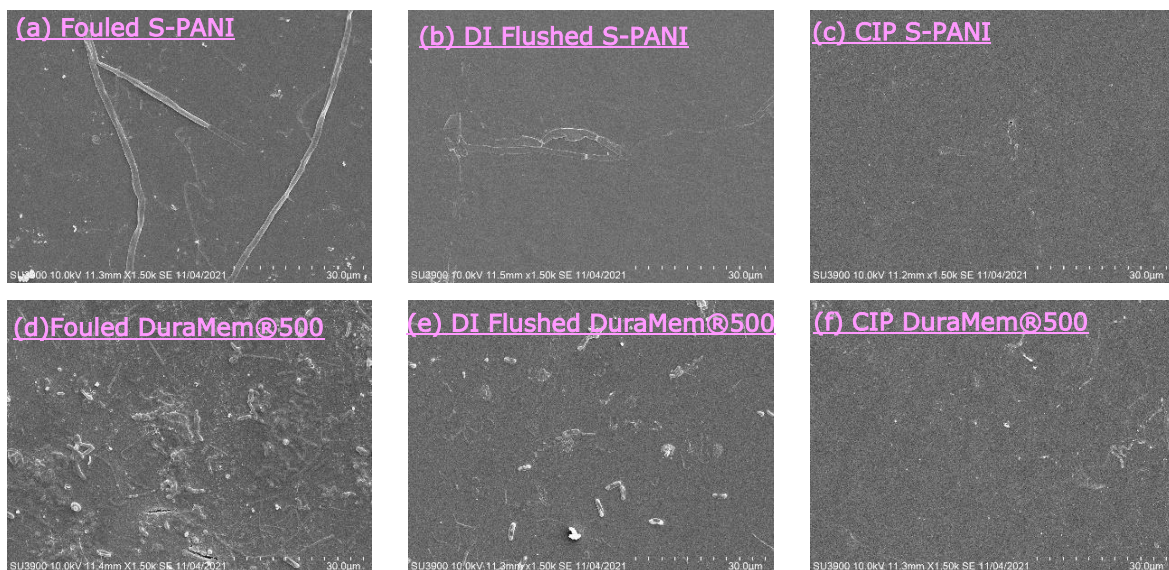


Fig. 4.9 SEM membrane surface images fouled S-PANI and DuraMem®500 in 20 mg L⁻¹ of artificial surface water feedstock (a, d), cleaned S-PANI and DuraMem®500 by dynamic flushing with DI water (b, e) and chemically cleaned in place (CIP) S-PANI and DuraMem®500 of (c, f), respectively.

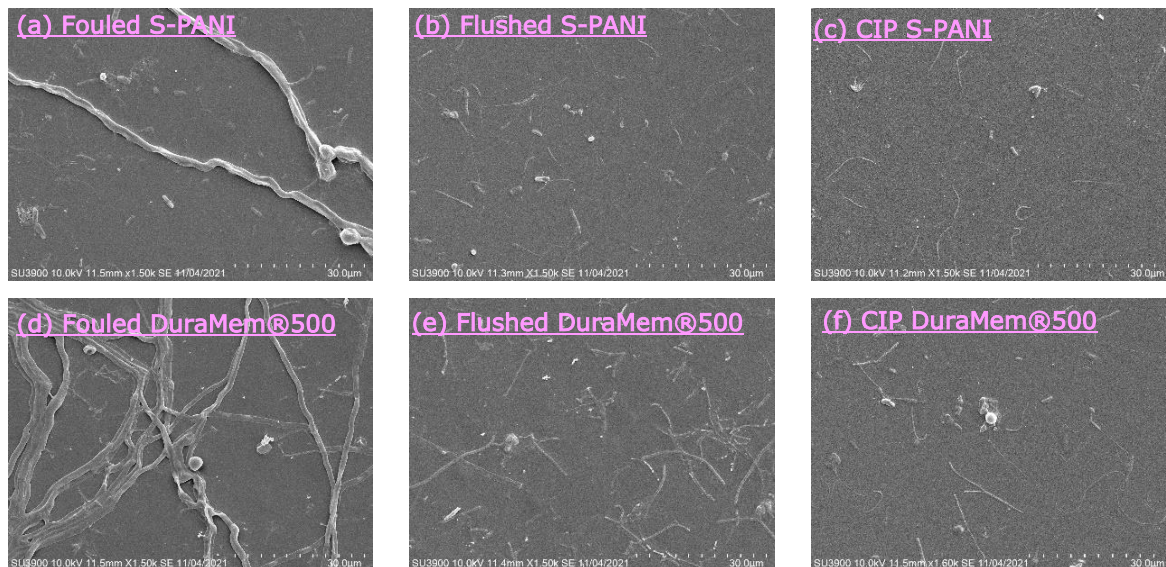


Fig. 4.10 SEM membrane surface images fouled S-PANI and DuraMem®500 in landfill leachate feedstock (a, d), cleaned S-PANI and DuraMem®500 by dynamic flushing with DI water (b, e) and chemically cleaned in place (CIP) S-PANI and DuraMem®500 of (c, f), respectively.

4.4 Conclusions

The performance of newly developed hydrophilic S-PANI membranes in the NF separation range was tested. Performance tests included organic matter removal and observing membrane fouling behaviour for a stabilized landfill leachate, artificially prepared surface water and seawater at different [DOC]. S-PANI performance was compared to a commercial NF membrane (DuraMem®500) and an optimized conventional adsorption/coagulation/flocculation/filtration treatment process. DOC removal for S-PANI membrane was regularly higher than the DuraMem®500 by 8-10% although both membranes experienced organic matter carry over (2-9%) at high salinity conditions. The membrane treatment revealed almost consistent DOC removal efficiencies surpassing the conventional treatment by 23-36% (surface water) and 16-31% (seawater), respectively, despite the variation in the feed [DOC]. In contrast, the conventional treatment DOC removal efficiency for the leachate transcended S-PANI and DuraMem®500 membranes by 7% and 14%, respectively, whereas the COD removal conformed the following order with marginal difference: SPANI > DuraMem®500 ≈ conventional treatment. The fouling study demonstrated how shifts in TMP were not proportional to the step increase in the [DOC]. S-PANI membrane showed limited development in real-time TMP, high flux recovery and less affinity towards organic foulants compared to the DuraMem®500 membrane as confirmed by foulant deposit

measurements over the membrane surface and SEM surface images for the pristine, fouled and chemically cleaned membranes. The results revealed that the developed S-PANI membranes exhibited a high and consistent organic matter removal efficiency at variable organic loads of different feed chemistries with genuine antifouling behaviour surpassing both conventional treatment and the commercial membrane contender. This makes S-PANI membrane an alternative solution to tackle stringent quality requirements for surface water and seawater, (pre)treatment including foulant rich streams in leachate and possibly also in food processing applications.

4.5 Acknowledgements

H.A. was supported by a University of Bath research scholarship. The authors thank the technician's team at the Department of Chemical Engineering and the Bio-imaging lab at the University of Bath for support and advice.

4.6 References

- [1] M. Sillanpää, M.C. Ncibi, A. Matilainen, M. Vepsäläinen, Removal of natural organic matter in drinking water treatment by coagulation: A comprehensive review, *Chemosphere*. 190 (2018) 54–71. <https://doi.org/10.1016/j.chemosphere.2017.09.113>.
- [2] J. Wenk, M. Aeschbacher, E. Salhi, S. Canonica, U. von Gunten, M. Sander, Chemical Oxidation of Dissolved Organic Matter by Chlorine Dioxide, Chlorine, And Ozone: Effects on Its Optical and Antioxidant Properties, *Environ. Sci. Technol.* 47 (2013) 11147–11156. <https://doi.org/10.1021/es402516b>.
- [3] J.M. Barazesh, C. Prasse, J. Wenk, S. Berg, C.K. Remucal, D.L. Sedlak, Trace Element Removal in Distributed Drinking Water Treatment Systems by Cathodic H₂O₂ Production and UV Photolysis, *Environ. Sci. Technol.* 52 (2018) 195–204. <https://doi.org/10.1021/acs.est.7b04396>.
- [4] J.G. Jacangelo, J. DeMarco, D.M. Owen, S.J. Randtke, Selected processes for removing NOM: an overview, *J. Am. Water Works Assoc.* 87 (1995) 64–77. <https://doi.org/10.1002/j.1551-8833.1995.tb06302.x>.

- [5] P.C. Singer, DBPs in drinking water: Additional scientific and policy considerations for public health protection, *J. Am. Water Works Assoc.* 98 (2006) 73–80. <https://doi.org/10.1002/j.1551-8833.2006.tb07779.x>.
- [6] M. Badruzzaman, N. Voutchkov, L. Weinrich, J.G. Jacangelo, Selection of pretreatment technologies for seawater reverse osmosis plants: A review, *Desalination*. 449 (2019) 78–91. <https://doi.org/10.1016/j.desal.2018.10.006>.
- [7] N. Voutchkov, *Desalination Engineering Planning and Design*, 2013. <https://doi.org/10.1017/CBO9781107415324.004>.
- [8] C. Öman, P.-Å. Hynning, Identification of organic compounds in munic*IP*A1 landfill leachates, *Environ. Pollut.* 80 (1993) 265–271. [https://doi.org/10.1016/0269-7491\(93\)90047-R](https://doi.org/10.1016/0269-7491(93)90047-R).
- [9] C.R. Evanko, D.A. Dzombak, Influence of Structural Features on Sorption of NOM-Analogue Organic Acids to Goethite, *Environ. Sci. Technol.* 32 (1998) 2846–2855. <https://doi.org/10.1021/es980256t>.
- [10] B. Bolto, D. Dixon, R. Eldridge, S. King, K. Linge, Removal of natural organic matter by ion exchange, *Water Res.* 36 (2002) 5057–5065. [https://doi.org/10.1016/S0043-1354\(02\)00231-2](https://doi.org/10.1016/S0043-1354(02)00231-2).
- [11] A. Matilainen, M. Sillanpää, Removal of natural organic matter from drinking water by advanced oxidation processes, *Chemosphere.* 80 (2010) 351–365. <https://doi.org/10.1016/j.chemosphere.2010.04.067>.
- [12] S. Mukherjee, S. Mukhopadhyay, M.A. Hashim, B. Sen Gupta, Contemporary Environmental Issues of Landfill Leachate: Assessment and Remedies, *Crit. Rev. Environ. Sci. Technol.* 45 (2015) 472–590. <https://doi.org/10.1080/10643389.2013.876524>.
- [13] C.B. Öman, C. Junestedt, Chemical characterization of landfill leachates – 400 parameters and compounds, *Waste Manag.* 28 (2008) 1876–1891. <https://doi.org/10.1016/j.wasman.2007.06.018>.
- [14] S. Renou, J.G. Givaudan, S. Poulain, F. Dirassouyan, P. Moulin, Landfill leachate treatment: Review and opportunity, *J. Hazard. Mater.* 150 (2008) 468–493. <https://doi.org/10.1016/j.jhazmat.2007.09.077>.

- [15] F. Knops, S. van Hoof, H. Futselaar, L. Broens, Economic evaluation of a new ultrafiltration membrane for pretreatment of seawater reverse osmosis, *Desalination*. (2007). <https://doi.org/10.1016/j.desal.2006.04.013>.
- [16] J.-S. Kang, S.C. Sung, J.J. Lee, H.-S. Kim, Application of ceramic membrane for seawater desalination pretreatment, *Desalin. Water Treat.* 3994 (2016) 1–6. <https://doi.org/10.1080/19443994.2016.1189702>.
- [17] J.Z. Hamad, C. Ha, M.D. Kennedy, G.L. Amy, Application of ceramic membranes for seawater reverse osmosis (SWRO) pre-treatment, *Desalin. Water Treat.* 51 (2013) 4881–4891. <https://doi.org/10.1080/19443994.2013.795211>.
- [18] G. Fernández, F. Plaza, G. Garralón, A. Garralón, J.I. Pérez, M.Á. Gómez, A comparative study of ultrafiltration and physicochemical process as pretreatment of seawater reverse osmosis, *Desalin. Water Treat.* 42 (2012) 73–79. <https://doi.org/10.1080/19443994.2012.683142>.
- [19] D. An, M. Chen, Y. Shen, Analyses of molecular weight distribution of organic matters with pre-oxidation and PAC–UF pretreatment before seawater reverse osmosis, *Desalin. Water Treat.* 51 (2013) 3920–3924. <https://doi.org/10.1080/19443994.2013.795000>.
- [20] C. Sun, L. Xie, X. Li, L. Sun, H. Dai, Study on different ultrafiltration-based hybrid pretreatment systems for reverse osmosis desalination, *Desalination*. 371 (2015) 18–25. <https://doi.org/10.1016/j.desal.2015.05.020>.
- [21] R.K. Henderson, R.M. Stuetz, S.J. Khan, Demonstrating ultra-filtration and reverse osmosis performance using size exclusion chromatography, *Water Sci. Technol.* 62 (2010) 2747–2753. <https://doi.org/10.2166/wst.2010.423>.
- [22] S. Meylan, F. Hammes, J. Traber, E. Salhi, U. von Gunten, W. Pronk, Permeability of low molecular weight organics through nanofiltration membranes, *Water Res.* 41 (2007) 3968–3976. <https://doi.org/10.1016/j.watres.2007.05.031>.
- [23] V. Yangali-Quintanilla, S.K. Maeng, T. Fujioka, M. Kennedy, G. Amy, Proposing nanofiltration as acceptable barrier for organic contaminants in water reuse, *J. Memb. Sci.* 362 (2010) 334–345. <https://doi.org/10.1016/j.memsci.2010.06.058>.

- [24] D. Trebouet, J.P. Schlumpf, P. Jaouen, J.P. Maleriat, F. Quemeneur, Effect of Operating Conditions on the Nanofiltration of Landfill Leachates: Pilot-Scale Studies, *Environ. Technol.* 20 (1999) 587–596. <https://doi.org/10.1080/09593332008616853>.
- [25] S. Jamaly, N.N. Darwish, I. Ahmed, S.W. Hasan, A short review on reverse osmosis pretreatment technologies, *DES.* 354 (2014) 30–38. <https://doi.org/10.1016/j.desal.2014.09.017>.
- [26] J. Suarez, B. Salgado, A. Casanas, J. Carlos Gonzalez, J. Pordomingo, One-year operational experience with ultrafiltration as pretreatment of seawater reverse osmosis desalination system (Maspalomas-I Plant), *Desalin. Water Treat.* 55 (2015) 2813–2821. <https://doi.org/10.1080/19443994.2014.959742>.
- [27] T. Nguyen, F.A. Roddick, L. Fan, Biofouling of Water Treatment Membranes: A Review of the Underlying Causes, Monitoring Techniques and Control Measures, (2012) 804–840. <https://doi.org/10.3390/membranes2040804>.
- [28] V. Kochkodan, N. Hilal, A comprehensive review on surface modified polymer membranes for biofouling mitigation, *Desalination.* 356 (2015) 187–207. <https://doi.org/10.1016/j.desal.2014.09.015>.
- [29] S. Jiang, Y. Li, B.P. Ladewig, A review of reverse osmosis membrane fouling and control strategies, *Sci. Total Environ.* 595 (2017) 567–583. <https://doi.org/10.1016/j.scitotenv.2017.03.235>.
- [30] A. Matin, Z. Khan, S.M.J. Zaidi, M.C. Boyce, Biofouling in reverse osmosis membranes for seawater desalination: Phenomena and prevention, *Desalination.* 281 (2011) 1–16. <https://doi.org/10.1016/j.desal.2011.06.063>.
- [31] S.F. Anis, R. Hashaikh, N. Hilal, Reverse osmosis pretreatment technologies and future trends: A comprehensive review, *Desalination.* 452 (2019) 159–195. <https://doi.org/10.1016/j.desal.2018.11.006>.
- [32] B. Van der Bruggen, Chemical modification of polyethersulfone nanofiltration membranes: A review, *J. Appl. Polym. Sci.* 114 (2009) 630–642. <https://doi.org/10.1002/app.30578>.
- [33] L.-P. Zhu, L. Xu, B.-K. Zhu, Y.-X. Feng, Y.-Y. Xu, Preparation and characterization of improved fouling-resistant PPESK ultrafiltration membranes with amphiphilic PPESK-graft-PEG

- copolymers as additives, *J. Memb. Sci.* 294 (2007) 196–206.
<https://doi.org/10.1016/j.memsci.2007.02.038>.
- [34] D.B. Mosqueda-Jimenez, R.M. Narbaitz, T. Matsuura, Impact of Membrane Surface Modification on the Treatment of Surface Water, *J. Environ. Eng.* 130 (2004) 1450–1459.
[https://doi.org/10.1061/\(ASCE\)0733-9372\(2004\)130:12\(1450\)](https://doi.org/10.1061/(ASCE)0733-9372(2004)130:12(1450)).
- [35] A.H. Nguyen, R.M. Narbaitz, T. Matsuura, Impacts of Hydrophilic Membrane Additives on the Ultrafiltration of River Water, *J. Environ. Eng.* 133 (2007) 515–522.
[https://doi.org/10.1061/\(ASCE\)0733-9372\(2007\)133:5\(515\)](https://doi.org/10.1061/(ASCE)0733-9372(2007)133:5(515)).
- [36] M. Zhou, H. Liu, J.E. Kilduff, R. Langer, D.G. Anderson, G. Belfort, High-Throughput Membrane Surface Modification to Control NOM Fouling, *Environ. Sci. Technol.* 43 (2009) 3865–3871. <https://doi.org/10.1021/es9003697>.
- [37] H. Ruan, B. Li, J. Ji, A. Sotto, B. Van der Bruggen, J. Shen, C. Gao, Preparation and characterization of an amphiphilic polyamide nanofiltration membrane with improved antifouling properties by two-step surface modification method, *RSC Adv.* 8 (2018) 13353–13363.
<https://doi.org/10.1039/C8RA00637G>.
- [38] H. Song, J. Shao, Y. He, J. Hou, W. Chao, Natural organic matter removal and flux decline with charged ultrafiltration and nanofiltration membranes, *J. Memb. Sci.* 376 (2011) 179–187.
<https://doi.org/10.1016/j.memsci.2011.04.022>.
- [39] Y. Zhao, N. Li, S. Xia, Polyamide nanofiltration membranes modified with Zn–Al layered double hydroxides for natural organic matter removal, *Compos. Sci. Technol.* 132 (2016) 84–92.
<https://doi.org/10.1016/j.compscitech.2016.06.016>.
- [40] K. Huang, X. Quan, X. Li, F.H. Tezel, B. Li, Improved surface hydrophilicity and antifouling property of nanofiltration membrane by grafting NH₂-functionalized silica nanoparticles, *Polym. Adv. Technol.* 29 (2018) 3159–3170. <https://doi.org/10.1002/pat.4438>.
- [41] A. Sotto, A. Boromand, S. Balta, J. Kim, B. Van der Bruggen, Doping of polyethersulfone nanofiltration membranes: antifouling effect observed at ultralow concentrations of TiO₂ nanoparticles, *J. Mater. Chem.* 21 (2011) 10311. <https://doi.org/10.1039/c1jm11040c>.

- [42] J. Wang, X. Gao, J. Wang, Y. Wei, Z. Li, C. Gao, O -(Carboxymethyl)-chitosan Nanofiltration Membrane Surface Functionalized with Graphene Oxide Nanosheets for Enhanced Desalting Properties, *ACS Appl. Mater. Interfaces*. 7 (2015) 4381–4389. <https://doi.org/10.1021/am508903g>.
- [43] L.Y. Ng, A.W. Mohammad, C.P. Leo, N. Hilal, Polymeric membranes incorporated with metal/metal oxide nanoparticles: A comprehensive review, *Desalination*. 308 (2013) 15–33. <https://doi.org/10.1016/j.desal.2010.11.033>.
- [44] Y.P. Tang, J.X. Chan, T.S. Chung, M. Weber, C. Staudt, C. Maletzko, Simultaneously covalent and ionic bridging towards antifouling of GO-imbedded nanocomposite hollow fiber membranes, *J. Mater. Chem. A*. 3 (2015) 10573–10584. <https://doi.org/10.1039/C5TA01715G>.
- [45] L. Upadhyaya, X. Qian, S. Ranil Wickramasinghe, Chemical modification of membrane surface — overview, *Curr. Opin. Chem. Eng.* 20 (2018) 13–18. <https://doi.org/10.1016/j.coche.2018.01.002>.
- [46] S. Zhao, Z. Wang, J. Wang, S. Yang, S. Wang, PSf/PANI nanocomposite membrane prepared by in situ blending of PSf and PANI/NMP, *J. Memb. Sci.* 376 (2011) 83–95. <https://doi.org/10.1016/j.memsci.2011.04.008>.
- [47] S. Zhao, Z. Wang, X. Wei, X. Tian, J. Wang, S. Yang, S. Wang, Comparison study of the effect of PVP and PANI nanofibers additives on membrane formation mechanism, structure and performance, *J. Memb. Sci.* 385–386 (2011) 110–122. <https://doi.org/10.1016/j.memsci.2011.09.029>.
- [48] B. Hudaib, V. Gomes, J. Shi, C. Zhou, Z. Liu, Poly (vinylidene fluoride)/polyaniline/MWCNT nanocomposite ultrafiltration membrane for natural organic matter removal, *Sep. Purif. Technol.* 190 (2018) 143–155. <https://doi.org/10.1016/j.seppur.2017.08.026>.
- [49] J. Alam, L.A. Dass, M.S. Alhoshan, M. Ghasemi, A.W. Mohammad, Development of polyaniline-modified polysulfone nanocomposite membrane, *Appl. Water Sci.* 2 (2012) 37–46. <https://doi.org/10.1007/s13201-011-0021-2>.
- [50] L. Xu, S. Shahid, A.K. Holda, E.A.C. Emanuelsson, D.A. Patterson, Stimuli responsive conductive polyaniline membrane: In-filtration electrical tuneability of flux and MWCO, *J. Memb. Sci.* 552 (2018) 153–166. <https://doi.org/10.1016/j.memsci.2018.01.070>.

- [51] S. Bhadra, D. Khastgir, N.K. Singha, J. Hee, Progress in Polymer Science Progress in preparation , processing and applications of polyaniline, 34 (2009) 783–810. <https://doi.org/10.1016/j.progpolymsci.2009.04.003>.
- [52] X. Zhang, J. Zhu, N. Haldolaarachchige, J. Ryu, D.P. Young, S. Wei, Z. Guo, Synthetic process engineered polyaniline nanostructures with tunable morphology and physical properties, Polymer (Guildf). 53 (2012) 2109–2120. <https://doi.org/10.1016/j.polymer.2012.02.042>.
- [53] H. Alhweij, I. Amura, J. Wenk, E.A.C. Emanuelsson, S. Shahid, Self-doped sulfonated polyaniline ultrafiltration membranes with enhanced chlorine resistance and antifouling properties, J. Appl. Polym. Sci. (2021) 50756. <https://doi.org/10.1002/app.50756>.
- [54] H. Alhweij, E.A. Carolina Emanuelsson, S. Shahid, J. Wenk, Simplified in-situ tailoring of cross-linked self-doped sulfonated polyaniline (S-PANI) membranes for nanofiltration applications, J. Memb. Sci. (2021) 119654. <https://doi.org/10.1016/j.memsci.2021.119654>.
- [55] H. Alhweij, E.A. Carolina Emanuelsson, S. Shahid, J. Wenk, High performance in-situ tuned self-doped polyaniline (PANI) membranes for organic solvent (nano)filtration, Polymer (Guildf). 245 (2022) 124682. <https://doi.org/10.1016/j.polymer.2022.124682>.
- [56] A. Matilainen, M. Vepsäläinen, M. Sillanpää, Natural organic matter removal by coagulation during drinking water treatment: A review, Adv. Colloid Interface Sci. 159 (2010) 189–197. <https://doi.org/10.1016/j.cis.2010.06.007>.
- [57] S. Al Aani, C.J. Wright, N. Hilal, Investigation of UF membranes fouling and potentials as pre-treatment step in desalination and surface water applications, Desalination. 432 (2018) 115–127. <https://doi.org/10.1016/j.desal.2018.01.017>.
- [58] T. Priya, B.K. Mishra, M.N.V. Prasad, Physico-chemical techniques for the removal of disinfection by-products precursors from water, in: Disinfect. By-Products Drink. Water, Elsevier, 2020: pp. 23–58. <https://doi.org/10.1016/B978-0-08-102977-0.00002-0>.
- [59] L. Llenas, G. Ribera, X. Martínez-Lladó, M. Rovira, J. de Pablo, Selection of nanofiltration membranes as pretreatment for scaling prevention in SWRO using real seawater, Desalin. Water Treat. 51 (2013) 930–935. <https://doi.org/10.1080/19443994.2012.714578>.

- [60] I. Monje-Ramirez, M.T.O. de Velásquez, Removal and transformation of recalcitrant organic matter from stabilized saline landfill leachates by coagulation–ozonation coupling processes, *Water Res.* 38 (2004) 2359–2367. <https://doi.org/10.1016/j.watres.2004.02.011>.
- [61] H. Alvarez-Vazquez, B. Jefferson, S.J. Judd, Membrane bioreactors vs conventional biological treatment of landfill leachate: a brief review, *J. Chem. Technol. Biotechnol.* 79 (2004) 1043–1049. <https://doi.org/10.1002/jctb.1072>.
- [62] L.K. Wang, V. Ivanov, J.-H. Tay, eds., *Environmental Biotechnology*, Humana Press, Totowa, NJ, 2010. <https://doi.org/10.1007/978-1-60327-140-0>.
- [63] A. Kudasheva, S. Sorribas, B. Zornoza, C. Téllez, J. Coronas, Pervaporation of water/ethanol mixtures through polyimide based mixed matrix membranes containing ZIF-8, ordered mesoporous silica and ZIF-8-silica core-shell spheres, *J. Chem. Technol. Biotechnol.* 90 (2015) 669–677. <https://doi.org/10.1002/jctb.4352>.
- [64] P. Marchetti, A.G. Livingston, Predictive membrane transport models for Organic Solvent Nanofiltration: How complex do we need to be?, *J. Memb. Sci.* 476 (2015) 530–553. <https://doi.org/10.1016/j.memsci.2014.10.030>.
- [65] M. Baalousha, M. Motelica-Heino, P. Le Coustumer, Conformation and size of humic substances: Effects of major cation concentration and type, pH, salinity, and residence time, *Colloids Surfaces A Physicochem. Eng. Asp.* 272 (2006) 48–55. <https://doi.org/10.1016/j.colsurfa.2005.07.010>.
- [66] J. Labanowski, V. Pallier, G. Feuillade-Cathalifaud, Study of organic matter during coagulation and electrocoagulation processes: Application to a stabilized landfill leachate, *J. Hazard. Mater.* 179 (2010) 166–172. <https://doi.org/10.1016/j.jhazmat.2010.02.074>.
- [67] C.C. Cleveland, J.C. Neff, A.R. Townsend, E. Hood, Composition, Dynamics, and Fate of Leached Dissolved Organic Matter in Terrestrial Ecosystems: Results from a Decomposition Experiment, *Ecosystems.* 7 (2004). <https://doi.org/10.1007/s10021-003-0236-7>.
- [68] S. Chen, J. Liu, Landfill leachate treatment by MBR: Performance and molecular weight distribution of organic contaminant, *Chinese Sci. Bull.* 51 (2006) 2831–2838. <https://doi.org/10.1007/s11434-006-2177-y>.

- [69] P. Jarvis, B. Jefferson, S.A. Parsons, Characterising natural organic matter flocs, *Water Supply*. 4 (2004) 79–87. <https://doi.org/10.2166/ws.2004.0064>.
- [70] M. Bogunović, T. Marjanović, I. Ivančev-Tumbas, Fate of Benzophenone, Benzophenone-3 and Caffeine in Lab-Scale Direct River Water Treatment by Hybrid Processes, *Int. J. Environ. Res. Public Health*. 18 (2021) 8691. <https://doi.org/10.3390/ijerph18168691>.
- [71] J. Sieliechi, B. Lartiges, S. Skali-Lami, J. Kayem, R. Kamga, Flocculation compaction during ballasted aggregation, *Water Res.* 105 (2016) 361–369. <https://doi.org/10.1016/j.watres.2016.09.015>.
- [72] A.N. Jones, J. Bridgeman, Investigating the characteristic strength of flocs formed from crude and purified Hibiscus extracts in water treatment, *Water Res.* 103 (2016) 21–29. <https://doi.org/10.1016/j.watres.2016.07.019>.
- [73] E.L. Sharp, P. Jarvis, S.A. Parsons, B. Jefferson, Impact of fractional character on the coagulation of NOM, *Colloids Surfaces A Physicochem. Eng. Asp.* 286 (2006) 104–111. <https://doi.org/10.1016/j.colsurfa.2006.03.009>.
- [74] M. Yan, D. Wang, J. Qu, J. Ni, C.W.K. Chow, Enhanced coagulation for high alkalinity and micro-polluted water: The third way through coagulant optimization, *Water Res.* 42 (2008) 2278–2286. <https://doi.org/10.1016/j.watres.2007.12.006>.
- [75] J. Świątlik, A. Dąbrowska, U. Raczyk-Stanisławiak, J. Nawrocki, Reactivity of natural organic matter fractions with chlorine dioxide and ozone, *Water Res.* 38 (2004) 547–558. <https://doi.org/10.1016/j.watres.2003.10.034>.
- [76] S.A. Parsons, B. Jefferson, E.H. Goslan, P.R. Jarvis, D.A. Fearing, Natural organic matter – the relationship between character and treatability, *Water Supply*. 4 (2004) 43–48. <https://doi.org/10.2166/ws.2004.0091>.
- [77] J.K. Edzwald, J. Haarhoff, Seawater pretreatment for reverse osmosis: Chemistry, contaminants, and coagulation, *Water Res.* (2011). <https://doi.org/10.1016/j.watres.2011.08.014>.
- [78] O.D. Schneider, L.A. Weinrich, E. Giraldo, M.W. LeChevallier, Impacts of salt type and concentration on coagulation of *humic acid* and silica, *J. Water Supply Res. Technol.* 62 (2013) 339–349. <https://doi.org/10.2166/aqua.2013.141>.

- [79] F. Duan, Jinming ; Wang, Jianhui ; Graham, Nigel ; Wilson, Coagulation of *humic acid* by aluminium sulphate in saline water conditions, 150 (2002) 1–14. [https://doi-org.ezproxy1.bath.ac.uk/10.1016/S0011-9164\(02\)00925-6%0A](https://doi.org.ezproxy1.bath.ac.uk/10.1016/S0011-9164(02)00925-6%0A).
- [80] J. Duan, N.J.D. Graham, F. Wilson, Coagulation of *humic acid* by ferric chloride in saline (marine) water conditions, *Water Sci. Technol.* 47 (2003) 41–48. <https://doi.org/10.2166/wst.2003.0012>.
- [81] Y. Wang, B. Gao, X. Xu, W. Xu, The effect of total hardness and ionic strength on the coagulation performance and kinetics of aluminum salts to remove *humic acid*, *Chem. Eng. J.* 160 (2010) 150–156. <https://doi.org/10.1016/j.cej.2010.03.028>.
- [82] H.N.. Dayarathne, M.J. Angove, R. Aryal, H. Abuel-Naga, B. Mainali, Removal of natural organic matter from source water: Review on coagulants, dual coagulation, alternative coagulants, and mechanisms, *J. Water Process Eng.* 40 (2021) 101820. <https://doi.org/10.1016/j.jwpe.2020.101820>.
- [83] R. Amal, J.. Raper, T.. Waite, Effect of fulvic acid adsorption on the aggregation kinetics and structure of hematite particles, *J. Colloid Interface Sci.* 151 (1992) 244–257. [https://doi.org/10.1016/0021-9797\(92\)90255-K](https://doi.org/10.1016/0021-9797(92)90255-K).
- [84] D. Mara, N. Horan, *Handbook of Water and Wastewater Microbiology*, Elsevier, 2003. <https://doi.org/10.1016/B978-0-12-470100-7.X5000-6>.
- [85] Aquatic chemistry: chemical equilibria and rates in natural waters, *Choice Rev. Online.* 33 (1996) 33-6312-33–6312. <https://doi.org/10.5860/CHOICE.33-6312>.
- [86] J. Duan, F. Wilson, N. Graham, J.H. Tay, Adsorption of *humic acid* by powdered activated carbon in saline water conditions, *Desalination.* 151 (2003) 53–66. [https://doi.org/10.1016/S0011-9164\(02\)00972-4](https://doi.org/10.1016/S0011-9164(02)00972-4).
- [87] G. Newcombe; Charge vs. Porosity, Some Influences on the Adsorption of Natural Organic Matter (NOM) by Activated Carbon, *Water Sci Techno.* 40 (1999) 191–198. <https://doi.org/https://doi.org/10.2166/wst.1999.0474>.

- [88] A. Matilainen, N. Vieno, T. Tuhkanen, Efficiency of the activated carbon filtration in the natural organic matter removal, *Environ. Int.* 32 (2006) 324–331. <https://doi.org/10.1016/j.envint.2005.06.003>.
- [89] E. Vuorio, R. Vahala, J. Rintala, R. Laukkanen, The evaluation of drinking water treatment performed with HPSEC, *Environ. Int.* 24 (1998) 617–623. [https://doi.org/10.1016/S0160-4120\(98\)00040-3](https://doi.org/10.1016/S0160-4120(98)00040-3).
- [90] S. Velten, D.R.U. Knappe, J. Traber, H.-P. Kaiser, U. von Gunten, M. Boller, S. Meylan, Characterization of natural organic matter adsorption in granular activated carbon adsorbers, *Water Res.* 45 (2011) 3951–3959. <https://doi.org/10.1016/j.watres.2011.04.047>.
- [91] P. Krzeminski, C. Vogelsang, T. Meyn, S.J. Köhler, H. Poutanen, H.A. de Wit, W. Uhl, Natural organic matter fractions and their removal in full-scale drinking water treatment under cold climate conditions in Nordic capitals, *J. Environ. Manage.* 241 (2019) 427–438. <https://doi.org/10.1016/j.jenvman.2019.02.024>.
- [92] E.L. Sharp, S.A. Parsons, B. Jefferson, Seasonal variations in natural organic matter and its impact on coagulation in water treatment, 363 (2006) 183–194. <https://doi.org/10.1016/j.scitotenv.2005.05.032>.
- [93] M.K. Ramseier, A. Peter, J. Traber, U. Von Gunten, Formation of assimilable organic carbon during oxidation of natural waters with ozone, chlorine dioxide, chlorine, permanganate, and ferrate, *Water Res.* 45 (2010) 2002–2010. <https://doi.org/10.1016/j.watres.2010.12.002>.
- [94] A. Sweity, Y. Oren, Z. Ronen, M. Herzberg, The influence of antiscalants on biofouling of RO membranes in seawater desalination, *Water Res.* 47 (2013) 3389–3398. <https://doi.org/10.1016/j.watres.2013.03.042>.
- [95] J.E. Kilduff, S. Mattaraj, G. Belfort, Flux decline during nanofiltration of naturally-occurring dissolved organic matter: effects of osmotic pressure, membrane permeability, and cake formation, *J. Memb. Sci.* 239 (2004) 39–53. <https://doi.org/10.1016/j.memsci.2003.12.030>.
- [96] C. Jarusutthirak, S. Mattaraj, R. Jiraratananon, Factors affecting nanofiltration performances in natural organic matter rejection and flux decline, *Sep. Purif. Technol.* 58 (2007) 68–75. <https://doi.org/10.1016/j.seppur.2007.07.010>.

- [97] A.W. Zularisam, A.F. Ismail, R. Salim, Behaviours of natural organic matter in membrane filtration for surface water treatment — a review, *Desalination*. 194 (2006) 211–231. <https://doi.org/10.1016/j.desal.2005.10.030>.
- [98] A. Braghetta, F.A. DiGiano, W.P. Ball, Nanofiltration of Natural Organic Matter: pH and Ionic Strength Effects, *J. Environ. Eng.* 123 (1997) 628–641. [https://doi.org/10.1061/\(ASCE\)0733-9372\(1997\)123:7\(628\)](https://doi.org/10.1061/(ASCE)0733-9372(1997)123:7(628)).
- [99] N. AlSawaftah, W. Abuwatfa, N. Darwish, G. Husseini, A Comprehensive Review on Membrane Fouling: Mathematical Modelling, Prediction, Diagnosis, and Mitigation, *Water*. 13 (2021) 1327. <https://doi.org/10.3390/w13091327>.
- [100] J. Cho, G. Amy, J. Pellegrino, Membrane filtration of natural organic matter: factors and mechanisms affecting rejection and flux decline with charged ultrafiltration (UF) membrane, *J. Memb. Sci.* 164 (2000) 89–110. [https://doi.org/10.1016/S0376-7388\(99\)00176-3](https://doi.org/10.1016/S0376-7388(99)00176-3).
- [101] S. Lee, J. Moon, S.-K. Yim, S.-H. Moon, J. Cho, The relationship between flux decline of NF membranes with NOM transport characteristics: convection vs. diffusion, *Desalination*. 147 (2002) 237–241. [https://doi.org/10.1016/S0011-9164\(02\)00542-8](https://doi.org/10.1016/S0011-9164(02)00542-8).
- [102] J. Kilduff, W.J. Weber, Transport and separation of organic macromolecules in ultrafiltration processes, *Environ. Sci. Technol.* 26 (1992) 569–577. <https://doi.org/10.1021/es00027a021>.
- [103] A. Braghetta, F.A. DiGiano, W.P. Ball, NOM Accumulation at NF Membrane Surface: Impact of Chemistry and Shear, *J. Environ. Eng.* 124 (1998) 1087–1098. [https://doi.org/10.1061/\(ASCE\)0733-9372\(1998\)124:11\(1087\)](https://doi.org/10.1061/(ASCE)0733-9372(1998)124:11(1087)).
- [104] S. Lee, J. Cho, M. Elimelech, Combined influence of natural organic matter (NOM) and colloidal particles on nanofiltration membrane fouling, *J. Memb. Sci.* 262 (2005) 27–41. <https://doi.org/10.1016/j.memsci.2005.03.043>.
- [105] A.G.F. and C.J.D. FELL, A Review of Fouling and Fouling Control in Ultrafiltration, 62 (1987) 117–136.
- [106] F. Liu, Hydrophilicity, in: *Enycl. Membr.*, Springer Berlin Heidelberg, Berlin, Heidelberg, 2015: pp. 1–1. https://doi.org/10.1007/978-3-642-40872-4_1677-1.

- [107] Y. Wu, S. Zhou, F. Qin, H. Peng, Y. Lai, Y. Lin, Removal of humic substances from landfill leachate by Fenton oxidation and coagulation, *Process Saf. Environ. Prot.* 88 (2010) 276–284. <https://doi.org/10.1016/j.psep.2010.03.002>.
- [108] J. Wiszniowski, D. Robert, J. Surmacz-Gorska, K. Miksch, S. Malato, J.-V. Weber, Solar photocatalytic degradation of *humic acids* as a model of organic compounds of landfill leachate in pilot-plant experiments: influence of inorganic salts, *Appl. Catal. B Environ.* 53 (2004) 127–137. <https://doi.org/10.1016/j.apcatb.2004.04.017>.
- [109] S. Hong, M. Elimelech, Chemical and physical aspects of natural organic matter (NOM) fouling of nanofiltration membranes, *J. Memb. Sci.* 132 (1997) 159–181. [https://doi.org/10.1016/S0376-7388\(97\)00060-4](https://doi.org/10.1016/S0376-7388(97)00060-4).
- [110] J. Duan, J. Gregory, Coagulation by hydrolysing metal salts, *Adv. Colloid Interface Sci.* 100–102 (2003) 475–502. [https://doi.org/10.1016/S0001-8686\(02\)00067-2](https://doi.org/10.1016/S0001-8686(02)00067-2).
- [111] Y. Smaoui, M. Chaabouni, S. Sayadi, J. Bouzid, Coagulation–flocculation process for landfill leachate pretreatment and optimization with response surface methodology, *Desalin. Water Treat.* 57 (2016) 14488–14495. <https://doi.org/10.1080/19443994.2015.1067837>.
- [112] V. Oloibiri, I. Ufomba, M. Chys, W.T.M. Audenaert, K. Demeestere, S.W.H. Van Hulle, A comparative study on the efficiency of ozonation and coagulation–flocculation as pretreatment to activated carbon adsorption of biologically stabilized landfill leachate, *Waste Manag.* 43 (2015) 335–342. <https://doi.org/10.1016/j.wasman.2015.06.014>.
- [113] W. Li, T. Hua, Q. Zhou, S. Zhang, F. Li, Treatment of stabilized landfill leachate by the combined process of coagulation/flocculation and powder activated carbon adsorption, *Desalination.* 264 (2010) 56–62. <https://doi.org/10.1016/j.desal.2010.07.004>.
- [114] A.R. Ishak, F.S. Hamid, S. Mohamad, K.S. Tay, Stabilized landfill leachate treatment by coagulation-flocculation coupled with UV-based sulfate radical oxidation process, *Waste Manag.* 76 (2018) 575–581. <https://doi.org/10.1016/j.wasman.2018.02.047>.
- [115] Y. Long, J. Xu, D. Shen, Y. Du, H. Feng, Effective removal of contaminants in landfill leachate membrane concentrates by coagulation, *Chemosphere.* 167 (2017) 512–519. <https://doi.org/10.1016/j.chemosphere.2016.10.016>.

- [116] D. Trebouet, J. Schlumpf, P. Jaouen, F. Quemeneur, Stabilized landfill leachate treatment by combined physicochemical–nanofiltration processes, *Water Res.* 35 (2001) 2935–2942. [https://doi.org/10.1016/S0043-1354\(01\)00005-7](https://doi.org/10.1016/S0043-1354(01)00005-7).
- [117] F. Kargi, M.Y. Pamukoglu, Repeated fed-batch biological treatment of pre-treated landfill leachate by powdered activated carbon addition, *Enzyme Microb. Technol.* 34 (2004) 422–428. <https://doi.org/10.1016/j.enzmictec.2003.11.016>.
- [118] F. Karginodot, Adsorbent supplemented biological treatment of pre-treated landfill leachate by fed-batch operation, *Bioresour. Technol.* 94 (2004) 285–291. <https://doi.org/10.1016/j.biortech.2004.01.003>.
- [119] Z. Liu, W. Wu, P. Shi, J. Guo, J. Cheng, Characterization of dissolved organic matter in landfill leachate during the combined treatment process of air stripping, Fenton, SBR and coagulation, *Waste Manag.* 41 (2015) 111–118. <https://doi.org/10.1016/j.wasman.2015.03.044>.
- [120] S.F.F.S. Zainal, H.A. Aziz, Potential of tin (IV) chloride for treatment in Alor Pongsu as stabilized landfill leachate, in: 2017: p. 040003. <https://doi.org/10.1063/1.5005683>.
- [121] Y. Wei, X. Dong, A. Ding, D. Xie, Characterization and coagulation–flocculation behavior of an inorganic polymer coagulant – poly-ferric-zinc-sulfate, *J. Taiwan Inst. Chem. Eng.* 58 (2016) 351–356. <https://doi.org/10.1016/j.jtice.2015.06.004>.
- [122] A.R. Mahdavi, A.A. Ghoresyhi, A. Rahimpour, H. Younesi, K. Pirzadeh, COD removal from landfill leachate using a high-performance and low-cost activated carbon synthesized from walnut shell, *Chem. Eng. Commun.* 205 (2018) 1193–1206. <https://doi.org/10.1080/00986445.2018.1441831>.
- [123] A.M. Hansen, T.E.C. Kraus, B.A. Pellerin, J.A. Fleck, B.D. Downing, B.A. Bergamaschi, Optical properties of dissolved organic matter (DOM): Effects of biological and photolytic degradation, *Limnol. Oceanogr.* 61 (2016) 1015–1032. <https://doi.org/10.1002/lno.10270>.
- [124] E. Gasia-Bruch, P. Sehn, V. García-Molina, M. Busch, O. Raize, M. Negrin, Field experience with a 20,000 m³/d integrated membrane seawater desalination plant in Cyprus, *Desalin. Water Treat.* 31 (2011) 178–189. <https://doi.org/10.5004/dwt.2011.2381>.

- [125] A. Seidel, Coupling between chemical and physical interactions in natural organic matter (NOM) fouling of nanofiltration membranes: implications for fouling control, *J. Memb. Sci.* 203 (2002) 245–255. [https://doi.org/10.1016/S0376-7388\(02\)00013-3](https://doi.org/10.1016/S0376-7388(02)00013-3).
- [126] A.R. Roudman, F.A. DiGiano, Surface energy of experimental and commercial nanofiltration membranes: effects of wetting and natural organic matter fouling, *J. Memb. Sci.* 175 (2000) 61–73. [https://doi.org/10.1016/S0376-7388\(00\)00409-9](https://doi.org/10.1016/S0376-7388(00)00409-9).
- [127] L.D. Nghiem, P.J. Coleman, C. Espendiller, Mechanisms underlying the effects of membrane fouling on the nanofiltration of trace organic contaminants, *Desalination*. 250 (2010) 682–687. <https://doi.org/10.1016/j.desal.2009.03.025>.
- [128] I.F. Amura, S. Shahid, A. Sarihan, J. Shen, D.A. Patterson, E.A.C. Emanuelsson, Fabrication of self-doped sulfonated polyaniline membranes with enhanced antifouling ability and improved solvent resistance, *J. Memb. Sci.* (2019) 117712. <https://doi.org/10.1016/j.memsci.2019.117712>.
- [129] L. Fan, J.L. Harris, F.A. Roddick, N.A. Booker, Influence of the characteristics of natural organic matter on the fouling of microfiltration membranes, *Water Res.* 35 (2001) 4455–4463. [https://doi.org/10.1016/S0043-1354\(01\)00183-X](https://doi.org/10.1016/S0043-1354(01)00183-X).
- [130] H. Yamamura, K. Kimura, Y. Watanabe, Mechanism Involved in the Evolution of Physically Irreversible Fouling in Microfiltration and Ultrafiltration Membranes Used for Drinking Water Treatment, *Environ. Sci. Technol.* 41 (2007) 6789–6794. <https://doi.org/10.1021/es0629054>.
- [131] H. Yamamura, K. Kimura, T. Okajima, H. Tokumoto, Y. Watanabe, Affinity of Functional Groups for Membrane Surfaces: Implications for Physically Irreversible Fouling, *Environ. Sci. Technol.* 42 (2008) 5310–5315. <https://doi.org/10.1021/es800406j>.
- [132] K.K. Kopeć, S.M. Dutczak, M. Wessling, D.F. Stamatialis, Tailoring the surface charge of an ultrafiltration hollow fiber by addition of a polyanion to the coagulation bore liquid, *J. Memb. Sci.* 369 (2011) 59–67. <https://doi.org/10.1016/j.memsci.2010.11.060>.
- [133] X. Jin, X. Huang, E.M.V. Hoek, Role of Specific Ion Interactions in Seawater RO Membrane Fouling by *Alginate acid*, *Environ. Sci. Technol.* 43 (2009) 3580–3587. <https://doi.org/10.1021/es8036498>.

- [134] J. Yang, S. Lee, E. Lee, J. Lee, S. Hong, Effect of solution chemistry on the surface property of reverse osmosis membranes under seawater conditions, *Desalination*. 247 (2009) 148–161. <https://doi.org/10.1016/j.desal.2008.12.020>.
- [135] D. Wu, Mi.R. Bird, The fouling and cleaning of ultrafiltration membranes during the filtration of model tea component solutions, *J. Food Process Eng.* 30 (2007) 293–323. <https://doi.org/10.1111/j.1745-4530.2007.00115.x>.

Supporting Information

Organic matter removal and antifouling performance of sulfonated polyaniline nanofiltration (S-PANI NF) membranes

Hassan Alhweij^{a,c,d}, Emma Anna Carolina Emanuelsson^{a,b}, Salman Shahid^{a,b,c}, Jannis Wenk^{a,c*}

^a Department of Chemical Engineering, University of Bath, Bath BA2 7AY, United Kingdom

^b Centre for Advanced Separations Engineering, University of Bath, Bath BA2 7AY, United Kingdom

^c Water Innovation and Research Centre (WIRC@Bath), University of Bath, Bath, BA2 7AY, United Kingdom

^d Stantec UK Limited, Dominion House, Warrington, WA3 6GD, United Kingdom

* Corresponding author

Jannis Wenk: j.h.wenk@bath.ac.uk

Materials S1

Aniline, ammonium persulfate (APS), 4-methylpyridine (4MP), *N*-methyl-2-pyrrolidone (NMP) and ammonium hydroxide solution were obtained from Sigma-Aldrich, UK. 3-aminobenzene sulfonic acid (metanilic acid), sodium hypochlorite, sodium hydroxide and hydrochloric acid (HCl) aqueous solution were obtained from VWR, UK. NOM extracted from natural source (Fulvic 25) was obtained from, Solufeed, UK. Sea-Salt ASTM D1141-98 was obtained from Lake products, USA. Hydrated ferric chloride and powder activated carbon (PAC, 95% pure, $\leq 40 \mu\text{m}$) were obtained from scientific laboratory suppliers, UK. Magnafloc[®]LT22S was provided by BASF, UK. Sand containing mainly SiO₂ was obtained from a drinking water treatment plant. All materials were used as received.

Solute fractionation S2

Five different commercially available membranes in the ultrafiltration (UF) and nanofiltration (NF) range were tested for 4 h for each test cycle. Flat sheet membrane coupons of different commercially available membranes were cut off for the testing in a filtration test cell with standard active membrane area of 14.6 cm². Table. S1 lists the specifications of the individual membranes.

Table. S 4.1 Details of utilised membranes for solute fractionation.

Membrane	Filtration spectrum	MWCO*, kg mol ⁻¹	Producer and brand name	Material
A	UF	30.0	Synder Filtration [™] , MK	Polyethersulfone
B	UF	10.0	Alfa Laval, RC70PP	Regenerated cellulose acetate
C	UF	3.0	Suez [™] , GK	Composite polyamide
D	UF	1.0	Alfa Laval, ETNA01PP	Composite fluoro polymer
E	NF	0.5	Evonik, DuraMem [®] 500	Modified Polyimide

*Molecular weight cut off (MWCO)

Conventional treatment S3

Adsorption by powder activated carbon (PAC), coagulation, flocculation, clarification by sedimentation and sand filtration tests were carried out using a jar test setup. Ferric chloride coagulant was chosen over ferric sulphate and aluminium based coagulants, due to its prevalent usage in seawater pre-treatment and better performance for NOM removal, respectively [1]. Phipps & Bird 900 model jar tester with 6.0 paddles and 1 L beakers was used to (a) mimic the operating conditions of conventional treatment plant, (b) determine the optimal PAC and ferric chloride dose rate and sequence c) identify the optimal dosed solution pH and (d) determine the maximum NOM removal through a series of conventional treatment processes.

Jar testing entails adjusting the amount of treatment chemicals and the sequence in which they are added to samples of aqueous solutions held in jars or beakers. The sample is then stirred so that the formation, development, and settlement of floc can be watched just as it would be in the full-scale treatment plant. The coagulation process takes place within few seconds and demands high mixing energy. Flocculation is the subsequent process which requires longer retention time (20 min) and low energy to overcome the repulsion forces leading to agglomeration of micro flocs. Higher energy (velocity gradient) or longer retention time than required were prevented to avoid floc shearing and subsequent performance deterioration of the clarification process. pH correction during the jar test experiments was carried out via the addition of hydrochloric acid aqueous solution and sodium hydroxide aqueous solution, as appropriate. The jar testing protocol can be summarized as follows:

- For each sample, several beakers (jars) were filled with equal amounts of DI water.
- A defined volume of NOM concentrate was added to each jar to form 10 mg C L⁻¹ DOC enriched aqueous solution. The process was repeated at higher concentrations of 20 and 100 mg C L⁻¹. For leachate, the solution was filtered through 0.45 µm Whatman™ filter paper and poured in the 1 L jars.
- The solution was mixed vigorously via the jar tester paddles at speed 200 rpm.

- Ferric chloride solution was prepared and dosed with step increase of 5 mg L^{-1} as Fe^{+3} to each jar without pH correction.
- The dosed sample was mixed at 200 rpm for 1 min and then the paddles speed was turned down to 30 rpm to initiate the micro-floc agglomeration. During the mixing stage, the dosed water pH was measured and recorded.
- After elapsed time of 20 min, the flocculators (paddles) were stopped and the jars were left stagnant for 30 min to allow for floc settlement.
- The supernatant was sampled via micro-syringe and the dissolved organic carbon concentration [DOC] was measured after sample filtration through $0.45 \mu\text{m}$ Whatman™ filter paper.
- To define the optimal pH operating range, the jar test experiment was repeated using a constant chemical dose (the chosen chemical dose at the highest DOC removal in previous steps). The dosed water pH was corrected in each jar using hydrochloric acid or sodium hydroxide aqueous solution, as appropriate.
- The optimal pH value was identified based on the highest DOC removal.
- The jar test was repeated, and both the chemical dose and the pH were tuned to explore the maximum DOC removal efficiency.

The experimental work was carried out to treat three distinctive streams a) artificial surface water, b) artificial seawater and c) landfill leachate from an existing site in Southwest England, Wiltshire, UK. The organic concentration in the artificial water stream was adjusted by adding diluted solution of Fulvic 25 to in order of 10, 20 and 100 mg C L^{-1} to DI water sample of known volume. All feed solutions were initially filtered through $0.45 \mu\text{m}$ Whatman™ filter paper. The calibration curves of the added organic feed solution are shown in Fig. S1. Salts were added accordingly to match the total hardness and conductivity of natural surface water and seawater

source. The solution was adjusted to pH ≈ 7.0 using hydrochloric acid. The NOM rejection during membrane experiments was calculated using the following equation:

$$R\% = \left(1 - \frac{C_t}{C_f}\right) \times 100 \quad \text{Equation S 4.1}$$

Where C_f and C_t represents the [DOC] in the feed and treated streams, respectively.

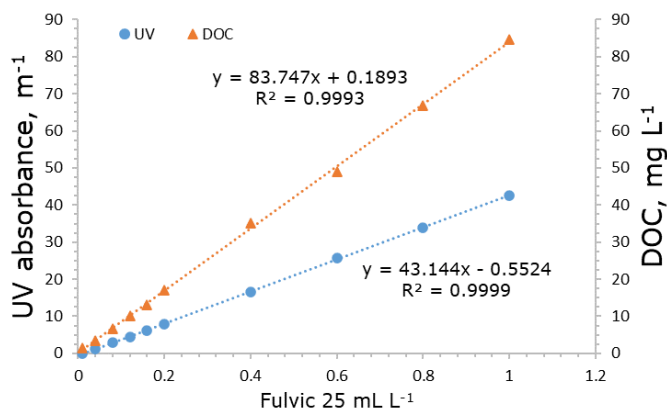


Fig. S 4.1 The calibration curve for colorimetric analysis of Fulvic 25 solution as a relation between the solution concentration (mL of fulvic 25 feedstock in L of DI water) and the UV₂₅₄ absorbance and the dissolved organic carbon (DOC).

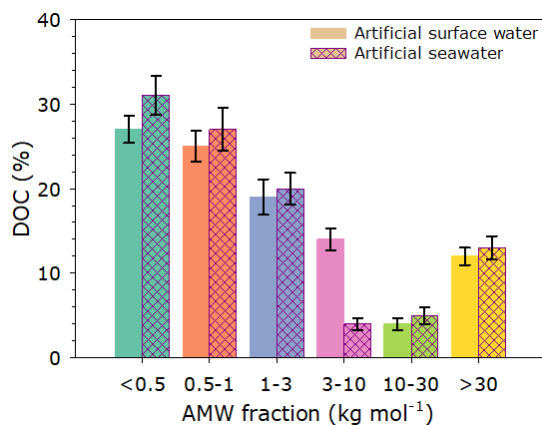


Fig. S 4.2 Apparent molecular weight distribution of the natural organic matter (measured DOC) in conventionally treated artificially prepared surface water and seawater at feed [DOC] of 20 mg C L⁻¹ with error bars representing one standard deviation calculated from the results of triplicate runs at the specific experimental conditions.

Table. S 4.2 The zeta potential of the treated artificial surface water, artificial seawater, and leachate by conventional and membrane processes.

Treatment process	pH	Zeta Potential, mV		
		Artificial surface water	Artificial seawater	Leachate
Conventional	5.5	-4.3±0.7	-6.6±0.8	-5.5±0.8
S-PANI membrane	≈7.0	-0.9±0.6	-6.5±1.0	-4.1±0.7
DURAMEM®500	≈7.0	-1.2±0.5	-6.4±0.9	-4.7±0.7

Table. S 4.3 The DOC removal through PAC adsorption of artificially prepared surface water and seawater sample at [DOC] of 20 mg L⁻¹.

Treatment process	pH	DOC removal%	
		Artificial surface water	Artificial seawater
PAC adsorption	5.5	17.2±1.8	21.5±1.3

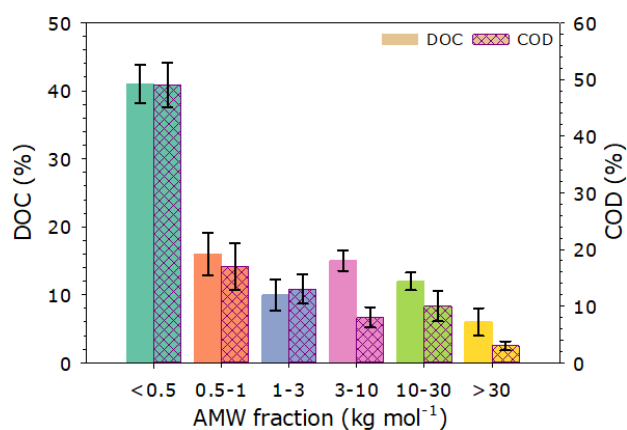


Fig. S4.3 Apparent molecular weight distribution of solute fractions of treated leachate effluent by conventional treatment with error bars representing one standard deviation calculated from the results of triplicate runs at the specific experimental conditions.

Membrane chemical cleaning procedure S4

During a chemical cleaning process, membrane samples were rinsed with 3.2 mM sodium hydroxide solution (around pH 11.5) and then soaked in the same solution for 30 min. afterwards, cleaning with mild acidic HCl aqueous solution at pH 5.0 for an equivalent period of 30 min. After that, the sample was flushed thoroughly, to rinsed out all residual contaminants.

SEM S5

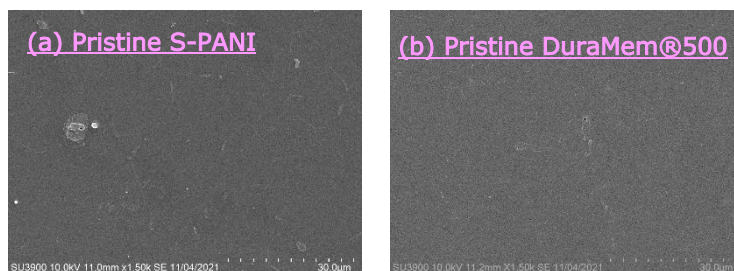


Fig. S4.4 The SEM surface images of the pristine a) S-PANI membrane and b) DuraMem@500 membrane.

References S6

- [1] J.K. Edzwald, J. Haarhoff, Seawater pretreatment for reverse osmosis: Chemistry, contaminants, and coagulation, Water Res. (2011). <https://doi.org/10.1016/j.watres.2011.08.014>.

Chapter 5

High performance in-situ tuned self-doped polyaniline (PANI) membranes for organic solvent (nano)filtration

The work presented in this chapter has been published to Polymer Journal Feb 2022. H. Alhweij, E.A. Carolina Emanuelsson, S. Shahid, J. Wenk, High performance in-situ tuned self-doped polyaniline (PANI) membranes for organic solvent (nano)filtration, Polymer. 245 (2022) 124682. <https://doi.org/10.1016/j.polymer.2022.124682>.

Context:

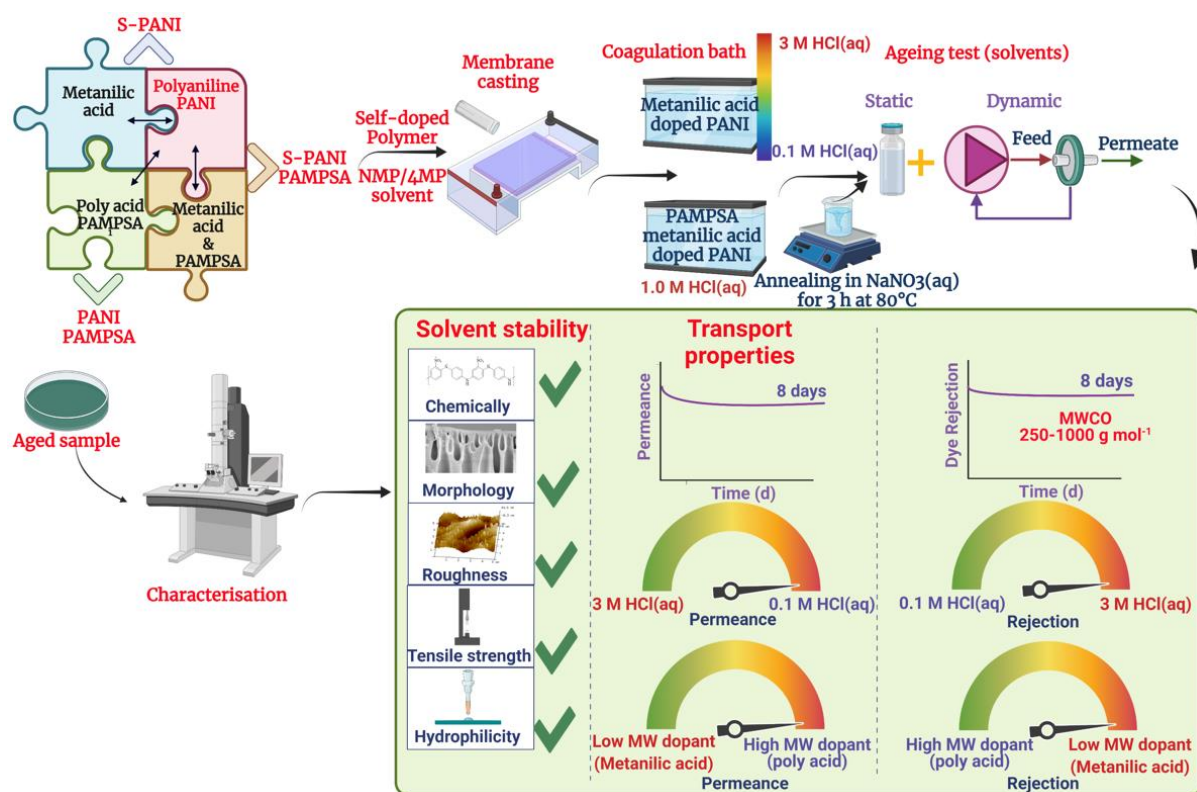
Polyaniline (PANI) membranes are attractive for organic solvent nanofiltration (OSN) due to the stimuli responsive behaviour. However, inadequate tuneability to cover the full nanofiltration (NF) separation range, prolonged post-treatment cross-linking using hazardous organic chemicals over a period of five days and poor permeance limit their widespread application. In this work, the authors systematically investigated, for the first time, a new simplified strategy to in-situ tune the performance of OSN PANI membranes from loose to tight NF separation range. This was inspired by previous work (chapter 3, <https://doi.org/10.1016/j.memsci.2021.119654>) in our research group: Alhweij et al “Simplified in-situ tailoring of cross-linked self-doped sulfonated polyaniline (S-PANI) membranes for nanofiltration applications. Briefly, presence of sulfonic groups as polymer crosslinking anchors and controlling the coagulation bath acidic strength resulted in instant stabilisation of the membrane selective layer, which hindered solvent/non-solvent exchange and enabled production of a tailored membrane morphology with a dense skin layer. This study focused simultaneous precipitation, cross-linking, and tuning of the permselective properties of PANI membranes to suit a broad range of OSN applications. The designed change in membrane transport properties takes place via a) controlling the cross-linking density by varying the coagulation bath acidic strength and b) self-doping PANI during the polymerisation process by incorporating organic acids at different molecular weight, acidity, and hydrophilicity, such as metanilic acid (MA) and poly (2-acrylamido-2-methyl-1-propanesulfonic acid) (PAMPSA). Incorporating different molecular weight organic acids facilitates cross-linking during polymer precipitation. Ageing tests in different solvents showed no observed physical or chemical deterioration, which was confirmed by various characterisation methods including Fourier transform infrared spectroscopy (FT-IR), scanning electron microscopy (SEM), atomic force microscopy (AFM), tensile strength and contact angle (CA) measurement. All membranes were stable during the long-term dynamic filtration tests with sequential feed of *Methanol (MeOH)*, *acetonitrile (ACN)* and *tetrahydrofuran (THF)*. The tuned membrane systems delivered *THF* permeance of 2.1 to 16.4 L m⁻² h⁻¹ bar⁻¹ with estimated molecular weight cut off (MWCO) from 250 to 1000 g mol⁻¹. PAMPSA doped membranes were successfully cross-linked followed by wet annealing post-treatment to obtain

membranes in NF range. The MA doped membranes which were prepared in 3 M HCl(aq) coagulation bath showed higher permeance and better rejection compared to *Glutaraldehyde* cross-linked PANI membranes. Given the ease of fabrication, modification and in-situ tuneable membrane performance, this work may represent a significant step forward in the fabrication of high performance OSN membranes for various applications. There is presently no published research on in-situ tuning of cross-linked PANI membranes with proven long-term solvent stability for OSN applications during the development and writing of this work.

Contributions:

Hassan Alhweij: Conceptualization, Methodology, Validation, Formal analysis, Investigation, Writing Original Draft, Writing Review & Editing, Visualization; Emma Anna Carolina Emanuelsson: Supervision, Funding acquisition; Salman Shahid: Conceptualization, Methodology, Supervision, Project administration, Writing Review & Editing; Jannis Wenk: Conceptualization, Writing Review & Editing, Visualization, Supervision, Project administration, Funding acquisition.

Graphical Abstract



High performance in-situ tuned self-doped polyaniline (PANI) membranes for organic solvent (nano)filtration

Hassan Alhweij^{a,c}, Emma Anna Carolina Emanuelsson^{a,b}, Salman Shahid^{a,b,c*}, Jannis Wenk^{a,c*}

^a Department of Chemical Engineering, University of Bath, Bath BA2 7AY, United Kingdom

^b Centre for Advanced Separations Engineering, University of Bath, Bath BA2 7AY, United Kingdom

^c Water Innovation and Research Centre (WIRC@Bath), University of Bath, Bath, BA2 7AY, United Kingdom

* Corresponding authors: Jannis Wenk: j.h.wenk@bath.ac.uk; Salman Shahid: s.shahid@bath.ac.uk

Abstract

Cross-linked polyaniline (PANI) membranes are attractive for organic solvent nanofiltration (OSN). However, inadequate tuneability to cover the full nanofiltration (NF) separation range, prolonged post-treatment cross-linking using hazardous organic chemicals and poor permeance limit their widespread application. This work introduces a new strategy to tune the transport properties of PANI membranes to suit the rejection spectrum of NF membranes without compromising permeance. Incorporating different molecular weight organic acids, metanilic acid (MA) and poly (2-acrylamido-2-methyl-1-propanesulfonic acid) (PAMPSA), facilitated cross-linking during polymer precipitation at different aqueous coagulation bath acidic strength using non-solvent induced phase separation (NIPS). Static ageing tests for PANI membranes immersed in *tetrahydrofuran* (THF) for 30 days showed no physical or chemical deterioration. All membranes were stable during long-term dynamic crossflow filtration tests over 250 h with sequential feed of *Methanol*, *acetonitrile* and *THF*. *THF* permeance was 2.1 to 16.4 L m⁻² h⁻¹ bar⁻¹ with apparent molecular weight cut off (MWCO) between 250 to 1000 g mol⁻¹. PAMPSA doped membranes were successfully cross-linked but required wet annealing post-treatment to obtain membranes in NF range. The MA doped membranes surpassed the performance of cross-linked PANI membranes with *glutaraldehyde* (organic cross-linker) showing 2.5 times higher permeance with better rejection. In comparison to commercial polyimide membranes, PANI membranes prepared in coagulation bath $\geq 0.5\text{M HCl(aq)}$ were stable in *N,N-dimethylformamide* (DMF) whereas the former suffered complete damage. This work represents a simplified technique to in-situ optimise permselective properties of OSN self-doped PANI membranes for various applications in food, pharmaceutical and petrochemical industries.

Keywords: Nanofiltration, organic solvent, polyaniline, high-performance, tuned.

5.1 Introduction

Organic solvent nanofiltration (OSN) is a pressure-driven technique which allows fractionation and purification for a diverse range of disperse mixtures in solvent streams [1,2]. Solutes with molecular weight (MW) between 200 and 2000 g mol⁻¹ are retained whereas small solvent molecules permeate through the membrane [3,4]. OSN membranes allow effective and consistent removal of impurities, high solvent recovery rates including flexibility to process feedstocks of fluctuating compositions without thermally affecting the quality of solutes, as alternative thermal separation processes [5–7]. Polymeric materials are the main building blocks for OSN membranes due to the ease of processing, lower fabrication costs and higher flexibility compared to inorganic materials such as ceramics [8]. Currently, integrally skinned asymmetric (ISA) polymeric membranes prepared via non-solvent induced phase separation (NIPS) are mostly used for OSN providing straightforward scale-up and low manufacturing cost [9,10]. During NIPS, gradual separation of membrane material from dope solution takes place by phase inversion in a non-solvent coagulation bath (typically water) [11]. As a result, an ISA membrane is formed which possesses same chemical composition with a skin-layer on the top of a porous and either finger-like or sponge-like support layer [12].

However, there are hurdles towards widespread practical applications of solvent stable membranes with high permeability and selectivity [13]. Ageing of OSN polymeric membranes has been a major issue resulting in loss of permeance and has also restricted application at ambient temperatures [14]. Efforts to overcome these challenges include development of new materials and strategies for solvent resistant, highly permeable, and selective membranes [15,16]. Chemical cross-linking is a common approach to render OSN membranes [17]. However, covalent bond cross-linking results in significant loss of solvent permeance due to a great reduction in interstitial spaces among polymer chains [18,19]. Both maintaining the stability of membranes in harsh solvent environments and enhancing the solvent permeance are critically important for high-performance OSN membranes, while the selection of a membrane for a particular solvent/solute system is challenging [19]. Control and tuneability of membrane pore size e.g., by polymer selection and cross-linking conditions play a crucial role in solvent

permeation [20]. Adjusting the molecular weight cut-off (MWCO) of polymeric membranes occurs either by incorporating certain functional groups into the polymer structure [21,22], changing polymer concentrations or solvent mixture ratios in dope solutions [23], altering phase inversion conditions [24], applying chemical or thermal membrane post-treatment [15], changing pH of the feedstock [25] or modifying cross-linking method [16].

Cross-linked polyaniline (PANI), an electrically conducting polymer, is an attractive starting material for OSN membranes. PANI is inexpensive, reusable, mechanically, chemically, and thermally stable, and allows controlled porosity through chemical doping [26–28]. PANI has been used to produce free-standing flat sheet NF membranes for water treatment [29] and cross-linked spiral-wound membranes for OSN applications [30,31]. Stimuli-responsive membranes can reversibly alter their physicochemical properties, pore size, and flux through external stimuli such as light and electric fields as well as changes in filtration conditions such as pH, temperature, ionic strength [32]. Tuneability of PANI membranes for OSN applications via applying electric fields has been investigated [33]. However, post-treatment for several days using hazardous organic chemicals is required to obtain chemically cross-linked solvent stable PANI or sulfonated polyaniline (S-PANI) membranes while significantly compromising solvent flux [34–36]. Given these challenges, developing PANI membranes for OSN applications require further research towards simplified in-situ tailored pore size with optimised cross-linking degree that suits different solvents for the whole NF filtration range.

Previous work in our research group presented a scalable approach to produce the first in-situ cross-linked S-PANI membranes at NF range using NIPS [37]. Briefly, presence of sulfonic groups as polymer cross-linking anchors and controlling the coagulation bath acidic strength resulted in instant stabilisation of the membrane selective layer, which hindered solvent/non-solvent exchange rate and enabled production of a tailored membrane morphology with a dense skin layer.

The aim of the present work is to introduce a novel technique to produce high performance PANI membranes with in-situ tuned transport properties to suit a broad range of OSN applications while exploiting the reported cross-linking method. The designed change in membrane performance is hypothesised to take place via a) controlling the cross-linking density by varying the coagulation bath acidic strength and b) self-doping PANI during the polymerisation process by incorporating organic

acids at different molecular weight, acidity, and hydrophilicity, such as metanilic acid (MA) and poly (2-acrylamido-2-methyl-1-propanesulfonic acid) (PAMPSA). Sulfonic polyacid like PAMPSA possess a flexible backbone that can strongly interact at molecular scale with imine nitrogen enabling the formation of a double-stranded structure with PANI [38,39]. In the case of low molecular weight MA, copolymerization with aniline takes place simultaneously in the presence of hydrochloric acid where the sulfonic acid $-SO_3H$ is covalently bound to the polymer structure resulting in compact free volume compared to PAMPSA [34,40]. To the best of our knowledge, a thorough investigation for tailoring in-situ tuned OSN self-doped PANI membranes with enhanced solvent stability, high permeance and solute selectivity has not been reported. The studied membranes cover the whole NF range, including the lower end of the ultrafiltration. Multiple dyes were tested as probe molecules to study the retention behaviour of the membranes. The physical, chemical and separation properties of the doped membranes were analysed by a variety of characterization techniques such as Fourier transform infrared spectroscopy (FT-IR), scanning electron microscopy (SEM), atomic force microscopy (AFM), tensile strength, contact angle (CA) measurement and lab-scale static and dynamic ageing tests. Benchmarking of solvent stability and transport properties for the proposed systems was compared to a laboratory cast chemically cross-linked S-PANI with *glutaraldehyde* (GA) following a preparation procedure reported elsewhere [34,35]. Also, the prepared membranes were compared to commercially modified polyimide membrane DuraMem[®] 500 of nominal MWCO 500 g mol⁻¹.

5.2 Experimental

5.2.1 Materials

Chemicals were obtained from various commercial suppliers and used as received. A list of chemicals is provided in the supporting information (SI), Materials S1. All solutions were prepared with deionised (DI) water produced from an ELGA deioniser (PURELAB Option).

5.2.2 Polymer synthesis

Previous work reported a modified synthesis method for sulfonation of aniline monomer before polymerisation (pre-sulfonation) [41]. In brief, ammonium persulfate aqueous solution was added dropwise to a glass beaker surrounded by ice containing aniline, metanilic acid (1:1 M ratio) and hydrochloric acid solution (1 M) within controlled time intervals for a prolonged time i.e., 13 h. The resulting S-PANI salt precipitate at $72\pm 1\%$ yield was filtered, washed, dried, sieved at $160\ \mu\text{m}$ and stored until required. The average MW was calculated around $47,000\ \text{g mol}^{-1}$ with a polydispersity of 1.93.

PANI PAMPSA polymer was synthesised following a procedure reported previously in our group [40]. In brief, aniline was dissolved in the PAMPSA acid solution at 4:1 monomer of PAMPSA molar ratio. Ammonium persulfate (1:1 APS to aniline M ratio) was dissolved in DI water and added into the mixture of aniline and acid continuously by using a peristaltic pump for a period of 13 h compared to 6 h as reported in the literature. The polymerisation temperature was set at 15°C and the total reaction time was 24 h. The reactant product was filtered, washed, dried, sieved at $160\ \mu\text{m}$ and stored until required. S-PANI PAMPSA was prepared following the same procedure whilst metanilic acid was added to aniline (1:1 aniline to metanilic acid M ratio).

Information on thermal degradation behaviour for the used polymers is important for OSN applications. Therefore, thermogravimetric analysis (TGA) for all polymers was studied (analytical details provided in SI, Polymer thermal analysis S2). A two-step derivative weight loss was observed in the TGA curve for all polymers (SI, Fig. S5.1). The first weight loss (1.1% for S-PANI and 2.5 to 2.7% for PANI-PAMPSA and S-PANI PAMPSA) at 100°C was attributed to evaporation of absorbed water molecules in the polymer matrix. PAMPSA doped polymer possess higher affinity to water [40] which might result in higher absorption and entrapment of water molecules. Both PANI-PAMPSA and S-PANI PAMPSA showed reasonably similar thermal behaviour with measured weight loss around 22% and 20% at 290°C , respectively. The second peak of both polymers starts at 200°C up to 335°C and 400°C for PANI-PAMPSA and S-PANI PAMPSA, respectively. The degradation rate for both polymers at temperature range 400 to 600°C was fluctuating between 31% and 46% with average rate of 38%. In contrast, S-PANI revealed higher thermal stability with the majority weight loss of second peak at

450°C. The second peak commenced around 300°C and lasts up to 600°C with final recorded degradation rate of 47%. The second weight loss for all polymers is associated with the instantaneous decompositions of the dopant functional groups at different stages and the degradation of the backbone units of PANI leading to the generation of substituted aromatic fragments [42]. The observed rise in weight loss around 200 to 300°C is unlikely to be linked to the structural decomposition of the PANI [43]. S-PANI degradation process started at 300°C which might be ascribed to the release of sulfonic groups as reported elsewhere [44]. PAMPSA dopant contains several molecular groups such as geminal dimethyl group, sulfomethyl group and amide [45]. The mechanism of the thermal decomposition of PAMPSA in its dopant form in PANI has not been fully investigated. It is assumed that the dopant will decompose into small fragments at earlier stages than polymer degradation rate.

5.2.3 Membrane fabrication

Simultaneous cross-linking and coagulation of the self-doped S-PANI, PANI-PAMPSA and S-PANI PAMPSA membranes was conducted via NIPS [37]. To understand the effect of the coagulation bath acidic strength for facilitating different cross-linking densities, S-PANI (21 wt%) was used to cast 200 µm membranes (clearance gap) at room temperature at a controlled relative humidity of ~30%. Membranes were formed after immersion precipitation at room temperature, considering a consistent evaporation time of 10 s before immersing the cast film into the coagulation bath of 0.1, 0.5, 1 and 3 M HCl(aq). For better understanding of the effect of different self-dopants, PANI-PAMPSA and S-PANI PAMPSA membranes were also prepared (21 wt%) at constant coagulation bath acidic strength of 1 M HCl(aq). Using higher polymer concentration (>21 wt%) was not viable due to gelling issues of the polymer solution. A reported procedure was followed to prepare the cross-linked S-PANI membrane with GA [35]. Immediately after casting, the membrane was fully immersed into a bath containing solution of cross-linking mixture of GA and 1 M HCl(aq) at room temperature. After 30 min, the membrane was transferred into a beaker along with the GA solution and *Acetone* (AC) was added to swell the membrane and facilitate cross-linking for 5 days whilst maintaining a constant volume of the cross-linker solution. All prepared membranes were washed sequentially in *Methanol*, DI water,

NaOH(aq) and then finally immersed in DI water to remove excess residual solvent, GA or HCl from the membrane.

Incorporation of the high MW polyacid was expected to increase the membrane permeance while decreasing the solute retention due to the high free volume and the stretch in the intersegmental spaces between the polymer chains [40]. Therefore, both PANI-PAMPSA and S-PANI PAMPSA were thermally annealed for 3 h at 80°C in aqueous solution containing sodium nitrate (33 wt%) to obtain membranes in NF range. Simultaneous wet annealing and dehydration occur due to the strong osmotic pressure difference between water in the polymer pores and the water in the NaNO₃(aq) [46]. The dope solution viscosity measurement was conducted using a procedure explained in SI, Viscosity S3. An overview of sample nomenclature and the conditions applied is provided in Table. 5.1.

Table 5.1 Preparation condition and properties of the tested membrane systems.

Membrane	Polymer	Coagulation solution	Post-treatment
M1	S-PANI	0.1 M HCl(aq)	-
M2	S-PANI	0.5 M HCl(aq)	-
M3	S-PANI	1.0 M HCl(aq)	-
M4	S-PANI	3.0 M HCl(aq)	-
M5	PANI-PAMPSA	1 M HCl(aq)	Annealing in NaNO ₃ (aq) for 3 h at 80°C
M6	S-PANI PAMPSA	1 M HCl(aq)	Annealing in NaNO ₃ (aq) for 3 h at 80°C
M7	S-PANI GA	GA/1 M HCl(aq)	GA/AC/DI water
M8	DuraMem® 500	-	Preservatives removal with solvent

5.2.4 Membrane characterisation

A detailed description, including suppliers of analytical equipment, is provided in SI, Membrane characterisation S4. In brief, the chemical properties of the membranes were determined using an FT-IR spectrometer. The morphological properties, such as membrane surface and cross-sectional area and top layer roughness were investigated by SEM and AFM. Mechanical analysis including tensile strength, stiffness and elongation at break was carried out to explore the effect of the cross-linking and ageing to membrane solvent stability. The hydrophilicity of the membranes was measured by sessile dynamic droplet penetration using a contact angle goniometer.

Solvent stability was determined by static and dynamic ageing tests. For static ageing, the membrane samples were soaked for 30 days in *tetrahydrofuran* (*THF*). The aged samples were analysed by FT-IR, SEM and AFM including the measurement of the tensile strength and CA. The cross-linking density was measured via determining the swelling degree and the gel content as surrogate using different polar protic (*Methanol*, *MeOH*) and polar aprotic solvents (*acetonitrile*, *ACN* and *THF*). Dynamic ageing test was carried out in crossflow filtration mode. Sequential feed of different solvents and dyes was applied over prolonged periods, see SI, Membrane characterisation S4.

5.3 Results and Discussion

5.3.1 FT-IR spectroscopy

Fig. 5.1 shows the FT-IR spectra determining the chemical compositions of the cross-linked samples prior and after static ageing test with *THF* solvent for 30 days. The spectra were recorded from 4000 to 650 cm^{-1} but were focussed over the range of 2000 to 650 cm^{-1} . Fig. 5.1a exhibits clear characteristic transmittance bands of M1-M7 which were observed at 1595 cm^{-1} (quinoid C = C stretching) and 1497 cm^{-1} (benzenoid C = C stretching) [34]. The presence of aromatic amine C – N stretching was observed at 1288 cm^{-1} for all samples. C – C bending for all samples was distinct at 816 cm^{-1} [47,48], and symmetric S = O stretching was detected at 1035 cm^{-1} and 704 cm^{-1} [49,50]. The spectra provide evidence of successful self-doping of aniline monomers. Based on the sulfonamide cross-linking mechanism it is expected that the amine/imine group reacts with the incorporated sulfonic groups of two dopants used (MA and PAMPSA) [37]. The cross-linked M1-M7 exhibit a peak shift towards 1148 cm^{-1} comparing to the original peak at 1168 cm^{-1} for the pristine membrane including a relative intensity change of the transmittance band at 1033 cm^{-1} , which is assigned to the stretch vibration of the sulfonic acid group, that is decreased after cross-linking (refer to pristine membranes FT-IR spectra in SI, Fig. S5.6a). The original peak (1168 cm^{-1}) was assigned to a strong asymmetric stretching vibration of S=O (sulfonate) whereas the new detected peak was linked to S=O stretching of sulfonamide bonds [51] which is in agreement with the reported sulfonamide formation elsewhere [52–54]. A transmittance band at 1111 cm^{-1} which is assigned to aromatic imine C = N stretching [55] was only noticed for the

pristine sample. The imine nitrogen double bond may break on either side of the quinoid ring reacting with the sulfonic group during the polymer re-assembly process leading to an increased benzoid to quinoid ring ratio which then prevents re-dissolution or dispersion when exposed to aprotic solvents [56]. The GA cross-linked membrane (M7) spectra is identical to M1-M7 which might be due to the presence of hydrochloric acid in the coagulation bath and the overlap of the GA cross-linker (incorporated at the aromatic imine) with the other transmittance bands. According to the reported cross-linking protocol, HCl was added as a catalyst for the reaction of GA with PANI [35].

Fig. 5.1b confirms no chemical structural changes occurred following static membrane ageing test i.e., no absence, addition or shifts of existing peaks were displayed. Also, the visual observation showed a transparent colour of the *THF* solvent beyond the test period confirmed the same. If detriment took place, discolouration of the solvent would have occurred showing light or vivid blue colour. FT-IR spectra for the commercial membrane were not interpreted given that no information on the actual modifications on the polyimide chemistry made were available. Instead, FT-IR spectra comparison was made to show that no deterioration or chemical structural changes were observed by static ageing as illustrated in SI, Fig. S5.6b.

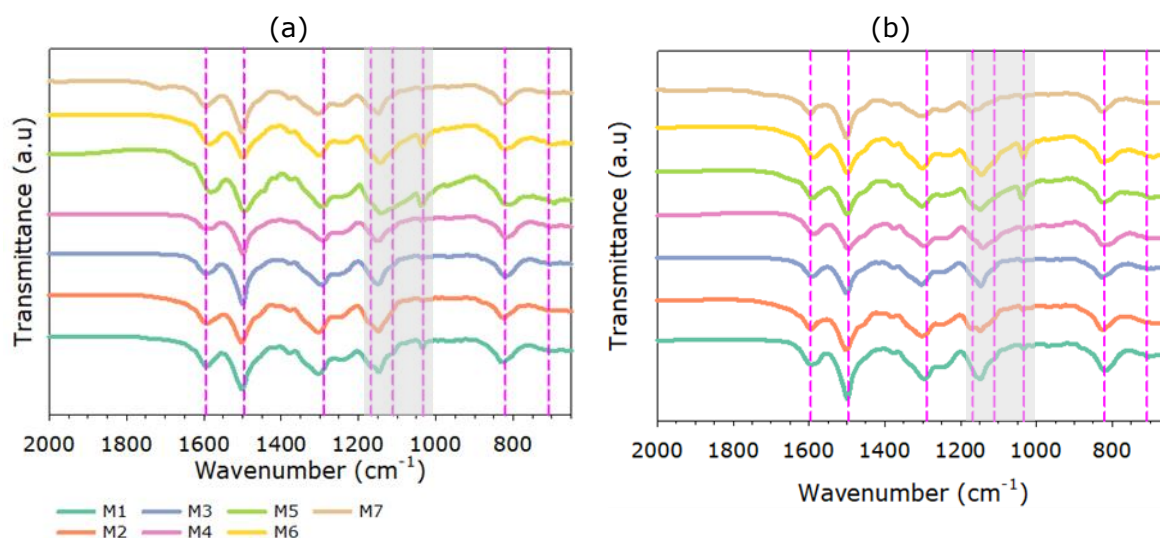


Fig. 5.1 FT-IR spectra of the cross-linked membranes M1-M7 a) before static ageing and b) after static ageing test.

5.3.2 Morphology

Both membrane morphology and structure were studied due to their significant effect on membrane transport properties [57]. Fig. S5.7 shows that the cross-section of all samples had characteristic ISA

structures which is identical to polymeric membranes prepared directly by NIPS [58]. M1-M4 and M7-M8 exhibited a skin-layer on top of a porous and finger-like transition layer with the same chemical composition. However, M1-M4 showed an increase in the density of the skin layer with suppressed macro-void structure (SI, Fig. S5.7b-e) compared to membranes produced in pure water (SI, Fig. S5.7a) or mild coagulation bath acidic strength. Simultaneous coagulation and cross-linking suppressed the formation of large macro-voids for S-PANI prepared membranes [37]. The morphology of membranes is greatly influenced by the kinetic aspects of the phase inversion process (particularly the non-solvent/solvent diffusion rates) [59]. Although the same polymer concentration (21 % wt) was used for all polymer solutions for membrane casting, M5-M6 showed different structures compared to other membranes with relatively dense but still porous, thin top layer and a more porous spongy layer underneath (SI, Fig. S5.7f-g). This could be ascribed by the potential effect of many factors. Polymer dope solutions of PANI-PAMPSA and S-PANI PAMPSA powders formed more viscous dope solution than S-PANI to certain extent by 28% and 30%, respectively, as shown in Table. 5.2. Increasing the dope solution viscosity leads to a more pronounced barrier effect during phase inversion, and the magnified top and middle section morphologies of membranes imply that the top layer becomes thicker [60]. Meanwhile, the size of sponge-like pores gradually shrinks, and the sub-layer grows denser [61,62]. However, the dope solution viscosity is not deemed to be a dominant governing factor in this instance. The measured viscosity is not substantially different meantime the dope solution of all samples is already too viscous for casting a membrane film. PAMPSA doped polymer possess high hydrophilicity [63] and needs a longer time to coagulate in the water bath to form the films. A slower coagulation rate is desirable to form membranes with sponge-like substructures [64]. Differences in membrane hydrophilicity between MA and PAMPSA doped polymers are shown and discussed at the contact angle analysis section following below. M7 exhibited a narrower bottom finger-like structure compared to the pristine S-PANI that presents large voids and cavities. This difference in the structure can be attributed to the inclusion of the cross-linker solution in the coagulation bath, causing a delayed demixing [65].

The structural stability after 30 days exposure to *THF* as a model solvent is shown in the cross-section SEM images in Fig. 5.2. Pristine S-PANI membranes experienced severe structural damage including a significant collapse in the transition layer (Fig. 5.2a). On the other hand, pristine PANI-PAMPSA and S-PANI PMPSA did not qualify for the SEM test due to the clear visual defects and the difficulties in preparing the membrane sample following significant loss in the polymer material. The SEM cross-sectional images did not show an apparent difference before and after the ageing test for all cross-linked membrane samples M1-M7 and commercial polyimide M8 which were structurally stable.

Table 5.2 Dope solution composition and viscosity.

Polymer	Membrane	Polymer concentration (wt%)	NMP/4MP* (wt%)	Solvent	Viscosity at 25°C (Pa s)
S-PANI	M1-M4, M7	21.0	72.7/6.3		24.3
PANI-PAMPSA	M4	21.0	72.7/6.3		31.2
S-PANI PAMPSA	M5	21.0	72.7/6.3		31.7

*NMP: *N*-methyl-2-pyrrolidone, 4MP: 4-methylpyridine.

Fig. S5.8 and Fig. 4.3 display the top surfaces for all membranes M1-M8 before and after ageing with *THF*, respectively. As shown in Fig. 4.3, all membranes show a smooth surface with no apparent pores or patterns.

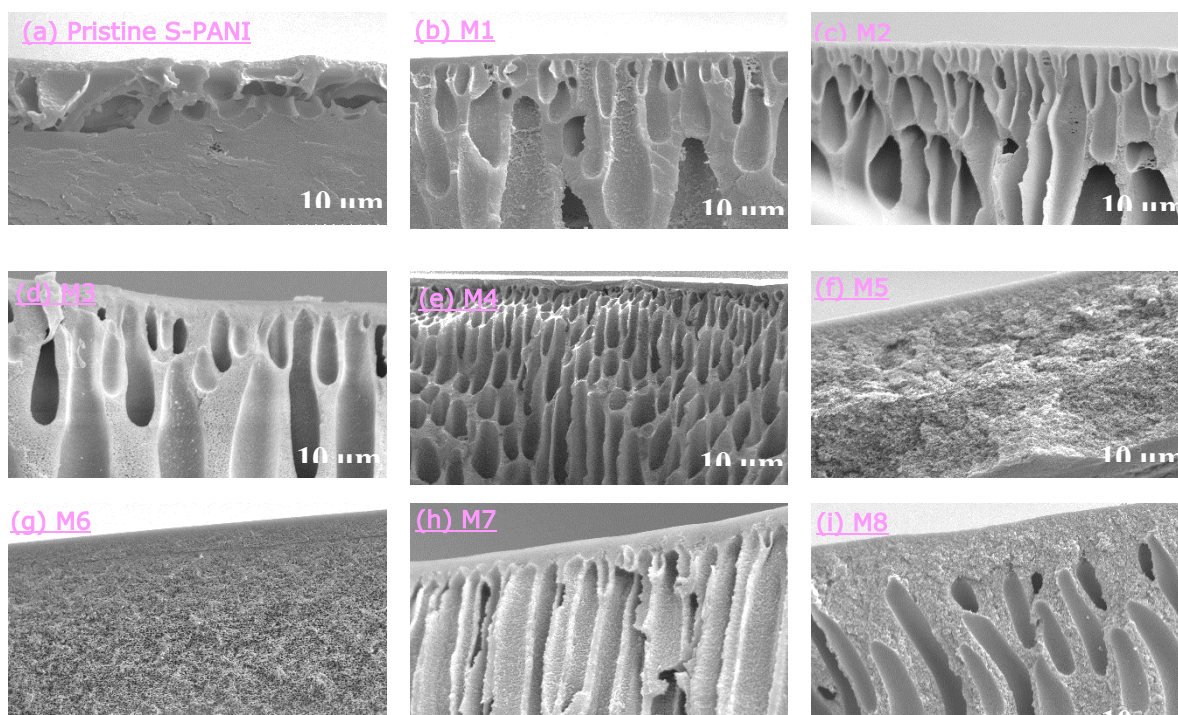


Fig. 5.2 SEM cross-sectional area images of M1-M8 membranes after static ageing test in *THF* solvent for 30 days.

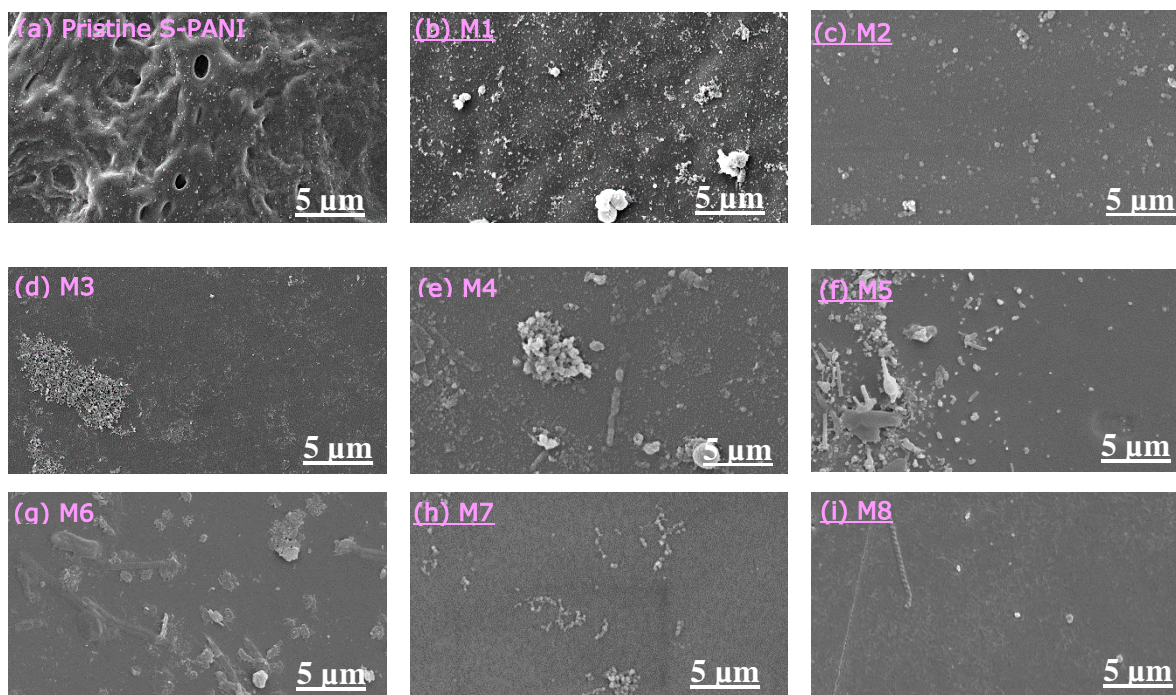


Fig. 5.3 SEM surface images of M1-M8 membranes after static ageing test in *THF* solvent for 30 days.

The randomly distributed, drop-like small particles present on all the top surfaces are most likely impurities deriving from the sample preparation process. Pristine S-PANI seems to have severe surface damages following the ageing test showing a rough and inconsistent topography with few pores as shown in Fig. 5.3a. There is no observable pin holes or deformations etc. on the surfaces either before or after ageing test for M1-M8. Since no difference was observed in the M1-M8 surfaces using SEM imaging. Therefore, stability tests were repeated using *N,N*-dimethylformamide (*DMF*) as a more aggressive solvent than *THF*. Following the same static ageing test procedure, all pristine membrane samples experienced immediate dissolution. M1 and M8 showed augmented discolouration over time and did not qualify for the SEM test by the end of the test period due to the degradation and formation of a gel-like polymer layer. In contrast, M2-M7 were structurally stable as shown in the SEM cross-sectional and surface images of the SI, Fig. S5.9 and Fig. S5.10, respectively.

AFM was used to identify differences in the surface roughness between the *THF* aged membranes with different cross-linking densities. The corresponding surface roughness parameters (mean roughness, R_a and root mean square roughness, R_q) data derived from AFM data give quantitative insights into the

surface morphology. Fig. S5.11 and Fig. 5.4 show the three-dimensional AFM images (scanning size of $5 \times 5 \mu\text{m}$) of M1-M8 before and after static ageing test, respectively. Fig. 5.4 shows that the surface of all M1-M8 membranes is smooth with few random size and shape bulges. Step increases in the coagulation bath acidic strength resulted in high solvent stability for M1-M4. Increasing the acidic strength by 10-fold (0.1 M to 1 M) diminished the increase in mean surface roughness (R_a) from 68% to 27% (SI, Fig. S5.12). This could be attributed to the higher consumption of sulfonic groups i.e., higher formation degree of sulfonamide. According to AFM analysis, M6 showed the highest solvent stability with R_a increase of 14% in comparison with M5 which showed the lowest stability with R_a of 217%. It was expected that M6 could surpass M5 in terms of solvent stability due to the abundance of functional groups which were introduced by both MA and PAMPSA. The GA cross-linked S-PANI (M7) showed less solvent stability than M3 and M4 whereas the commercial polyimide R_a increased by 161%. The initial lower roughness value exhibited by M8 may be due to the spreading of a layer of pore preservatives. Thus, the washing out of pore preservatives before and during the static aging may cause the roughness to increase. The observed increase in surface roughness during long-term solvent exposure for all membrane samples could be attributed to the clustering effect which is associated with slight changes in the polymer configuration due to the solvent polarity [66,67]. Even though all membranes tested in this study remained stable after the static aging, changes to the surface property in the microscopic scale suggest that the actual membrane performance of these membranes may be influenced when exposed to harsh solvents over prolonged periods. These results were consistent with qualitative SEM observations in Fig. 4.3 and Fig. 5.4.

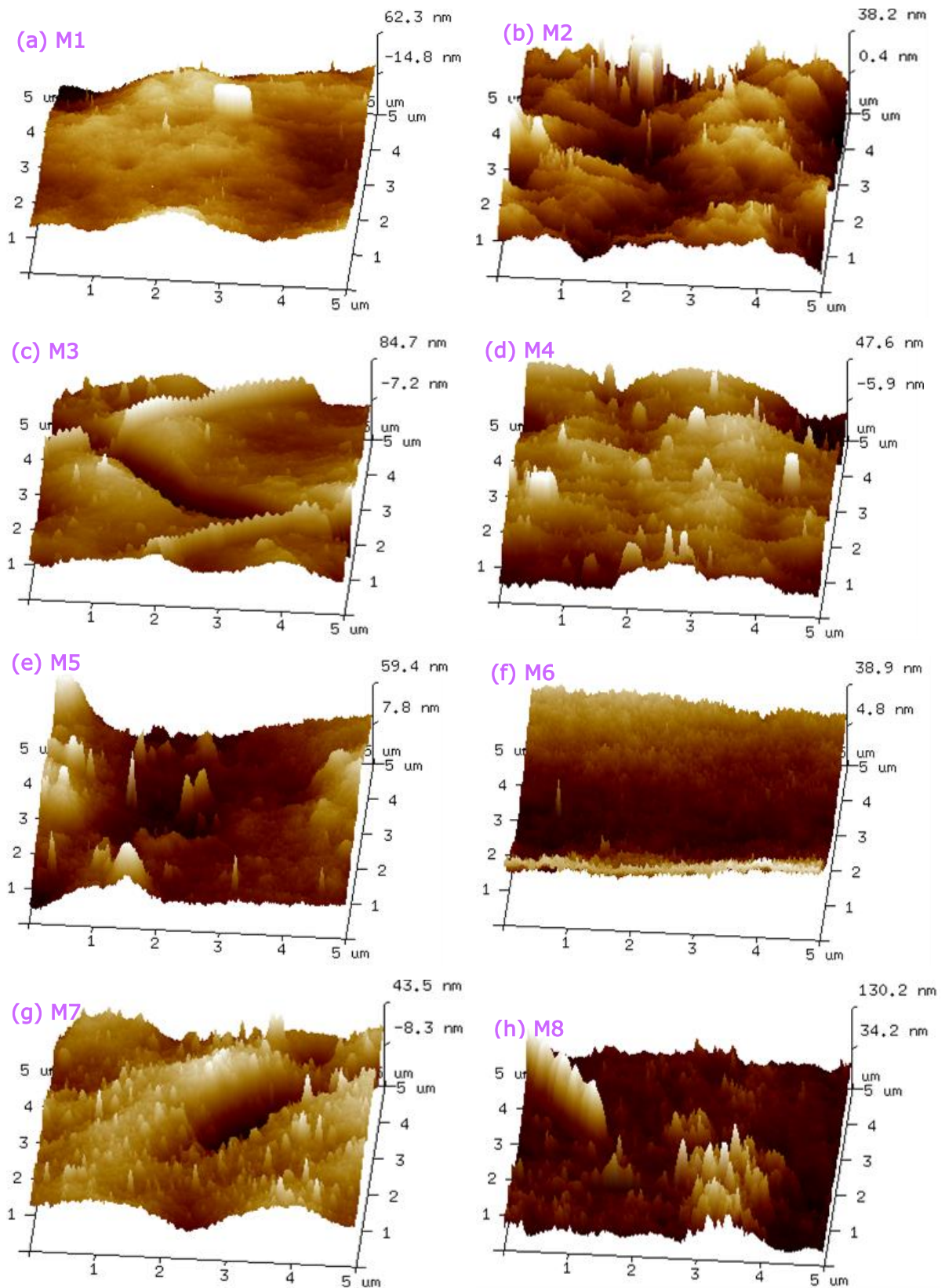


Fig. 5.4 AFM three-dimensional images of membranes M1-M8 top surface layer after static ageing test with THF for 30 days.

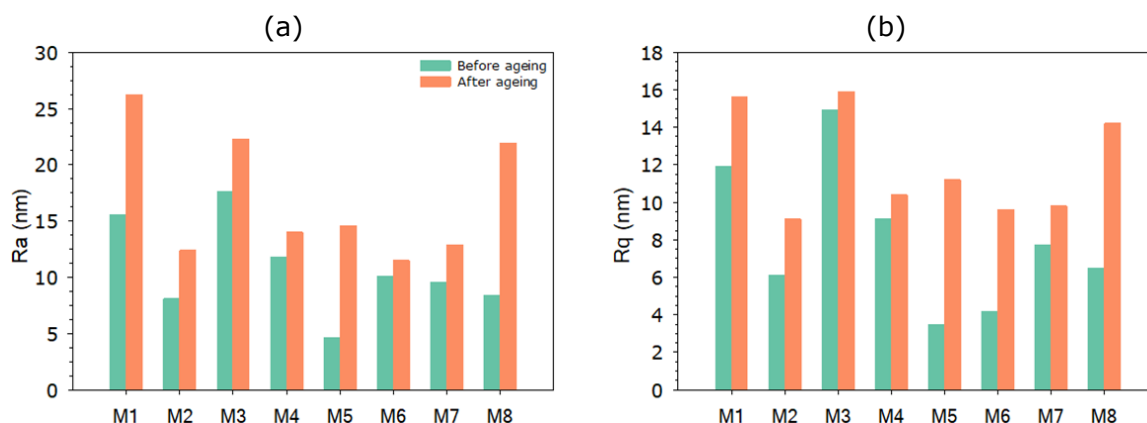


Fig. 5.5 Surface roughness before and after static ageing test with *THF* solvent for 30 days a) mean roughness, R_a , and b) root mean square roughness, R_q .

5.3.3 Mechanical analysis

A customised free-standing flat sheet membrane batch of M1-M7 was prepared exclusively to scrutinise the changes in mechanical behaviour before and after soaking in *THF* solvent for 30 days at room temperature as shown in the stress-strain curves SI, Fig. S5.13 to Fig. S5.19. Casting the membranes over a support layer makes distinguishing the potential changes in mechanical properties after ageing challenging because the membrane tensile strength and stiffness, for instance, will be primarily dominated by the support layer. As such, the tensile strength of the commercial membrane which was supplied cast over support layer was not measured due to little changes, while values were also not comparable with M1-M7 (GPa versus MPa unit scale, respectively). The membranes showed some signs of curling in the air after they were gently wiped to remove the solvent on their surfaces. Therefore, the membranes were fixed in between two glass plates while being soaked in DI water for a week to remove entrapped solvent.

The tensile strength and Young's modulus (slope of linear region of the plot) which indicates the elasticity of the membrane film are shown in Fig. 5.6. The tensile strength and Young's modulus of M1-M4 (before ageing) was in the order $M4 \approx M3 > M2 > M1$. A step increase in the tensile strength and Young's modulus (74% and 30%, respectively) was observed for M1 (before ageing) compared to the pristine S-PANI prepared in pure water coagulation bath. M7 possessed a tensile strength just under M3 which is 121% over the pristine S-PANI while the Young's modulus for both samples was in closed proximity. In contrast, M5 and M6 showed the smallest tensile strength step increases of 35% and 44%, respectively, compared to the pristine PANI PAMPSA and S-PANI PAMPSA. Although both M5 and

M6 have sponge-like sub-layer structure which should enhance the mechanical strength, the high volume in between the polymer chains seems to primarily affect the mechanical properties. M6 showed higher Young's modulus than M5 by 35% which could be attributed to the abundance of the sulfonic groups making the membrane more brittle [41]. Overall, the results emphasised how increasing the cross-linking density of macromolecular chains would have led to an enhanced tensile strength and Young's modulus of the polymeric membrane films [68].

Although the sample edges were placed in the test machine using padding material between the sample and metallic clamps to avoid any mechanical damage, the elongation at break data (SI, Table. S5.1) supported by visual observation showed signs of inevitable and consistent pre-mature break in the area closed to the fixing clamps at higher applied tension force.

The ageing had a negligible effect on the mechanical stability for all membranes. The slight fluctuation in tensile strength and Young's modulus for most of the analysed samples falls in the range of the standard deviation of the tested samples before ageing except M6 which showed a decrease in Young's modulus by 25%. This might be attributed to residual solvent in the tested polymeric sample. The dense three-dimensional network makes the membranes more mechanically stable due to the limited freedom for motion by the individual segments of the molecules and steric hindrance of chain movement even during exposure to solvents.

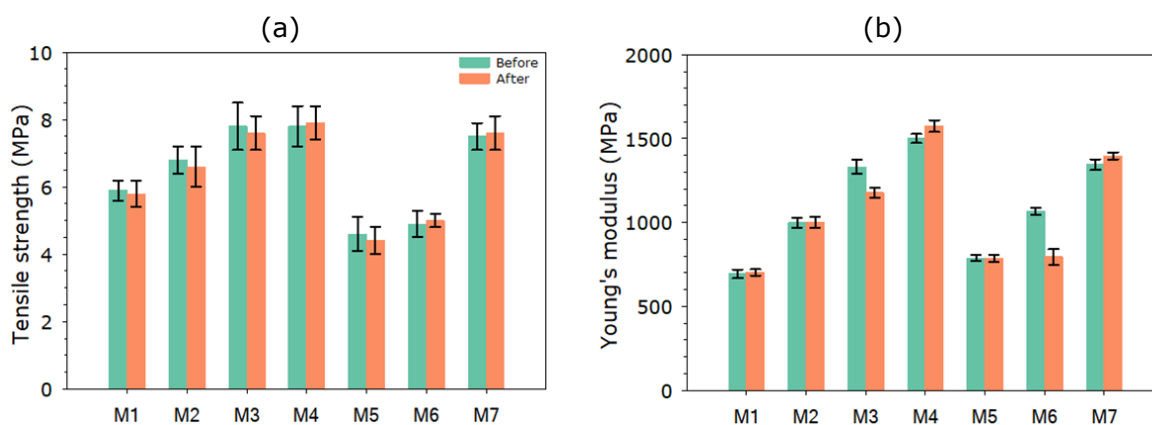


Fig. 5.6 a) Tensile strength and b) Young's modulus of the cross-linked membranes M1-M7 before and after static ageing test with *THF* for 30 days with the error bars representing single standard deviation.

5.3.4 Contact angle

The hydrophilicity was investigated by measuring the apparent contact angle (CA) of the membrane surface by using water contact angle goniometry. As expected, self-doped PANI membranes showed high hydrophilicity with broad ranging CA from 53° to 10° after 180 seconds of membrane-water droplet contact as indicated in Fig. 5.7. The increase of the coagulation bath acidic strength resulted in sequential decline in the membrane surface CA in the order $M1 > M2 > M3 \approx M4$. This could be attributed to the formation of a highly dense skin layer [58,69]. The hydrophilicity followed the opposite order of the contact angle: $M1 < M2 < M3 \approx M4$. Self-doping PANI with PAMPSA polyacid significantly improved the membrane hydrophilicity showing CA around 23° and 10° for M5 and M6, respectively, after 180 seconds which was the lowest measured value across all tested membranes. Preparing membranes with hydrophilic groups is favourable due to their low fouling tendency [70]. Both GA cross-linked S-PANI (M7) and the commercial modified polyimide showed a good hydrophilicity with an approximate CA around 37°.

The surface hydrophilicity of membranes can greatly affect the membrane performance in different solvents, especially for polar solvents [71]. Results in Fig. 5.7 show that the membrane exposure to *THF* solvent for 30 days slightly altered the hydrophilicity of the membrane surfaces, leading to a varying degree in decline of CA which ranged from 3% (M6) to 26% (M5). The hydrophilicity of the cross-linked membranes after the ageing tests still followed the same order compared to the fresh membrane samples. The variation in the membrane CA could be attributed to a slight increase in top layer surface roughness (as shown in AFM analysis) which enhanced the intrinsically hydrophilic active surface area. For hydrophilic materials, the apparent contact angle decreases when surface roughness increases in contrast with the hydrophobic materials [72]. Exposure of polymeric membranes to organic solvent was thought to initiate rearrangement of the polymer chain at the membrane top layer which results in changes in membrane intrinsic properties such as swelling and surface hydrophilicity [73–75]. Localised hydrophilicity of membranes with hydrophilic functional groups takes place due to the tendency of the last to form small clusters following pre-treatment of membranes with organic solvents [66]. In contrast, M7 and M8 revealed a marginal increase in the measured CA by 3% and 6%,

respectively. Overall, all tailored membranes showed high and relatively solvent stable hydrophilic property in consistent with results obtained from AFM.

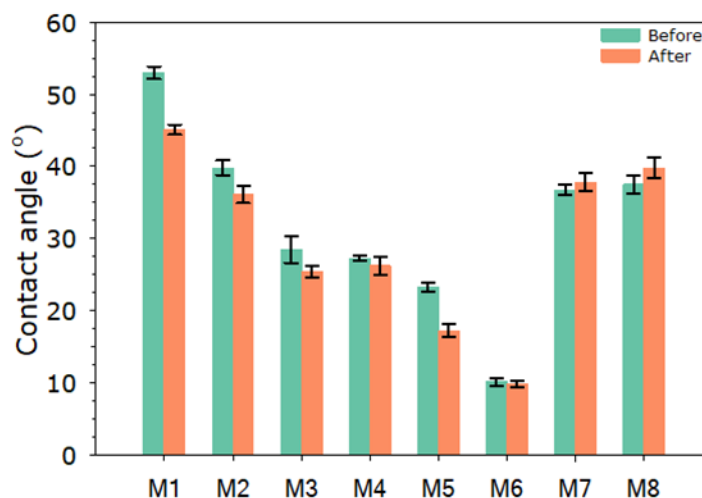


Fig. 5.7 Dynamic contact angle with single standard deviation after 180 seconds of membrane-water droplet contact for the membranes M1-M8 before and after ageing with *THF* for 30 days.

5.3.5 Swelling degree and gel content

The chemical structure of a given polymer determines its solubility in various solvents where the solubility favours structural similarity [76]. This means that polymer solubility potential increased if the solubility parameters of polymer and solvent are equal. The reported Hansen solubility parameter of undoped PANI is $22.2 \text{ MPa}^{0.5}$ at 25°C [77] compared to $29.6 \text{ MPa}^{0.5}$ for *MeOH*, $24.4 \text{ MPa}^{0.5}$ for *ACN*, $19.5 \text{ MPa}^{0.5}$ for *THF* and $24.86 \text{ MPa}^{0.5}$ for *DMF* [78,79]. Therefore, it was anticipated that all prepared membranes might favour the interaction with *ACN*, *THF* and *DMF* over *MeOH* given the fact that PANI Hansen solubility parameter falls in between the solubility parameter of these three solvents. Swelling degree and gel content measurements were carried out to assess the stability of cross-linked and commercial membranes M1-M8. Fig. 5.8a shows that all membranes have a relatively low swelling degree (below 16%) in both polar protic and aprotic solvents. The swelling degree was as low as 3% for the used solvents. Nevertheless, M5 showed higher swelling degree than M3 and M6 which were prepared at identical coagulation bath conditions (1 M *HCl*(aq)). This could be attributed to the availability of high free volume that is not occupied by the polymer chains which allows diffusion of solvent molecules. However, M6 showed low swelling compared to PANI-PAMSA which might be due to the presence of more polar groups which increase membrane stability against solvents [55].

Although M7 was expected to reveal the least swelling due to the prolonged cross-linking period in the presence of low MW cross-linker (GA), it showed an approximate swelling between M3 and M4. As envisaged, all prepared membranes exhibited higher swelling with ACN and THF than MeOH due to the closed proximity of Hansen solubility parameters. Additionally, it was found that all the membranes have a gel content higher than 98% after soaking in THF for 30 days (Fig. 5.8b), indicating the stabilities of these membranes. The swelling degree and gel content test in DMF was only carried out for M2-M7 because both M1 and M8 degraded and dissolved over time. The swelling degree in DMF was in the range of 19% to 32% which is higher than the other three solvents demonstrating the following order: M4≈M7<M3<M2≈M6<M5 as shown in the SI, Fig. S5.20a. The gel content test shows slight changes in the dry mass deterioration from 1.0% to 10.0% as the following M4<M7<M3<M2<M6<M5 which is nearly similar to the swelling degree trend (SI, Fig. S5.20b). The visual observation emphasises that M2-M7 membranes were stable in DMF providing no change in solvent colour after the 30 days soaking period, except a slight discolouring in the first 30 min.

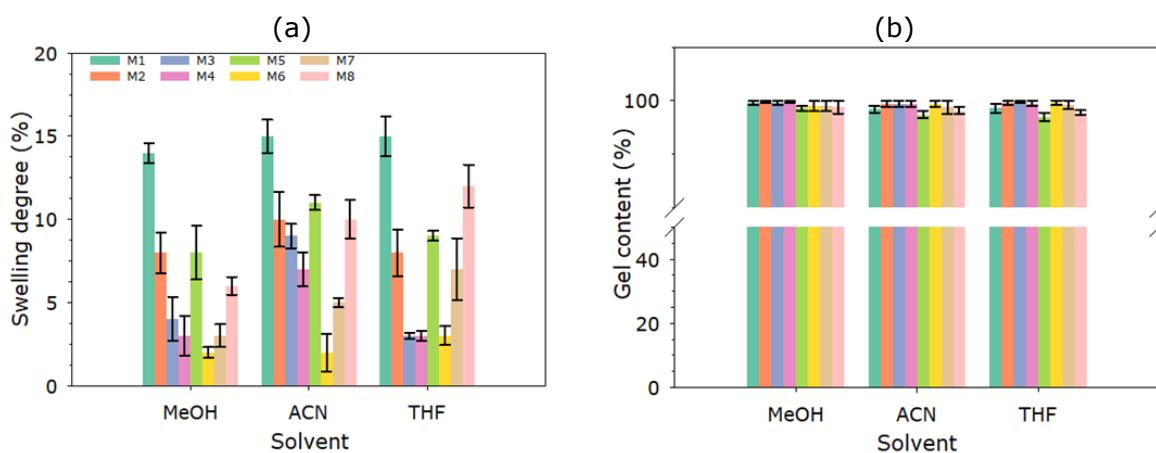


Fig. 5.8 Mass swelling degree and gel content of the cross-linked and commercial membranes M1-M8 in different polar protic and polar aprotic solvents.

5.3.6 Membrane transport properties

Long-term performance of M1-M8 was tested over 250 h in a crossflow filtration mode using sequential feed solutions of rose bengal, congo red, acid red 1, and methyl orange in DI water, MeOH, ACN and THF. The DI water and pure solvent permeance was measured after an initial period of membrane compaction as shown in Fig. 5.9. The water flux of a hydrophilic membrane gives a good indication of its MWCO, and therefore of its separation performance in water [80]. The water permeance was in the

range of 25 to 1.2 L m⁻² h⁻¹ bar⁻¹ under an operating pressure of 3 to 10 bar. The obtained membrane performance is in the NF range at approximate pure water permeance 5-50 L m⁻² h⁻¹ bar⁻¹ with transmembrane pressure around 2-10 bar [58,81]. The permeance of membranes in prepared acidic coagulation bath was in the order: M1>M2>M3>M4 which experienced a permeance decline by 52%, 61%, 75% and 92%, respectively, compared to the pristine S-PANI (prepared in DI water coagulation bath). Latter membrane showed a permeance around 52 L m⁻² h⁻¹ bar⁻¹. Doping PANI with different functional groups revealed different performance for the cross-linked M4 and M5 membranes with DI water permeance around 100 and 85 L m⁻² h⁻¹ bar⁻¹ before the wet annealing process. This represents a permeance decline of 31% and 41% for M4 and M5, respectively, compared to the samples prepared in the DI water coagulation bath. Although cross-linking of M4 and M5 resulted in solvent stable membranes, the permeance data indicate transport properties at the UF range which was verified by solute rejection of reactive red 120 dye in aqueous solution. Therefore, membrane post-treatment was required to shift the solvent stable membrane performance to the NF range. The membrane wet annealing temperature and time were optimised to 80°C and 3 h in aqueous solution containing sodium nitrate (33 wt%). The permeance of M4 and M5 membranes declined by 90 and 98%, respectively, following the annealing process. The wet annealing was favoured over heat-treatment and drying of membranes via vacuum oven as reported elsewhere [33]. Dry annealing was reported to cause a shift in the PANI-PAMPSA permeance below 1.0 L m⁻² h⁻¹ bar⁻¹ which might be due to further pore tightening with potential pore collapse including a higher densification of the top selective layer than desirable. It is worth noting that pristine PAMPSA doped membranes in this work showed over 50% decline in permeance compared to previous results reported in literature which could be attributed to the increased polymer concentration in dope solution and extended polymerisation period [40]. The GA cross-linked membrane showed the least DI water permeance 1.2 L m⁻² h⁻¹ bar⁻¹ which showed 98% decline compared to pristine S-PANI. The permeance of the commercial M8 membrane was close to M3-M5 i.e., around 9.5 L m⁻² h⁻¹ bar⁻¹.

To ensure reproducible solvent filtration results, the membranes were tested before triggering irreversible structural ageing. The available characterisation results indicated that no membrane ageing

occurred over the static test period of 30 days with *THF* and therefore the membranes were expected to demonstrate stable and consistent performance. The membranes were tested for OSN of polar solvents. After testing each system with *MeOH*, the same coupon module was systematically tested with ACN and then *THF*. A thorough system wash was performed for a 4 h to allow for steady state fluxes to be achieved before pure ACN and then *THF* solvent was put through. Polar solvents were chosen because hydrophilic cross-linked membranes show a higher permeance for polar solvents compared to non-polar solvents [82]. The solvent permeance followed the trend of DI water permeance revealing a stable permeance in the range of 21 to 0.9 L m⁻² h⁻¹ bar⁻¹. A permeance decline of 23-49%, 13-50% and 31-55% was observed with *MeOH*, ACN and *THF* solvents, respectively, compared to DI water. Unlike in aqueous solution, the interactions between solvent and OSN membranes are more complex. Different types of solvents may interact with a same membrane in an extremely dissimilar way as explained in the swelling section. As such, reorganisation of the membrane material may take place, leading to differences in porosity and changes in rejection [83]. Although a slight solvent permeance difference was observed for all membranes in the order: ACN>*MeOH*>*THF*. An explanation as to why the permeance in ACN is generally higher than in other common solvents can be attributed to a decrease in viscosity of the fluids. ACN (MW 41 g mol⁻¹) has a dynamic viscosity of 0.38 cP at 25°C compared to 0.6 and 0.46 cP for *MeOH* and *THF* [84]. Although *MeOH* (MW 32 g mol⁻¹) possess higher viscosity than *THF* (MW 72 g mol⁻¹), its higher permeance could be explained by the low MW. It would be difficult to conclude the effect of different solvents to the transport properties in this work due to the slight differences in permeance and the effect of other factors such as solvent polarity, membrane swelling, degree of cross-linking, hydrophilicity, and surface interactions.

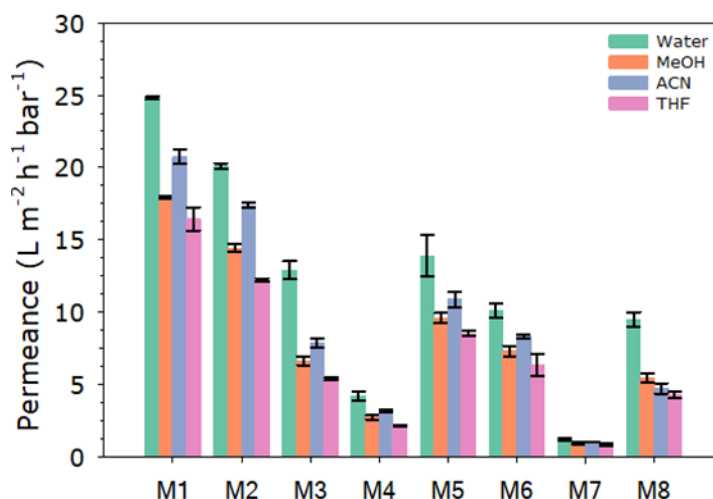


Fig. 5.9 DI water and pure *Methanol*, *acetonitrile*, and *tetrahydrofuran* solvent permeance of M1-M8 membranes. Dyes of different MW range from 327 to 1470 g mol⁻¹ were dissolved in mixtures of 50 mL DI water and 1,450 mL of *MeOH*, ACN, and *THF* as feed solution (10 mg L⁻¹ as active dye). The calibration curves for colorimetric analysis of all dyes are shown in SI, Fig. S5.2-S5.5. Fig. 5.10 indicates that the permeance of all tested systems is overall lower when dye solutions are used as feed, as compared to DI water or pure solvent feeds. The approximate permeance decline due to membrane fouling with dye solutes for all prepared membranes is between 10% to 20% in contrast with the commercial M8 which suffered a decline ranging from 33% to 47%. In general, M1-M7 membranes experienced lower dye solution permeance decline in all solvents compared to water feed solution. In general, both solvent viscosity and the state of the solvent in the membrane strongly influence the solute mobility [3]. Also, the complex interaction between the water and dye solute molecules enlarges the effective solute size and increases the solute rejection in water with respect to that in other solvent such as *Methanol* [85]. On the other hand, M8 suffered surplus flux decline with solvent feeds compared to water which could be explained by the membrane swelling causing a decrease in the polymeric matrix free volume and narrowing the porous structure [86]. This agrees with the AFM and swelling test experiments which revealed how M8 showed high swelling degree and increase in surface roughness compared to most of the prepared membranes. M8 was more vulnerable and sensitive towards long-term solvent exposure. Both pore blocking and dye solute deposition can be partially involved in the flux decline of loose NF membranes with a larger pore size [87]. Also, concentration polarisation increased concentration of dye

solution over the membrane surface reducing the driving force towards the permeate side and hence diminishing the overall permeance. This indicates a favourable interaction between the membranes and the dye and can also contribute to higher retentions as the dye adsorbed on the membrane surface and into the pores.

Solute retention of M1-M8 is shown in Fig. 5.10 as a function of the molar mass of the dyes, thus constructing an apparent MWCO curve in all solvents for these membranes as shown in SI, Fig. S5.21-S5.28. The MWCO is defined as the molecular weight (molecular mass) that a 90% retention of the solute (marker) in the feedstock [88]. The use of different markers e.g., dyes/molecules with different MW [85], polymers [89], and others such as oligostyrenes [90] has been the subject of much debate due to the variability between different techniques leading to inconsistencies between reported results. The use of dye, for instance, might not reflect the actual MWCO by size exclusion mechanism due to the potential involvement of other mechanisms such as adsorption and Donnan Exclusion [91]. Nonetheless, dyes of different MW are commonly used as a marker to estimate the MWCO of the OSN membranes as reported elsewhere [13,71,92,93]. At this work, membrane MWCO was measured using wide range of dyes with molecular weight ranging from 327 to 1470 g mol⁻¹. The MWCO was obtained by interpolation of discrete rejection points of different dyes to illustrate the apparent MWCO curve. The crossflow rig was running for prolonged periods which is thought to help in demonstrating the size exclusion mechanism. The dye adsorption could reach a saturation limit after an extended operation time. The dye retention was diminished by 10% after 2 to 3 hours of filtration for all membrane systems. The retention was then stabilised for the remainder of the test period. This indicates that the diminished rejection could be associated with the limited dye adsorption. This was appraised to be a sensible approach towards defining the MWCO and was therefore labelled as “apparent MWCO”.

The solute rejection trends indicate that the smaller the molecular weight of the dye, the lower its retention for all membranes. The obtained results show that the retention of the solute is almost independent on the solvent used. The average standard deviation of the solute rejection was marginal and between 1.0% to 4.0% for all solvents. For all the studied systems, the rejection rate was in the order: Water>THF>MeOH>ACN. The rejection trend inversely followed the trend of feed solution permeance. Membrane swelling was found to be minimal, and it was concluded that swelling did not

govern the retention rate for the prepared PANI membranes. However, the swelling might have a small impact to the solute rejection for the commercial M8. The apparent MWCO of the membranes in order: M4>M7>M3>M6>M5>M8>M2>M1 whereas the membrane permeance was in the order: M1>M2>M5>M3>M6>M8>M4>M7. All prepared membranes showed MWCO in the OSN range from approximately 1000 to 320 g mol⁻¹. The core performance data of the tailored systems were compared with the commercial and tailored systems reported in literature as shown in Table. 5.3.

Table 5.3 Comparison of membrane performance with other published data using polymeric membranes with THF solvent.

Membrane	Permeance (L m ⁻² h ⁻¹ bar ⁻¹)	Estimated MWCO	Reference
Poly(ether ether ketone)	0.2	400	[14,94]
Polybenzimidazole	0.68	~400	[95]
PANI	0.3	150-250	[96]
PIM-1/AlOx ⁽¹⁾	~2-3	~204	[97]
Modified Polyimide ⁽²⁾	~2.2	~200	[98]
Silicone polymer-based composite ⁽³⁾	~4.6	~405	[99]
Perfluorodioxole copolymer	~0.13	~350 ⁽⁴⁾	[100]
Nanocellulose	~0.3	~3000	[101]
SolSep NF010206 ⁽⁵⁾	3.0	300	[102]
Polyamide thin film composite	2.6	~370	[103]
Composite polyamide	~4.0	~625	[104]
Polybenzimidazole hollow fibre	~1.1	~500	[105]
M1	16.4	1000	This work
M2	12.2	740	This work
M3	5.4	545	This work
M4	2.1	250-300	This work
M5	8.5	700	This work
M6	6.3	645	This work
M7	0.8	300-330	This work
M8	4.2	590	This work ⁽⁶⁾

(1) Polymers of intrinsic microporosity (PIMs).

(2) Test of the commercial membrane DuraMem300 was carried out at 30°C.

(3) Commercial GMT-oNF-2 (GMT Membrantechnik GmbH, Rheinfelden, Germany) with an active layer of PDMS (Polydimethylsiloxane) on a PAN (Polyacrylonitrile) support.

(4) 94% rejection of Safranin O (MW, 351 g mol⁻¹).

(5) Commercial, material type is not available.

(6) Commercial modified polyimide DuraMem500.

Table. 5.3 shows that the *THF* permeance of the tailored membranes range from 2.1 to 16.4 L m⁻² h⁻¹ bar⁻¹ with estimated MWCO from 250 to 1000 g mol⁻¹. Commercial modified polyimide M8 showed a comparable *THF* performance of 4.2 L m⁻² h⁻¹ bar⁻¹ and estimated MWCO around 590 g mol⁻¹. The estimated MWCO in this work agrees with reported work elsewhere which showed a MWCO around 600 g mol⁻¹ using polystyrenes solutes as MWCO marker [106]. Table. 4.3 elucidates that the obtained performance of the tailored membranes in terms solvent permeance and solute rejection a) exceeded the performance of laboratory developed membranes and b) good contender to commercially scaled membranes.

These results indicate that the membranes exhibit good stability over a long-term period whilst still maintaining the excellent separation performances. The membranes could be tailored to suit widespread applications by changing the cross-linking degree without compromising model solvent stability such as *MeOH*, *ACN* and *THF*. Altering the coagulation bath acidic strength or incorporating different MW of self-dopant (MA and PAMPSA) resulted in tuned performance properties to suit loose and tight OSN applications. The introduction of sulfonic groups helped to facilitate the cross-linking reaction and hence enhance the chemical stability, permeance and hydrophilicity.

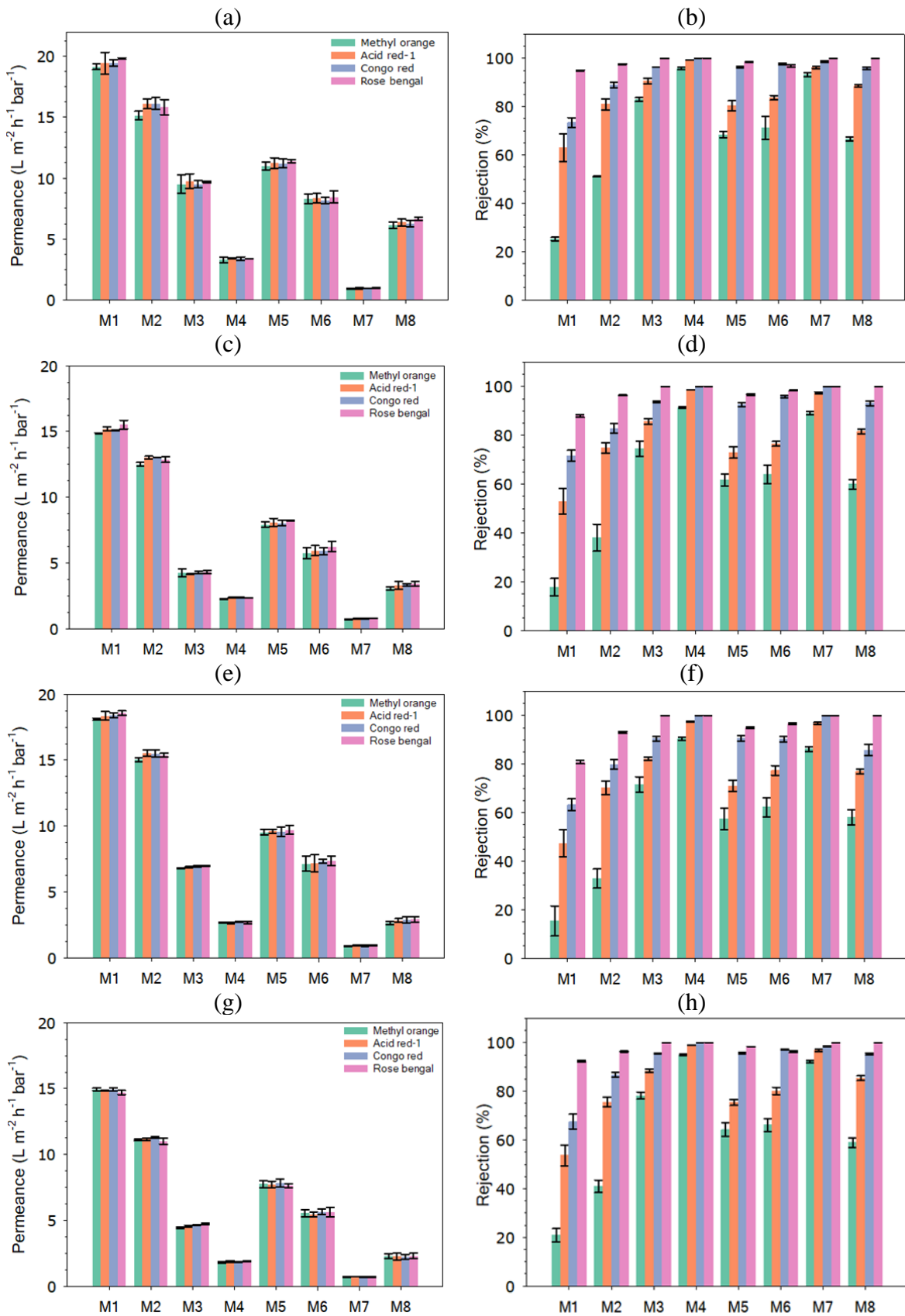


Fig. 5.10 Dye solution permeance and solute rejection in (a,b) aqueous solution (c,d) *MeOH* (e,f) *ACN* and (g,h) *THF* solvents.

5.4 Conclusions

A new simplified strategy to enhance and tune the performance of OSN PANI membranes for loose and tight NF range applications was introduced in this work. Incorporating different MW acid dopants in the PANI backbone and altering the coagulation bath acidic strength facilitated cross-linked membranes with tuned transport properties whilst improving solvent stability. The polymers were synthesised by oxidation polymerisation of aniline in the presence of different MW acid dopants such as MA and/or PAMPSA to produce S-PANI, PANI-PAMPSA and S-PANI PAMPSA. TGA test revealed that S-PANI was thermally stable up to 450°C compared to 290°C for PANI PAMPSA and S-PANI PAMPSA which is vital for OSN applications. Simultaneous coagulation and cross-linking took place by using NIPS for producing self-doped PANI membranes. Membrane solvent stability was assessed by conducting a static ageing test by immersing the membrane samples in harsh solvent (*THF*) for 30 days followed by multitude characterisation techniques such as FT-IR, SEM, AFM, tensile strength, swelling degree and gel content test. FT-IR spectra revealed a successful self-doping and cross-linking of all membranes with no changes in the chemical structure after static ageing. The mechanical analysis, swelling degree, gel content and SEM surface and cross-sectional images did not indicate any structural damage or morphological deterioration of all cross-linked membranes. The AFM surface roughness analysis suggested that all membranes possess a smooth membrane surface with few random size and shape bulges before and after ageing although mean surface roughness was increased following ageing. Membranes prepared in higher acidic strength coagulation bath are deemed to have higher cross-linking degree showing higher solvent stability with less swelling and little increase in mean surface roughness after static ageing. The dynamic ageing crossflow filtration test over 250 h using sequential dye feed solutions of *MeOH*, *ACN* and *THF* showed that all membranes have a steady-state performance. The *THF* permeance of the tailored membranes range from 2.1 to 16.4 L m⁻² h⁻¹ bar⁻¹ with estimated MWCO from 250 to 1000 g mol⁻¹. The S-PANI membrane prepared in 3 M HCl(aq) showed higher permeance (2.5 times) and rejection than cross-linked PANI with GA over 5 days. The commercial modified polyimide showed a comparable *THF* performance of 4.2 L m⁻² h⁻¹ bar⁻¹ and estimated MWCO around 590 g mol⁻¹. However, the static ageing test indicated that the prepared membranes in higher coagulation

bath acidic strength (≥ 0.5 M HCl(aq)) were stable in *DMF* compared to commercial modified polyimide which suffered complete damage. Given the ease of fabrication, modification and the in-situ tuned membrane performance, this work may represent a significant step forward in the fabrication of high performance OSN membranes for various applications.

5.5 Acknowledgements

H.A. was supported by a University of Bath research scholarship. The authors thank the technicians' team at the Department of Chemical Engineering and the Bio-imaging lab at the University of Bath for support and advice.

5.6 References

- [1] H. Werhan, A. Farshori, P. Rudolf von Rohr, Separation of lignin oxidation products by organic solvent nanofiltration, *J. Memb. Sci.* 423–424 (2012) 404–412. <https://doi.org/10.1016/j.memsci.2012.08.037>.
- [2] P. Marchetti, M.F. Jimenez Solomon, G. Szekely, A.G. Livingston, Molecular Separation with Organic Solvent Nanofiltration: A Critical Review, *Chem. Rev.* 114 (2014) 10735–10806. <https://doi.org/10.1021/cr500006j>.
- [3] P. Vandezande, L.E.M. Gevers, I.F.J. Vankelecom, Solvent resistant nanofiltration: separating on a molecular level, *Chem. Soc. Rev.* 37 (2008) 365–405. <https://doi.org/10.1039/B610848M>.
- [4] S. Darvishmanesh, T. Robberecht, P. Luis, J. Degrève, B. Van der Bruggen, Performance of Nanofiltration Membranes for Solvent Purification in the Oil Industry, *J. Am. Oil Chem. Soc.* 88 (2011) 1255–1261. <https://doi.org/10.1007/s11746-011-1779-y>.
- [5] X.Q. Cheng, Y.L. Zhang, Z.X. Wang, Z.H. Guo, Y.P. Bai, L. Shao, Recent Advances in Polymeric Solvent-Resistant Nanofiltration Membranes, *Adv. Polym. Technol.* 33 (2014) n/a-n/a. <https://doi.org/10.1002/adv.21455>.
- [6] K. Werth, P. Kaupenjohann, M. Knierbein, M. Skiborowski, Solvent recovery and deacidification by organic solvent nanofiltration: Experimental investigation and mass transfer

- modeling, *J. Memb. Sci.* 528 (2017) 369–380. <https://doi.org/10.1016/j.memsci.2017.01.021>.
- [7] C. Wang, M.J. Park, D.H. Seo, E. Drioli, H. Matsuyama, H. Shon, Recent advances in nanomaterial-incorporated nanocomposite membranes for organic solvent nanofiltration, *Sep. Purif. Technol.* 268 (2021) 118657. <https://doi.org/10.1016/j.seppur.2021.118657>.
- [8] M.H. Davood Abadi Farahani, D. Ma, P. Nazemizadeh Ardakani, Nanocomposite membranes for organic solvent nanofiltration, *Sep. Purif. Rev.* 49 (2020) 177–206. <https://doi.org/10.1080/15422119.2018.1526805>.
- [9] Y.H. See Toh, F.W. Lim, A.G. Livingston, Polymeric membranes for nanofiltration in polar aprotic solvents, *J. Memb. Sci.* 301 (2007) 3–10. <https://doi.org/10.1016/j.memsci.2007.06.034>.
- [10] K. Vanherck, P. Vandezande, S.O. Aldea, I.F.J. Vankelecom, Cross-linked polyimide membranes for solvent resistant nanofiltration in aprotic solvents, *J. Memb. Sci.* 320 (2008) 468–476. <https://doi.org/10.1016/j.memsci.2008.04.026>.
- [11] M. Mulder, *Basic Principles of Membrane Technology*, Springer Netherlands, Dordrecht, 1996. <https://doi.org/10.1007/978-94-009-1766-8>.
- [12] Loeb Sidney Sourirajan Srinivasa, High flow porous membranes for separating water from saline solutions, US3133132A, 1964.
- [13] Y. Li, Z. Guo, S. Li, B. Van der Bruggen, Interfacially Polymerized Thin-Film Composite Membranes for Organic Solvent Nanofiltration, *Adv. Mater. Interfaces.* 8 (2021) 2001671. <https://doi.org/10.1002/admi.202001671>.
- [14] J. da Silva Burgal, L. Peeva, A. Livingston, Negligible ageing in poly(ether-ether-ketone) membranes widens application range for solvent processing, *J. Memb. Sci.* 525 (2017) 48–56. <https://doi.org/10.1016/j.memsci.2016.10.015>.
- [15] A. Asadi Tashvigh, Y. Feng, M. Weber, C. Maletzko, T.-S. Chung, 110th Anniversary: Selection of Cross-Linkers and Cross-Linking Procedures for the Fabrication of Solvent-Resistant Nanofiltration Membranes: A Review, *Ind. Eng. Chem. Res.* 58 (2019) 10678–10691. <https://doi.org/10.1021/acs.iecr.9b02408>.
- [16] A. Asadi Tashvigh, L. Luo, T.-S. Chung, M. Weber, C. Maletzko, Performance enhancement in organic solvent nanofiltration by double crosslinking technique using sulfonated

- polyphenylsulfone (sPPSU) and polybenzimidazole (PBI), *J. Memb. Sci.* 551 (2018) 204–213. <https://doi.org/10.1016/j.memsci.2018.01.047>.
- [17] K. Hendrix, S. Vandoorne, G. Koeckelberghs, I.F.J. Vankelecom, SRNF membranes for edible oil purification: Introducing free amines in crosslinked PEEK to increase membrane hydrophilicity, *Polymer (Guildf)*. 55 (2014) 1307–1316. <https://doi.org/10.1016/j.polymer.2013.11.039>.
- [18] D. Bhanushali, S. Kloos, C. Kurth, D. Bhattacharyya, Performance of solvent-resistant membranes for non-aqueous systems: solvent permeation results and modeling, *J. Memb. Sci.* 189 (2001) 1–21. [https://doi.org/10.1016/S0376-7388\(01\)00356-8](https://doi.org/10.1016/S0376-7388(01)00356-8).
- [19] H.J. Zwijnenberg, S.M. Dutczak, M.E. Boerrigter, M.A. Hempenius, M.W.J. Luiten-Olieman, N.E. Benes, M. Wessling, D. Stamatialis, Important factors influencing molecular weight cut-off determination of membranes in organic solvents, *J. Memb. Sci.* 390–391 (2012) 211–217. <https://doi.org/10.1016/j.memsci.2011.11.039>.
- [20] J. Liu, X. Kong, J. Jiang, Solvent nanofiltration through polybenzimidazole membranes: Unravelling the role of pore size from molecular simulations, *J. Memb. Sci.* 564 (2018) 782–787. <https://doi.org/10.1016/j.memsci.2018.07.086>.
- [21] L. Shao, X. Cheng, Z. Wang, J. Ma, Z. Guo, Tuning the performance of polypyrrole-based solvent-resistant composite nanofiltration membranes by optimizing polymerization conditions and incorporating graphene oxide, *J. Memb. Sci.* 452 (2014) 82–89. <https://doi.org/10.1016/j.memsci.2013.10.021>.
- [22] M. Peyravi, A. Rahimpour, M. Jahanshahi, Thin film composite membranes with modified polysulfone supports for organic solvent nanofiltration, *J. Memb. Sci.* 423–424 (2012) 225–237. <https://doi.org/10.1016/j.memsci.2012.08.019>.
- [23] J. da Silva Bural, L. Peeva, P. Marchetti, A. Livingston, Controlling molecular weight cut-off of PEEK nanofiltration membranes using a drying method, *J. Memb. Sci.* 493 (2015) 524–538. <https://doi.org/10.1016/j.memsci.2015.07.012>.
- [24] K. Vanherck, A. Cano-Odena, G. Koeckelberghs, T. Dedroog, I. Vankelecom, A simplified

- diamine crosslinking method for PI nanofiltration membranes, *J. Memb. Sci.* 353 (2010) 135–143. <https://doi.org/10.1016/j.memsci.2010.02.046>.
- [25] D. Ormerod, B. Sledsens, G. Vercammen, D. Van Gool, T. Linsen, A. Buekenhoudt, B. Bongers, Demonstration of purification of a pharmaceutical intermediate via organic solvent nanofiltration in the presence of acid, *Sep. Purif. Technol.* 115 (2013) 158–162. <https://doi.org/10.1016/j.seppur.2013.05.007>.
- [26] A. Nasar, F. Mashkoo, Application of polyaniline-based adsorbents for dye removal from water and wastewater—a review, *Environ. Sci. Pollut. Res.* 26 (2019) 5333–5356. <https://doi.org/10.1007/s11356-018-3990-y>.
- [27] M. Sairam, S.K. Nataraj, T.M. Aminabhavi, S. Roy, C.D. Madhusoodana, Polyaniline Membranes for Separation and Purification of Gases, Liquids, and Electrolyte Solutions, *Sep. Purif. Rev.* 35 (2006) 249–283. <https://doi.org/10.1080/15422110600859727>.
- [28] L. Xu, S. Shahid, A.K. Holda, E.A.C. Emanuelsson, D.A. Patterson, Stimuli responsive conductive polyaniline membrane: In-filtration electrical tuneability of flux and MWCO, *J. Memb. Sci.* 552 (2018) 153–166. <https://doi.org/10.1016/j.memsci.2018.01.070>.
- [29] I.I. Yusoff, R. Rohani, A.W. Mohammad, Investigation of the formation characteristics of polyaniline and its application in forming free-standing pressure filtration membranes, *J. Polym. Res.* 23 (2016) 177. <https://doi.org/10.1007/s10965-016-1068-4>.
- [30] M. Sairam, X.X. Loh, Y. Bhole, I. Sereewatthanawut, K. Li, A. Bismarck, J.H.G. Steinke, A.G. Livingston, Spiral-wound polyaniline membrane modules for organic solvent nanofiltration (OSN), 349 (2010) 123–129. <https://doi.org/10.1016/j.memsci.2009.11.039>.
- [31] S. Monjezi, M. Soltanieh, A.C. Sanford, J. Park, Polyaniline membranes for nanofiltration of solvent from dewaxed lube oil, *Sep. Sci. Technol.* 54 (2019) 795–802. <https://doi.org/10.1080/01496395.2018.1512617>.
- [32] D. Wandera, S.R. Wickramasinghe, S.M. Husson, Stimuli-responsive membranes, *J. Memb. Sci.* 357 (2010) 6–35. <https://doi.org/10.1016/j.memsci.2010.03.046>.
- [33] A. Sarihan, S. Shahid, J. Shen, I. Amura, D.A. Patterson, E.A.C. Emanuelsson, Exploiting the electrical conductivity of poly-acid doped polyaniline membranes with enhanced durability for

- organic solvent nanofiltration, *J. Memb. Sci.* 579 (2019) 11–21. <https://doi.org/10.1016/j.memsci.2019.02.030>.
- [34] I.F. Amura, S. Shahid, A. Sarihan, J. Shen, D.A. Patterson, E.A.C. Emanuelsson, Fabrication of self-doped sulfonated polyaniline membranes with enhanced antifouling ability and improved solvent resistance, *J. Memb. Sci.* (2019) 117712. <https://doi.org/10.1016/j.memsci.2019.117712>.
- [35] X.X. Loh, M. Sairam, A. Bismarck, J.H.G. Steinke, A.G. Livingston, K. Li, Crosslinked integrally skinned asymmetric polyaniline membranes for use in organic solvents, 326 (2009) 635–642. <https://doi.org/10.1016/j.memsci.2008.10.045>.
- [36] M. Sairam, X.X. Loh, Y. Bhole, I. Sereewatthanawut, K. Li, A. Bismarck, J.H.G. Steinke, A.G. Livingston, Spiral-wound polyaniline membrane modules for organic solvent nanofiltration (OSN), *J. Memb. Sci.* 349 (2010) 123–129. <https://doi.org/10.1016/j.memsci.2009.11.039>.
- [37] H. Alhweij, E.A. Carolina Emanuelsson, S. Shahid, J. Wenk, Simplified in-situ tailoring of cross-linked self-doped sulfonated polyaniline (S-PANI) membranes for nanofiltration applications, *J. Memb. Sci.* (2021) 119654. <https://doi.org/10.1016/j.memsci.2021.119654>.
- [38] L. Sun, H. Liu, R. Clark, S.C. Yang, Double-strand polyaniline, *Synth. Met.* 84 (1997) 67–68. [https://doi.org/10.1016/s0379-6779\(96\)03839-8](https://doi.org/10.1016/s0379-6779(96)03839-8).
- [39] A.A. Nekrasov, O.L. Gribkova, T.V. Eremina, A.A. Isakova, V.F. Ivanov, V.A. Tverskoj, A.V. Vannikov, Electrochemical synthesis of polyaniline in the presence of poly(amidosulfonic acid)s with different rigidity of polymer backbone and characterization of the films obtained, *Electrochim. Acta.* 53 (2008) 3789–3797. <https://doi.org/10.1016/j.electacta.2007.08.060>.
- [40] L.L. Xu, S. Shahid, D.A. Patterson, E.A.C. Emanuelsson, Flexible electro-responsive in-situ polymer acid doped polyaniline membranes for permeation enhancement and membrane fouling removal, *J. Memb. Sci.* 578 (2019) 263–272. <https://doi.org/10.1016/j.memsci.2018.09.070>.
- [41] H. Alhweij, I. Amura, J. Wenk, E.A.C. Emanuelsson, S. Shahid, Self-doped sulfonated polyaniline ultrafiltration membranes with enhanced chlorine resistance and antifouling properties, *J. Appl. Polym. Sci.* (2021) 50756. <https://doi.org/10.1002/app.50756>.

- [42] J. Zhou, G. Tzamalís, N.A. Zaidi, N.P. Comfort, A.P. Monkman, Effect of thermal aging on electrical conductivity of the 2-acrylamido-2-methyl-1-propanesulfonic acid-doped polyaniline fiber, *J. Appl. Polym. Sci.* 79 (2001) 2503–2508. [https://doi.org/10.1002/1097-4628\(20010328\)79:13<2503::AID-APP1058>3.0.CO;2-T](https://doi.org/10.1002/1097-4628(20010328)79:13<2503::AID-APP1058>3.0.CO;2-T).
- [43] Y. Wei, K.F. Hsueh, Thermal analysis of chemically synthesized polyaniline and effects of thermal aging on conductivity, *J. Polym. Sci. Part A Polym. Chem.* 27 (1989) 4351–4363. <https://doi.org/10.1002/pola.1989.080271312>.
- [44] L.C. Mendes, A.P.S. Falco, M.S. Pinho, P.O. Marques, Sulfonated polyaniline: influence of sulfonation routes on its thermal and structural characteristics, *Mater. Res.* 14 (2011) 466–471. <https://doi.org/10.1590/S1516-14392011005000070>.
- [45] L. Hechavarría, Polyaniline–poly(2-acrylamido-2-methyl-1-propanosulfonic acid) composite thin films: structure and properties, *Thin Solid Films.* 441 (2003) 56–62. [https://doi.org/10.1016/S0040-6090\(03\)00864-2](https://doi.org/10.1016/S0040-6090(03)00864-2).
- [46] D.M. Stevens, B. Mickols, C. V. Funk, Asymmetric reverse osmosis sulfonated poly(arylene ether sulfone) copolymer membranes, *J. Memb. Sci.* 452 (2014) 193–202. <https://doi.org/10.1016/j.memsci.2013.10.042>.
- [47] S. Bhadra, N.H. Kim, J.H. Lee, Synthesis of water soluble sulfonated polyaniline and determination of crystal structure, *J. Appl. Polym. Sci.* 117 (2010) 2025–2035. <https://doi.org/10.1002/app.32152>.
- [48] S.S. An, H.H. Yoon, G. Das, Amperometric urea biosensors based on sulfonated graphene/polyaniline nanocomposite, *Int. J. Nanomedicine.* (2015) 55. <https://doi.org/10.2147/IJN.S88315>.
- [49] Y. Liu, X. Yue, S. Zhang, J. Ren, L. Yang, Q. Wang, G. Wang, Synthesis of sulfonated polyphenylsulfone as candidates for antifouling ultrafiltration membrane, *Sep. Purif. Technol.* 98 (2012) 298–307. <https://doi.org/10.1016/j.seppur.2012.06.031>.
- [50] X.-S. Wang, Q.-F. An, T. Liu, Q. Zhao, W.-S. Hung, K.-R. Lee, C.-J. Gao, Novel polyelectrolyte complex membranes containing free sulfate groups with improved pervaporation dehydration of ethanol, *J. Memb. Sci.* 452 (2014) 73–81. <https://doi.org/10.1016/j.memsci.2013.10.028>.

- [51] C. Topaçli, A. Topaçli, Infrared spectra simulation for some sulfonamides by using semi-empirical methods, *Spectrosc. Lett.* 35 (2002) 207–217. <https://doi.org/10.1081/SL-120003806>.
- [52] T. Sata, Ion exchange membranes and separation processes with chemical reactions, *J. Appl. Electrochem.* 21 (1991) 283–294. <https://doi.org/10.1007/BF01020210>.
- [53] G. Chamoulaud, D. Bélanger, Chemical Modification of the Surface of a Sulfonated Membrane by Formation of a Sulfonamide Bond, *Langmuir.* 20 (2004) 4989–4995. <https://doi.org/10.1021/la036285l>.
- [54] B.P. TrIPathi, T. Chakrabarty, V.K. Shahi, Highly charged and stable cross-linked 4,4'-bis(4-aminophenoxy)biphenyl-3,3'-disulfonic acid (BAPBDS)-sulfonated poly(ether sulfone) polymer electrolyte membranes impervious to *Methanol*, *J. Mater. Chem.* 20 (2010) 8036. <https://doi.org/10.1039/c0jm01183e>.
- [55] J. Shen, S. Shahid, A. Sarihan, D.A. Patterson, E.A.C. Emanuelsson, Effect of polyacid dopants on the performance of polyaniline membranes in organic solvent nanofiltration, *Sep. Purif. Technol.* 204 (2018) 336–344. <https://doi.org/10.1016/j.seppur.2018.04.034>.
- [56] P. Chapman, X.X. Loh, A.G. Livingston, K. Li, T.A.C. Oliveira, Polyaniline membranes for the dehydration of *tetrahydrofuran* by pervaporation, 309 (2008) 102–111. <https://doi.org/10.1016/j.memsci.2007.10.016>.
- [57] Z. Wang, J. Ma, The role of nonsolvent in-diffusion velocity in determining polymeric membrane morphology, *Desalination.* 286 (2012) 69–79. <https://doi.org/10.1016/j.desal.2011.11.006>.
- [58] Nidal Hilal; Ahmad Fauzi Ismail; Chris J Wright, *Membrane Fabrication*, CRC Press, 2015. <https://doi.org/10.1201/b18149>.
- [59] A.K. Holda, I.F.J. Vankelecom, Integrally skinned PSf-based SRNF-membranes prepared via phase inversion—Part A: Influence of high molecular weight additives, *J. Memb. Sci.* 450 (2014) 512–521. <https://doi.org/10.1016/j.memsci.2013.08.050>.
- [60] C.M. Kee, A. Idris, Permeability performance of different molecular weight cellulose acetate hemodialysis membrane, *Sep. Purif. Technol.* 75 (2010) 102–113.

- <https://doi.org/10.1016/j.seppur.2010.08.013>.
- [61] G.R. Guillen, G.Z. Ramon, H.P. Kavehpour, R.B. Kaner, E.M. V Hoek, Direct microscopic observation of membrane formation by nonsolvent induced phase separation, *J. Memb. Sci.* 431 (2013) 212–220. <https://doi.org/10.1016/j.memsci.2012.12.031>.
- [62] M. Sadrzadeh, S. Bhattacharjee, Rational design of phase inversion membranes by tailoring thermodynamics and kinetics of casting solution using polymer additives, *J. Memb. Sci.* 441 (2013) 31–44. <https://doi.org/10.1016/j.memsci.2013.04.009>.
- [63] J.E. Yoo, J.L. Cross, T.L. Bucholz, K.S. Lee, M.P. Espe, Y.-L. Loo, Improving the electrical conductivity of polymer acid-doped polyaniline by controlling the template molecular weight, *J. Mater. Chem.* 17 (2007) 1268. <https://doi.org/10.1039/b618521e>.
- [64] G.R. Guillen, Y. Pan, M. Li, E.M. V Hoek, Preparation and Characterization of Membranes Formed by Nonsolvent Induced Phase Separation: A Review, (2011) 3798–3817. <https://doi.org/10.1021/ie101928r>.
- [65] G.T. Caneba, D.S. Soong, Polymer Membrane Formation through the Thermal-Inversion Process. 2. Mathematical Modeling of Membrane Structure Formation, *Macromolecules.* 18 (1985) 2545–2555. <https://doi.org/10.1021/ma00154a032>.
- [66] B. Van der Bruggen, J. Geens, C. Vandecasteele, Fluxes and rejections for nanofiltration with solvent stable polymeric membranes in water, ethanol and n-hexane, *Chem. Eng. Sci.* 57 (2002) 2511–2518. [https://doi.org/10.1016/S0009-2509\(02\)00125-2](https://doi.org/10.1016/S0009-2509(02)00125-2).
- [67] K. Rezzadori, F.M. Penha, M.C. Proner, G. Zin, J.C.C. Petrus, M. Di Luccio, Impact of Organic Solvents on Physicochemical Properties of Nanofiltration and Reverse-Osmosis Membranes, *Chem. Eng. Technol.* 42 (2019) 2700–2708. <https://doi.org/10.1002/ceat.201900020>.
- [68] K. Majdzadeh-Ardakani, B. Nazari, Improving the mechanical properties of thermoplastic starch/poly(vinyl alcohol)/clay nanocomposites, *Compos. Sci. Technol.* 70 (2010) 1557–1563. <https://doi.org/10.1016/j.compscitech.2010.05.022>.
- [69] C.J.W. Nidal Hilal, Mohamed Khayet, *Membrane Modification*, CRC Press, 2016. <https://doi.org/10.1201/b12160>.
- [70] Y. Li, Y. Su, X. Zhao, X. He, R. Zhang, J. Zhao, X. Fan, Z. Jiang, Antifouling, High-Flux

- Nanofiltration Membranes Enabled by Dual Functional Polydopamine, *ACS Appl. Mater. Interfaces*. 6 (2014) 5548–5557. <https://doi.org/10.1021/am405990g>.
- [71] N.A.A. Sani, W.J. Lau, N.A.H.M. Nordin, A.F. Ismail, Influence of organic solvents and operating conditions on the performance of polyphenylsulfone (PPSU)/copper-1,3,5-benzenetricarboxylate (Cu-BTC) solvent resistant nanofiltration (SRNF) membranes, *Chem. Eng. Res. Des.* 115 (2016) 66–76. <https://doi.org/10.1016/j.cherd.2016.09.021>.
- [72] T.T. Chau, W.J. Bruckard, P.T.L. Koh, A.V. Nguyen, A review of factors that affect contact angle and implications for flotation practice, *Adv. Colloid Interface Sci.* 150 (2009) 106–115. <https://doi.org/10.1016/j.cis.2009.07.003>.
- [73] N.A.A. Sani, W.J. Lau, A.F. Ismail, Morphologies and separation characteristics of polyphenylsulfone-based solvent resistant nanofiltration membranes: Effect of polymer concentration in casting solution and membrane pretreatment condition, *Korean J. Chem. Eng.* 32 (2015) 743–752. <https://doi.org/10.1007/s11814-014-0281-2>.
- [74] B. Van der Bruggen, J. Geens, C. Vandecasteele, Influence of organic solvents on the performance of polymeric nanofiltration membranes, *Sep. Sci. Technol.* 37 (2002) 783–797. <https://doi.org/10.1081/SS-120002217>.
- [75] S. Darvishmanesh, J. Degrève, B. Van der Bruggen, Performance of Solvent-Pretreated Polyimide Nanofiltration Membranes for Separation of Dissolved Dyes from *Toluene*, *Ind. Eng. Chem. Res.* 49 (2010) 9330–9338. <https://doi.org/10.1021/ie101050k>.
- [76] K.T.N. Van Krevelen, D.W. Properties of Polymers, Elsevier Science, 2009.
- [77] L.W. Shacklette, C.C. Han, Solubility and Dispersion Characteristics of Polyaniline, *MRS Proc.* 328 (1993) 157. <https://doi.org/10.1557/PROC-328-157>.
- [78] Charles M. Hansen, Hansen Solubility Parameters: A User's Handbook, Second Edition, CRC Press Taylor & Francis Group, 2007.
- [79] Y. Wan, H. He, Z. Huang, P. Zhang, J. Sha, T. Li, B. Ren, Solubility, thermodynamic modeling and Hansen solubility parameter of 5-norbornene-2,3-dicarboximide in three binary solvents (*Methanol*, ethanol, ethyl acetate + *DMF*) from 278.15 K to 323.15 K, *J. Mol. Liq.* 300 (2020)

112097. <https://doi.org/10.1016/j.molliq.2019.112097>.
- [80] A. Buekenhoudt, F. Bisignano, G. De Luca, P. Vandezande, M. Wouters, K. Verhulst, Unravelling the solvent flux behaviour of ceramic nanofiltration and ultrafiltration membranes, *J. Memb. Sci.* 439 (2013) 36–47. <https://doi.org/10.1016/j.memsci.2013.03.032>.
- [81] R.W. Baker, *Membrane Technology and Applications*, John Wiley & Sons, Ltd, Chichester, UK, 2004. <https://doi.org/10.1002/0470020393>.
- [82] H. Siddique, Y. Bhole, L.G. Peeva, A.G. Livingston, Pore preserving crosslinkers for polyimide OSN membranes, *J. Memb. Sci.* 465 (2014) 138–150. <https://doi.org/10.1016/j.memsci.2014.03.031>.
- [83] H.M. Tham, K.Y. Wang, D. Hua, S. Japip, T.-S. Chung, From ultrafiltration to nanofiltration: Hydrazine cross-linked polyacrylonitrile hollow fiber membranes for organic solvent nanofiltration, *J. Memb. Sci.* 542 (2017) 289–299. <https://doi.org/10.1016/j.memsci.2017.08.024>.
- [84] I.M. Smallwood, *Handbook of Organic Solvent Properties*, Butterworth-Heinemann, 2012.
- [85] X. Yang, Experimental observations of nanofiltration with organic solvents, *J. Memb. Sci.* 190 (2001) 45–55. [https://doi.org/10.1016/S0376-7388\(01\)00392-1](https://doi.org/10.1016/S0376-7388(01)00392-1).
- [86] T.S. Anokhina, A.A. Yushkin, I.S. Makarov, V.Y. Ignatenko, A. V. Kostyuk, S. V. Antonov, A. V. Volkov, Cellulose composite membranes for nanofiltration of aprotic solvents, *Pet. Chem.* 56 (2016) 1085–1092. <https://doi.org/10.1134/S0965544116110025>.
- [87] J. Lin, C.Y. Tang, W. Ye, S.-P. Sun, S.H. Hamdan, A. Volodin, C. Van Haesendonck, A. Sotto, P. Luis, B. Van der Bruggen, Unraveling flux behavior of superhydrophilic loose nanofiltration membranes during textile wastewater treatment, *J. Memb. Sci.* 493 (2015) 690–702. <https://doi.org/10.1016/j.memsci.2015.07.018>.
- [88] Y.H.S. Toh, X.X. Loh, K. Li, A. Bismarck, A.G. Livingston, In search of a standard method for the characterisation of organic solvent nanofiltration membranes, 291 (2007) 120–125. <https://doi.org/10.1016/j.memsci.2006.12.053>.
- [89] C.J. Davey, Z.-X. Low, R.H. Wirawan, D.A. Patterson, Molecular weight cut-off determination of organic solvent nanofiltration membranes using poly(propylene glycol), *J. Memb. Sci.* 526

- (2017) 221–228. <https://doi.org/10.1016/j.memsci.2016.12.038>.
- [90] Y.H. See-Toh, M. Silva, A. Livingston, Controlling molecular weight cut-off curves for highly solvent stable organic solvent nanofiltration (OSN) membranes, *J. Memb. Sci.* 324 (2008) 220–232. <https://doi.org/10.1016/j.memsci.2008.07.023>.
- [91] L. Xu, S. Shahid, J. Shen, E.A.C. Emanuelsson, D.A. Patterson, A wide range and high resolution one-filtration molecular weight cut-off method for aqueous based nanofiltration and ultrafiltration membranes, *J. Memb. Sci.* 525 (2017) 304–311. <https://doi.org/10.1016/j.memsci.2016.12.004>.
- [92] M. Bastin, K. Hendrix, I. Vankelecom, Solvent resistant nanofiltration for *acetonitrile* based feeds: A membrane screening, *J. Memb. Sci.* 536 (2017) 176–185. <https://doi.org/10.1016/j.memsci.2017.05.003>.
- [93] L. Pérez-Manríquez, P. Neelakanda, K.-V. Peinemann, Tannin-based thin-film composite membranes for solvent nanofiltration, *J. Memb. Sci.* 541 (2017) 137–142. <https://doi.org/10.1016/j.memsci.2017.06.078>.
- [94] J. da Silva Burgal, L.G. Peeva, S. Kumbharkar, A. Livingston, Organic solvent resistant poly(ether-ether-ketone) nanofiltration membranes, *J. Memb. Sci.* 479 (2015) 105–116. <https://doi.org/10.1016/j.memsci.2014.12.035>.
- [95] D. Chen, S. Yu, M. Yang, D. Li, X. Li, Solvent resistant nanofiltration membranes based on crosslinked polybenzimidazole, *RSC Adv.* 6 (2016) 16925–16932. <https://doi.org/10.1039/C5RA27044H>.
- [96] M. Sairam, X. Xing, K. Li, A. Bismarck, J. Hans, G. Steinke, A. Guy, Nanoporous asymmetric polyaniline films for filtration of organic solvents, 330 (2009) 166–174. <https://doi.org/10.1016/j.memsci.2008.12.067>.
- [97] E.K. McGuinness, F. Zhang, Y. Ma, R.P. Lively, M.D. Losego, Vapor Phase Infiltration of Metal Oxides into Nanoporous Polymers for Organic Solvent Separation Membranes, *Chem. Mater.* 31 (2019) 5509–5518. <https://doi.org/10.1021/acs.chemmater.9b01141>.
- [98] I. Sereewatthanawut, F.W. Lim, Y.S. Bhole, D. Ormerod, A. Horvath, A.T. Boam, A.G.

- Livingston, Demonstration of Molecular Purification in Polar Aprotic Solvents by Organic Solvent Nanofiltration, *Org. Process Res. Dev.* 14 (2010) 600–611. <https://doi.org/10.1021/op100028p>.
- [99] S. Zeidler, U. Kätzel, P. Kreis, Systematic investigation on the influence of solutes on the separation behavior of a PDMS membrane in organic solvent nanofiltration, *J. Memb. Sci.* 429 (2013) 295–303. <https://doi.org/10.1016/j.memsci.2012.11.056>.
- [100] J. Chau, P. Basak, J. Kaur, Y. Hu, K.K. Sirkar, Performance of a composite membrane of a perfluorodioxole copolymer in organic solvent nanofiltration, *Sep. Purif. Technol.* 199 (2018) 233–241. <https://doi.org/10.1016/j.seppur.2018.01.054>.
- [101] A. Mautner, K.-Y. Lee, P. Lahtinen, M. Hakalahti, T. Tammelin, K. Li, A. Bismarck, Nanopapers for organic solvent nanofiltration, *Chem. Commun.* 50 (2014) 5778–5781. <https://doi.org/10.1039/C4CC00467A>.
- [102] G. Székely, J. Bandarra, W. Heggie, B. Sellergren, F.C. Ferreira, Organic solvent nanofiltration: A platform for removal of genotoxins from active pharmaceutical ingredients, *J. Memb. Sci.* 381 (2011) 21–33. <https://doi.org/10.1016/j.memsci.2011.07.007>.
- [103] M.F. Jimenez Solomon, Y. Bhole, A.G. Livingston, High flux membranes for organic solvent nanofiltration (OSN)—Interfacial polymerization with solvent activation, *J. Memb. Sci.* 423–424 (2012) 371–382. <https://doi.org/10.1016/j.memsci.2012.08.030>.
- [104] X. Zheng, A. Zhou, Y. Wang, X. He, S. Zhao, J. Zhang, W. Li, Modulating hydrophobicity of composite polyamide membranes to enhance the organic solvent nanofiltration, *Sep. Purif. Technol.* 223 (2019) 211–223. <https://doi.org/10.1016/j.seppur.2019.04.078>.
- [105] A. Asadi Tashvigh, T.-S. Chung, Robust polybenzimidazole (PBI) hollow fiber membranes for organic solvent nanofiltration, *J. Memb. Sci.* 572 (2019) 580–587. <https://doi.org/10.1016/j.memsci.2018.11.048>.
- [106] P. Marchetti, A.G. Livingston, Predictive membrane transport models for Organic Solvent Nanofiltration: How complex do we need to be?, *J. Memb. Sci.* 476 (2015) 530–553. <https://doi.org/10.1016/j.memsci.2014.10.030>.

Supporting Information

High performance in-situ tuned self-doped polyaniline (PANI) membranes for organic solvent (nano)filtration

Hassan Alhweij^{a,c,d}, Emma Anna Carolina Emanuelsson^{a,b}, Salman Shahid^{a,b,c*}, Jannis Wenk^{a,c*}

^a Department of Chemical Engineering, University of Bath, Bath BA2 7AY, United Kingdom

^b Centre for Advanced Separations Engineering, University of Bath, Bath BA2 7AY, United Kingdom

^c Water Innovation and Research Centre (WIRC@Bath), University of Bath, Bath, BA2 7AY, United Kingdom

^d Stantec UK Limited, Dominion House, Warrington, WA3 6GD, United Kingdom

* Corresponding authors

Jannis Wenk: j.h.wenk@bath.ac.uk

Salman Shahid: s.shahid@bath.ac.uk

Materials S1

Aniline, ammonium persulfate (APS), 4-methylpyridine (4MP), *N*-methyl-2-pyrrolidone (NMP), ammonium hydroxide solution, *N,N*-dimethylformamide (DMF), glutaraldehyde (GA), poly(2-acrylamido-2-methyl-1-propanesulfonic acid) (PAMPSA, MW 800,000 g mol⁻¹), reactive red 120 (MW 1469.98 g mol⁻¹), rose bengal (MW 1017.6 g mol⁻¹), congo red (MW 696.66 g mol⁻¹), acid red 1 (MW 509.42 g mol⁻¹), and methyl orange (MW 327.33 g mol⁻¹) were obtained from Sigma-Aldrich, UK. Acetone (AC), Methanol (MeOH), acetonitrile (ACN), tetrahydrofuran (THF), 3-aminobenzene sulfonic acid (metanilic acid), sodium hydroxide, sodium nitrate (NaNO₃) and hydrochloric acid (HCl) aqueous solution were obtained from VWR, UK. Commercial modified polyimide DuraMem® 500 flat sheet membrane (nominal MWCO 500 g mol⁻¹) was obtained from Evonik, UK.

Polymer thermal analysis S2

Thermogravimetric analysis (TGA) for all polymers was studied using Setaram Setsys Evolution 16 TGA-Differential thermal analysis (DTA)-Differential scanning calorimetry (DSC). The instrument was equipped with Pfeiffer GSD 320 mass spectrometer to monitor the mass change over a change in temperature with the detection of evolved gases during the experiment. All polymer samples were heated from 30 to 600°C with an airflow rate of 60 mL min⁻¹ and a heating rate of 10°C min⁻¹. Fig. S5.1 shows the TGA results which elucidate the change of weight during controlled heating as a percentage of the initial polymer sample weight and the derivative weight with respect to temperature up to 600°C.

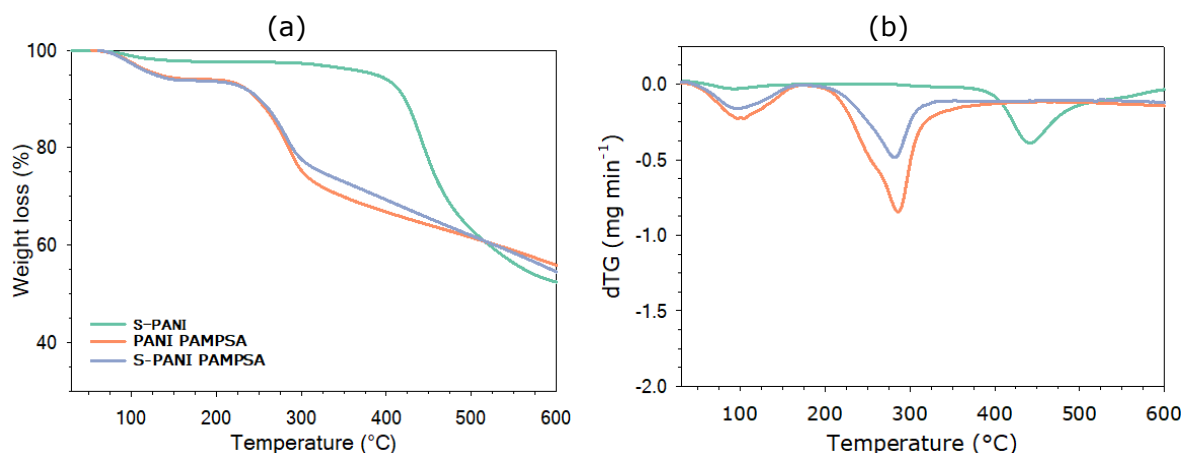


Fig. S5.1 TGA curves for S-PANI, PANI-PAMPSA and S-PANI PAMPSA polymers (a) weight loss (b) derivative weight loss with respect to temperature from room temperature to 600°C.

Viscosity S3

Stress-controlled rheometer (Discovery HR-3, TA Instruments, USA) equipped with a sandblasted plate-plate stainless steel geometry (40 mm) at 25°C. Approximately 1 mL of the sample was placed between the plates (with a plate-plate gap of 0.5 mm) and the flow curve was measured to study the viscosity response of the sample to shearing, with a shear rate ranging from 0.01 to 100 s⁻¹.

Membrane characterisation S4

FT-IR

The chemical composition of the membranes was determined using FT-IR spectrometer (PIKE Technologies Inc, USA) fitted with an attenuated total reflectance (ATR) accessory. All spectra were recorded with 32 scans and 4 cm⁻¹ resolutions over a range of wave number from 4000 to 650 cm⁻¹.

SEM

The morphological properties, such as membrane surface and cross-sectional area were investigated by SEM (SU3900, Hitachi, Japan). To analyse membrane morphology, SEM images on both the surface and the cross-section of membranes were captured at an acceleration voltage of 10 kV. A representative cross-section was obtained by fracturing membranes in liquid nitrogen. Samples were mounted onto SEM stubs and coated with gold using a sputter coater (S150B, Edwards, USA).

AFM

The topography of the membrane surface and roughness were determined by AFM, Nanoscope IIIa, Digital Instruments. Non-contact probe (Nu Nano Ltd, UK) was used to ensure soft tapping mode in air.

Mass swelling degree and gel content

A set of organic solvents such as *Methanol* (*MeOH*), *acetonitrile* (*ACN*) and *tetrahydrofuran* (*THF*) were used to determine the membrane swelling degree and gel content. In terms of polarity, *MeOH* is polar protic solvent whereas *ACN* and *THF* are polar aprotic solvents. M1-M8 were cut into small

samples (2 × 2 cm) and dried in the vacuum oven. The dried membrane samples (of known mass) were allowed to equilibrate with an excess of the solvent in a sealed flask at 25°C for 1 h. The swollen membranes were taken from the solvent and quickly dried with filter paper to remove solvent from the external surface. The mass of the swollen membranes was then determined. The mass swelling degree (SD) was calculated using the following equation:

$$SD = (m_{wet} - m_{dry})/m_{dry} \quad \text{Equation S 5.1}$$

where m_{wet} is the mass of the swollen membrane after equilibrium and m_{dry} is the mass of the dry membrane.

The gel content of the M1-M8 membranes in the solvents was determined by immersing the membrane sample in the solvent for 30 days (same conditions as per swelling test) including for *DMF*. After two weeks, the membrane samples were removed from the solvent and dried in the vacuum oven. The mass change of the dry membrane before and after soaking in the solvent indicates membrane dissolution. The gel content is a parameter that is used to define the polymer stability in different solvent was calculated by using the following equation:

$$Gel\ content\ \% = (W_a/W_b) \times 100 \quad \text{Equation S 5.2}$$

where W_b and W_a is the dry weight of the membrane sample before and after solvent soaking, respectively. Membranes that showed no swelling or dissolution in *DMF* and had a gel content higher than 90%, are designated cross-linked [67].

Mechanical analysis

Tensile strength was measured to assess the effect of the cross-linking degree and the mechanical stability following membrane ageing with solvent. An Instron 3369 mechanical tester was used and dried membrane casts without a support layer were cut into rectangular strips of approximately 70 mm × 6 mm for testing. All tests were conducted with a pull speed of 2 mm min⁻¹ at room temperature. The membrane thickness was measured using standard micrometre. The reported mechanical data is an average of three different membrane samples.

Contact angle

The hydrophilicity of the membranes was measured (3 times per sample) by sessile dynamic droplet penetration using a contact angle goniometer (Contact Angle System OCA 15Pro, Dataphysics, Germany). A small droplet of water (2.0 μL) was placed onto the membrane surface at a dosing rate of 1.0 $\mu\text{L s}^{-1}$ using a Hamilton syringe. The software SCA20 was used to calculate the dynamic effective contact angle (CA).

Membrane transport properties

Membrane filtration experiments were conducted using a stainless-steel solvent resistant pilot scale crossflow rig with an active membrane area of 14.6 cm^2 . The schematic of the experimental set-up is illustrated in previous work [194]. Permeate flow rates were measured using a digital scale connected to a computer. The membrane permeance J_p ($\text{L m}^{-2} \text{hr}^{-1} \text{bar}^{-1}$) by using the following equation:

$$J_p = \frac{\Delta W}{A \cdot \Delta P \cdot t \cdot \rho_p} \quad \text{Equation S 5.3}$$

Where ΔW (kg) is the obtained permeate weight during a fixed time slot, ρ_s (kg m^{-3}) is the permeate density at room temperature, A (m^2) is the membrane coupon active surface area (filtration area), t is the time intervals between each measurement and ΔP (bar) represents the differential pressure at the membrane, which is maintained by chemical resistant dual-acting pump.

Once the membrane wetted, the membrane was not used after it has been removed from the filtration cell, even if it has been kept wet. As the sealing process in the filtration cell compresses the membrane at the seal point, any misalignment when the membrane is re-used will lead to leaks and by-passing of the membrane. This is undesirable as data generated with a misaligned membrane will not be representative of the membrane type. A stable membrane performance was achieved after 1 h of filtration for all membrane samples. However, the reported DI water permeance was reported after 4 h to ensure full pre-conditioning and consistency.

To define the effect on the membranes' solutes retention, different batches of dye feed solutions ranging from 327 to 1470 g mol^{-1} were used in order. Methyl orange, acid red 1, congo red and rose bengal dye

powders were separately dissolved in solvent. For a typical dye solution, 10 mg of active dye powder was added to a mixture of 50 mL DI water and 1,450 mL solvent at room temperature. The dye powder was dissolved and stirred using a magnetic stirrer at 200 rpm until the dye powder was completely dissolved.

Each membrane sample was placed in the crossflow rig and the pure solvent permeance was measured over running period of 12 h for solvent pre-conditioning and preliminary stability check. Afterwards, the membrane solute rejection was measured by sequential feed of dye solution for 12 h per cycle. The membrane was washed with solvent for 4 h after each cycle to washout the dye residual and ensure cleanliness of the system for each used dye. Once each solvent cycle completed, the membrane washed for 4 h with DI water to prepare the membrane for test with the next solvent. The sequence of the solvent feed as the following *MeOH*, *ACN* and then *THF*. By doing so, the total ageing test of each sample involves around 205 h (8.5 days) running time. The crossflow rig was primed with DI water to maintain membrane wettability while being idle for next day use.

The dye concentration in the feed and permeate samples were measured via UV absorbance using an Agilent Carry 100 UV-Vis spectrometer (Agilent Corporation). For calibrations curves see Fig. S5.2-S5.5. The dye rejection was calculated using the following equation:

$$R\% = \left(1 - \frac{C_p}{C_f}\right) \times 100 \quad \text{Equation S 5.4}$$

Where C_p is the dye solution concentration in the permeate and C_f is that in the feed.

DuraMem[®] membranes contain a polyethylene glycol preservative which was washed out prior to use with *Acetone*. The resulting permeate was discarded after flushing the preservative from a new membrane disk.

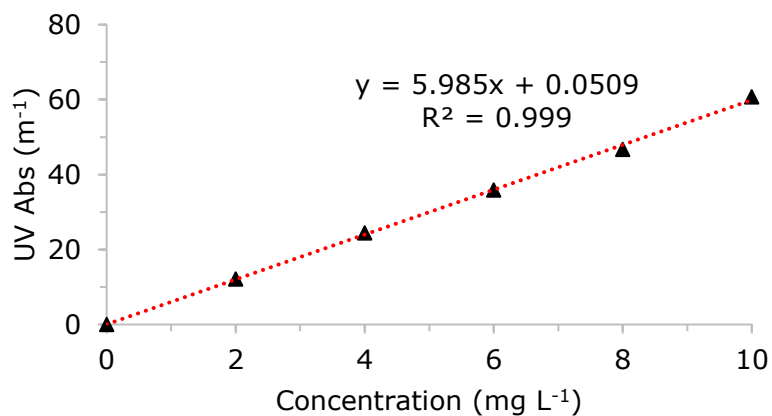


Fig. S5.2 The calibration curve for colorimetric analysis of methyl orange solution as a relation between the solution concentration and the UV absorbance (peak absorption at wavelength 461 nm).

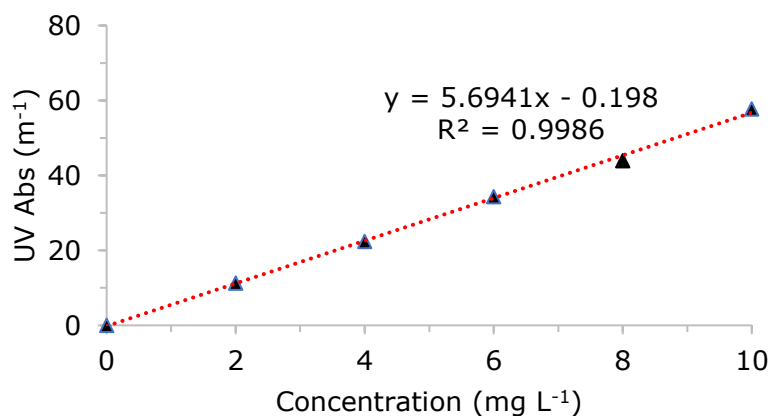


Fig. S5.3 The calibration curve for colorimetric analysis of acid red 1 dye solution as a relation between the solution concentration and the UV absorbance (peak absorption at wavelength 530.5 nm).

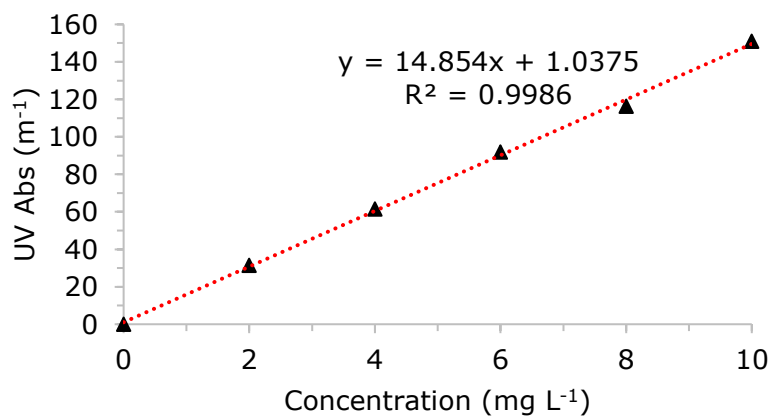


Fig. S5.4 The calibration curve for colorimetric analysis of congo red dye solution as a relation between the solution concentration and the UV absorbance (peak absorption at wavelength 496.5 nm).

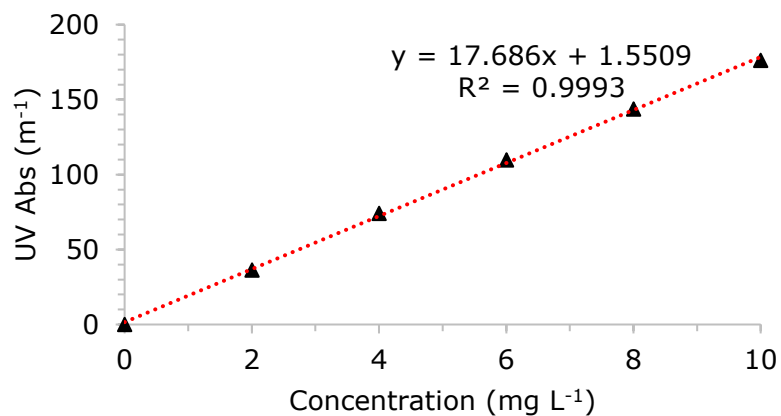


Fig. S5.5 The calibration curve for colorimetric analysis of rose bengal dye solution as a relation between the solution concentration and the UV absorbance (peak absorption at wavelength 548 nm).

FT-IR spectra S5

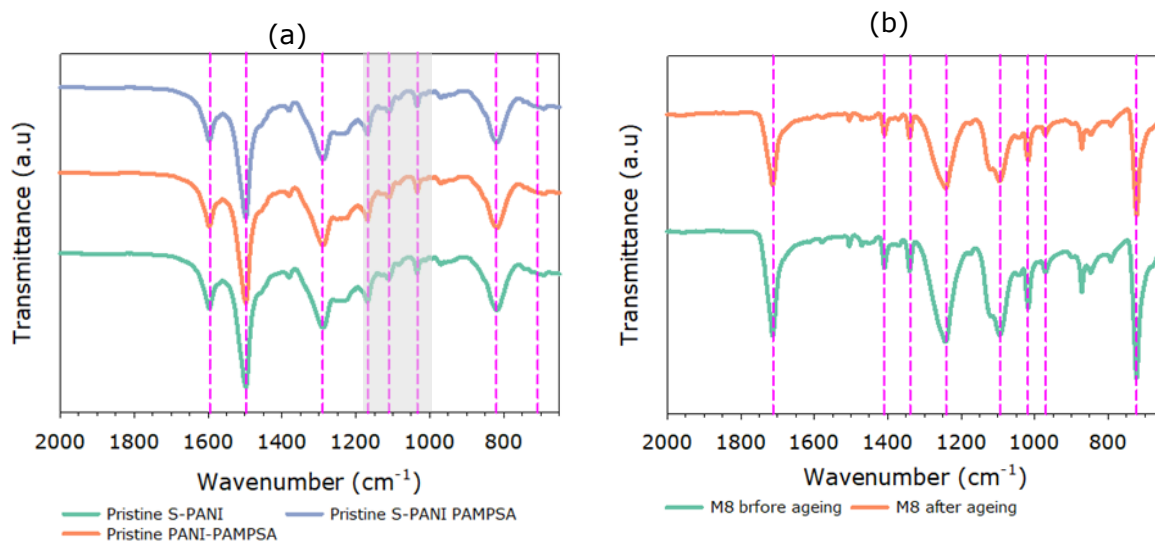


Fig. S5.6 FT-IR spectra of a) pristine S-PANI, PANI-PAMPSA and S-PANI PAMPSA and b) commercial modified polyimide membrane DuraMem@500 before and after static ageing test.

Membrane SEM S6

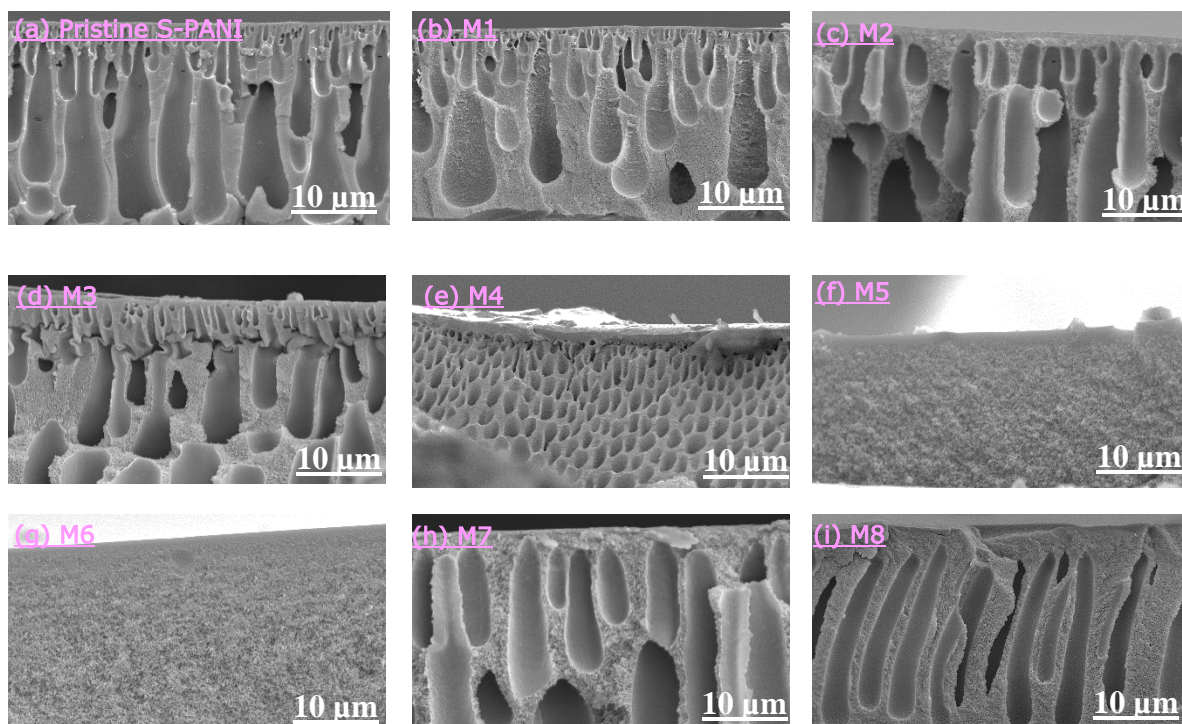


Fig. S5.7 SEM cross-sectional area images of M1-M8 membranes before static ageing test in *THF* solvent.

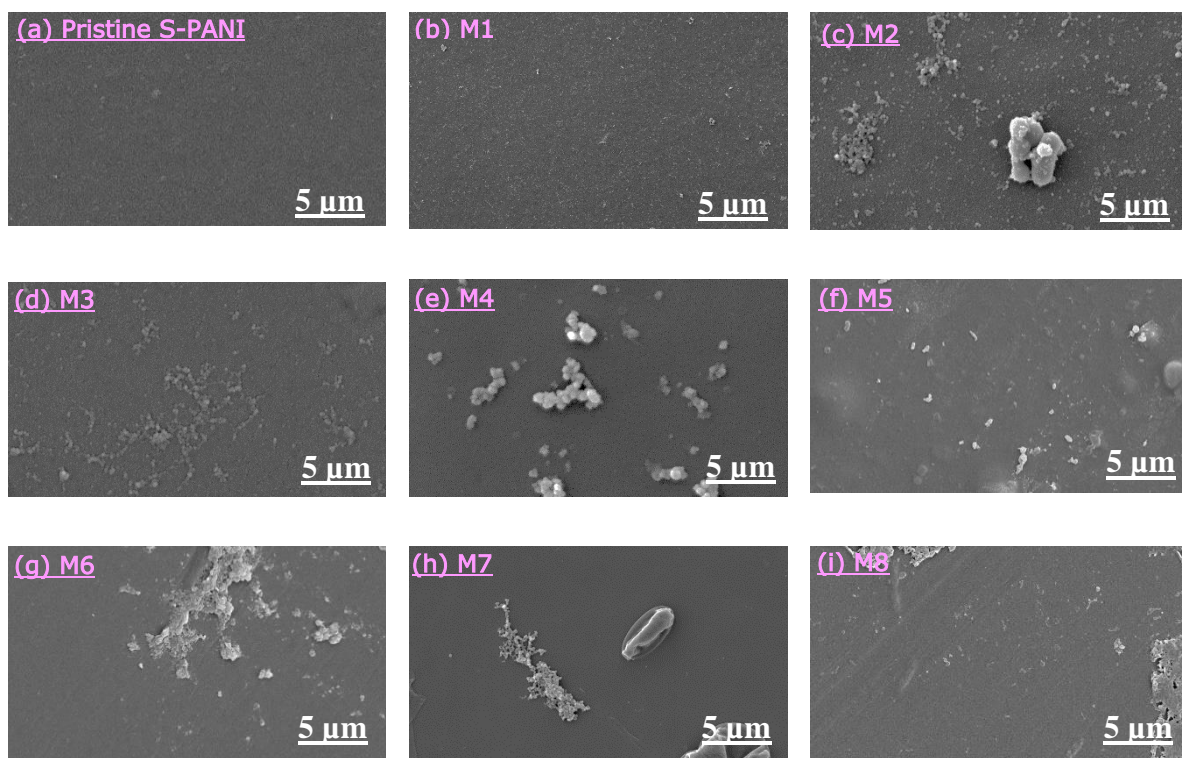


Fig. S5.8 SEM surface images of M1-M8 membranes before static ageing test in *THF* solvent.

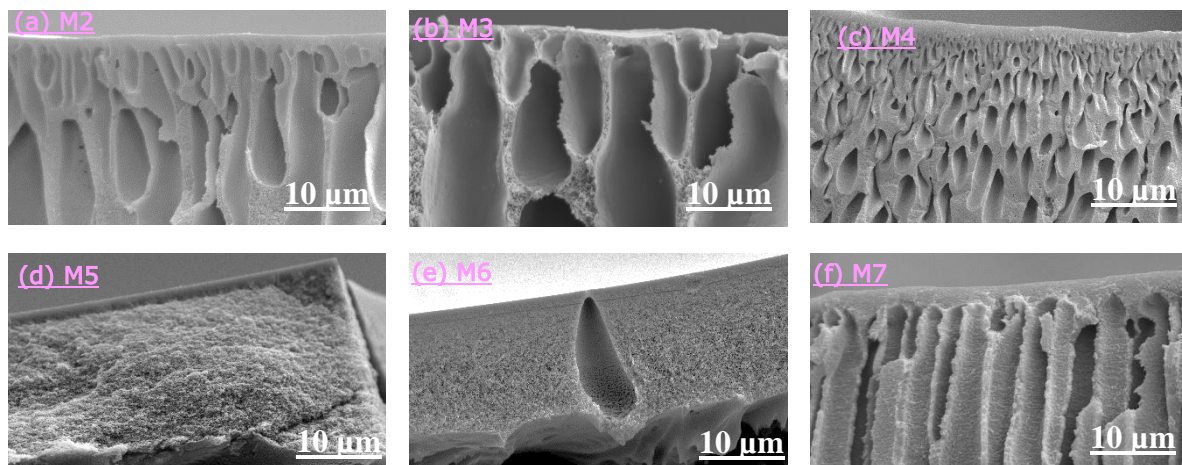


Fig. S5.9 SEM cross-sectional area images of M2-M7 membranes after static ageing test in *DMF* solvent for 30 days.

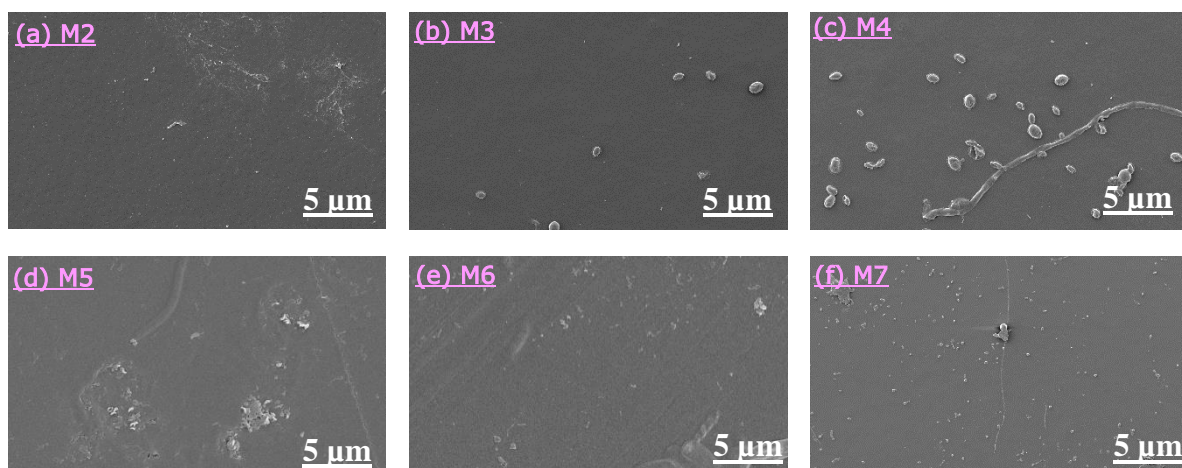


Fig. S5.10 SEM surface images of M2-M7 membranes after static ageing test in *DMF* solvent for 30 days.

Membrane AFM S7

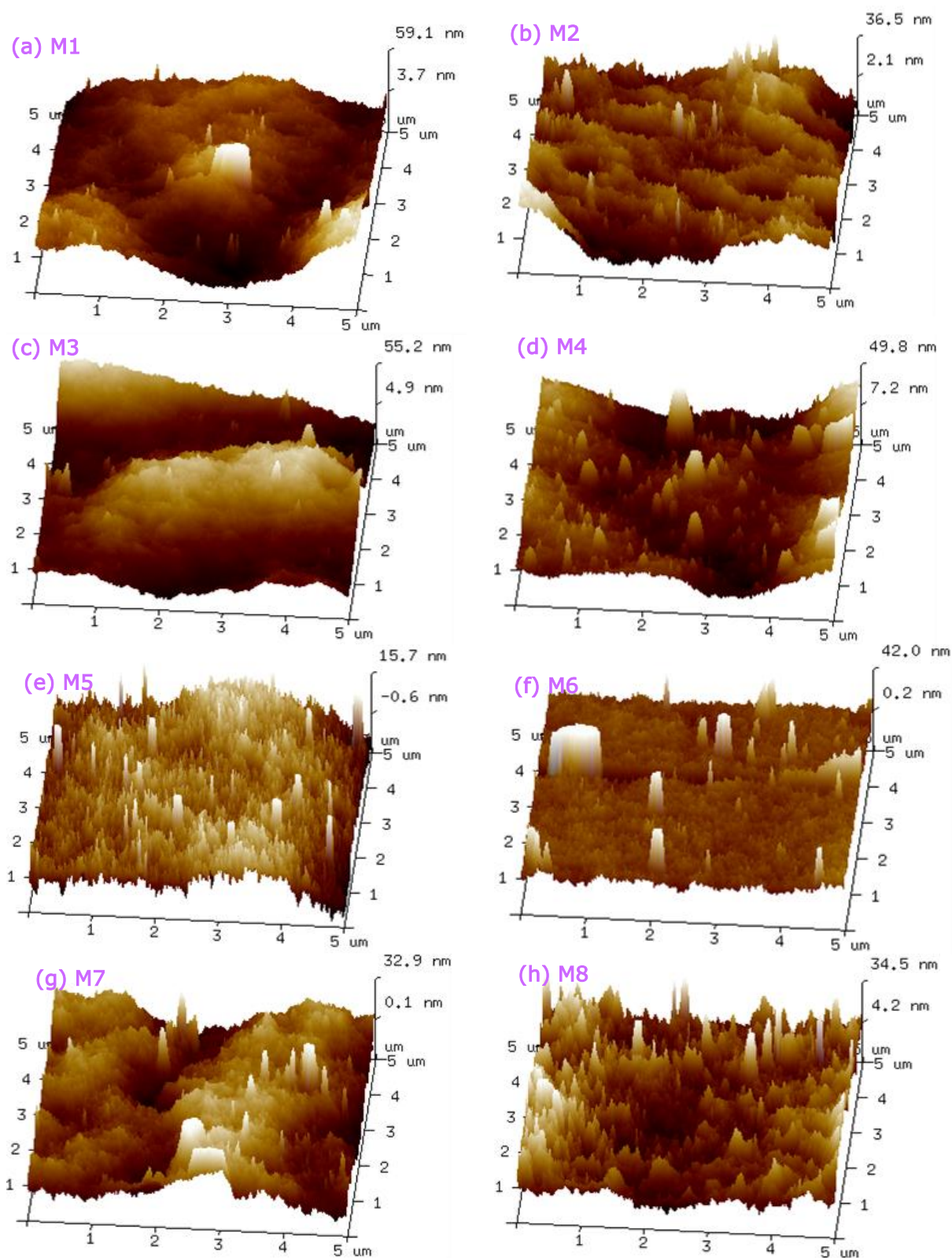


Fig. S5.11 AFM three dimensional images of membranes M1-M8 top surface layer before static ageing test in THF solvent.

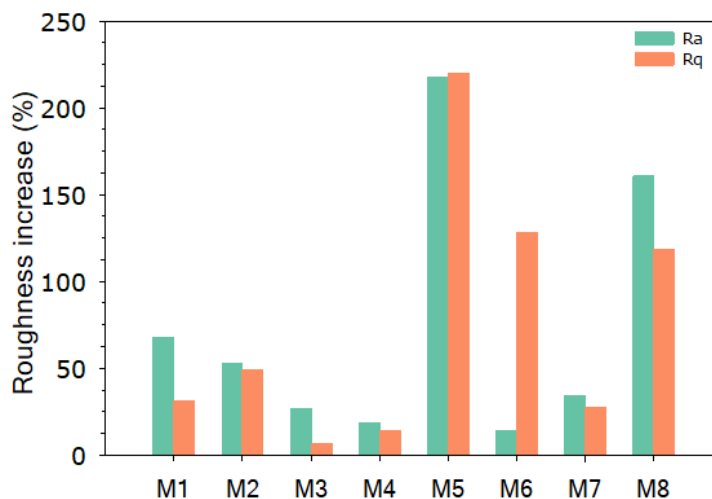


Fig. S5.12 The percentage increase in the membranes M1-M8 top layer mean roughness, Ra and root mean square roughness, Rq roughness after static ageing test with *THF* solvent for 30 days.

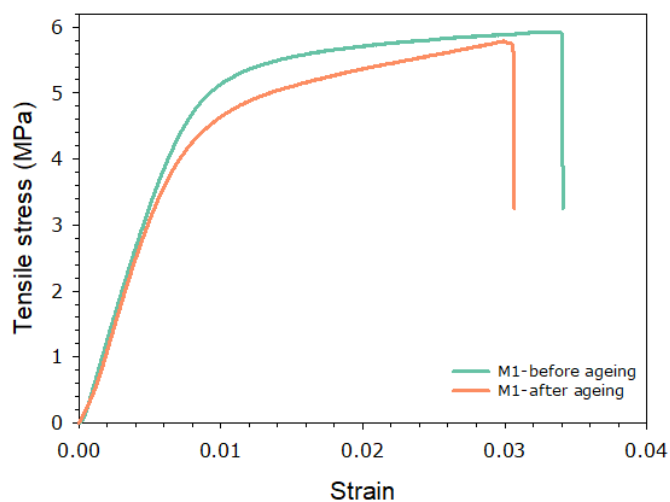


Fig. S5.13 The stress-strain curves of the M1 membrane film before and after static ageing test with *THF* solvent for 30 days.

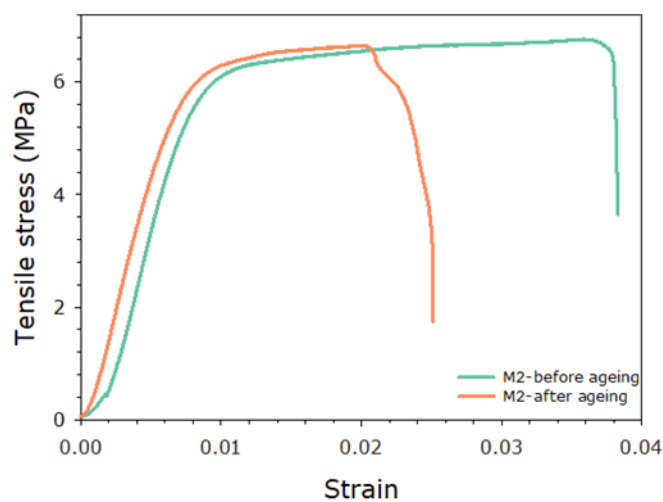


Fig. S5.14 The stress-strain curves of the M2 membrane film before and after static ageing test with *THF* solvent for 30 days.

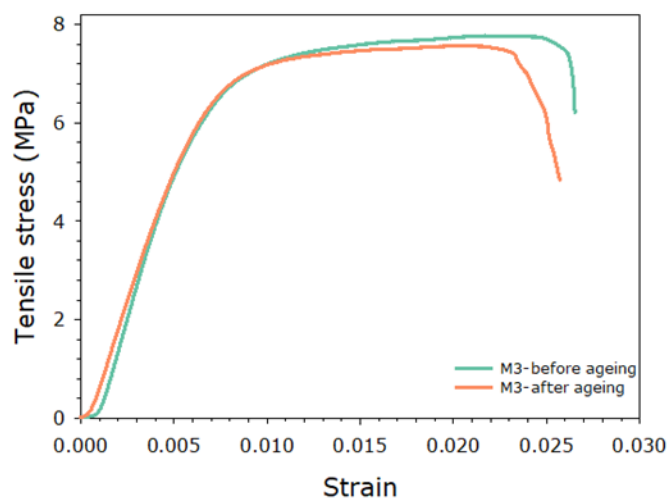


Fig. S5.15 The stress-strain curves of the M3 membrane film before and after static ageing test with *THF* solvent for 30 days.

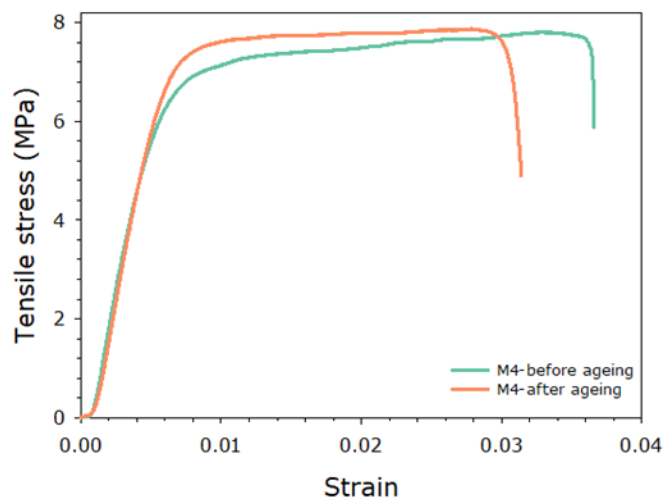


Fig. S5.16 The stress-strain curves of the M4 membrane film before and after static ageing test with *THF* solvent for 30 days.

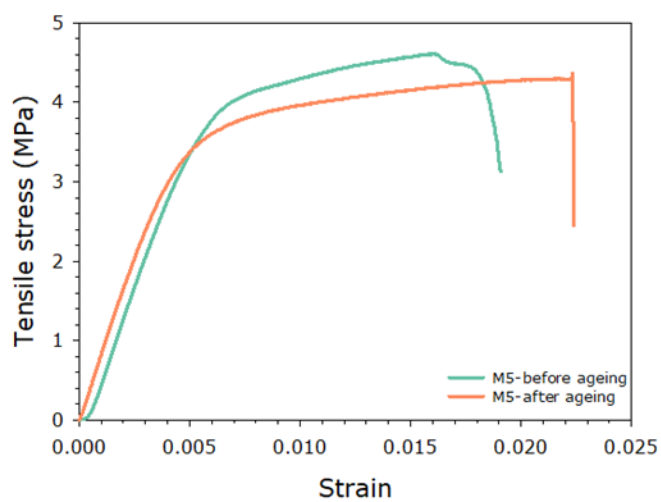


Fig. S5.17 The stress-strain curves of the M5 membrane film before and after static ageing test with *THF* solvent for 30 days.

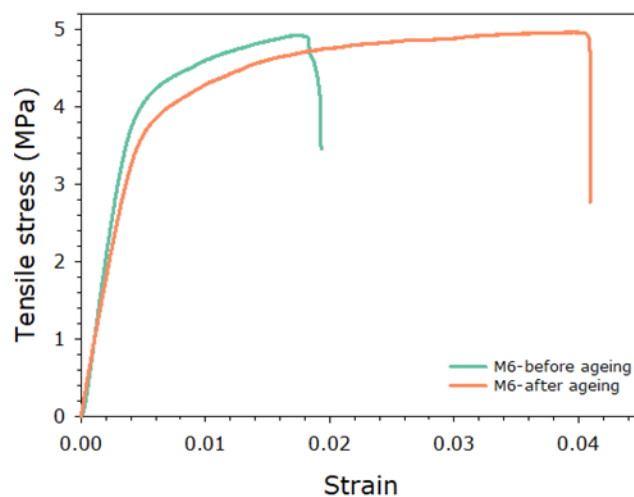


Fig. S5.18 The stress-strain curves of the M6 membrane film before and after static ageing test with *THF* solvent for 30 days.

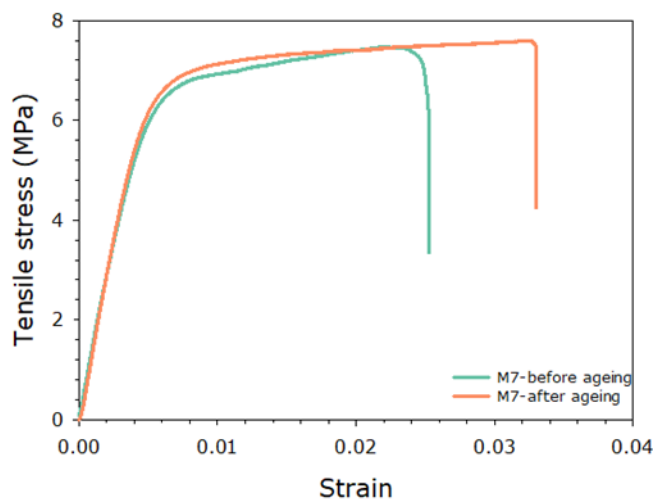


Fig. S5.19 The stress-strain curves of the M7 membrane film before and after static ageing test with *THF* solvent for 30 days.

Table. S5.1 Elongation at break of the M1-M7 free-standing membrane films before and after ageing with *THF* solvent for 30 days.

Membrane	Elongation at break, %	
	before ageing	after ageing
M1	3.4±0.3	3.1±0.4
M2	3.8±0.2	2.0±0.3
M3	2.7±0.5	2.6±0.6
M4	3.7±0.4	3.1±0.4
M5	1.6±0.5	2.2±0.5
M6	1.9±0.4	2.5±0.3
M7	2.5±0.6	3.3±0.7

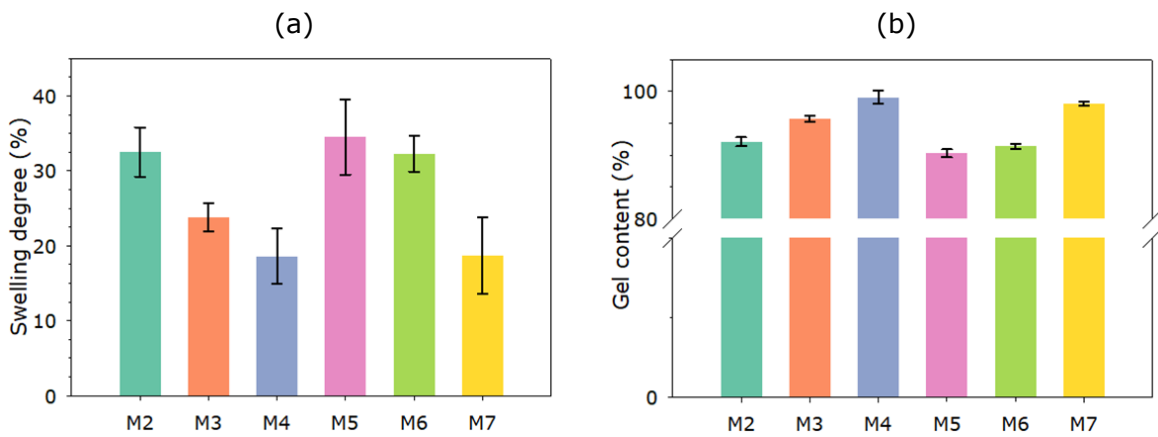


Fig. S5.20 Mass swelling degree and gel content of the cross-linked membranes M2-M7 in DMF solvent.

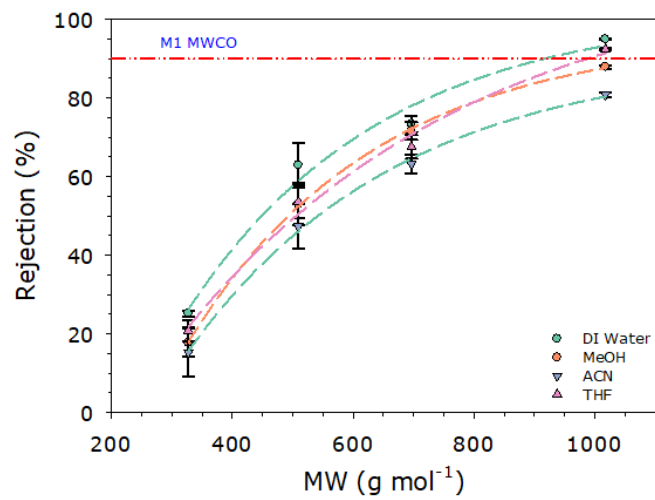


Fig. S5.21 The dye retention and apparent MWCO of the S-PANI membrane (M1) prepared in 0.1 M HCl(aq) coagulation bath.

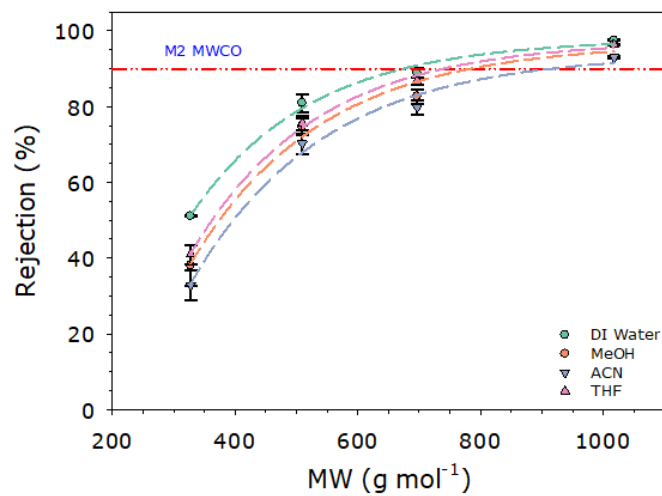


Fig. S5.22 The dye retention and apparent MWCO of the S-PANI membrane (M2) prepared in 0.5 M HCl(aq) coagulation bath.

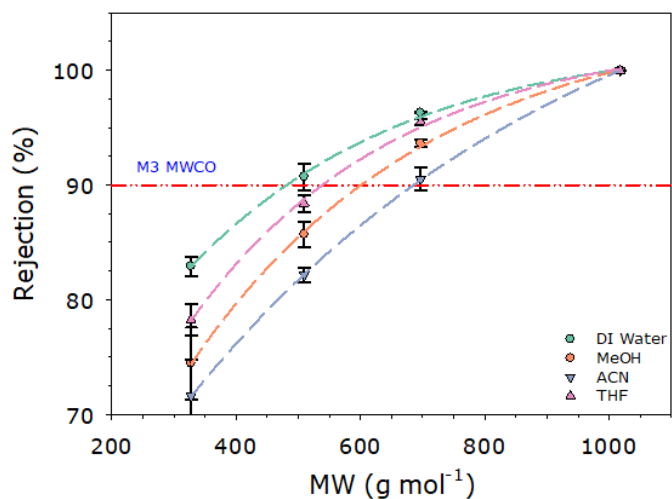


Fig. S5.23 The dye retention and apparent MWCO of the S-PANI membrane (M3) prepared in 1.0 M HCl(aq) coagulation bath.

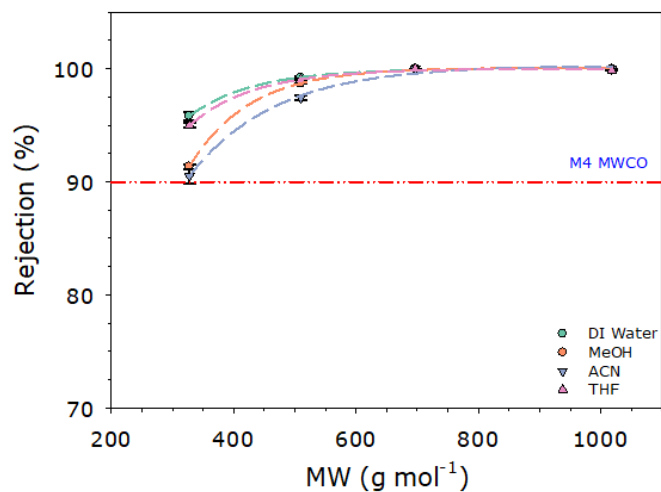


Fig. S5.24 The dye retention and apparent MWCO of the S-PANI membrane (M4) prepared in 3.0 M HCl(aq) coagulation bath.

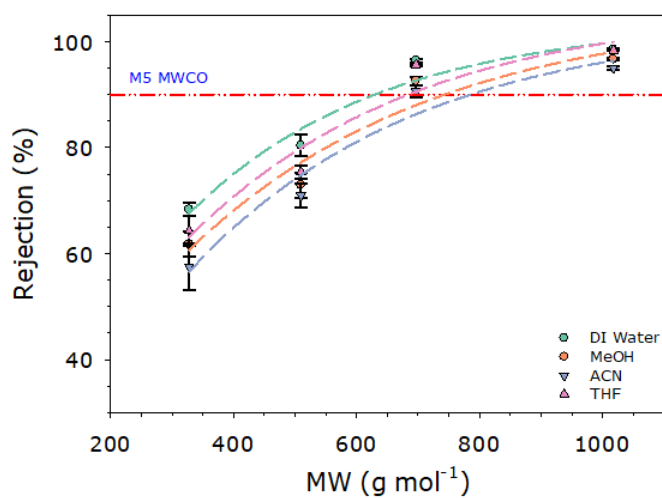


Fig. S5.25 The dye retention and apparent MWCO of PANI-PAMPSA membrane (M4) prepared in 1.0 M HCl(aq) coagulation bath.

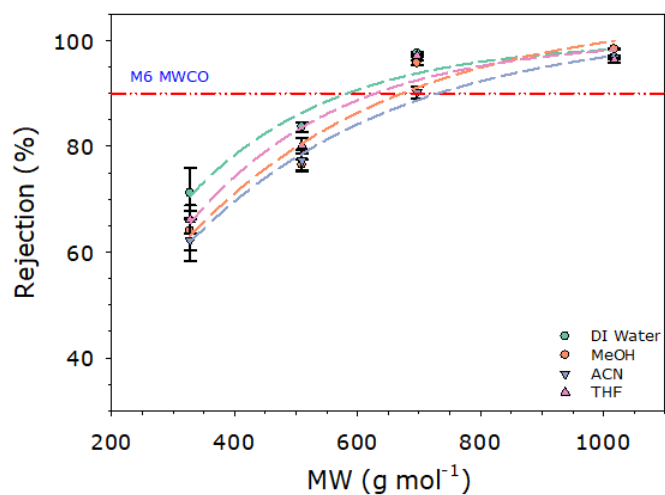


Fig. S5.26 The dye retention and apparent MWCO of the S-PANI PAMPSA membrane (M6) prepared in 1.0 M HCl(aq) coagulation bath.

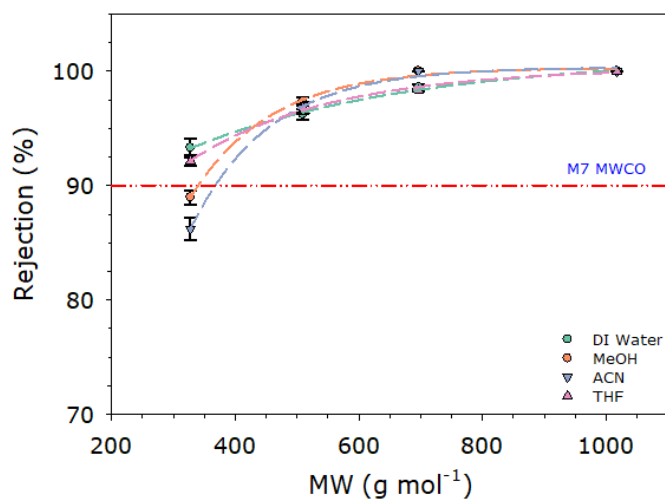


Fig. S5.27 The dye retention and apparent MWCO of the S-PANI membrane (M7) cross-linked with glutaraldehyde.

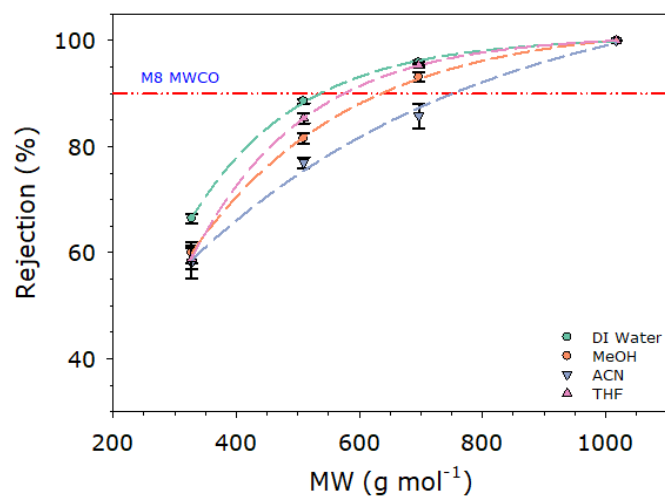


Fig. S5.28 The dye retention and apparent MWCO of the commercial modified polyimide (M8).

Chapter 6

General discussions of the published work

This chapter draws the story line and delve into the meaning, importance and relevance of the results presented in this thesis.

6.1 Discussions

Membrane long-term durability is crucial under complicated operating conditions for water treatment. Herein, sulfonation reaction of aniline monomer before polymerisation was adopted by the introduction of sulfonic acid groups ($-\text{SO}_3\text{H}$) and S-PANI membranes were facilely fabricated in the UF separation range (MWCO \approx 25 kDa). The S-PANI pure water permeance was $\approx 69.7 \pm 1.9 \text{ L m}^{-2} \text{ h}^{-1} \text{ bar}^{-1}$ and the results were reproducible with permeance variance of different polymer batches around 6.3%. Sulfur atom of a sulfonating agent bonded to the oxygen atoms that possess higher electronegativity and acted as electrophilic centre by reacting with the delocalised π electron system of the aromatic ring. The incorporation of $-\text{SO}_3\text{H}$ groups into the preferential positions of the polymer aromatic ring altered the membrane properties such as improved hydrophilicity and decreased anion exchange between the polymer and electrolyte during oxidation and reduction. This was attributed to the electron-withdrawing effect of the sulfonate groups which reduced the electron density on amino groups and the reactivity of polymer backbone with chemical agents. As such, Orton re-arrangement was inhibited upon the exposure to free chlorine (250 ppm NaOCl at different pH) for three consecutive days. The soaked S-PANI membranes in free chlorine solution did not compromise the membrane morphology, surface roughness, and chemical properties as confirmed by SEM imaging, AFM analysis and the FT-IR, respectively. Meanwhile, the permselectivity was not sacrificed and the slight permeance changes ($\pm 10\%$) were associated with the pH stimuli responsiveness. In contrast, the electron rich moieties (aromatic rings) of PANI membranes were susceptible to direct chlorination including sequential (step) chlorination of amides followed by intermolecular rearrangement, forming various aromatic substitution products. This led to degradation of membranes by creating void space openings resulting in complete damage of the membrane structure as confirmed by visual observation, SEM images, higher water flux and/or solute carryover into the membrane permeate. Despite the high hydrophilicity of the S-PANI membranes which forms a hydration layer at their surface to prevent foulants from adsorbing on the surface, a zero rate of TMP increase over time was not obtained, including critical flux, during the trial. The highest fouling propensity was observed with the *alginate acid* followed by the *humic acids*

and the *BSA*. The relatively higher TMP growth with the *alginate acid* model foulant was associated with the charged hydrophilic organic macromolecules that possess higher intermolecular bridging (gelation) compared to the hydrophobic *humic acids* used here. The bulky nature and the positive charge of the *BSA* molecules which were fully retained by both PANI and S-PANI membranes would have resulted in deposited foulant cake layer without further pore blocking. The hydrodynamic conditions may have created a continuous shear force to the foulant deposits leading to the least TMP growth in comparison with the *alginate acid* and *humic acids*. The S-PANI membrane demonstrated less TMP increase than PANI which could be explained by the reduced foulant adsorption due to the formation of the hydration layer by the zwitterionic surface. This positioned the S-PANI membranes in a premium stage for UF applications where intrinsic antifouling behaviour and chlorine-resistant are vital.

Nevertheless, the application of the developed S-PANI membranes was limited to the UF range and broad reaching application was imminent upon tailoring membranes with higher permselective properties at NF range and beyond. As such, a novel method that involves simultaneous coagulation and crosslinking was explored using NIPS technique. This was achieved by altering the composition of the aqueous coagulation bath in the presence of cross-linkable groups in the chain end or the side-chains of the polymer backbone. The exposure of the S-PANI dope solution to a high acidic strength coagulation bath (1-3 M HCl) helped to yield cross-linked membranes in the NF range, due to fourfold factors: (a) associated acid doping with cross-linking, (b) interaction between sulfonic and amine groups, (c) pH effects on polymer re-assembly, and (d) delayed demixing. NF S-PANI membranes with MWCO $\approx 680 \text{ g mol}^{-1}$ (sucrose octa-acetate) and pure water permeance $5 \pm 1 \text{ L m}^{-2} \text{ h}^{-1} \text{ bar}^{-1}$ were obtained at coagulation bath acidic strength of 3 M HCl(aq). The membrane showed less rejection for the PEG 1000 (MWCO $\approx 900 \text{ g mol}^{-1}$) which was attributed to solutes carry-over to the permeate under applied pressure due to the wiggling effect of the linear PEG. The crosslinked membranes showed relative changes in the FT-IR spectra which were attributed to the partial consumption of the sulfonic acid groups due to the formation of sulfonamide groups as a result of nucleophilic $\text{S}_{\text{N}}1$ substitution between an electron pair donor (secondary amine) and an electron pair acceptor (sulfonic group). Also, reactions occur between *NMP*/*4MP* solvents and HCl(aq) in the coagulation bath which involve degradation of *NMP* potentially impacting polymer precipitation during re-assembly and the polymer-polymer

bonding. Changes in the chemical state of the sulfur and nitrogen bonding following the cross-linking reaction were also confirmed in the XPS spectra. Additionally, the crosslinked membranes were less structured than the pristine membrane as confirmed by the XRD analysis which can be ascribed to shrinkage of the intersegmental distance of polymer chains. The analysis of the carbon gradient in the coagulation bath over time served for better understanding of the kinetics during the precipitation process. A dramatic solvent/non-solvent demixing rate took in total 2 h was observed for the pristine SPANI compared to delayed demixing (~24 h) in coagulation bath with high acidic strength (1-3 M HCL) where crosslinking was taking place. This kinetics explained the SEM cross-sectional images which showed the formation of finger-like voids for the pristine S-PANI compared to a dense selective layer with suppressed macro voids for the crosslinked systems. The dense three-dimensional network with limited freedom for motion by the individual segments of the molecules' steric hindrance to chain movement resulted in higher thermal stability for the crosslinked membranes and improved mechanical strength by 2.3 times higher than the pristine S-PANI membrane. The crosslinking was verified by measuring the swelling degree and gel content using different grades of organic solvents. Moreover, the tailored crosslinked membranes exhibited continuous and higher decline in the dynamic contact angle compared to the pristine sample which illustrates higher hydrophilicity and less affinity towards foulant matter for the former system. The developed fabrication method helped to tailor chemically and thermally stable S-PANI NF membranes and eliminates the need for additional solvent-based post-treatment that caused a high compromise in the pure water permeance and demands for high applied pressure (20 bar versus 7 bar). The developed S-PANI NF membrane was trialed in crossflow mode for NOM removal from artificial surface water, artificial seawater and an actual leachate obtained from an existing landfill site. The S-PANI was compared with a commercial membrane and conventional adsorption-coagulation-flocculation, optimised for NOM removal. S-PANI NF membranes showed best NOM separation performance for both surface and seawater followed by the commercial membrane and conventional treatment. For landfill leachate conventional treatment had the best performance followed by S-PANI NF membranes. S-PANI performed slightly better in removal of COD (74%) compared to the commercial membrane (70%) and conventional treatment (70%). Both membranes

performed consistent with increasing salinity and NOM concentration, while experiencing a modest carryover at higher salinity. During long-term fouling S-PANI exhibited slower growth in TMP, less affinity towards organic matter and higher flux recovery compared to the commercial membrane, particularly at high NOM concentration. This is the first study to investigate S-PANI membranes for water treatment applications and under high-fouling conditions. Results indicate S-PANI NF membranes are promising for such applications. In addition, this study also provides an inter-process comparison for NOM removal over an extreme range of water matrix conditions.

The utilisation of the crosslinked S-PANI membranes in the OSN applications could play a significant role in sustainable development for altering conventional separation technologies such as solvent extraction, crystallisation, evaporation, precipitation, and ion exchange. The latter technologies are accompanied with high costs and energy use, and low separation efficiency limit their sustainability compared to facile operation, small footprint, relatively low energy requirements, scalable capacities, and high separation efficiency in mass separation or chemical conversion for the membrane processes. However, each application requires different membrane properties which prompted the need for more selective and permeable membrane performances. Crosslinked PANI membranes were foreseen as a promising solution for OSN applications due to the thermal, chemical, mechanical stability and the stimuli responsive behaviour at variable electric fields. Nonetheless, post-treatment of PANI membranes for several days using hazardous organic chemicals was essential to obtain chemically cross-linked solvent stable PANI or S-PANI membranes while significantly compromising solvent flux. Given these challenges, developing PANI membranes for OSN applications required further research towards simplified in-situ tailored pore size with optimised cross-linking degree that suits different solvents for the whole NF filtration range. We presented in previous work (chapter 3) a scalable approach to produce the first in-situ cross-linked S-PANI membranes at NF range using NIPS which inspired the present work in chapter 5 for facile simultaneous coagulation and crosslinking in acidic coagulation bath with a presence of crosslinker in the polymer chains. The fabrication of high performance (*THF* permeance was 2.1 to 16.4 L m⁻² h⁻¹ bar⁻¹ with apparent MWCO between 250 to 1000 g mol⁻¹) PANI membranes with in-situ tuned transport properties to suit a broad range of OSN applications was successful and took place by a) controlling the cross-linking density by varying the

coagulation bath acidic strength and b) self-doping PANI during the polymerisation process by incorporating organic acids at different molecular weight, acidity, and hydrophilicity, such as MA and PAMPSA. The latter, PAMPSA, possess a flexible backbone that can strongly interact at molecular scale with imine nitrogen enabling the formation of a double-stranded structure with PANI whereas the low molecular weight MA, resulted in compact free volume due to the copolymerisation with aniline in the presence of hydrochloric acid which led to desired changes in membrane performance. The successful crosslinking was confirmed by the FT-IR. Higher crosslinking degree was achieved by increasing the gradient of the coagulation bath acidic strength. The increased crosslinking degree reflected higher mechanical strength, improved stability in different grades of organic solvents with lower gel content and swelling degree and denser selective layer and suppressed macro voids as exhibited by the SEM cross-sectional images. The PAMPSA doped membranes showed different structures compared to other membranes with relatively dense but still porous, thin top layer and a more porous spongy layer underneath. This was ascribed to the high dope solutions viscosity and the high hydrophilicity of PAMPSA doped polymer which needs a longer time to coagulate in the water bath to form the films. Long-term performance tested over 250 h in a crossflow filtration mode using sequential feed solutions of different dyes (MW range from 327 to 1470 g mol⁻¹) in *MeOH*, *ACN* and *THF*. Membranes with higher crosslinking degree showed an order in permeance decline (52-92%) and increase in solute selectivity. PAMPSA doped membranes were only in the tight UF separation range (MWCO \approx 1.5 kDa) due to the high MW of the acid dopant which increased the intersegmental spaces. Therefore, membrane post-treatment by wet annealing was applied to narrow the membrane's solute rejection to NF range without substantial compromise to the membrane permeance as experienced in dry annealing process. The OSN filtration results were reproducible without any irreversible structural ageing. The characterisation results (SEM, AFM, mechanical properties, and hydrophilicity) indicated that no membrane ageing occurred over the static test period of 30 days with *THF*. These results indicate that the membranes exhibit good stability over a long-term period whilst still maintaining the excellent separation performances. The membranes could be tailored to suit widespread applications by changing the cross-linking degree without compromising model solvent stability such as *MeOH*, *ACN* and *THF*.

Chapter 7

General conclusions and future work

This chapter draws conclusions from all the research conducted as part of this PhD and presented in this thesis. It also provides recommendations for future work.

7.1 Conclusions

Membrane processes are rapidly growing and may replace a significant proportion of conventional separation processes in many areas such as water and wastewater treatment at commercial scale. Despite the commercialisation of membrane technology for over four decades, next generation of polymeric membranes by using new classes of materials with novel preparation protocols is vital to overcome limitations such as membrane fouling propensity, chlorine intolerance and solvent stability. To combat fouling development, strategies like a) feed water pre-treatment, b) chlorination, c), membrane surface modification, d) blending of membrane dope solution with organic or inorganic material to enhance hydrophilicity i.e., decrease affinity towards foulants, and e) development of polymeric membrane material that possess intrinsic antifouling property. Likewise, laborious post-treatment using toxic and hazardous organic compounds were used to facilitate crosslinking and therefore enhance permselective properties and organic solvent stability. Herein, these challenges were addressed and solved by developing membrane materials that possess enhanced intrinsic antifouling behaviour with antibacterial growth, chlorine resistance, solvent stability, and the in-situ tuneability of the permselective properties at UF and NF separation range. PANI was chosen as a starting material of interest due to its hydrophilic and antibacterial nature, simple and low-cost synthesis, thermal and chemical stability, and unique doping/dedoping chemistry. However, the pristine PANI membranes are chlorine intolerant and retain solutes rejection not below the UF separation range. Although obtaining PANI membrane at NF range had been successful, this was achieved at the cost of flux and demanding laborious post-treatment cross-linking procedures that involves toxic and hazardous organic compounds. This work has systematically tackled these issues by the following approaches: a) introduction of electron-withdrawing sulfonate groups ($-\text{SO}_3\text{H}$) into the aromatic polymer chain to improve the antifouling behaviour and chlorine resistance, b) facile fabrication of S-PANI membranes in NF separation range via exploiting the polymer crosslinking sites

(sulfonic and amide groups) during the precipitation process in acidic coagulation bath and c) in-situ crosslinking and tuneability of membrane transport properties during membrane fabrication process to suit broad range of OSN applications via incorporating organic acids of different MW, chemistry and hydrophilicity, such as MA and PAMPSA in different coagulant bath of different acidic strength.

PANI and S-PANI powder were synthesised by oxidation polymerisation and subsequently, ISA membranes were prepared using the NIPS technique. The cast-film was immersed in aqueous coagulation bath containing DI water and all prepared membranes showed MWCO in UF separation range. The results showed that the S-PANI membranes withstood chlorine exposure (250 ppm for 3 consecutive days in acidic to basic conditions) whereas PANI membranes suffered critical structural damage and completely lost their ability to reject the probe molecule. Dynamic filtration test which investigated the real-time development of TMP using model foulants such as *alginate acid*, *humic acid* and *BSA* suggests S-PANI membranes acquire better antifouling properties including a high flux recovery ratio in comparison to the PANI membranes. The filtration results suggest that the presence of sulfonated groups ($-\text{SO}_3\text{H}$) make PANI a promising material to overcome outstanding challenges, such as, fouling propensity and membrane longevity. However, the obtained MWCO of the S-PANI membrane was around 25 kDa and more efforts were essential to improve the solute rejection without substantial compromise to the membrane flux using simplified preparation techniques to prevent the laborious post-treatment cross-linking techniques reported in literature. It was hypothesised the sulfonic groups in the polymer backbone provides the anchor to cross-link the polymer while precipitating in an acidic aqueous coagulation bath. The results showed a potential interaction between the sulfonic groups and the nitrogen resulting in a more amorphous matrix compared to the pristine S-PANI produced in pure water coagulation bath. The simultaneous cross-linking and coagulation resulted in an instant formation of a dense selective layer, which diminished the demixing rate. The membrane conformation was altered with suppressed macro-voids, reduced porosity, improved tensile strength, enhanced hydrophilicity, and a significant improvement in *DMF* solvent stability over

an observation time of two weeks. Coagulation bath acidic strength of 3 M HCl(aq) led to in-situ formation of membranes in NF range with MWCO \approx 680 g mol⁻¹ (sucrose octa-acetate). This new simplistic, time, chemical and cost savings scalable approach can be effortlessly applied to design new classes of S-PANI membranes in NF range without the complications of using laborious post modification cross-linking methods. The performance of S-PANI NF membranes was compared to a commercial NF membrane (DuraMem[®]500) and an optimised conventional adsorption/coagulation/flocculation/filtration treatment process. Performance tests included organic matter removal and observing membrane fouling behaviour for a stabilised landfill leachate, artificially prepared surface water and seawater at different [DOC]. Performance DOC removal for S-PANI membrane was regularly higher than the DuraMem[®]500 by 8-10% although both membranes experienced organic matter carry over (2-9%) at high salinity conditions. The membrane treatment revealed almost consistent DOC removal efficiencies surpassing the conventional treatment despite the variation in the feed [DOC]. In contrast, the conventional treatment DOC removal efficiency for the leachate transcended S-PANI and DuraMem[®]500 membranes by 7% and 14%, respectively, whereas the COD removal conformed the following order with marginal difference: SPANI > DuraMem[®]500 \approx conventional treatment. The fouling study demonstrated limited development in real-time TMP, high flux recovery and less affinity towards organic foulants compared to the DuraMem[®]500 membrane as confirmed by foulant deposit measurements over the membrane surface and SEM surface images for the pristine, fouled and chemically cleaned membranes. The results revealed that the developed S-PANI membranes exhibited a high and consistent organic matter removal efficiency at variable organic loads of different feed chemistries with genuine antifouling behaviour surpassing both conventional treatment and the commercial membrane contender. The results underline that the developed S-PANI membranes exhibited a high and consistent NOM removal efficiencies in variable organic loads of different feed chemistries with genuine antifouling behaviour surpassing commercial contenders. Consequently, the S-PANI membrane could be considered as an alternative solution

to tackle more stringent quality requirements for surface water, seawater, leachate (pre)treatment and foulant rich solutions such as food processing.

The simplified crosslinking technique inspired further work for in-situ tuning the permselective properties of PANI membranes by incorporating different MW acid dopants in the PANI backbone and altering the coagulation bath acidic strength. PANI was synthesised by oxidation polymerisation of aniline in the presence of different MW acid dopants such as MA and/or PAMPSA to produce S-PANI, PANI-PAMPSA and S-PANI PAMPSA. Simultaneous coagulation and cross-linking took place by using NIPS for producing self-doped PANI membranes. The produced membranes were soaked in *THF* for 30 days to investigate the static ageing. The mechanical analysis, swelling degree, gel content and SEM surface and cross-sectional images did not indicate any structural damage or morphological deterioration of all cross-linked membranes. The AFM surface roughness analysis suggested that all membranes possess a smooth membrane surface with few random size and shape bulges before and after ageing although mean surface roughness was increased following ageing. Membranes prepared in higher acidic strength coagulation bath are deemed to have higher cross-linking degree showing higher solvent stability with less swelling and little increase in mean surface roughness after static ageing. The dynamic ageing crossflow filtration test over 250 h using sequential dye feed solutions of *MeOH*, *ACN* and *THF* showed that all membranes have a steady-state performance. The transport properties test revealed a successful tailoring of membranes with wide range of *THF* permeance range from 2.1 to 16.4 L m⁻² h⁻¹ bar⁻¹ and estimated MWCO from 250 to 1000 g mol⁻¹. The static ageing test indicated that the prepared membranes in higher coagulation bath acidic strength (≥ 0.5 M HCl) were stable in *DMF* compared to commercial modified polyimide which suffered complete damage. Given the ease of fabrication, modification and the in-situ tuned membrane performance, this work may represent a significant step forward in the fabrication of high performance OSN membranes for various applications. Overall, the aims and objectives pursued by this study were attained. However, future work is needed as explained in the following section.

7.2 Future work and impact

Despite advances and discoveries over several decades, the field of membrane treatment includes several knowledge gaps. These gaps mainly concern a standard approach for the identification and characterisation of the membranes for different applications. Most of the commercially and laboratory prepared membranes have no consistency in terms of a) selection of probe molecules for MWCO determination, b) fouling tendencies because most of the studies are carried out using model foulants of different concentrations at short running time which does not reflect the actual operating conditions and real membrane-foulant affinity, and c) static and dynamic ageing protocol in organic solvents. The main barriers to addressing these knowledge gaps are a) affordability limitations of existing analytical techniques, including high cost of solute and analytical instruments which need for specialised personnel, b) size exclusion (sieving) is not the only separation mechanism and contribution of other mechanisms might interfere with solute selectively such as charge interaction (Donnan exclusion effect), and solute-membrane affinity (e.g., hydrophobic attraction, hydrogen bonding), c) the highly variable load of foulants that possess different surface charges and morphologies with complex and diverse nature in water, wastewater or saline water make understanding the fouling mechanisms too challenging, and d) different types of solvents may interact with a same membrane in an extremely dissimilar way which is subjective to the membrane hydrophilicity/hydrophobicity and also solvent polarity. Future work is therefore proposed for the wider membrane field. Finally, the future work and impact that this thesis can have on water and wastewater treatment is described below.

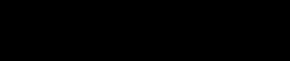
7.2.1 Future work on the specific topics of this thesis


- Self-doping of PANI membranes with sulfonic groups, for instance, helped to facilitate cross-linking in acidic coagulation bath, enhanced the chlorine resistance and enhanced the antifouling behaviour. However, the effect of different types of self-dopants and cross-linking techniques to the PANI membranes' stimuli responsive behaviour at


different pH and electric potential have not been investigated. This has a potential impact on pore size tuneability and defouling behaviour during membrane cleaning cycles using stimuli responsive property.


- The development of S-PANI membranes in reverse osmosis separation range with acceptable compromise to membrane flux has not yet been achieved/investigated.
- S-PANI membrane-foulant interactions are not well understood and further works is required to study the adhesion forces considering different types of foulants with different surface charges in different feed water chemistry such as pH and temperature.
- Fabrication of S-PANI spiral wound modules to investigate the performance of the membrane at pilot scale and compare it with the bench scale results worth investigating.
- Development of mixed matrix adsorptive S-PANI membranes for water and wastewater treatment.
- Investigation of the recyclability and reuse of PANI membranes.
- Exploration of the possibility to tune the permselective properties of S-PANI membranes by using pore forming agents at different concentrations.
- Examine alternative in-situ cross-linking methods such as the use of inorganic free radical initiators in the coagulation bath.
- Explore alternative sustainable and environmentally friendly solvents for membrane preparation to substitute the toxic and hazardous *NMP* solvent.

Appendix: Statement of Authorship

This declaration concerns the article entitled:			
Self-doped sulfonated polyaniline ultrafiltration membranes with enhanced chlorine resistance and antifouling properties.			
Publication status (tick one)			
Draft manuscript	<input type="checkbox"/>	Submitted	<input type="checkbox"/>
		In review	<input type="checkbox"/>
		Accepted	<input type="checkbox"/>
		Published	<input checked="" type="checkbox"/>
Publication details (reference)	Alhweij H, Amura I, Wenk J, Emanuelsson EAC, Shahid S. Self-doped sulfonated polyaniline ultrafiltration membranes with enhanced chlorine resistance and antifouling properties. J Appl Polym Sci. 2021;138:e50756. https://doi.org/10.1002/app.50756 .		
Copyright status (tick the appropriate statement)			
I hold the copyright for this material		<input type="checkbox"/>	Copyright is retained by the publisher, but I have been given permission to replicate the material here
			<input checked="" type="checkbox"/>
Candidate's contribution to the paper (provide details, and also indicate as a percentage)	<p>The candidate contributed to:</p> <p>Formulation of ideas: 70% The paper idea was originally planned by the candidate HA and the co-supervisors SH and EE which covered the chlorine resistance study. Afterwards, the further detailed work which was particularly focused on the fouling study was developed between the candidate and JW.</p> <p>Design of methodology: 75% The candidate designed the methodology for experiments and analysis with feedback from all co-authors.</p> <p>Experimental work: 90% The candidate prepared all S-PANI membranes with advanced training and consultation provided by Dr Ida Amura and Dr Adam Sarihan. The optimisation for polymer synthesis procedure and membrane preparations were conducted by the candidate. All experimental work was carried out by the candidate including valuable feedback from the SH and JW.</p> <p>Presentation of data in journal format: 75% The candidate wrote the manuscript and prepared graphs and tables under the supervision of SH and JW and with input from EE. JW has provided substantial feedback to enhance the quality of the conducted work.</p>		
Statement from Candidate	This paper reports on original research I conducted during the period of my Higher Degree by Research candidature.		
Signed			Date
			11/03/2022

This declaration concerns the article entitled:			
Simplified in-situ tailoring of cross-linked self-doped sulfonated polyaniline (S-PANI) membranes for nanofiltration applications.			
Publication status (tick one)			
Draft manuscript	<input type="checkbox"/>	Submitted	<input type="checkbox"/>
		In review	<input type="checkbox"/>
		Accepted	<input type="checkbox"/>
		Published	<input checked="" type="checkbox"/>
Publication details (reference)	H. Alhweij, E.A. Carolina Emanuelsson, S. Shahid, J. Wenk, Simplified in-situ tailoring of cross-linked self-doped sulfonated polyaniline (S-PANI) membranes for nanofiltration applications, J. Memb. Sci. (2021) 119654. https://doi.org/10.1016/j.memsci.2021.119654 .		
Copyright status (tick the appropriate statement)			
I hold the copyright for this material	<input type="checkbox"/>	Copyright is retained by the publisher, but I have been given permission to replicate the material here	<input checked="" type="checkbox"/>
Candidate's contribution to the paper (provide details, and also indicate as a percentage)	<p>The candidate contributed to:</p> <p>Formulation of ideas: 80% The paper idea was originally planned by the candidate HA and presented to the co-supervisors SH, JW and EE. The co-authors provided feedback and advised about the steps forward.</p> <p>Design of methodology: 85% The detailed methodology and analysis were designed by the candidate with feedback from all co-authors. JW has given ongoing feedbacks to improve the work quality. JW has also helped with interdisciplinary consultation with Dr Matthew Jones and Simon Lewis at the University of Bath chemistry department.</p> <p>Experimental work: 90% The candidate prepared and tested all membrane systems. The data collection was performed at the EPSRC National Facility for XPS ("HarwellXPS"), operated by Cardiff University and UCL, under Contract No. PR16195.</p> <p>Presentation of data in journal format: 80% The candidate wrote the manuscript and prepared graphs and tables under the supervision of SH and JW and with input from EE. JW has provided substantial feedback to enhance the quality of the conducted work.</p>		
Statement from Candidate	This paper reports on original research I conducted during the period of my Higher Degree by Research candidature.		
Signed		Date	11/03/2022

This declaration concerns the article entitled:			
Organic matter removal and antifouling performance of sulfonated polyaniline nanofiltration (S-PANI NF) membranes.			
Publication status (tick one)			
Draft manuscript	<input type="checkbox"/>	Submitted	<input type="checkbox"/>
		In review	<input checked="" type="checkbox"/>
		Accepted	<input type="checkbox"/>
		Published	<input type="checkbox"/>
Publication details (reference)	H. Alhweij, E.A. Carolina Emanuelsson, S. Shahid, J. Wenk, Organic matter removal and antifouling performance of sulfonated polyaniline nanofiltration (S-PANI NF) membranes.		
Copyright status (tick the appropriate statement)			
I hold the copyright for this material		<input type="checkbox"/>	Copyright is retained by the publisher, but I have been given permission to replicate the material here
			<input checked="" type="checkbox"/>
Candidate's contribution to the paper (provide details, and also indicate as a percentage)	<p>The candidate contributed to:</p> <p>Formulation of ideas: 85% The paper idea was originally planned by the candidate HA and presented to JW who provided feedback and advised about the steps forward.</p> <p>Design of methodology: 85% The detailed methodology and analysis were designed by the candidate with feedback from JW who has given ongoing feedbacks to improve the work quality.</p> <p>Experimental work: 90% The candidate prepared and tested all membrane systems.</p> <p>Presentation of data in journal format: 70% The candidate wrote the manuscript and prepared graphs and tables with help and contribution offered by JW.</p>		
Statement from Candidate	This paper reports on original research I conducted during the period of my Higher Degree by Research candidature.		
Signed			Date
			11/03/2022

This declaration concerns the article entitled:			
High performance in-situ tuned self-doped polyaniline (PANI) membranes for organic solvent (nano)filtration.			
Publication status (tick one)			
Draft manuscript	<input type="checkbox"/>	Submitted	<input type="checkbox"/>
		In review	<input type="checkbox"/>
		Accepted	<input type="checkbox"/>
		Published	<input checked="" type="checkbox"/>
Publication details (reference)	H. Alhweij, E.A. Carolina Emanuelsson, S. Shahid, J. Wenk, High performance in-situ tuned self-doped polyaniline (PANI) membranes for organic solvent (nano)filtration, Polymer. 245 (2022) 124682. https://doi.org/10.1016/j.polymer.2022.124682 .		
Copyright status (tick the appropriate statement)			
I hold the copyright for this material		<input type="checkbox"/>	Copyright is retained by the publisher, but I have been given permission to replicate the material here
			<input checked="" type="checkbox"/>
Candidate's contribution to the paper (provide details, and also indicate as a percentage)	<p>The candidate contributed to:</p> <p>Formulation of ideas: 85% The paper idea was originally planned by the candidate HA and presented to SH and JW. The co-authors provided feedback and advised about the steps forward.</p> <p>Design of methodology: 85% The detailed methodology and analysis were designed by the candidate with feedback from JW who has given ongoing feedbacks to improve the work quality.</p> <p>Experimental work: 90% The candidate prepared and tested all membrane systems.</p> <p>Presentation of data in journal format: 80% The candidate wrote the manuscript and prepared graphs and tables under the supervision of JW with input from SH and EE. JW has provided substantial feedback to enhance the quality of the conducted work.</p>		
Statement from Candidate	This paper reports on original research I conducted during the period of my Higher Degree by Research candidature.		
Signed			Date 11/03/2022